

EVALUATION AND RESPONSE OF AGED FLEXIBLE AIRFIELD PAVEMENTS AT
AMBIENT TEMPERATURES USING THE FALLING WEIGHT DEFLECTOMETER

By

CHARLES WILLIAM MANZIONE

A DISSERTATION PRESENTED TO THE GRADUATE SCHOOL
OF THE UNIVERSITY OF FLORIDA IN
PARTIAL FULFILLMENT OF THE REQUIREMENTS
FOR THE DEGREE OF DOCTOR OF PHILOSOPHY

UNIVERSITY OF FLORIDA

1988

UNIVERSITY OF FLORIDA



3 1262 08552 3420

DEDICATION

This dissertation is dedicated to my greatest blessings and joy, Karen and Michael, in loving appreciation for their understanding, comfort and endless love.

ACKNOWLEDGMENTS

There are many people the author would like to recognize and thank for their part in making this research a success. Knowing that it is impossible to cite all the individuals involved, the author wishes to express his sincere appreciation to every person who has contributed toward the completion of this study.

The author owes sincere gratitude to Captain (Dr.) Randall W. Brown for his key role in getting this research started and for his sound advice and friendship. The author also thanks the Air Force Engineering and Services Center (AFESC) for their fiscal and logistical support.

The author is especially grateful to Mr. Albert J. Bush and Mr. Dennis Mathews both from Waterways Experiment Station for providing monthly logistical support and technical expertise. The assistance of Mr. William D. Brunson, airfield manager at Duke Field, is also appreciated.

The author owes sincere thanks to Dr. Byron E. Ruth for his interest and guidance in the research as committee chairman and for the giving of his time to educate the author. A very special thanks goes to Dr. Michael C. McVay for serving as committee cochairman, offering words of encouragement, and for sacrificing his time to help the author in every way possible.

Gratitude is expressed to Dr. Mang Tia, Professor Walter H. Zimpfer, and Dr. Robert S. Mansell for their willingness to serve as committee members and for offering friendly advice. Special words of thanks

are extended to Drs. Frank C. Townsend, John L. Davidson, and David G. Bloomquist for helping shape my formative years as a geotech and for always being available for assistance.

The author wishes to acknowledge the invaluable contribution of the Florida Department of Transportation, especially that of Mr. Ed Leitner, Ms. Teresa Bailey, and other personnel of the Bituminous Materials Research section.

Special recognition goes to Captain John J. Gill, the author's good friend and study partner, for his quick wit and for helping to keep it all in perspective.

The contributions of Messrs. Danny Richardson, Bill Studstill, Kirk Waite, and Ed Dobson are also appreciated.

The author wishes to commend Ms. Candace Leggett for her professional skill and assistance in preparing this manuscript.

TABLE OF CONTENTS

	<u>Page</u>
ACKNOWLEDGMENTS.....	iii
LIST OF TABLES.....	ix
LIST OF FIGURES.....	xii
ABSTRACT.....	xvi
CHAPTERS	
1 INTRODUCTION.....	1
1.1 Problem Statement.....	1
1.2 Study Objectives.....	3
1.3 Scope of Work.....	4
2 REVIEW OF THE LITERATURE.....	5
2.1 Introduction.....	5
2.2 Design and Performance of Asphalt Concrete Airfield Pavements.....	6
2.2.1 Background.....	6
2.2.2 Horizontal Strain Criteria in the Asphalt Layer.....	7
2.2.3 Vertical Strain at the Top of the Subgrade.....	8
2.3 Nondestructive Testing (NDT) and Conventional Analysis Procedures.....	10
2.3.1 Description of NDT Equipment.....	10
2.3.2 Use of the Falling Weight Deflectometer (FWD) and Conventional Analysis Procedures.....	12
2.3.3 Performance Predictions Using AIRPAVE.....	15
2.4 Causes and Effects for Failure in Flexible Pavement Systems.....	16
2.4.1 General.....	16
2.4.2 Cracking in Asphalt Concrete Pavement.....	18
2.4.3 Rutting in Asphalt Concrete Pavement.....	23
2.5 Rheological Properties of Asphalt Cement and Asphalt Mixtures as Related to Pavement Performance.....	25
2.5.1 Asphalt Cement Properties.....	26
2.5.2 Asphalt Mixture Properties.....	27

3	AIRFIELD DESCRIPTION AND FIELD TESTING.....	32
3.1	Introduction.....	32
3.2	Airfield Description.....	33
3.2.1	Topography and Climatology.....	33
3.2.2	Test Locations and Layout.....	35
3.2.3	Site Layer Profiles.....	42
3.2.4	Construction History.....	46
3.2.5	Aircraft Traffic Data.....	48
3.3	Field Testing and Environmental Monitoring.....	50
3.3.1	Selection and Description of the Falling Weight Deflectometer (FWD).....	50
3.3.2	FWD Field Testing Procedures.....	58
3.3.3	Measurement of Subgrade Moisture.....	59
3.3.4	Measurement and Prediction of Pavement Thermal Profiles.....	65
4	LABORATORY TESTING AND EVALUATION OF PAVEMENT MATERIALS.....	75
4.1	Introduction.....	75
4.2	Classification of Subgrade Materials.....	75
4.3	Determination of Air Void Content in Field Extracted Bituminous Mixtures.....	76
4.4	Determination of Maximum Density of Bituminous Layers.....	80
4.5	Determination of Asphalt Content and Gradation by Quantitative Extraction.....	81
4.6	Testing and Evaluation of Recovered Asphalts Using Penetration and Viscosity Measurements.....	87
4.7	Asphalt Viscosity Testing Using the Schwyer Constant Stress Rheometer for the Determination of Temperature and Shear Susceptibility.....	97
4.7.1	Background.....	97
4.7.2	Equipment and Test Procedures.....	97
4.7.3	Data Acquisition and Analysis.....	98
4.7.4	Relationship Between Viscosity and Temperature.....	102
4.8	Diametral Testing of Bituminous Field Samples.....	105
4.8.1	General.....	105
4.8.2	Laboratory Equipment.....	106
4.8.2.1	Loading System.....	106
4.8.2.2	Electronic Control Console.....	106
4.8.2.3	Recording System.....	110
4.8.2.4	Temperature Control System.....	110
4.8.3	Preparation of Test Specimens.....	110
4.8.4	Preconditioning of Test Specimens.....	113
4.8.5	Dynamic Resilient Modulus Test.....	115
4.8.6	Indirect Tensile Test (Quick).....	117
4.8.7	Static Creep Test (Fracture Energy).....	118

5	RESULTS AND ANALYSES OF DIAMETRAL TESTING.....	120
5.1	Introduction.....	120
5.2	Dynamic Resilient Modulus.....	120
5.3	Tensile Strength.....	126
5.4	Indirect Static Creep.....	130
5.5	Summary.....	134
6	ANALYSES OF FIELD MEASURED FWD DATA.....	136
6.1	Introduction.....	136
6.2	Computer Programs and Data Input.....	137
6.3	Analysis of Site 3.....	138
6.4	Analysis of Site 2.....	150
6.5	Analysis of Site 1.....	164
6.6	Summary.....	171
7	STRESS ANALYSES FOR PAVEMENT REHABILITATION.....	172
7.1	Introduction.....	172
7.2	Stress Analysis on the As-Constructed Pavements.....	173
7.2.1	Input Parameters.....	173
7.2.2	Comparison of Pavement Response Using As-Constructed and Improved Material Design Methods.....	175
7.3	Rehabilitation of Existing Pavements.....	187
7.3.1	Rehabilitation of Site 3.....	187
7.3.2	Rehabilitation of Site 2.....	191
7.3.3	Rehabilitation of Site 1.....	192
7.4	Summary.....	194
8	CONCLUSIONS AND RECOMMENDATIONS.....	197
8.1	Conclusions.....	197
8.2	Recommendations.....	201

APPENDICES

A	SUBGRADE MOISTURE PROFILES.....	205
B	FIELD THERMAL PROFILES.....	207
C	GRADATION TEST RESULTS.....	216
D	PENETRATION-VISCOSITY CORRELATIONS.....	218
E	SCHWEYER RHEOMETER TEST RESULTS ON RECOVERED FIELD CORES.....	223
F	DIAMETRAL TEST RESULTS ON FIELD CORES.....	230
G	FIELD FWD TEST RESULTS.....	256

REFERENCES..... 304
BIOGRAPHICAL SKETCH..... 314

LIST OF TABLES

<u>Table</u>	<u>Page</u>
2.1 Typical Layered Elastic Methods of Matching Deflection Basins.....	14
2.2 Primary Types and Causes of Surface Distress in Asphalt Concrete Pavements.....	17
3.1 Site Layer Profiles In and Out of Wheel Path.....	45
3.2 Construction History.....	47
3.3 Annual Traffic Volume at Duke Field.....	49
3.4 Aircraft Characteristics for C-130.....	52
3.5 Typical Drop Sequence and Load.....	58
3.6 Field Moisture Contents (w %) by Month.....	63
3.7 Parametric Study of Mean Pavement Temperature (MPT).....	74
4.1 Summary of Subgrade Classification.....	77
4.2 Maximum Density, Unit Weight, and Air Void Content for Bituminous Layers In and Out of Wheel Path.....	79
4.3 Penetration, Absolute Viscosity, and Air Void Content for Recovered Asphalts Inside the Wheel Path.....	89
5.1 Results From Indirect Tensile Test With Viscosity and Air Void Content at 25 C (77 F).....	127
7.1 Input Parameters and Results of Stress Analysis at 86 F on Original Pavements.....	176
7.2 Input Parameters and Results of Stress Analysis at 23 F on Original Pavements.....	177
7.3 Input Parameters and Results of Stress Analysis at 86 F on Original Pavements Using the Texaco Air-Blown Asphalt.....	180
7.4 Input Parameters and Results of Stress Analysis at 23 F on Original Pavements Using the Texaco Air-Blown Asphalt.....	181

7.5	Input Parameters and Results of Stress Analysis at 86 F on Full-Depth Asphalt Concrete Pavements Using the Texaco Air-Blown Asphalt.....	184
7.6	Input Parameters and Results of Stress Analysis at 23 F on Full-Depth Asphalt Concrete Pavements Using the Texaco Air-Blown Asphalt.....	185
7.7	Summary of Critical Response Parameters for the As-Constructed Design Using Original and Texaco Air-Blown Asphalts.....	186
7.8	Input Parameters and Results of Stress Analysis for Overlay Rehabilitation at Site 3.....	190
7.9	Input Parameters and Results of Stress Analysis for Overlay Rehabilitation at Site 2.....	193
7.10	Input Parameters and Results of Stress Analysis for Recycling Rehabilitation at Site 1.....	195
A.1	Results of Gravimetric and Volumetric Moisture Contents Measured in the Field.....	205
C.1	Gradation and Asphalt Content of Bituminous Layers.....	216
D.1	Correlation Between Penetration and Viscosity.....	218
E.1	Schweyer Rheometer Test Results on Asphalts Recovered From Site 1.....	223
E.2	Schweyer Rheometer Test Results on Asphalts Recovered From Site 2.....	225
E.3	Schweyer Rheometer Test Results on Asphalts Recovered From Site 3.....	227
F.1	Dynamic Resilient Modulus Test Results on 1AC-1.....	230
F.2	Dynamic Resilient Modulus Test Results on 1AC-2.....	231
F.3	Dynamic Resilient Modulus Test Results on 1SA.....	234
F.4	Dynamic Resilient Modulus Test Results on 2AC-1.....	237
F.5	Dynamic Resilient Modulus Test Results on 2AC-2.....	239
F.6	Dynamic Resilient Modulus Test Results on 2AC-3.....	240
F.7	Dynamic Resilient Modulus Test Results on 2SA.....	241
F.8	Dynamic Resilient Modulus Test Results on 3AC-1.....	243
F.9	Dynamic Resilient Modulus Test Results on 3AC-2.....	245

F.10	Dynamic Resilient Modulus Test Results on 3SA.....	247
F.11	Indirect Tensile Test Results.....	252
F.12	Fracture Energy Parameters and Creep Test Data.....	253
G.1	Results of FWD Tests on Site 1 (Test 1).....	256
G.2	Results of FWD Tests on Site 1 (Test 2).....	258
G.3	Results of FWD Tests on Site 1 (Test 3).....	260
G.4	Results of FWD Tests on Site 1 (Test 4).....	262
G.5	Results of FWD Tests on Site 1 (Test 5).....	264
G.6	Results of FWD Tests on Site 1 (Test 6).....	266
G.7	Results of FWD Tests on Site 1 (Test 7).....	268
G.8	Results of FWD Tests on Site 1 (Test 8).....	270
G.9	Results of FWD Tests on Site 2 (Test 1).....	272
G.10	Results of FWD Tests on Site 2 (Test 2).....	274
G.11	Results of FWD Tests on Site 2 (Test 3).....	276
G.12	Results of FWD Tests on Site 2 (Test 4).....	278
G.13	Results of FWD Tests on Site 2 (Test 5).....	280
G.14	Results of FWD Tests on Site 2 (Test 6).....	282
G.15	Results of FWD Tests on Site 2 (Test 7).....	284
G.16	Results of FWD Tests on Site 2 (Test 8).....	286
G.17	Results of FWD Tests on Site 3 (Test 1).....	288
G.18	Results of FWD Tests on Site 3 (Test 2).....	290
G.19	Results of FWD Tests on Site 3 (Test 3).....	292
G.20	Results of FWD Tests on Site 3 (Test 4).....	294
G.21	Results of FWD Tests on Site 3 (Test 5).....	296
G.22	Results of FWD Tests on Site 3 (Test 6).....	298
G.23	Results of FWD Tests on Site 3 (Test 7).....	300
G.24	Results of FWD Tests on Site 3 (Test 8).....	302

LIST OF FIGURES

<u>Figure</u>		<u>Page</u>
3.1	State Map of Florida Showing Location of Duke Field.....	34
3.2	Plan View of Duke Field Showing Locations of the Three Test Sites.....	36
3.3	Detail of Test Sites.....	37
3.4	Site 1: Severe Block Cracking With Spalling.....	39
3.5	Site 2: Longitudinal Crack at Edge of Wheel Path.....	40
3.6	Site 2: Rutting in Wheel Path.....	41
3.7	Site 3: Longitudinal and Transverse Cracking.....	43
3.8	Site 3: Cracking Through Entire Pavement Thickness.....	44
3.9	Wheel Gear Configuration for C-130 Aircraft.....	51
3.10	C-130 Aircraft: Front and Rear View.....	53
3.11	Main Landing Gear. a) Side View; b) Front View.....	54
3.12	Falling Weight Deflectometer (FWD).....	56
3.13	Location of Loading Plate and Spacing of Geophones.....	57
3.14	Schematic of Installed Moisture Tube.....	60
3.15	Nuclear Moisture Gage.....	61
3.16	Monthly Subgrade Moisture Contents: High, Low, and Average Values. a) Center of Pavement; b) Edge of Pavement.....	64
3.17	Schematic of Installed Temperature Profile Device (TPD).....	68
3.18	Installing the Temperature Profile Device (TPD).....	69
3.19	Temperature Measurement System.....	70
3.20	Nomograph for Determining Pavement Profile Temperatures.....	72
4.1	Grain Size Distribution for the Subgrade Soils.....	78

4.2	Gradation Range for Group A.....	83
4.3	Gradation Range for Group B.....	84
4.4	Gradation Range for Group C.....	85
4.5	Gradation Comparison of All Groups.....	86
4.6	Relationship Between Penetration at 77 F and Absolute Viscosity at 140 F.....	90
4.7	Relationship Between Penetration at 77 F and Constant Power Viscosity at 77 F.....	91
4.8	Relationship Between Penetration at 77 F and Constant Power Viscosity at 59 F.....	92
4.9	Range of Hardening for the Asphalt Cements.....	96
4.10	The Schweyer Rheometer Test System. a) Schweyer Rheometer; b) IBM 9000 Computer.....	99
4.11	F-Tube (left) and G-Tube.....	100
4.12	Temperature Susceptibility Curves for the Asphalt Cements.....	104
4.13	Machine Test System (MTS).....	107
4.14	Loading System.....	108
4.15	Electronic Control Console.....	109
4.16	Recording System.....	111
4.17	Temperature Control Chamber with Dummy Sample and Thermal Probe.....	112
4.18	Strain Gaged Sample Ready for Indirect Tensile Testing.....	114
4.19	Typical Creep Response Curve for Asphalt Concrete.....	115
5.1	Dynamic Resilient Modulus Test Results.....	122
5.2	Dynamic Resilient Modulus Test Results Using Modified Equations.....	123
5.3	Modulus Ratios as a Function of Air Voids.....	125
5.4	Tensile Strength Test Results.....	129
5.5	Results of Fracture Energy Tests.....	131

5.6	Results of Fracture Energy Tests Using Modified Equation.....	133
5.7	Correlation Between Mix Viscosity, n_{100} , and Constant Power Viscosity, $n_{100}^{0.01}$	135
6.1	Surface Deflection as a Function of Load at Site 3 (Most Linear Response).....	140
6.2	Surface Deflection as a Function of Load at Site 3 (Least Linear Response).....	141
6.3	Change in E_1 and E_2 With Temperature for Cracked and Uncracked Pavement at Site 3.....	143
6.4	E_2 as a Function of Temperature at Site 3.....	144
6.5	E_1 as a Function of n_{100} for Cracked and Uncracked Pavements (All Sites).....	145
6.6	E_2 as a Function of n_{100} for Cracked and Uncracked Pavements (All Sites).....	147
6.7	Comparison of E_4 Values as a Function of Temperature at Site 3.....	148
6.8	Extreme Temperature Deflection Response at Site 3 (Normalized to 18-kip Load).....	149
6.9	Measured and Predicted Deflection Basins in Wheel Path at Site 3 (Normalized to 18-kip Load).....	151
6.10	Measured and Predicted Deflection Basins Outside Wheel Path at Site 3 (Normalized to 18-kip Load).....	152
6.11	Surface Deflection as a Function of Load at Site 2 (Most Linear Response).....	153
6.12	Surface Deflection as a Function of Load at Site 2 (Least Linear Response).....	154
6.13	E_2 as a Function of Temperature at Site 2.....	156
6.14	Comparison of E_4 Values as a Function of Temperature at Site 2.....	157
6.15	Extreme Temperature Deflection Response at Site 2 (Normalized to 18-kip Load).....	158
6.16	Comparison of Low Temperature Deflection Response Between Sites 2 and 3 (Normalized to 18-kip Load).....	160
6.17	Comparison of High Temperature Deflection Response Between Sites 2 and 3 (Normalized to 18-kip Load).....	161

6.18	Measured and Predicted Deflection Basins in Wheel Path at Site 2 (Normalized to 18-kip Load).....	162
6.19	Measured and Predicted Deflection Basins Outside Wheel Path at Site 2 (Normalized to 18-kip Load).....	163
6.20	Surface Deflection as a Function of Load at Site 1 (Most Linear Response).....	165
6.21	Surface Deflection as a Function of Load at Site 1 (Least Linear Response).....	166
6.22	E_1 as a Function of Temperature at Site 1.....	167
6.23	Extreme Temperature Deflection Response at Site 1 (Normalized to 18-kip Load).....	168
6.24	Comparison of E_4 Values as a Function of Temperature at Site 1.....	170
7.1	Comparison of Modulus-Temperature Relationships Between the Duke Field and Texaco Air-Blown Asphalts.....	182
7.2	Radial Distances Used in Pavement Stress Analyses.....	189
B.1	Temperature Profile (Test 1).....	207
B.2	Temperature Profile (Test 2).....	208
B.3	Temperature Profile (Test 3).....	209
B.4	Temperature Profile (Test 4).....	210
B.5	Temperature Profile (Test 5).....	211
B.6	Temperature Profile (Test 6).....	212
B.7	Temperature Profile (Test 7).....	213
B.8	Temperature Profile (Test 8).....	214

Abstract of Dissertation Presented to the Graduate School
of the University of Florida in Partial Fulfillment of the
Requirements for the Degree of Doctor of Philosophy

EVALUATION AND RESPONSE OF AGED FLEXIBLE AIRFIELD PAVEMENTS
AT AMBIENT TEMPERATURES USING THE FALLING WEIGHT DEFLECTOMETER

By

Charles William Manzione

April 1988

Chairman: Byron E. Ruth
Cochairman: Michael C. McVay
Major Department: Civil Engineering

A research study was conducted to evaluate the response of aged flexible airfield pavements at varying ambient temperatures using the Falling Weight Deflectometer (FWD). Eight field tests were performed on three sites at Duke Field, Florida, at pavement surface temperatures ranging from 30 to 130 F. Monthly subgrade moisture readings were taken along with the measuring of pavement temperature profiles during each test. Laboratory tests were conducted on collected asphalt concrete and sand asphalt cores. Tests included low-temperature rheology tests, indirect resilient modulus and indirect static creep tests (fracture energy). The analysis of the test data provided a reliable and effective method for predicting the asphalt modulus and fracture energy using asphalt viscosity and air void content.

Backcalculation of layer moduli using measured FWD data was performed by the layered elastic computer program BISDEF. The asphalt

concrete modulus (E_1) was computed using the developed asphalt modulus prediction equations, while BISDEF iterated for the base and subgrade layer moduli. This technique greatly reduced the errors in determining E_1 from the iteration process. Uncracked segments of pavement gave good results using the prediction equations for all asphalt layers. However, adjustments to E_1 were necessary to accommodate the degradation of modulus due to pavement cracking. It was found that the reduction in E_1 values was largely dependent on the degree of cracking. In a severely cracked test section, the modulus values for all layers remained almost constant throughout the entire range of test temperatures. Modulus values of the cracked sections could only be analyzed using FWD data obtained over a large temperature range.

Stress analyses were performed using the elastic layer program, BISAR. Results indicated that the tensile stresses in the sand asphalt layer far exceeded maximum strengths. The original pavement was under-designed and poorly maintained to meet current mission demands.

Specific scenarios were presented for the pavement rehabilitation. Efforts were focused on the prevention of reflective cracking in the new pavement layers while reducing stresses in the base and subgrade layers.

CHAPTER 1 INTRODUCTION

1.1 Problem Statement

The United States Air Force has approximately 4,000 miles of runways throughout the world of which approximately 40 percent are flexible. Ninety percent of the airfield pavements are more than twenty years old (design life) and 25 percent are significantly deteriorated with anticipated replacement costs in the billions of dollars (1). Some runways have been temporarily closed to air traffic prompting immediate repair before being reopened. Other airfields have been neglected to the point where serious distressed conditions threaten their closing unless restorative action is taken. Many airfield pavements have steadily deteriorated and soon could be rendered unsafe to accomplish Air Force mission objectives.

Flexible pavement design has been relatively unaltered over the past twenty years. Acceptable design is achieved when rutting (permanent deformation), resilient (recoverable) deformation, and cracking in the surface courses have been restricted to tolerable limits. The engineer normally bases his analysis on one of the following: 1) layered elastic theory, 2) transfer functions, 3) nondestructive insitu tests, and 4) simple laboratory tests (2,3).

When evaluating flexible pavements, these methods do not account for the changing rheological properties of the asphalt binder caused by age-hardening and seasonal temperature changes. Also, variations in

soil moisture, especially in silts and clays, can have dramatic effects on subgrade and subbase properties. The rheological properties of the asphalt cement and existing soil conditions can substantially affect both the short and long term performance of a flexible pavement.

The Air Force is concerned primarily with maintaining existing air-field pavements since there is very little new construction being done. Presently, rehabilitation of isolated problem areas and overlay work is accomplished based on evaluations and recommendations by the Air Force Engineering and Services Center (AFESC) and base engineers. Air Force installations normally receive comprehensive pavement evaluations by AFESC every five to seven years. Evaluations are either destructive (e.g., conducting subgrade plate load tests) or nondestructive using the Falling Weight Deflectometer (FWD). During an evaluation, there is neither enough time or manpower to conduct both destructive and nondestructive tests (NDT). Cores recovered during NDT are used in obtaining layer thicknesses for input into layered elastic computer programs. Currently, no laboratory strength or modulus tests are conducted on the asphalt concrete.

The AFESC acquired the FWD to speedily but accurately perform NDT evaluations. Deflection basin data obtained by the FWD are used in an iterative analysis to match the deflection basin and backcalculate layer moduli. Layer moduli are then used in another program which uses Miner's theory to compute life expectancy (passes to failure).

Problems arise using iterative approaches in that unique solutions cannot be guaranteed and different sets of elastic moduli can produce similar deflection basins. In 4-layer systems, for example, moduli computed for the intermediate layers (base and subbase) are often times

reversed with the base yielding substantially lower values. In addition, iterative methods using FWD data have shown to be more reliable in predicting the elastic modulus of the subgrade and least reliable in predicting the modulus of the layers at the surface. Other concerns come about when applying Miner's theory (cumulative damage or fatigue) to predict the long term performance of flexible pavements. This is especially true in aged airfield systems that already show the signs of advanced distress (e.g., rut depths over one inch and/or severe block cracking). Life expectancy can differ greatly depending on the time of the year the evaluation is done. The fatigue approach has merit, but other factors can also effect the long term performance of asphalt concrete such as air void content and age-hardening of the binder.

A need, therefore, exists to understand what factors impact the response and performance of flexible pavements and how to incorporate them into a rational analysis. Only then can an accurate assessment of flexible pavement response and performance be made.

1.2 Study Objectives

The primary objective of this research was to study the effects that load and seasonal variations (temperature and moisture) have on the response and performance of an aged asphalt concrete pavement using field and laboratory measurements.

The secondary objective was to determine from laboratory tests which factors and to what degree affect the resilient and creep properties of bituminous mixtures and how to incorporate these factors into the rational evaluation of flexible airfield pavements.

1.3 Scope of Work

Nondestructive field tests were conducted on an aged airfield pavement, Duke Field, located in Crestview, Florida, using the FWD. Eight tests were performed at three selected sites under extreme climatic conditions during the 6-month testing phase. Subgrade moisture and pavement temperature profiles were measured using semi-permanently installed devices. Also, asphalt concrete and sand asphalt cores were collected for a number of laboratory tests, including rheology and indirect tensile tests. These were used to establish relationships between viscosity and temperature and used to predict the moduli of the bituminous mixtures. Other tests allowed the correlation between penetration and viscosity that can be used in moduli prediction equations when more exact methods are not performed.

The FWD data were analyzed to correctly assess the pavement layer moduli for both cracked and uncracked sections. Analyses were then performed to determine if the pavement stresses and strains produced by past loading conditions were high enough to initiate the failure that existed. Finally, scenarios for pavement rehabilitation were offered to help minimize the potential for further degradation of the airfield.

CHAPTER 2 REVIEW OF THE LITERATURE

2.1 Introduction

The ability to structurally characterize pavement systems using nondestructive testing (NDT) and predict their performance has intrigued the pavement engineer for many years. Often, the engineer is left with the task of selecting the correct pavement parameters such as modulus, Poisson's ratio, and thickness for input into a mechanistic (analytical) computer program, then go on to predict the expected life of the pavement system. The approach is further complicated by the task of defining failure, investigating the various modes and mechanisms for it, and correlating it with assumedly correct NDT measurements. The airfield offers even more elusive data for the engineer to obtain, especially traffic volume information accounting for aircraft wander, wheel gear configuration, and taxiway usage. Considering this, the literature review will help to serve two purposes,

- 1) to discuss current airfield design methodology along with the uses of NDT and conventional analytical procedures as it relates to the performance of asphalt concrete pavements, and
- 2) to define concepts, modes, and mechanisms for failure in asphalt concrete pavements which are used to predict flexible pavement response and performance.

2.2 Design and Performance of Asphalt Concrete Airfield Pavements

2.2.1 Background

Design procedures for conventional flexible and rigid airfield pavements, developed from data gathered over forty years of accelerated traffic testing, have served the airfield requirements well in the past. However, in the 1960s the engineering profession began to consider design concepts that departed from conventional design approaches that were widely used (4). As experience was gained with new approaches, the potential for cost savings in the life-cycle design of pavements became obvious, particularly in a predictive-type design system which considered new usages and maintenance strategies. What became apparent was that empirical design methodology would not relate to stress analyses, deflection analyses, or performance predictions.

Design procedures available today handle two modes of structural deterioration either by limiting values of certain parameters or by accounting for cumulative damage according to Miner's hypothesis. This treatment implies the prediction of pavement performance on having a value of "nonfailed" or "failed." In other words, failure occurs once a limiting strain value is exceeded. For the design and evaluation of pavement systems, these criteria are used extensively by pavement engineers, including those in the USAF. Unfortunately, this methodology does not realistically predict deterioration of pavements in the field.

For the design system, two types of strain are considered: 1) horizontal tensile strain at the bottom of the asphalt layer and/or stabilized layer and 2) vertical strain at the top of the subgrade. To fully understand the design rationale for asphalt pavement systems, one

must first look closely at the development of the strain criteria for the asphalt and subgrade layers.

2.2.2 Horizontal Strain Criteria in the Asphalt Layer

Under traditional design approaches, failure in the asphalt layer occurs when a specific number of load repetitions results in enough cumulative strain (allowable strain) to equal the computed strain for one load repetition. This allowable strain will vary depending on the number of anticipated load repetitions and the elastic modulus of the asphalt layer (5). According to Himeno et al. (6), this cumulative damage (fatigue) is a function of the wheel load, vehicle speed, transverse wheel position, and the temperature gradient in the asphalt pavement layer.

The performance criteria for horizontal tensile strain are based on the total number of strain repetitions which are determined from a repetitive load, flexural beam test. The procedures for such tests are described by Deacon and Monismith (7). These tests are conducted for each temperature condition, therefore a value of limiting horizontal tensile strain can be determined for the pavement design life. Barker and Brabston (4) stated that researchers generally recognize that the fatigue strength of bituminous materials is highly dependent not only on the type of mix, but on temperature, stress history, and mode of testing. A few researchers, including Ruth and Davis (8), contend that increasing temperature is the greatest factor in relieving accumulated stresses in the asphalt layer through increased flow. This flow can partially or completely negate the cumulative fatigue damage.

2.2.3 Vertical Strain at the Top of the Subgrade

Gerritsen et al. (9) reported that most subgrade soils are not linear elastic materials. They added, however, that their behavior can reasonably be predicted by a linear elastic representation, provided the elastic modulus is determined under conditions similar to those prevailing in the pavement structure. Ruth (personal communication 1987) thought that under dynamic loading conditions, a linear elastic assumption for the subgrade is appropriate provided the pavement structure is relatively stiff. However, since dynamic measurements of the subgrade are not often available, the Shell Pavement Design Manual suggests the use of the California Bearing Ratio (CBR). It cautions that deviations using this method can be as high as a factor of two. However, since the design and analysis of flexible pavements depend on properly predicting strain at the subgrade surface, careful assessment of the subgrade modulus must be made.

Environmental effects can play a significant role in altering strain predictions in the subgrade. In asphalt concrete pavements, where the bituminous layer is of moderate thickness, a temperature change can alter the vertical stress transferred to the subgrade. Lambe and Whitman (10) offered the opinion that the elastic modulus in soil is stress dependent and decreases with increasing vertical stress. The resilient modulus is also very sensitive to changes in moisture conditions. Monismith and Finn (11) reported that the presence of water in the pavement system is one of the most important environmental factors to consider, because it affects the response of the pavement to load. Hicks (12) showed that increased saturation lead to reduced resilient moduli values for granular materials. This could result in higher

pavement deflections and associated distress. Darter et al. (13) listed the more common types of distress from increased pavement deflections as distortion, corrugation, rutting, depression, and potholes.

A suitable method for characterizing subgrade materials in the laboratory, according to Seed and Fead (14), is the resilient modulus test using the standard triaxial device. Recently, however, McVay and Taesiri (15) reported that conventional triaxial testing was incapable of reproducing the moving wheel stress path demonstrated in the laboratory by Ishihara (16) using a hollow cylinder. Unlike the standard triaxial device, the hollow cylinder is able to continuously rotate the principal stress planes, and in effect, simulate the stress path produced by the moving wheel in the field. Ishihara showed that under drained conditions (typical for low-volume airfield pavements), axial strains produced in the hollow cylinder were 25 percent greater than measured in the standard triaxial device after only three cycles under similar stresses. Although both studies suggested further investigation into this phenomenon, its relative importance in pavement design today is still undecided.

The subgrade strain criteria were developed based on data from conventionally designed pavement sections for which a performance life could be assumed. Peattie (17) presented strain criteria based on stress. His criteria are for 1,000,000 strain repetitions and are a function of CBR. Edwards and Valkering (18) using the Shell CBR design curves for 1,000,000 strain repetitions, arrived at a subgrade strain criteria between 0.8×10^{-3} and 0.9×10^{-3} in./in. but gave no reason for this. Witczak (19) developed subgrade strain criteria based on assumed values of asphalt concrete moduli. All the comparisons made by Barker

and Brabston (4) indicated that for a given resilient strain, the specimens of a weaker soil exhibited larger permanent strain than those of a stronger soil. They concluded that the allowable resilient strain for a weaker soil would have to be less than that for a stronger soil if the amount of permanent strain is to be equal.

2.3 Nondestructive Testing (NDT) and Conventional Analysis Procedures

2.3.1 Description of NDT Equipment

Smith and Lytton (20) gave four general classes of NDT equipment that are routinely used to collect deflection data: static deflection equipment, automated beam equipment, steady-state dynamic deflection equipment, and impulse deflection equipment.

Static load devices measure the response of a pavement to slowly applied loads. The most routinely used of this type of device is the Benkelman beam. This device requires a loaded truck to create the deflection basin to be measured. Normally, only the maximum deflection is measured with beams. Technical difficulties in using this device include 1) ensuring the front supports are kept out of the deflection basin and 2) the inability to accurately define the basin itself.

The automated beam deflection equipment simply automates the Benkelman beam. This device called the La Croix Deflectograph has been widely used in Europe and other parts of the world but has not been used much in the U.S. Although it allows for continuous recordings of data, it still has the same inherent limitations of the Benkelman beam.

Devices that produce a sinusoidal vibration are classified as steady-state dynamic deflection equipment. These devices, including the Dynaflect and the Road Rater, place a static load on the pavement along

with a sinusoidal vibratory force produced by a dynamic force generator. Velocity transducers are positioned on the pavement surface and measure the deflections. A static preload is applied to prevent bouncing on the pavement. However, this preload must increase as the dynamic force increases. Some researchers feel that this preload changes the existing stress state in the pavement and may cause altered response to the load (21). Given this, an inertial reference is used to compare the deflection change with the change in the magnitude of the dynamic force.

The last category of NDT equipment are the impulse deflection devices. These devices deliver a transient force impulse to the pavement surface which produces a dynamic deflection basin. The equipment uses a weight that is raised and dropped from a predetermined height, striking the impact plate which transmits the force directly to the pavement surface. The advantage of using this type of NDT device is that the drop height and weight can be easily changed to vary the generated force impulse. In this way, loadings can be obtained for a wide range of actual field loading conditions. Also, the static preload is relatively small, so the deflection basin produced most closely approximates the deflections produced by a moving wheel. The most widely used impulse device is the Falling Weight Deflectometer (FWD). The Air Force has adopted the FWD as its primary source for nondestructive testing.

Nazarian and Stokoe (22) cited the fundamental advantage of steady-state devices over impulse devices is the ability of the former to vary the loading frequency to minimize the effect of rebounding shock waves caused by a rigid layer at shallow depth below the subgrade. This

critical depth is a function of the natural frequency of the pavement layers, especially that of the subgrade. Although Nazarian confessed that encountering such conditions in practice is rare, he admitted that users of steady-state equipment do not adjust the frequency to account for this phenomenon. Furthermore, impulse devices can not be adjusted for the effects of reflecting waves, and if not considered in the final analysis, large errors in deflection measurements may result.

2.3.2 Use of the Falling Weight Deflectometer (FWD) and Conventional Analysis Procedures

The FWD was developed and employed based on early work conducted in the 1960's by the Technical University of Denmark and the National Danish Road Laboratory (23). The FWD was designed to simulate a heavy moving wheel load at normal traffic speed while obtaining very accurate deflection measurements at large distances from the load. According to Sorensen and Hayven (24), proper assessment of the subgrade modulus is vital since it contributes some 60 to 80 percent of the center deflection. A study by Uddin et al. (25) determined that the theoretical deflection basin was most influenced by even a small change in subgrade modulus and changes in the surface asphalt layer thickness. Moreover, deflection basins were less influenced by changes in assumed moduli of thin asphalt layers and changes in thickness of the intermediate layers.

Marchionna et al. (26) stated that the FWD can be used to estimate bearing capacity of pavement systems and evaluate remaining pavement life in terms of fatigue distress using computed moduli. In a study to determine the structural properties of flexible pavements through the use of NDT, Lytton et al. (27) ranked the FWD above other NDT devices when comparing such factors as reliability, accuracy, and accessibility to test sites, speed of operation, and cost.

The quick, accurate calculation of the insitu moduli is the goal of the FWD and accompanying layered elastic programs. Uddin et al. (28) reported that the inverse application of layered theory by fitting a measured deflection basin using an iterative procedure is the most promising for predicting insitu moduli. During the past few years a number of self-iterative approaches have been made available to handle flexible pavement systems. Typical layered elastic programs are shown in Table 2.1.

The two self-iterative programs used primarily by the U.S. Air Force for flexible pavements are BISDEF (also for rigid) and FPEDD1. BISDEF is a layered linear elastic program developed by the COE. The subroutine BISAR (Bitumen Structures Analysis in Roads) was developed by Shell in 1972. FPEDD1 (Flexible Pavement Evaluation from Dynamic Deflections) was developed by layered program ELSYM5. BISDEF was developed for use on a microcomputer for quick calculations in the field. FPEDD1 requires a main frame computer for downloading to a personal computer.

The use of elastic layer analysis for the prediction of stresses, strains, and deformations in the asphalt concrete layer is generally accepted. However, there is concern about how well it predicts response in unbound layers, although its suitability for bound layers is well documented. Ros et al. (29) measured insitu the stresses and strains at various locations in trial sections using standard wheel loads at different speeds and temperatures. They found good correlation between the values measured in the field and those calculated using BISAR. Correlation was especially good at high asphalt stiffness. Halim et al. (30) and Waterhouse (31) also achieved good agreement using elastic layer

Table 2.1 Typical Layered Elastic Methods of Matching Deflection Basins

Program Name	Number of Layers	Starting Moduli User Input or Automatic	Elastic Layered Program	Nonlinear Stress Effects	Microcomputer or Mainframe
EMOD	2	Auto	N/A	No	Main
CHEVDEF	4	User	CHEVRON BISAR	No	Micro/Main
MODCOMP	5	User	CHEVRON	No	Micro
FPEDDI	5	Auto	ELSYM5	No	Main
IMD	4	User	CHEVRON	No	Main
ISDEM	4	User	ISSEM4	No	Main
OAF	4	User	ELSYM5	Yes	Main
FPOD	4	User	ELSYM5	Yes	Main
BISDEF	4	Use/Auto	BISAR	No	Micro/Main

Source: Lytton et al. (27)

theory. However, Brown and Pappin (32) questioned the ability of elastic layer theory to predict response in the soil layers, although they found it appropriate for the asphalt layer.

There are other methods for determining insitu moduli from NDT data. Lytton et al. (27) listed them categorically as 1) equivalent thickness methods, 2) finite element methods, 3) dynamic analysis methods, and 4) wave propagation methods. Ruth et al. (33) developed a series of algorithms using measured FWD deflections to determine the insitu moduli in the pavement system. Their study revealed that for narrow ranges of asphalt thickness, good prediction of the asphalt concrete modulus was achieved. Moduli predictions for the base and subbase were slightly better with the greatest consistency coming from predicting the subgrade modulus. They recommended verifying these moduli predictions with an other form of analysis, or through laboratory resilient modulus testing, or the use of asphalt viscosity-modulus relationships.

2.3.3 Performance Predictions Using AIRPAVE

The AIRPAVE program was developed by the Army Corps of Engineers (COE) for evaluating military airfield pavements. The program uses the resilient moduli, layer thicknesses, and Poisson's ratios to calculate the stresses and strains produced in the pavement system due to a selected aircraft wheel load (5). AIRPAVE makes use of the linear, elastic layer program BISAR to calculate stresses and strains at critical locations in the pavement structure (34). Calculated stresses and strains are compared with fatigue algorithms developed from laboratory and field test data and empirically correlated to predict the number of

cycles to failure. Information on aircraft load, wheel gear configuration, and passes-to-coverage ratios for seventeen aircraft types are stored in an AIRPAVE data file called ACDATA.

The program calculates the horizontal tensile strain at the bottom of the first layer. Therefore, multiple asphalt concrete layers must be combined into a single thickness. Vertical stresses and strains are normally calculated at the top of the subgrade, although AIRPAVE does give some flexibility in computing the vertical stresses and strains at other locations.

2.4 Causes and Effects for Failure in Flexible Pavement Systems

2.4.1 General

The types of distress seen in asphalt pavement is highly recognized and the causes behind them are at least generally understood. Table 2.2 lists the types and causes of distress common to bituminous pavements. Failure in these systems can be primarily attributed to either cracking, excessive rutting, or a combination of both.

Through the use of numerous pavement surveys taken in this country and around the world, Finn (35) stated that load related cracking is the number one priority item for improving and extending the performance of asphalt pavement systems. Furthermore, he reported that load-induced cracking is one of the first observable signs of distress and that excessive cracking could occur with little or no distortion. When reviewing the results of the AASHTO Road Test, he found cracking often led to other forms of distress such as rutting, and that it appeared to be more pronounced during cold weather than warm. Information as to when and where these cracks developed was lacking and only recently have

Table 2.2 Primary Types and Causes of Surface Distress in Asphalt Concrete Pavements

Type of Distress	Causes or Factors
1. Rutting	Consolidation Lateral movement (shear) Traffic High temperatures Low viscosity Low stability Poor compaction Foundation quality Drainage
2. Fatigue Cracking (Load-Induced)	Traffic--volume and loads Asphalt viscosity Layer moduli Layer thickness Drainage Material quality
3. Thermal Cracking	Binder shrinkage Thermal contraction Low temperatures Asphalt hardening Fast cooling rates
4. Combined Load and Thermal Cracking	Combination of factors named in 2 and 3 above
5. Raveling and Weathering	Deterioration Asphalt hardening Time
6. Disintegration	Stripping--loss of bond Chemical reactivity Traffic abrasion

Source: Ruth et al. (36)

full scale modeling been done to better understand the response of asphalt pavement at low temperature and its relationship with cracking (36).

2.4.2 Cracking in Asphalt Concrete Pavement

Traditionally, cracking in flexible pavements is thought to stem from load or thermal effects with little regard for the combined effects of the two. Anderson et al. (37) reported that low-temperature transverse cracking has been recognized as the most common nontraffic associated failure mode and is a serious problem in Canada and parts of the United States. Hugo and Kennedy (38) emphasized that the design of asphalt pavements must consider the distress due to cracking from both load and nonload associated factors or a combination of the two.

The most recognized concept for use in the evaluation of load-induced failure, is cracking in asphalt concrete due to fatigue distress (39,40). Fatigue failure in asphalt pavements is the result of repeated stresses below the tensile strength of the material. There are many references, such as Witczak (41) and Barksdale (42), on the subject of fatigue in asphalt concrete. The Air Force criterion for cracking is based on limiting stress/strain conditions that are calculated by AIRPAVE. The allowable tensile strain at the bottom of the asphalt concrete layer is given by equation 2.1 and is dependent upon the asphalt modulus and the number of aircraft coverages (5).

$$\text{Allowable Strain}_{AC} = 10^{-A} \quad (2.1)$$

where

$$A = \frac{N + 2.665 \log \left(\frac{E_{AC}}{14.22} \right) + 0.392}{5}$$

$$N = \log (\text{aircraft coverages})$$

$$E_{AC} = \text{asphalt modulus}$$

Since the fatigue life of asphalt concrete has been shown experimentally to be dependent on temperature, researchers have proposed modifications to fatigue life predictions taking into account seasonal temperature variations. Rauhut and Kennedy (43) proposed such adjustments and offered those given by others. They did, however, recognize the difficulty in evaluating fatigue life of actual pavements in the field, since reliable test data existed for only a limited number of asphalt concrete mixtures. Furthermore, they pointed out that no fatigue test can accurately simulate the complex mechanisms at work in the field. Recently, Himeno et al. (6) offered a new fatigue failure criteria based on energy dissipation. They found that bending fatigue damage at the bottom of the mix slab is greatest in the spring and can be ignored in the summer and winter.

Ruth and Maxfield (44) found the fatigue concept did not apply to specimens from test roads in Florida. Their conclusion was that the fracture of asphalt concrete was related to the accumulation of creep strain and that fracture strain is dependent on asphalt viscosity and loading conditions. Ruth et al. (45) emphasized that during warm weather, temperatures are high enough to relieve stresses and strains, and thus offset the cumulative damage of fatigue. Nevertheless, they did not discount the concept of fatigue when asphalt pavements are subjected to repetitive short-term loads where their rheological properties remain fairly consistent. Asphalt binder viscosity and shrinkage were clearly demonstrated as major factors leading to cracking. Ruth et al. (46) reported that cracking will occur when a critical condition is imposed on the asphalt pavement. They described a critical condition as "any combination of materials, environmental, and loading

characteristics which produce stresses or strains equivalent to those required for fracture" (46:53). Specific factors responsible for fracture include excessive binder hardening and rapid cooling to sufficiently low temperatures relative to the asphalt viscosity.

Resistance to thermal contraction during rapid cooling is the mechanism causing high tensile stresses to develop in the asphalt layer. Simply, as the temperature decreases, the asphalt wants to contract but is resisted by the friction developed between the asphalt layer and the base, and by the length of the pavement in the longitudinal direction. This results in tensile stresses which are greater in the longitudinal direction. During rapid cooling, these stresses build rapidly with little chance for thermal creep to relieve them. Several researchers (47,48,49) have postulated that cracking occurs when the thermally induced tensile stresses exceed the tensile strength of the asphalt concrete. This mechanism was confirmed by laboratory and field investigations by the above researchers.

Ruth (50) concluded that cracking could be reduced by using asphalt binders of lower viscosity and improved rheological behavior at low temperatures. Fabb (51) remarked that low viscosity and low temperature susceptibility are vital to reducing the temperature required for fracture. Ruth et al. (46) stated that temperature susceptibility per se is not a critical factor since apparent viscosities will change according to the creep strain rate that is induced by cooling the pavement at different rates. They added that low-temperature viscosity is critical since viscosity controls the creep rate and fracture characteristics of asphalt concrete. Schmidt (52) reported that the glass transition temperature of the asphalt is a more definitive measure of nonload

associated cracking behavior than measured viscosities since at that temperature the asphalt behaves elastically while higher temperatures result in viscoelastic response. Therefore, almost no potential for stress relaxation exists below the glass transition temperature.

To deal with the effects of thermally induced stresses and strains in the asphalt concrete, a computer program CRACK was developed by Ruth et al. (46). This program computes the thermal stress, incremental creep strains, and stress-strain energy developed at each time-temperature increment during cooling of the pavement. The thermal analysis was combined with the ELSYM5 stress analysis program to combine the effects of load and nonload induced stresses. A second program CRACK-2, developed by Hugo (53), permits the subdivision of the asphalt surface into two layers, each with their own low-temperature thermal characteristics.

Reflection cracking is another form of cracking that severely affects much of North America and is considered the number one pavement performance problem (54). Ponniah et al. (55) reported in a recent paper that reflection cracking is caused by thermal cycles and/or load induced stresses. Ignored, it can markedly decrease the structural performance of the pavement through deterioration caused by the ingress of water. They further added the importance of fracture mechanics in determining the design method which offers the best alternative for reducing stress concentrations around the crack front. Analyses can be used to evaluate the relative effectiveness of such treatments as geogrid reinforcement, stress absorbing membrane interlayers (SAMI), and composite interlayers.

Aside from the conventional forms of thermally induced cracking, lies the potential for thermal rippling or curling. In a recent study by Ruth et al. (36) on low-temperature pavement response using a test-pit facility, load-deflection data clearly indicated that the asphalt pavement layer was uplifted from the base during cooling cycles then settled as the temperature increased. They stated

it seems clear from these observations that the unusual response observed was caused by the contraction and bending characteristics of the asphalt concrete layer under a thermal gradient and continued cooling . . . however, the actual mechanism that led to this behavior was unclear.

(36:328)

Curling is a phenomenon normally associated with portland cement concrete slabs and not asphalt concrete pavements. However, at low temperatures, the stiffness of asphalt concrete is high enough that its behavior can approach that of concrete. The mechanism of curling in asphalt concrete may be different than that for portland cement concrete in that the former exhibits viscoelastic response (creep). This creep could develop from the stresses induced by the uplifted slab causing it to settle.

Ruth et al. (36) concluded that if this curling effect demonstrated in the test pit occurs in actual pavements, it could explain some failures and causes of longitudinal wheel path cracking. They emphasized the importance of combining the properties of the asphalt with the combined effects of thermal and load in the failure analysis of asphalt concrete pavements.

2.4.3 Rutting in Asphalt Concrete Pavement

Gerlack et al. (56) described rut formation as a result of permanent deformations of the individual pavement layers caused by progressive stiffening of the pavement elements due to traffic loading. Ruth (personal communication 1987) stated, however, that as the pavement stiffens through consolidation and age-hardening, the potential for further rutting is reduced. Furthermore, he cautioned that one must distinguish rutting caused by consolidation from that caused by plastic flow (low stability).

Work conducted by Freeme et al. (57) showed that permanent deformation tends to occur within the asphalt layer under traffic loads at a rate which depends predominately on the grading and properties of the binder. They added that high stability asphalt mixes will deform less than those with a low stability under the same loading and temperature conditions. Barker and Brabston (4) reported that rutting can also occur in the subgrade whereby little or none is assumed to occur in the asphalt layers. Monismith et al. (58) stated the propensity for rutting in thick pavement sections is dependent upon the stiffness and thickness of the asphalt concrete and the stiffness of the subgrade. Given two pavement systems with identical layer moduli and loading conditions, more rutting can be expected in a system with a thinner bituminous layer. This is due to the higher compressive stresses transferred into the foundation layers resulting in greater deformations.

The intricacies of rut prediction is complex; however, models do exist. Monismith et al. (58) offered a rut depth prediction model using creep moduli for each sublayer in the pavement system. With computed

vertical normal stresses and corresponding creep moduli, rut depths can be estimated using the following relationship:

$$\text{rut depth} = \sum_{i=1}^n \frac{\sigma_i}{E_{ci}} h_i \quad (2.2)$$

where

h_i = thickness of sublayer

σ_i = average vertical stress in layer

E_{ci} = creep modulus for average temperature in sublayer

Barber (59) gave the following expression for a two layer flexible pavement system with an asphalt wearing course over a granular base:

$$\text{rut depth} = 1.9431 \left\{ \frac{P_k^{1.3127} \times t_p^{0.0499} \times R^{0.3249}}{[\log (1.25 T_{ac} + T_{base})]^{3.4202} \times C_1^{1.6877} \times C_2^{0.1156}} \right\} \quad (2.3)$$

$$\text{std error} = 0.411$$

$$r = 0.8779$$

where

P_k = equivalent single wheel load (ESWL), kips

t_p = tire pressure, psi

T_{ac} = thickness of ac, in.

T_{base} = thickness of base, in.

C_1 = CBR on top of base

C_2 = CBR on top of subgrade

R = repetition of load or passes

Barker (60) presented the following prediction based on the ratio of permanent strain to resilient strain in the subgrade:

$$\epsilon_p/\epsilon_r = 0.14 \times \frac{70,800^R}{M_r} \quad (2.4)$$

where

$$R = 0.4 \text{ (stress repetitions)}^{0.12}$$

$$M_r = \frac{\sigma_d}{\epsilon_r}, \text{ ksi}$$

σ_d = repeated deviator stress in laboratory triaxial test, ksi

ϵ_r = measured resilient strain in laboratory triaxial test,
in./in.

ϵ_p = measured permanent strain in laboratory triaxial device,
in./in.

This model assumes all rutting occurs in the subgrade.

Monismith et al. (58) stated that to estimate rutting in taxiway sections on airfields, aircraft wander (passes-per-coverage) must be considered. Accordingly, these procedures were developed by the COE.

2.5 Rheological Properties of Asphalt Cement and Asphalt Mixtures as Related to Pavement Performance

Rheology involves the study and evaluation of the time-temperature dependent response (flow) of materials which are subjected to an applied force. The rheological properties of bituminous mixtures can be altered by either time, applied stress, or temperature. Moreover, this alteration can be quite complex and even today is not fully understood. The performance of asphalt concrete is greatly dependent on the properties of asphalt binder itself. Unfortunately, conventional asphalt mix design is based on empirical approaches as the Marshall and Hveem mix design methods (39). Such methods do not account for asphalt properties

as failure stress, failure strain, temperature and shear susceptibility, and stiffness. Conventional asphalt viscosity tests (e.g., absolute and kinematic) are run at high temperatures and are not able to predict the low-temperature behavior of asphalt cements.

2.5.1 Asphalt Cement Properties

Schweyer (61) stated that in general as the temperature is decreased, asphalt becomes more viscous and will eventually exhibit glassiness where elastoviscous behavior is seen. Brittle fracture may result from its inability to flow and relieve built-up stresses. Jongepier and Kuilman (62) characterized asphalt as a viscoelastic liquid. At low temperatures elastic behavior is observed, while at high temperatures it flows like a viscous fluid. In the intermediate temperature ranges, asphalt exhibits both elastic and viscous properties. By using combinations of Hookean springs (elastic component) and Newtonian dashpots (viscous component) it is possible to mathematically represent the behavior of asphalt. The models, Maxwell, Kelvin, Van der Poel, Burgers, and Kuhn and Rigden are among those kinds used to represent the stress-strain-time relationship of asphalt. Burns and Schweyer take the Kuhn and Rigden model one step further by accounting for the shear susceptibility of the material. Full description and capabilities of each model, along with their inherent limitations, are given by Teng (63).

Duthie (64) described the rheological parameters of asphalt as its viscosity, temperature susceptibility, and shear susceptibility. Viscosity or consistency is simply defined as the applied shear stress over the shear rate. Temperature susceptibility is the degree of the change in viscosity with change in temperature. At low temperatures, asphalts may become more shear susceptible, i.e., the change in creep strain is

not proportional to the change in applied stress. This inability to creep can result in the accumulation of stresses which can ultimately lead to failure through cracking.

Measurement of the above mentioned parameters at low temperature can be difficult since asphalt behaves elastically with relatively low creep rates. Therefore standard creep or viscosity tests would take an extremely long time to obtain appreciable deformation at low stress levels. High stress levels are required to achieve the desired deformation, but shear susceptible asphalts may give results outside the range of interest.

Schweyer et al. (65) reported that different asphalts having nearly the same high temperature properties behaved quite differently at low temperatures. They emphasized that absolute viscosity tests rather than empirical tests should be used near the glass transition zone. This understanding among researchers led to the development of the Schweyer Constant Stress Rheometer (66). Keyser and Ruth (67) concluded that the Schweyer rheometer is an excellent device for the low-temperature (e.g., -10 C (14 F) and lower) measurement of asphalt properties, especially those that are highly shear susceptible. Furthermore, they added that the concepts developed by Schweyer provided values of shear and strain rates encountered in the laboratory, applicable to those measured in the field.

2.5.2 Asphalt Mixture Properties

A number of laboratory tests exist to characterize asphalt mixtures including compression, bending (flexure), tensile, and shear. Tests are normally conducted to obtain the failure characteristics. However, the increasing trend toward mechanistic approaches and the use of elastic

theory, has led researchers to define the stress-strain behavior of bituminous mixtures (68). A study by the Highway Research Board (69) showed that it is very difficult to uniquely characterize the stress-strain properties of asphalt mixtures. This is due to the variability of materials and the nature of pavement structures. A distinct disadvantage in conducting the aforementioned tests is the effect of time or rate of loading which are disregarded by elastic equations used in analyzing the data. Creep effects are normally ignored due to the complexities involved by introducing them into the analysis. Many researchers including Gonzalez et al. (70), Kennedy (71), and Puyana (72) have recommended the indirect tensile test as the most suitable for routine pavement characteristics in terms of practicality, simulation of actual loading conditions, economy, and ease of testing. Mamlouk (73) emphasized the importance of dynamic testing to most realistically simulate the actual stress conditions of pavements. He cited that the magnitude, shape, and duration of moving wheel stress pulses can only be accounted for in dynamic testing.

Deacon (74) stated that four variables have a considerable effect on the stiffness of asphalt paving mixtures: air void content, asphalt content, viscosity, and filler content. Temperature, and its effect on asphalt viscosity, was considered the major external factor on stiffness and mixture behavior. Deacon also reported that linear response increased with increasing load frequency, decreasing temperature and air void content, and increasing asphalt content, asphalt viscosity, or filler content.

Bazin and Saunier (75) studied the variation in modulus for different asphalt mixtures. They reported that for correct binder amounts and

normal air void contents, (e.g., 4 to 8 percent), the other parameters had little effect on stiffness when compared to the effects of variation in binder type, temperature, and time of loading. They suggested a linear relationship between the log of modulus and air void content. Ruth et al. (76) gave a modulus ratio for air void contents to 9 percent. They suggested a 11.5 percent decrease in dynamic modulus for every 1 percent increase in air void content up to 9 percent.

Ruth et al. (46) were the first to present modulus relationships based on direct evaluation of measured asphalt viscosity at different temperatures. The dynamic modulus equations were developed for dense-graded mixtures given a loading duration of 0.1 seconds. Required for computation is the asphalt viscosity obtained for a particular temperature as measured in the Schweyer rheometer.

Limited work has been done to define the failure limits of asphalt concrete mixtures in terms of stresses and strains. Ruth et al. (77) stated that as temperature decreases, the failure stress increases but remains constant below some transition temperature dependent on asphalt properties. Finn (78) reported asphalt tensile strengths ranging from 290 to 580 psi for fast loading rates. Ruth and Olson (79) reported failure stresses consistently between 380 and 440 psi and chose a value of 400 psi as typical. They also demonstrated that as temperature decreases, the strain at failure also decreases. Pavlovich and Goetz (80) determined from direct tension tests that temperature is the most significant factor affecting limiting strains. Strain rate has some effect but not as much as temperature. Ruth and Maxfield (44) reported that failure strain is primarily a function of viscosity. It was shown by Ruth et al. (46) that energy required for fracture decreased as the

viscosity increased and that fracture energy may be the best measure for predicting failure response in asphalt mixtures.

From the above studies, it is well documented that as the asphalt binder hardens, the tolerance for strain decreases. As a result, brittle failure of the asphalt concrete becomes more likely. Binder hardening can be both instantaneous, due to changes in temperature, and time dependent. Page et al. (81) blamed the premature hardening of asphalt binders on plant hot-mix operations and in-service aging. Kumar and Goetz (82) stated that the most important factor associated with binder hardening is the oxidation of the asphalt throughout the entire pavement thickness. Hardening at the surface is generally greater due to ultraviolet radiation and higher temperatures experienced.

It is important to point out that the type of asphalt binder plays a big part in the hardening of bituminous mixes. Some asphalts subjected to the same exposure conditions are less susceptible to hardening than others. The reasons for this are not well known. Currently, research is being conducted at the University of Florida to specifically address the issues associated with the hardening of asphalt with respect to its chemical identity. The study proposes the use of infrared spectroscopy to determine the susceptibility of the asphalt to further oxidation under plant mixing and in-service environments (83).

Since hardening of the asphalt increases its viscosity, the energy required for fracture is reduced. Page et al. (81) further reported that when the asphalt binder attains a critical degree of hardness for a specified structural support system, the stress and strains imposed by traffic loadings can exceed the tolerance of the asphalt concrete. This will result in fracture of the material and the development of pavement

cracking. During rapid thermal cooling, the critical temperature required for cracking increases as the viscosity increases (46). This critical temperature can become even higher as the asphalt continues to harden, causing cracking earlier than expected in the life of the pavement. Huffman (84) stated that softer asphalts delayed cracking, and cracking became evident when the viscosity at 25 C (77 F) exceeded 5 megapoises (Mp). Potts et al. (85) found viscosities in excess of 10 Mp resulted in pavement cracking and poor performance. They also showed that in-service air void contents in excess of 4 percent generally were associated with poor pavements. Page et al. (81) concluded that although the effects of age and air void content on binder hardening are not clearly distinguishable, the recovered asphalt viscosity usually indicated harder asphalt for higher air void content samples.

CHAPTER 3 AIRFIELD DESCRIPTION AND FIELD TESTING

3.1 Introduction

A flexible airfield pavement subjected to a wide range of environmental and loading conditions was desired for this study. After discussing this matter with officials at the Air Force Engineering and Services Center (AFESC), Duke Field (Eglin AFB Auxiliary Field 3) became the prominent choice. Specifically, Duke Field was selected for the following reasons:

- 1) its proximity to the University of Florida (five hours by car) would make necessary monthly trips both geographically and economically feasible,
- 2) its close proximity to AFESC (ninety minutes) would allow for the lending of needed equipment (e.g., FWD) and technical personnel,
- 3) accessibility to the airfield, especially during the day, was virtually unlimited,
- 4) the entire airfield, excluding parking aprons, was comprised of asphalt wearing courses and offered a vast selection of sites for study, and
- 5) a wide range of pavement temperatures are experienced.

Another key consideration was that the research was to begin at the same time the AFESC was scheduled to perform its periodic airfield inspection

of Duke Field. This enabled the team to evaluate the FWD data first hand before choosing testing locations for study.

3.2 Airfield Description

3.2.1 Topography and Climatology

Duke Field, located in Crestview, Florida, is some 14 miles north of Eglin AFB, 23 miles north of the Gulf of Mexico, and 6 miles south of Interstate 10 just off U.S. 85 (Figure 3.1). Land areas surrounding the airfield consist primarily of well-draining sands and sandy loams. The terrain is undulating in most directions with the elevation on the airfield being approximately 85 ft.

Climatic data have been recorded since 1939 (86). Annual temperatures range from a mean daily maximum of 90 F in August to a mean daily minimum of 42 F in January. The summer months average forty-one days above 90 F with a recorded high of 106 F, while the winter months average seventeen days below 32 F with a recorded low of 6 F. During this study ambient air temperatures ranged from a low of 26 F in January to a high of 91 F in July. Pavement surface temperatures during this period ranged between 30 and 130 F.

Annual rainfall amounts average 62 in. per year with September being the wettest (7.3 in.) and October the driest (3.3 in.). Thunderstorms are a common occurrence in the area averaging twelve per month from May to September. The airfield itself retains little surface moisture after heavy rains due to adequate surface runoff, well-draining soils, and infiltration through cracks in the pavement.



Figure 3.1 State Map of Florida Showing Location of Duke Field

3.2.2 Test Locations and Layout

Three sites were chosen to test, analyze, and correlate data to properly characterize the pavement conditions at Duke Field. As mentioned previously, the initial research effort ran concurrently with the periodic evaluation of the airfield by the Pavement Evaluation Team (PET) from the AFESC. The three sites were selected for monthly evaluations after analyzing the FWD data obtained by the PET for the entire airfield. Sites were chosen on taxiways instead of runways because of easier access and known loading conditions. Figure 3.2 shows the location of each site with respect to the entire airfield. Site 1 is located at the north end of the parallel taxiway, site 2 at the south end, and site 3 is located on the third ladder taxiway. The basis for selection were 1) a uniform FWD test response over a sufficient segment of taxiway and 2) varying degrees of surface distress present between sites. These locations were chosen during ideal testing conditions, i.e., overcast skies, and air temperatures around 55 F.

The horizontal layout of the test grid was basically similar for each site. Eleven longitudinal stations (10 ft. spacing) and six transverse stations (6 to 8 ft. spacing) were marked off at each site. The longitudinal stations were offset between 6 and 7 ft. from the taxiway centerline. This approximated the wheel path for the main landing gear of the C-130 aircraft. Data obtained from the wheel path could then be compared with those taken from the transverse stations outside the loading area. Figure 3.3 depicts the location and spacing of the FWD test stations, cores, and environmental instrumentation at each test site.

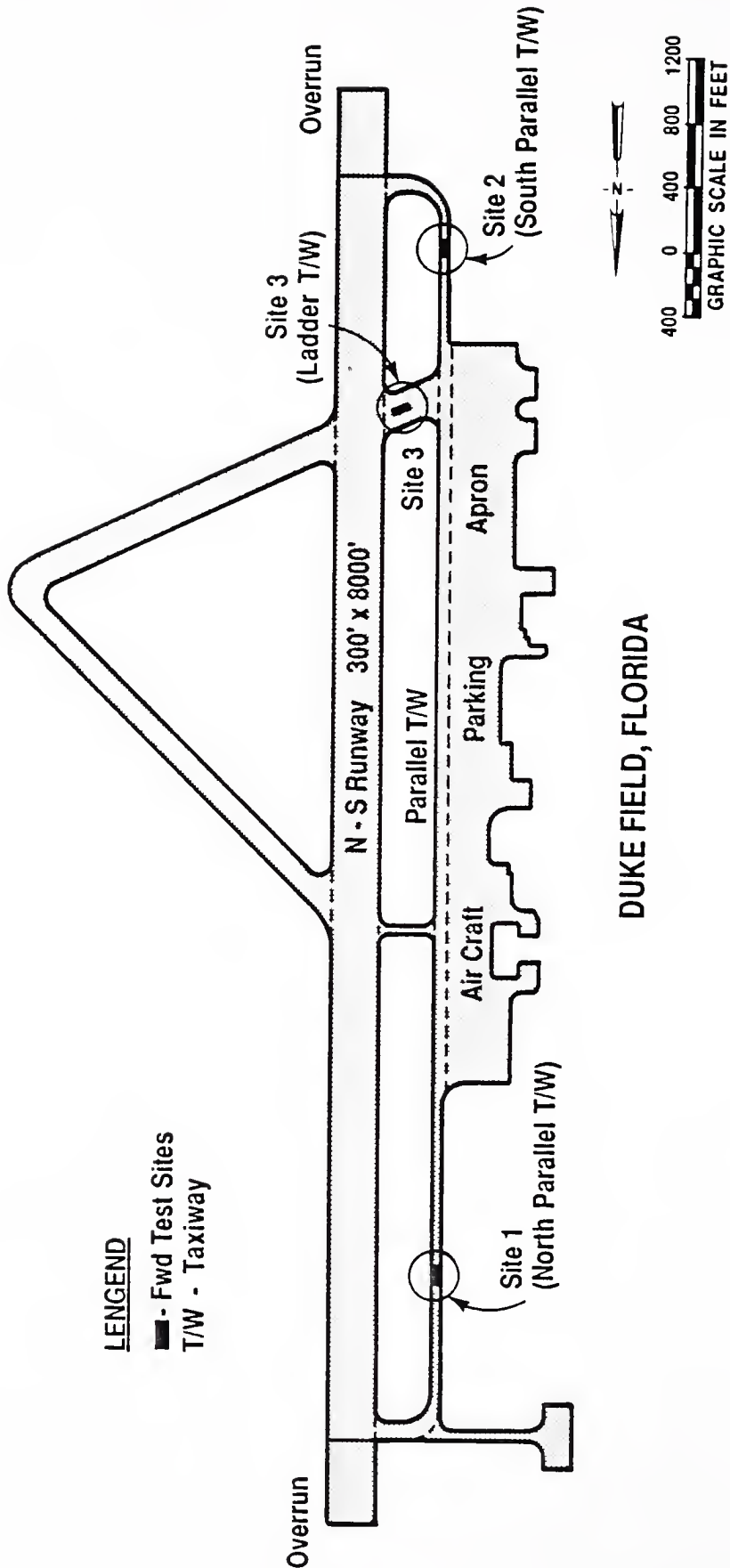


Figure 3.2 Plan View of Duke Field Showing Locations of the Three Test Sites

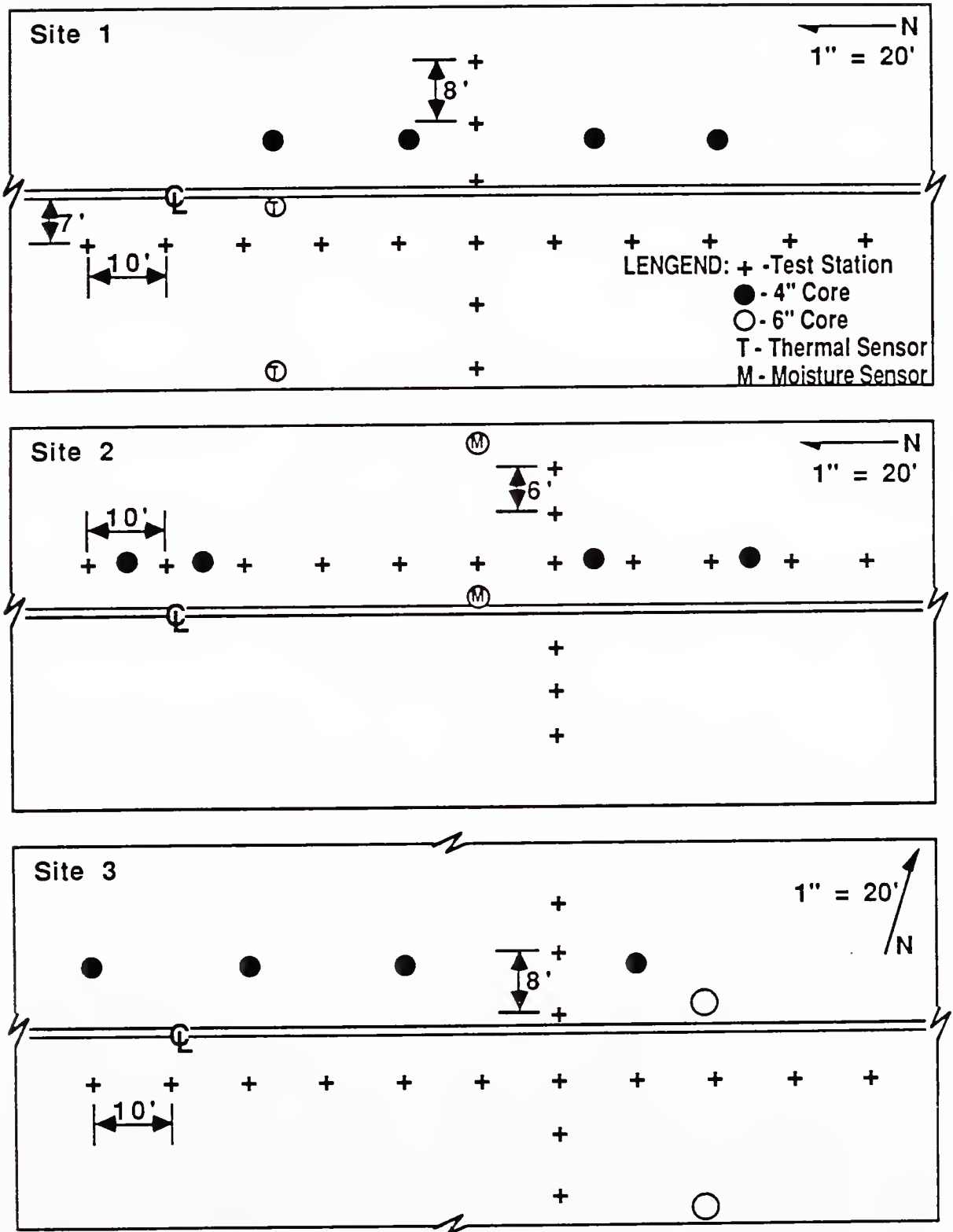


Figure 3.3 Detail of Test Sites

Special test stations were designated within each site to evaluate the uncracked characteristics of the pavement. A primary concern was to choose a station or stations that yielded results free of cracking influence. However, site 1 had such a high crack density that it was impossible to isolate an uncracked section within the site.

One reason for selecting the sites was based on visible surface conditions. Site 1 showed extensive 4 to 5 ft. block cracking (Figure 3.4) which extended over the entire width of the pavement. Crack widths up to 1 in. were measured with some spalling evident. Block cracking of the asphalt concrete is caused mainly by shrinkage, and thermal contraction resulting from daily temperature cycling. It is not load-associated, although aircraft wheel loadings can increase its severity (87). Rutting up to 0.75 in. was measured at the center of the wheel path at site 1 classifying it as medium severity (> 0.5 - 1 in.) by Federal Highway Administration standards. Ravelling has begun to occur and could present operational hazards in the near future if left unchecked. As of this report, no operational restrictions apply to this site.

Site 2 displayed moderate 10 to 15 ft. block cracking which traversed the entire width. Load-induced longitudinal cracking was obvious at this site and is shown in Figure 3.5. Rutting here was more pronounced measuring 1.5 in. at the wheel path center (Figure 3.6). Rutting exceeding 1 in. is classified high severity and is used to quantify failure in Air Force flexible pavements. The rut basin was more than 10 ft. wide which gave indication to excessive strains in deeper layers, perhaps the subgrade. The longitudinal crack at the edge of the wheel path was a direct result from this rutting. Crack widths



Figure 3.4 Site 1: Severe Block Cracking With Spalling



Figure 3.5 Site 2: Longitudinal Crack at Edge of Wheel Path



Figure 3.6 Site 2: Rutting in Wheel Path

at site 2 were up to 0.75 in. and were as wide at the edge of the pavement as they were near the wheel path.

From a visual standpoint, site 3 showed the least distress. This feature displayed 20 to 30 ft. transverse and longitudinal cracking with no evidence of rutting (Figure 3.7). Most of the stations were out of the immediate vicinity of cracking. However, cracking did extend the entire width of this 150 ft. wide ladder taxiway. A core taken in a cracked portion of the pavement revealed that cracking propagated the entire thickness (Figure 3.8). Crack widths at this site also measured up to 1 in. The lack of cracking and rutting at site 3 were initially explained by the increase in aircraft wander (higher pass-to-coverage ratios) and the decrease in aircraft weight after landing. Other explanations dealing with asphalt rheology and mix parameters are discussed in the next chapter.

One surface distress condition common to all three sites was the moderate degree of weathering present. This form of distress, exhibited by the wearing away of the binder material, leaves the surface rough and pitted. Normally, it is an indication of significant binder hardening (87).

3.2.3 Site Layer Profiles

All three sites had similar layer profiles with respect to material type but varied somewhat in layer thickness. Each site consisted of two or more asphalt concrete layers, a sand asphalt base, all overlying a uniform, well-draining sand subgrade. The profiles for typical sections both in and out of the wheel path are given in Table 3.1 for each site. Construction history is discussed in the next section.



Figure 3.7 Site 3: Longitudinal and Transverse Cracking



Figure 3.8 Site 3: Cracking Through Entire Pavement Thickness

Table 3.1 Site Layer Profiles In and Out of Wheel Path

Type Layer	No. Cores Taken In/Out	Site					
		1 (in.)		2 (in.)		3 (in.)	
		In	Out	In	Out	In	Out
AC surface course	4/1	2.0	1.6	1.6	1.5	1.7	1.5
AC	4/1	1.8	2.3	1.5	1.3	1.8	2.5
AC	3/1	NA		1.8	1.9	NA	
Total AC Thickness:		3.8	3.9	4.9	4.7	3.5	4.0
Sand Asphalt	4/1	7.5	7.8	6.4	6.5	8.0	9.5

Stratigraphy data were obtained from four 4-in. and two 6-in. core samples extracted from each site. Core locations within each feature are shown in Figure 3.3. At sites 1 and 2 there appears to be no significant decrease in layer thickness inside the wheel path as opposed to outside. This tends to indicate that rutting occurred primarily in the subgrade and was not due to additional consolidation or plastic flow in the bituminous layers. However, it is entirely feasible that the areas inside the wheel paths were built up with subsequent overlays where initial thicknesses were greater and where upon trafficking, densification occurred. This was verified through specific gravity tests where the densities in the asphalt concrete layers were generally higher in the wheel path. At least some rutting, therefore, can be attributed to additional consolidation of the flexible layers.

Extracted materials were taken back to the laboratory and subjected to a variety of tests to determine their physical properties. These tests will be discussed in detail in the next two chapters.

3.2.4 Construction History

The existing airfield is the product of several construction and repair projects (88). Initial construction was performed in 1941-42 by the U.S. Engineering Division (USED). The runways and taxiways were originally designed for capacity gross loads of 34 kips. Site 3 was the only evaluated feature built during initial construction and was once used as a NE/SW runway. Sites 1 and 2 were added in 1949 by the Army Corps of Engineers (COE). Since 1962, several overlay/rejuvenation projects have been accomplished by the USAF at all three sites. Table 3.2 gives the summary of the construction history pertaining to the three locations studied in this report.

Table 3.2 Construction History

Feature Description	Approximate Construction Period	Design Thickness (in.) and Type	Remarks
Site 1 North End Parallel Taxiway	1949	5.0 Sand Asphalt (SA)	Original Construction, COE
	1962	2.0 Asphalt Conc. (AC)	Surface Course, USAF
	1973	1.5 AC	Overlay, USAF
Site 2 South End Parallel Taxiway	1949	5.0 SA	Original Construction, COE
	1962	2.0 AC	Surface Course, USAF
	1973	1.5 AC	Overlay, USAF
	1974	1.5 AC	Overlay, USAF
Site 3 Ladder Taxiway	1942	5.0 SA	Original Construction, USED
	1962	2.0 AC	Surface Course, USAF
	1974	1.5 AC	Overlay, USAF

Source: USAF (86)

Detailed construction information is lacking for Duke Field. Therefore, reasonable assumptions must be made on the types and grades of asphalts used in construction in order to estimate the binder hardening characteristics.

3.2.5 Aircraft Traffic Data

During World War II, the traffic consisted mainly of 4,000- to 8,000-lb. aircraft averaging between 145 and 275 cycles per day (88). Since 1971, traffic primarily consisted of specially configured C-130 aircraft operated by the 919th Special Operations Group (SOG). Supporting the SOG was the main reason for the complete resurfacing of existing runways and taxiways between 1972 and 1974. According to officials at Duke Field, the increased weight of the C-130 caused extensive cracking to the pavement surface (only one asphalt concrete layer existed at that time) and prompted the overlay construction (89).

From available traffic information, the C-130 has averaged between 1,000 and 3,000 operations per year since 1971 accounting for 99 percent of the total generated traffic at Duke Field. Since 1979 there have been approximately 1,650 operations per year. Flying is normally done at night between 9 p.m. and 12 mid-night with missions generally lasting two to four hours. However, there is no data describing specific taxiway usage during this time period. From climatic data including wind roses, and from observations made over many years, approximately 80 percent of the traffic traverses down site 1 (north end) and takes off in a southerly direction on the active N/S runway. The same percentage of aircraft are also recovered on site 3. Rarely do the aircraft need the entire length of the runway to be recovered at the south end (site 2). Site 2 receives about 20 percent of the total launched and

recovered aircraft. Paradoxically, at least from initial observations, this feature exhibited the greatest amount of rutting. This will be examined more closely in subsequent chapters.

The number of passes of an aircraft over a pavement feature does not necessarily represent an equivalent number of coverages at a particular point on the pavement surface. To account for this wander, engineers have determined the number of passes required for one coverage in terms of pass-to-coverage ratios (P/C) for all aircraft types (5). The higher the P/C, the more wander taken by the design aircraft. Factors that effect the P/C are 1) aircraft type, 2) wheel gear configuration, 3) type of pavement system (rigid or flexible), and 4) pavement designation (primary or secondary usage).

Traffic volume information is given below in Table 3.3.

Table 3.3 Annual Traffic Volume at Duke Field

Site	Annual Traffic Cycles (passes)	Usage	P/C (C-130)	Annual Coverages
1	1,320	Primary	2.09	632
2	330	Primary	2.09	158
3	1,320	Secondary	4.05	326

It is important to point out that the P/C applies only to the asphalt layer, and more specifically, the pavement surface since one is dealing with aircraft coverages at a point. Failure in the subgrade is based on repetitions (passes) because of the effect of lateral distribution of loads in deeper layers. Simply, the wandering of aircraft will have less an influence on the stress distribution in the subgrade than it will at the asphalt surface.

Other factors affect the distribution of stress in flexible pavements. These include load, gear type and configuration, tire pressure, and tire contact area. Figure 3.9 depicts the wheel gear configuration for the C-130 aircraft, and Table 3.4 gives its physical characteristics (90). The design category and group index are used to classify like aircraft into specific design groups which are used for design and evaluation purposes. The C-130 sits alone in design group 4 as no other aircraft has its unique physical features. Figures 3.10 and 3.11 offer an indication as to the size and wheel gear arrangement for the C-130 type aircraft stationed at Duke Field.

3.3 Field Testing and Environmental Monitoring

3.3.1 Selection and Description of the Falling Weight Deflectometer (FWD)

The FWD is the nondestructive testing choice of the USAF. It was chosen for this study because of the AFESC's ability to support the research. The AFESC, along with the COE, provided the necessary equipment and technical services for the project. Initially, the Center was interested in performing a year-long evaluation to determine the effects of seasonal variations (e.g., temperature and moisture) on NDT results and associated pavement performance. Since this initial focus, the research has evolved into many distinct facets including laboratory as well as field testing. The intent was to determine the ability of the FWD deflection data to accurately predict layer moduli values in response to varying environmental and pavement distressed conditions. This being the case, the FWD was a good selection to carry out the investigation.

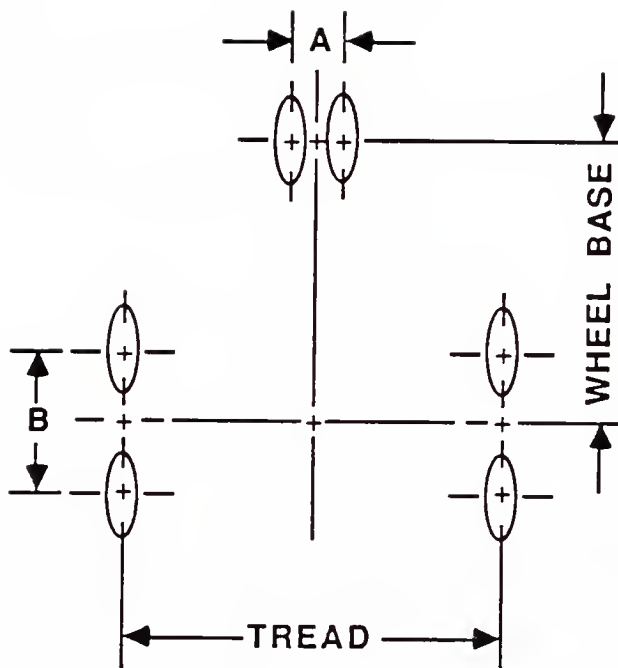


Figure 3.9 Wheel Gear Configuration for C-130 Aircraft

Table 3.4 Aircraft Characteristics for C-130

Characteristic	Description
Common Name	Hercules
Maximum Gross Weight (kips)	175
Design Category, AFM 86-2	4
Group Index, AFR 93-5	8
Maximum Single Wheel Load, Main Gear (kips)	41.9
Contact Pressure, Main Gear (psi)	105
Contact Area, Main Gear (in. ²)	400
Tire Width (in.)	17.6
Tread Width (in.)	172
Wheel Base (in.)	388
A (see Figure 3.9)	24 in.
B (see Figure 3.9)	60 in.

Source: USAF (90)



Figure 3.10 C-130 Aircraft: Front and Rear View



a) Side View



b) Front View

Figure 3.11 Main Landing Gear

The Dynatest 8000 FWD Test System chosen for this research simulates the effects of a moving aircraft single wheel load. The system is normally capable of applying loads up to 26,000 lbs. for a pulse duration between 25 and 30 msec (86). The test load allows for nonlinear and visco-elastic stress-strain response and very accurate deflection measurements (\pm 0.5 percent).

The Dynatest FWD used in this study is shown in Figure 3.12 and consisted of three main components,

- 1) a FWD,
- 2) a system processor (8600), and
- 3) a Hewlett-Packard Integral Personal Computer (IPC).

The FWD was a light-weight, trailer-mounted device which was towed by a Suburban van. It came equipped with seven velocity transducers (geophones) to measure deflections and a 12-in. impact plate with load cell. The six outer sensors can have spacings preset to any desired configuration. The arrangement used in this research is illustrated in Figure 3.13.

The 8600 System Processor controlled the FWD operation. It also supplied the power to the IPC and performed scanning and conditioning of the eight transducers (one load plus seven deflection). The system processor monitored the status of the FWD unit to ensure correct measurements were obtained and safety precautions followed.

The IPC allowed for the input of control and site/test identification, as well as displaying, printing, and storing of the FWD test data. Other features allowed it to edit (e.g., change load and/or drop sequence), sort, and further process test information. The light weight of the IPC made it easy to transport from the field to the office in



Figure 3.12 Falling Weight Deflectometer (FWD)

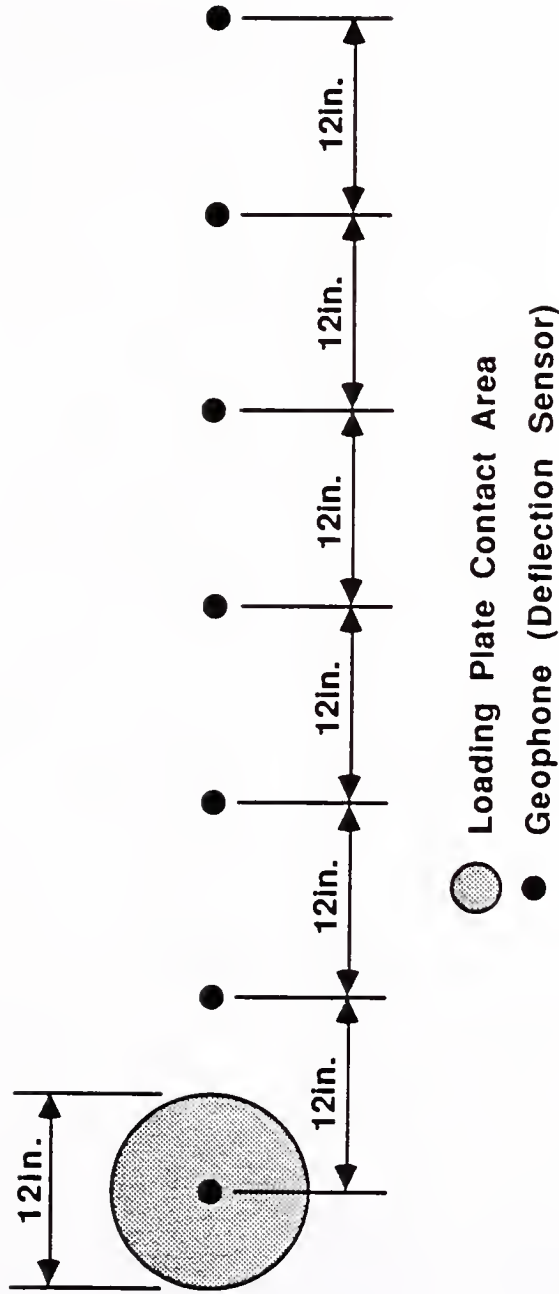


Figure 3.13 Location of Loading Plate and Spacing of Geophones

order to run various programs designed to match deflection basins, compute layer moduli, and predict pavement life expectancy.

3.3.2 FWD Field Testing Procedures

Once the IPC was programmed to include information as test and site description and loading, the FWD was ready to test. The testing sequence was the same for all three sites, i.e., longitudinal followed by transverse stations. Once completed, the special stations were tested. These locations were specific areas within the site that appeared free from cracking effects.

Each FWD test station received four drops, starting from the highest drop height working down to the lowest. The first drop was considered a seating load. The normal drop configuration and load is given in Table 3.5. A load of 12,000 lbs. most closely approximates the contact stress of a C-130 aircraft, although the total wheel load was 41,900 lbs.

Table 3.5 Typical Drop Sequence and Load

Drop Sequence (IPC)	Load
4	26,000
4 or 3	26,000 or 17,000
2	12,000
1	9,000

The research team was able to complete the testing of all three sites in just over two hours. Eight tests were performed during the six month field testing phase of the study. Tests were conducted at different times during the day under all weather conditions. Results are discussed in Chapter 6.

3.3.3 Measurement of Subgrade Moisture

To accurately interpret and analyze FWD data, subgrade moisture contents and pavement thermal profiles were measured using installed equipment. For moisture determination, two aluminum access tubes were installed at site 2. Water contents were obtained using a nuclear moisture device at subgrade depths of 2, 3, 4, 5 and 6 ft. below the pavement surface. A schematic showing the installed access tube is given in Figure 3.14. Tubes were placed at the center and at the edge of the taxiway to monitor horizontal as well as vertical moisture gradients.

The Troxler 3220 Depth Moisture Gauge pictured in Figure 3.15 was calibrated for Florida sands and gave water contents in volumetric units using the following equation (91):

$$\theta = 0.361 \text{ CR} - 0.769 \quad (3.1)$$

where,

CR = ratio of neutron count rate in the soil to the
standard count rate in the shield

Volumetric values are mostly used in agricultural sciences where soils do not ordinarily undergo appreciable settlements. In civil engineering applications, however, volumetric measurements are impractical, therefore gravimetric (mass) values are used. Equation 3.2 was used to convert volumetric water contents to mass values (92).

$$w = \frac{\theta (\rho_w)}{(\rho_b)} \quad (3.2)$$

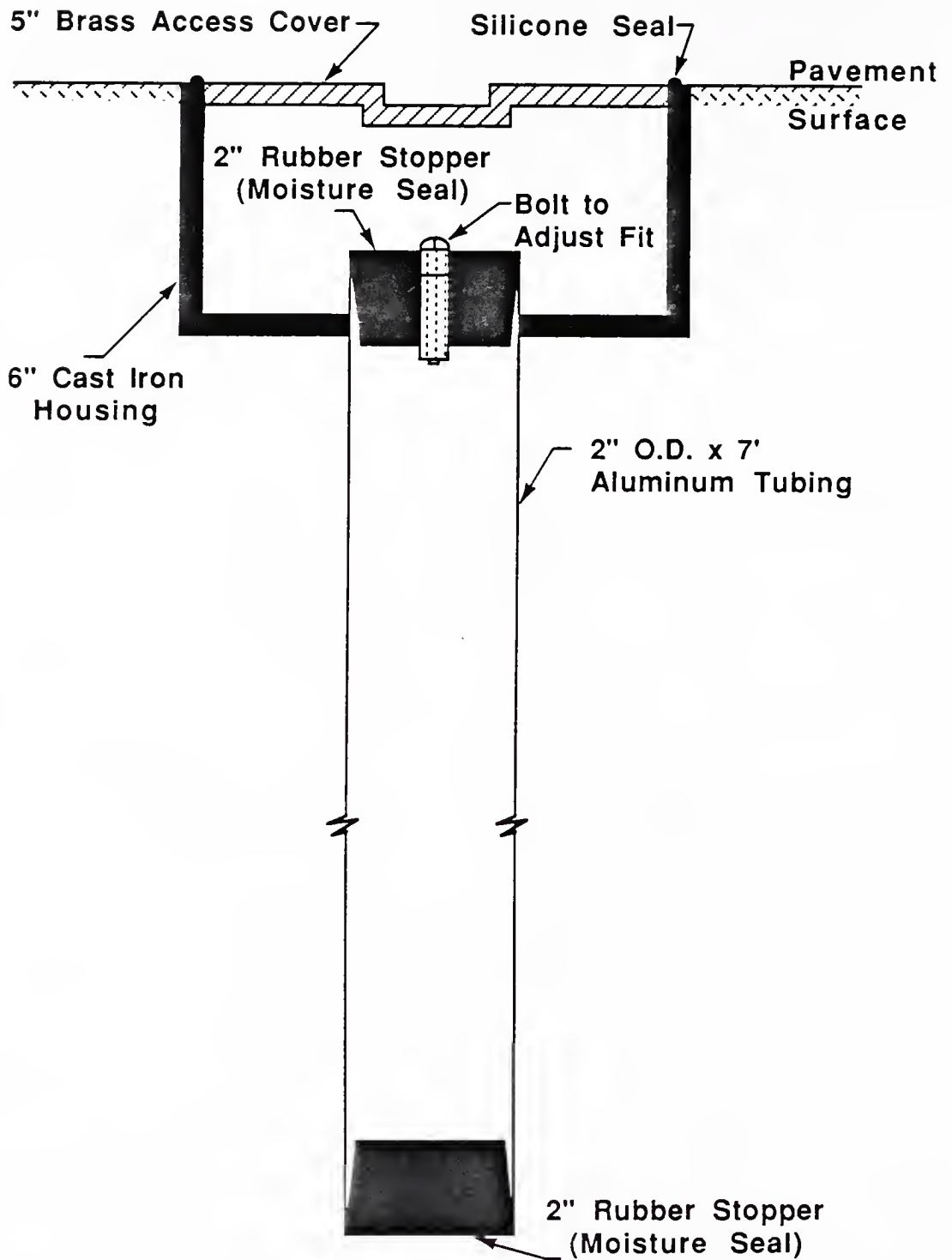


Figure 3.14 Schematic of Installed Moisture Tube



Figure 3.15 Nuclear Moisture Gage

where,

w = gravimetric water content

θ = volumetric water content

ρ_w = density of water, normally 1 gm/cc

ρ_b = dry bulk density, gm/cc

An average ρ_b value of 2.15 gm/cc was calculated from gravimetric and volumetric readings listed in Appendix A. Hillel (92) reported a ρ_b value of 1.6 gm/cc as typical for uncompacted sandy soils. Lambe and Whitman (10) gave a maximum value of 2.21 gm/cc for fine to coarse compacted sands.

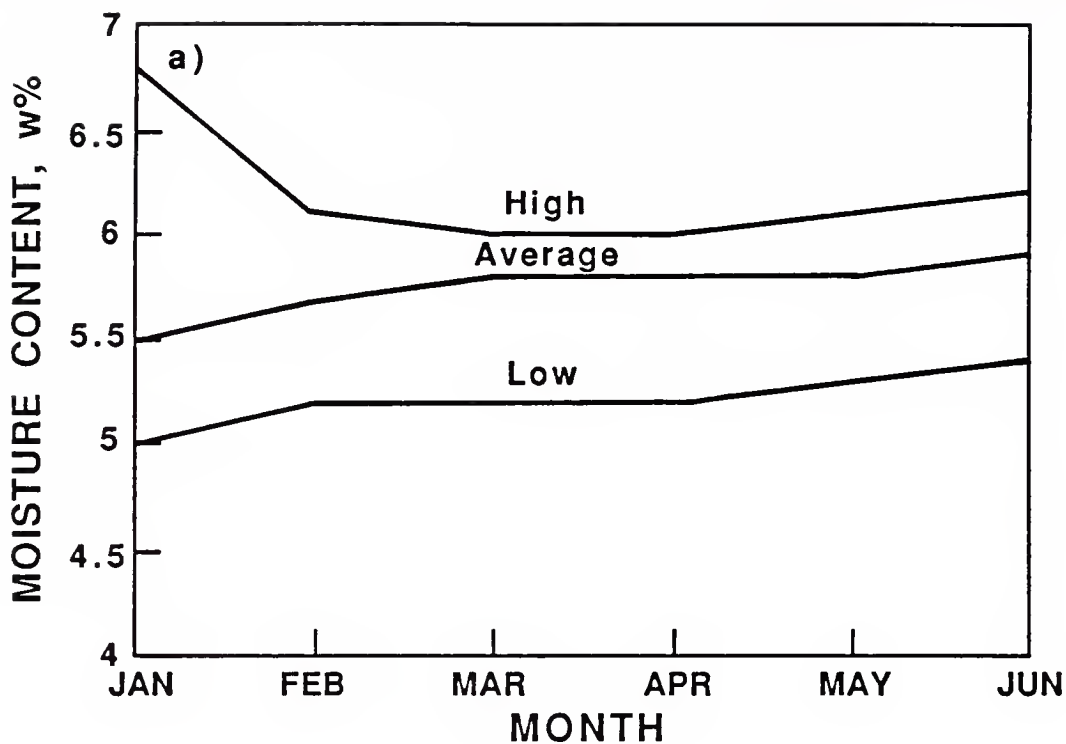
Monthly mass water contents determined from equation 3.2, are presented in Table 3.6. Graphical illustrations representing the high, low, and average values for moisture content are shown in Figure 3.16. Little fluctuation of water content was observed throughout the entire six-month study. There existed, however, a small moisture gradient across the pavement section. The taxiway edge displayed a 10 to 20 percent decrease in values of w from the centerline. A plausible reason for this stems from the evapotranspiration of adjacent field moisture resulting in higher soil suctions at the edge of the pavement. This, in turn, pulls water from the center causing small horizontal gradients to develop. In the vertical direction, there was a general reduction in water content with depth. Surface cracks allowing the infiltration of water into the subgrade can result in higher soil moisture near the surface, especially after heavy rains. In contrast, the decreased water contents at depth seemed to indicate the absence of a water table. Maximum capillary rise for the type soil at Duke Field is approximately 3 ft. (10). Since no increase in water content was observed at 6 ft.,

Table 3.6 Field Moisture Contents (w %) by Month

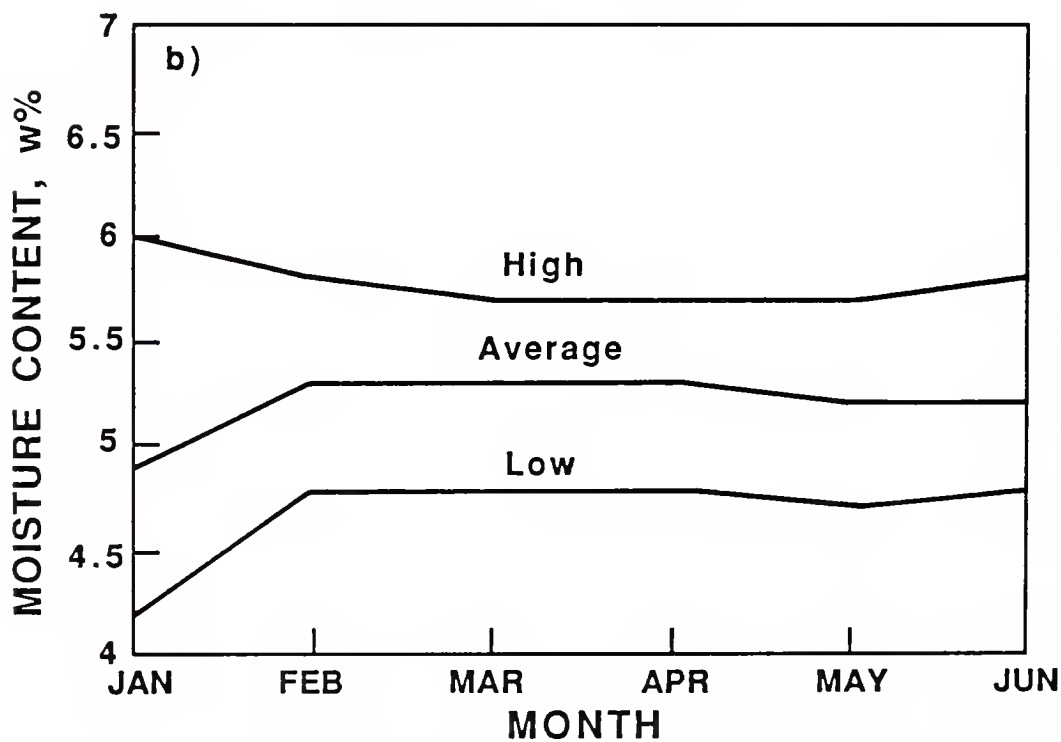
Depth (ft.)	January		February		March	
	<u>Center</u>	<u>Edge</u>	<u>Center</u>	<u>Edge</u>	<u>Center</u>	<u>Edge</u>
2	6.8	6.0	6.1	5.5	6.0	5.5
3	5.3	4.8	6.0	5.8	6.0	5.7
4	5.0	4.8	5.8	5.4	5.9	5.5
5	5.2	4.2	5.5	4.8	5.7	4.9
6	5.3	4.5	5.2	4.8	5.2	4.8
AVE	5.5	4.9	5.7	5.3	5.8	5.3

Depth (ft.)	April		May		June	
	<u>Center</u>	<u>Edge</u>	<u>Center</u>	<u>Edge</u>	<u>Center</u>	<u>Edge</u>
2	*	*	6.1	5.7	6.2	5.8
3	*	*	6.0	5.5	5.9	5.5
4	*	*	5.9	5.2	6.0	5.2
5	*	*	5.8	4.8	5.8	4.8
6	*	*	5.3	4.7	5.4	4.8
AVE	*	*	5.8	5.2	5.9	5.2

* Did not test



a) Center of Pavement



b) Edge of Pavement

Figure 3.16 Monthly Subgrade Moisture Contents:
High, Low, and Average Values

the water table appeared to be of no influence to at least 9 ft. below the pavement surface.

Due to the relatively low water content of the subgrade soil excess pore water pressures are not generated under repeated aircraft loadings. Given similar loading conditions, the small variation of subgrade moisture present would not be enough to significantly alter its modulus.

3.3.4 Measurement and Prediction of Pavement Thermal Profiles

The accurate measurement of temperatures within a flexible pavement is extremely important to correctly assess its structural response to changing load and environmental conditions. Measuring thermal gradients at predetermined points in the pavement profile presented an interesting challenge. A device was designed using nonconductive tubing and thermocouple wire that could be sealed from moisture intrusion and made flush with the pavement surface. Information on the theory and use of thermocouples presented by Schimmelpfennig (93) and Holman (94) was used to design, calibrate, and construct the devices.

Trial tests were performed in the laboratory at temperatures ranging from 32 to 144 F using type T (copper-constantan) thermocouple wire. Water bath temperatures were verified with a Fluk 80T-150 temperature probe accurate to 0.01 F. Relative voltages were recorded between the measuring junction (tip of thermal couple) and reference junction using a standard Fluk True RMS multimeter accurate to 0.01 mv. Type T thermocouples show high sensitivity (± 1 F) when working in thermal ranges below 600 F.

The reference junction must be known in order to compute temperature from measured voltages. Normally, the reference temperature (RT) in the laboratory is set at 32 F (ice bath). However, maintaining this

temperature in the field is impractical and therefore sophisticated devices are available to simulate this ice bath electronically. Since the RT in the field approximates the ambient temperature, laboratory calibration included recording relative voltages for five different RTs (e.g., 32, 54, 74, 93, and 113 F). A correct reading of the RT is essential to precisely measure pavement temperatures. This is because the voltage generated is proportional to the relative temperature between the two junctions. For example, if the ambient air temperature (RT) is 50 F and a point within the pavement is 50 F, then the potential difference is zero (0.00 on the multimeter). However, if the RT rises to 60 F but the actual pavement temperature remains at 50 F, then a negative potential will develop. Errors in the measured temperature are directly related to the errors induced by incorrectly assessing the RT.

From the laboratory data, a plot of millivolt output versus temperature was made and a linear regression analysis performed for each of the five RTs. Very good correlations were obtained with R^2 values averaging 0.999. A multiple regression analysis was then performed for the entire range of temperatures and equation 3.3 developed. Using this equation, several trials were conducted to predict actual temperatures at different RTs. Deviations from the actual temperatures varied between 0.1 and 1.2 F. Considering the sensitivity of the thermocouple, the predicted values were within acceptable limits. This equation was subsequently used to measure temperature profiles in the field.

$$MT = 0.7933 + 43.6560 (MV) + 0.9891 (RT) \quad (3.3)$$

$$(N = 25 \quad R^2 = 0.9996)$$

where

MT = measured temperature (F)

MV = output from volt meter (mv)

RT = reference temperature (F)

Two temperature profile devices (TPD) were constructed using 2-in. PVC tubing, styrofoam (for added insulation), and thermocouple wire. Illustrated in Figure 3.17 is a schematic of the installed TPD. Six thermocouple sensors were prepositioned on each of the two devices at points determined from a previous airfield evaluation (88). Note from Figure 3.17 that four thermocouple sensors were placed in the asphalt concrete layer. These, along with the surface temperature reading, allowed for five thermal recordings within the top 3.5 in. of pavement, where the largest temperature gradients were expected. The other two sensors were placed in the sand asphalt and subgrade layers, respectively.

The two TPDs were placed in previously drilled 6-in. core holes at site 1, one at the centerline and one at the edge of the pavement. The exposed thermocouples were covered with a slurry sand-asphalt mixture and butted up firmly against the side of the core to secure intimate contact with the existing pavement (Figure 3.18). The core was back-filled with a cold-mix asphalt and lightly tamped.

To obtain six simultaneous readings, a temperature measurement system was built which consisted of a six-position switch box and two multimeters (Figure 3.19). The meter on the left recored the RT using the Fluk 80T-150 temperature probe, while the one on the right measured the voltage output from the TPD. The styrofoam mat was used to reduce heat

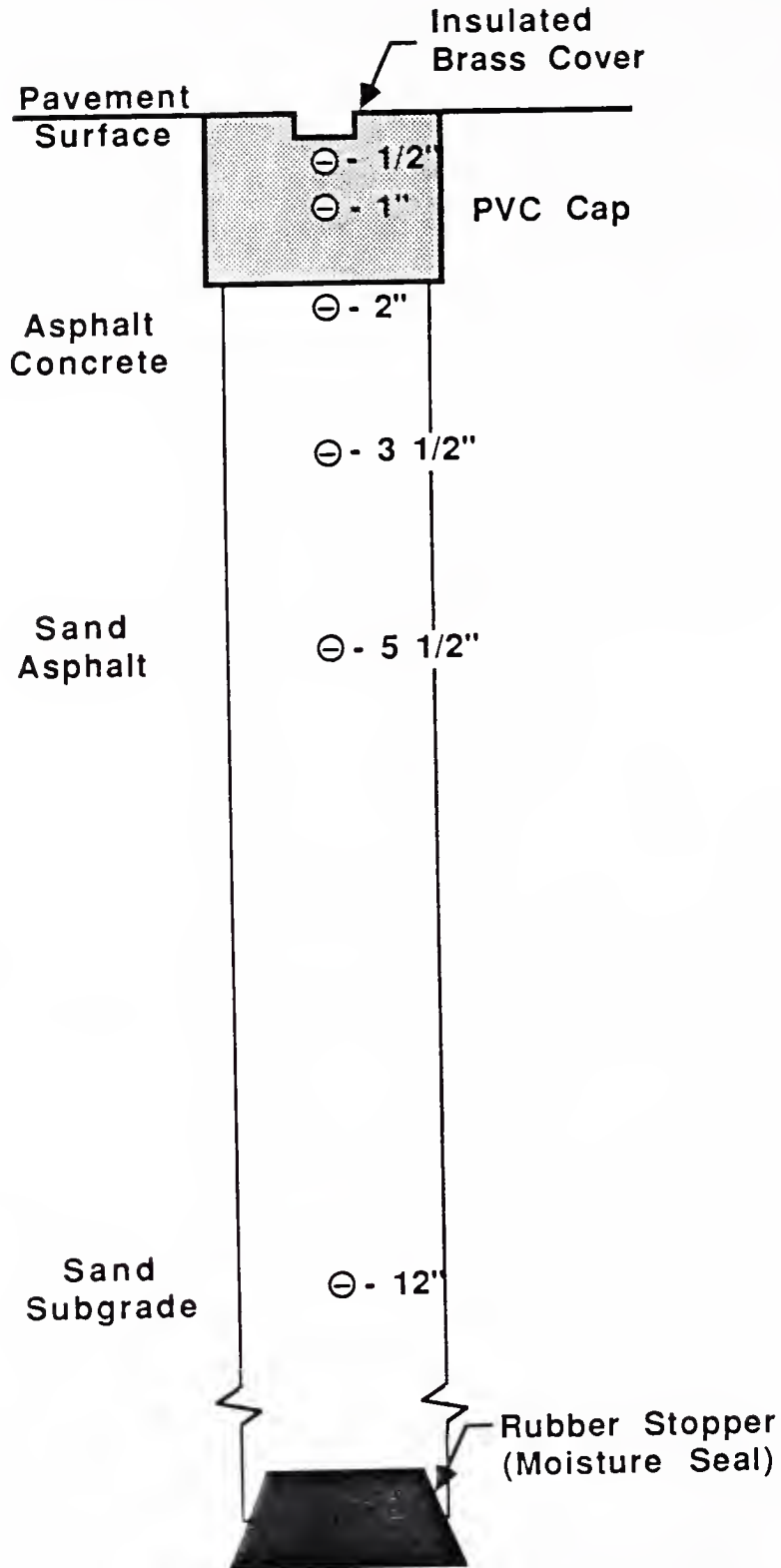


Figure 3.17 Schematic of Installed Temperature Profile Device (TPD)



Figure 3.18 Installing the Temperature Profile Device (TPD)

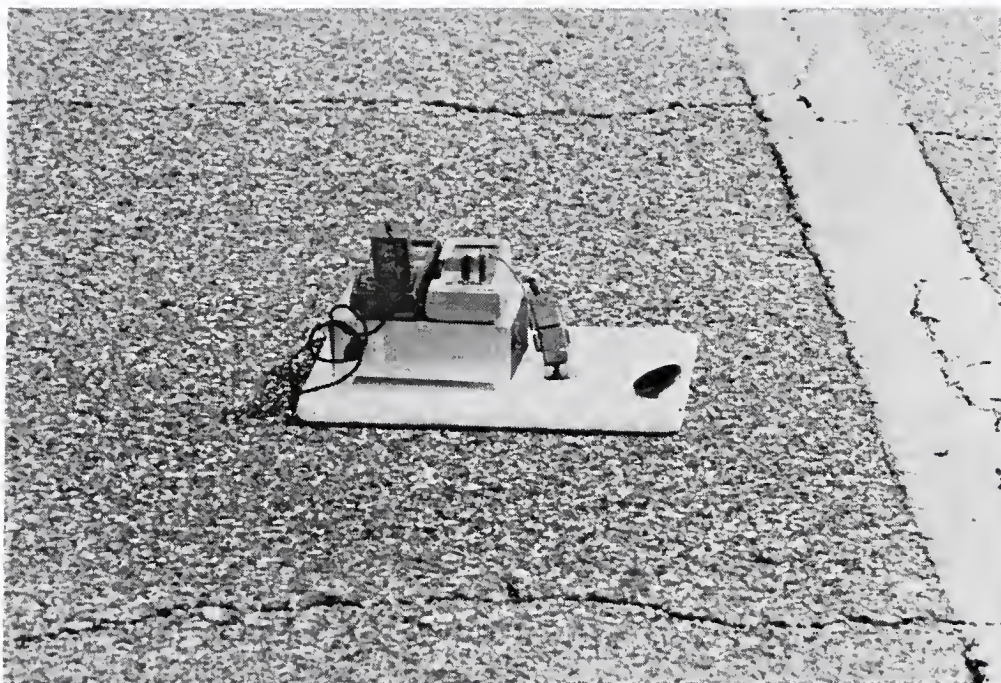


Figure 3.19 Temperature Measurement System

loss from the TPD and limit the effects of heat gain on the reference junction.

A nomograph was developed for temperatures typically experienced in Florida throughout the year. It can be used for quick, approximate temperature measurements. An example for using the nomograph is shown in Figure 3.20, and is outlined below.

Given: Reference Temperature (RT) = 74 F
Output on voltmeter = 0.5 mv @ 3.5 in.

Find: Pavement Temperature @ 3.5 in.

- Procedure:
- 1) Locate 0.5 mv on abscissa and read up until intersection with RT (diagonal line).
 - 2) Read across to pavement temperature.

Answer: 96.0 F

A parametric study was undertaken to compare measured field temperatures with predicted temperatures using the 5-day mean pavement temperature model developed by Southgate and Deen (95). This model utilizes the prior 5-day mean air temperature added to the current pavement surface temperature to arrive at the mean pavement temperature (MPT). A Fortran computer program is available to quickly compute the MPT and is presented by Bush (96).

In order to calculate the MPT from actual field measurements, thermal profiles were first plotted as shown in Appendix B. An average was then obtained for the entire depth of asphalt concrete, arriving at the

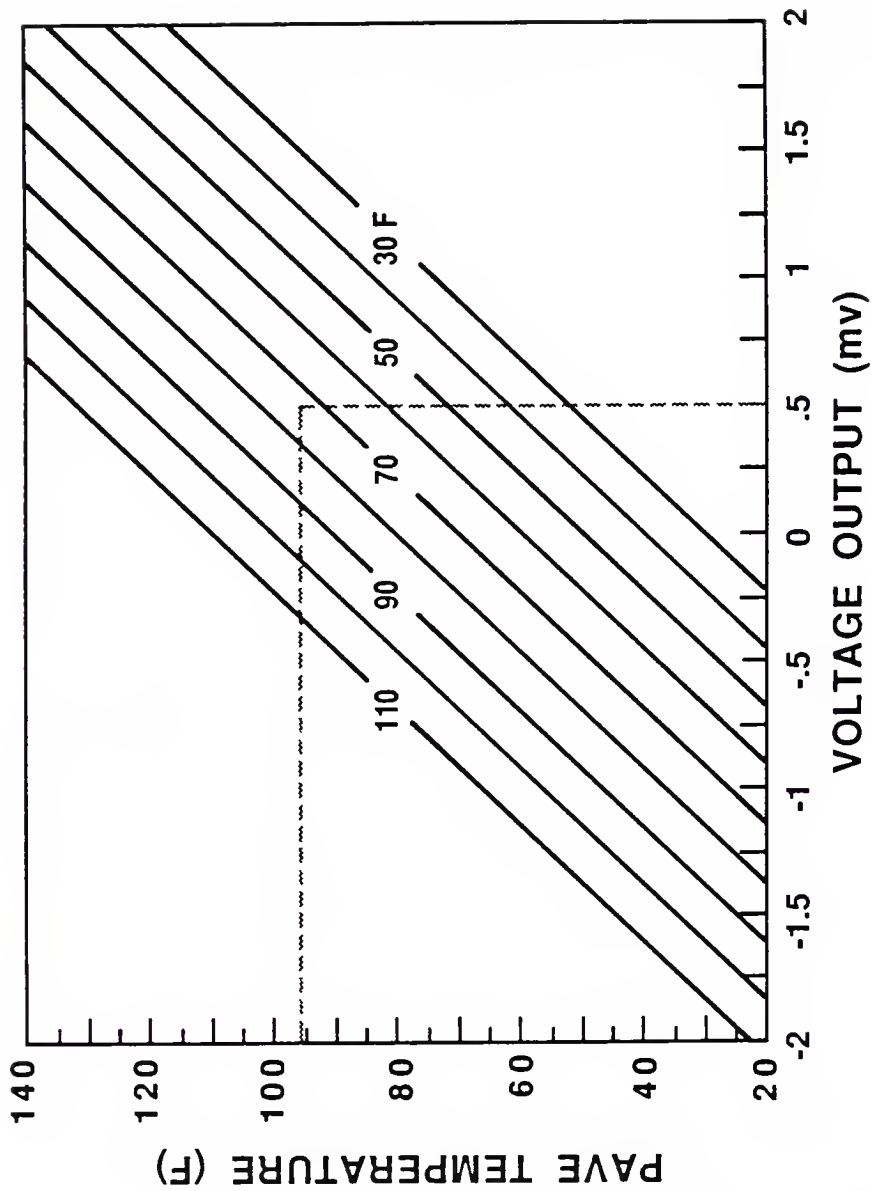


Figure 3.20 Nomograph for Determining Pavement Profile Temperatures

mean pavement temperature (MPT). Since horizontal thermal gradients did not appear to be significant, the MPT was taken as an average between the center and edge TPD. Finally, the measured MPT was compared with the computed 5-day MPT for 3.5 and 5.5 in. layer thicknesses.

From the results given in Table 3.7, satisfactory agreement exists between the measured MPT and the predicted MPT using the 5-day model. The best correlations came during uniform gradient conditions. However, it did not fair as well under positive or negative gradient situations. This was somewhat expected due to the highly empirical nature of the model. One inherent flaw shown by the data is the apparent trend of the model to predict higher MPTs with decreasing layer thickness, regardless of gradient conditions present. During thermal cooling, lower temperatures are expected near the surface which results in a lower MPT at 3.5 in. than at 5.5 in. Using the 5-day model, the opposite occurred.

In summary, thermocouples provided very reliable pavement temperatures which appeared to respond correctly to changing thermal conditions. The predicted 5-day model is best used for initial estimates but should not be relied upon to accurately define pavement temperatures. This is especially true when predicting resilient characteristics of bituminous layers where differences of just a few degrees could result in significant errors.

Table 3.7 Parametric Study of Mean Pavement Temperature (MPT)

Test	Pavement Thickness (in.)	Measured MPT (F)	5-Day MPT (F)	Diff.	Thermal (a) Gradient
1	3.5	55.2	52.8	2.4	Uniform
	5.5	54.8	51.6	3.2	
2	3.5	34.1	39.0	-4.9	Positive
	5.5	35.3	38.9	-3.6	
3	3.5	57.3	59.5	-2.2	Uniform
	5.5	56.9	58.2	-1.3	
4	3.5	70.7	75.1	-4.4	Uniform
	5.5	70.6	72.9	-2.3	
5	3.5	89.7	95.5	-5.8	Negative
	5.5	88.0	92.1	-4.1	
6	3.5	120.0	114.1	5.9	Negative
	5.5	114.8	109.6	5.2	
7	3.5	77.6	85.0	-7.4	Positive
	5.5	78.9	82.3	-3.4	
8	3.5	91.1	91.0	0.1	Negative
	5.5	92.6	87.9	4.7	

Note:

- (a) Uniform - No appreciable gradient exists
 Positive - Pavement temperature increasing with depth
 Negative - Pavement temperature decreasing with depth

CHAPTER 4
LABORATORY TESTING AND EVALUATION OF PAVEMENT MATERIALS

4.1 Introduction

Laboratory tests were performed on core material extracted from the Duke Field test sites to determine the physical classifications and properties of the pavement layers. Discussed in this chapter are the basic procedures and the results obtained from the following tests:

- 1) subgrade sieve analysis and specific gravity
- 2) bulk specific gravity
- 3) maximum density
- 4) asphalt content and gradation
- 5) penetration
- 6) absolute viscosity
- 7) Schweyer rheometer
- 8) indirect resilient modulus
- 9) indirect tensile (quick)
- 10) indirect static creep (fracture energy)

Results from the last three tests (indirect) are discussed in greater detail in Chapter 5.

4.2 Classification of Subgrade Materials

Subgrade soils from each site were classified according to the AASHTO and Unified systems using grain-size analysis (10,97). The results of the sieve analyses along with a sensory assessment of the

materials are presented in Table 4.1. A corresponding grain-size distribution is shown in Figure 4.1 for all three sites. From the distribution curve, a Uniformity Coefficient (C_u) close to 2.0 was computed for each feature indicating that the subgrade sands were uniform in size. The low percentage of fines further identified the soils as clean, poorly-graded sands.

Specific gravities were 2.63 and 2.64 for sites 1 and 2, respectively, and slightly lower at 2.58 for site 3. The specific gravities at sites 1 and 2 were close to the value of 2.65 given for quartz (98). The lower value computed for site 3 was attributed to the small amount of organic content found in the soil.

4.3 Determination of Air Void Content in Field Extracted Bituminous Mixtures

Two specific tests were conducted to obtain air void contents for both the asphalt concrete and the sand asphalt layers. Tests included the determination of bulk specific gravity (AASHTO T 166-78) on each core specimen and maximum theoretical specific gravity (AASHTO T 209-82) on selected cores for each layer. Table 4.2 lists representative values of unit weight and air voids for both in and out of the wheel path. The data clearly show a marked increase in density inside the wheel path with a corresponding decrease in air void content for each layer. There appears even greater densification in the surface courses as compared to underlying layers. This densification may appear significant from the standpoint of reduced air voids, but it accounts for less than 0.1 in. of additional consolidation in the surface courses. Site 3, which displayed no measurable rutting, exhibited extremely high densities in the surface and binder courses both in and out of the wheel path. The

Table 4.1 Summary of Subgrade Classification

	Sieve No.	Diameter (mm)	Site		
			1	2	3
			Percent Passing		
Sieve Analysis	20	0.840	99.84	99.16	99.34
	40	0.420	72.35	70.23	67.03
	60	0.250	15.89	20.04	19.36
	100	0.149	3.74	6.08	7.27
	140	0.105	1.68	2.24	4.29
	200	0.074	0.78	1.10	2.49
	wet ^(a)	<0.074	1.60	4.30	5.70
Uniformity Coefficient, Cu			1.7	2.1	2.2
Specific Gravity, Gs			2.63	2.64	2.58
Plasticity			none	none	none
Description			fine sand	fine sand	fine sand
Color			orange	medium tan	light brown
Odor			none	none	burnt ^(b)
Classifications	AASHTO		A-3	A-3	A-3
	Unified		SP	SP	SP

NOTE

- (a) Wet sieve analysis performed to verify low percentage of fines
(b) Organic content of 1.09 % determined from AASHTO T 267-80

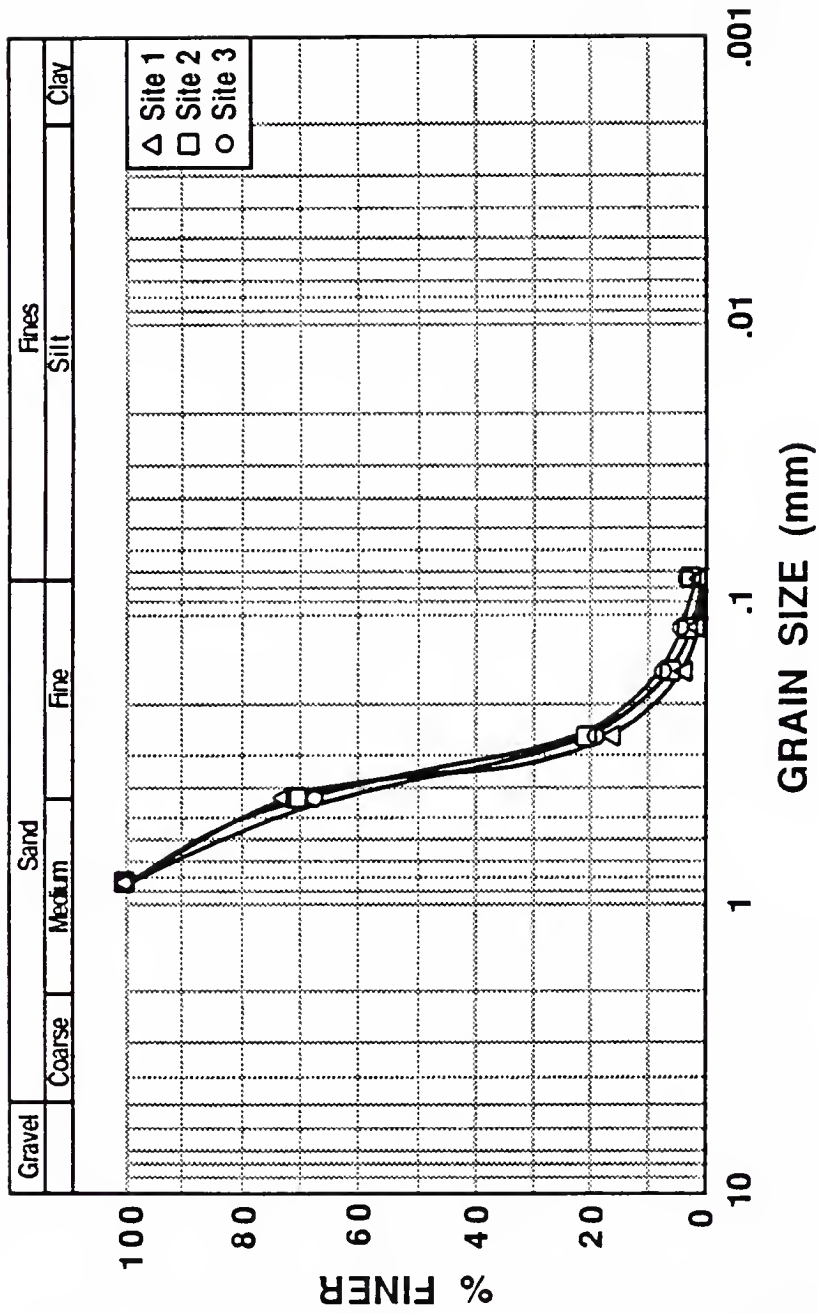


Figure 4.1 Grain Size Distribution for the Subgrade Soils

Table 4.2 Maximum Density, Unit Weight, and Air Void Content for Bituminous Layers In and Out of Wheel Path

Layer Type-No.	Number Cores Taken In/Out	Site								
		1 (pcf)		2 (pcf)		3 (pcf)				
		MTD	In (% AV)	Out (% AV)	MTD	In (% AV)	Out (% AV)	MTD	In (% AV)	Out (% AV)
AC-1 Surface Course	4/2	152.1	141.7 (6.8)	136.4 (10.1)	152.3	143.6 (5.7)	139.0 (8.6)	153.9	146.1 (5.0)	143.3 (6.7)
AC-2	4/2	142.2	130.4 (8.2)	129.8 (8.5)	148.5	130.2 (12.3)	129.1 (13.1)	149.8	143.0 (4.4)	141.5 (5.4)
AC-3	3/2		NA		141.7	129.1 (9.0)	127.4 (10.0)		NA	
SA-1 Top half	3/2	152.9	111.6 (27.1)	108.4 (29.2)	153.5	114.1 (25.5)	111.9 (27.0)	152.1	114.7 (25.9)	114.6 (25.9)
SA-2 Bottom half	3/2	152.9	111.9 (26.8)	108.5 (29.0)	153.5	116.0 (24.3)	113.9 (25.4)	152.1	116.7 (22.5)	117.1 (21.8)

NOTE

$$\% \text{ AV} = 100 - 100 \left(\frac{\text{unit weight}}{\text{MTD}} \right)$$

low air void contents tend to suggest good compaction during construction. Sites 1 and 2 exhibited appreciable rutting (0.75 and 1.5 in., respectively) when compared to site 3, but this could be attributed to the subgrade and not necessarily to consolidation in the bituminous layers.

Unlike the higher density courses at site 3, sites 1 and 2 had binder courses of substantially lower densities (127.4 to 130.4 pcf). A careful examination of the core material revealed a low-weight, porous aggregate comprising the mix. These reduced densities could have possibly resulted in lower overall strengths of the binder layers, thus influencing the transfer of higher stresses to the underlying material. This premise will be discussed in Chapter 5.

The low densities and associated high air void contents of the sand asphalt are typical for the type construction used back in the forties. In conferring with officials at the Florida Department of Transportation (FDOT), the popular construction method used then was an asphalt emulsion combined with the natural soil and compacted in approximately 4-in. lifts. This technique, called a sand bituminous road mix or SBRM, suited the era quite well. Today, however, it is unacceptable for use in quality road construction because of the difficulty of controlling aggregate gradation, asphalt content, and compaction in the field.

4.4 Determination of Maximum Density of Bituminous Layers

Tests for maximum specific gravity were done in accordance with AASHTO T 209-82. Six-inch cores selected from each site were tested to determine maximum densities for each asphalt pavement layer. Table 4.2 presents the maximum theoretical density.

Air void contents were calculated using the MTD. Given similar mixtures, for every 1 percent increase in air void content, there is a proportional decrease in bulk unit weight. Air void contents of an asphalt concrete pavement which exceed the Marshall Mix Design criteria of 3 to 5 percent can result in significant reductions in strength, demonstrate high deformability, and exhibit lower fracture strain tolerance. The data in Table 4.2 shows air void contents above 5 percent for every asphalt concrete layer except inside the wheel path of site 3. Air void content is an indicator of the durability and performance life of flexible pavements. Therefore, this could, in part, explain the higher degree of cracking seen at sites 1 and 2. Lower MTDs in the underlying asphalt concrete layers confirmed the use of low-weight aggregates.

The relatively high MTDs and air voids (21.0 to 29.2 percent) for the sand asphalt indicated poor field compaction during airfield construction. Today, sand asphalt hot mix (SAHM), and not SBRM, is used to meet design specifications which require air voids below 16 percent and minimum asphalt contents of 6 percent (99).

4.5 Determination of Asphalt Content and Gradation by Quantitative Extraction

Quantitative extraction was done on representative cores from each site and layer in accordance with AASHTO T 164-80. The paving mixtures were extracted using a solvent, trichloroethylene, to separate the bitumen from the aggregate. The asphalt content was calculated by the difference between the mass of the original sample and the mass of the

extracted aggregate, moisture content, and ash from an aliquot of the extract. Sieve analyses were performed on the separated aggregate to determine the gradation of each bituminous layer. Results from these tests are presented in Appendix C.

Plots of the sieve analyses are given in Figures 4.2 through 4.4. Layers of similar gradation were grouped together and designated either Group A, B, or C. A final comparison is made of all three groups in Figure 4.5 using the average values from the first three plots. Plots for Group A and B give the maximum density based on maximum aggregate size and is shown by a dashed line through the origin. A deviation from this line represents a more uniformly graded mixture. Design specifications, however, stipulate the range of deviation allowed that will still meet strength and compaction requirements.

Six of the seven asphalt concrete layers were placed in Group A and are shown in Figure 4.2. The gradation band shows well-graded mixtures with an average filler content (< No. 200) of 5.1 percent. Mineral filler contents under 6 percent are desired for reasons of stability.

Site 2, layer 2, was the only asphalt concrete layer in Group B (Figure 4.3). This mixture was more uniformly graded than the other asphalt concrete mixtures which accounted for its high air void content (13.6 percent). The amount of mineral filler present was 5.0 percent.

Group C (Figure 4.4) contained the sand asphalt mixtures for all three sites. These layers were uniformly graded and displayed high air void contents (21 to 29 percent). Mineral filler ranged between 2.6 and 6.2 percent.

The binder contents for the asphalt concrete fell between 4.8 and 6.4 percent, while for the sand asphalt values ranged between 3.6 and

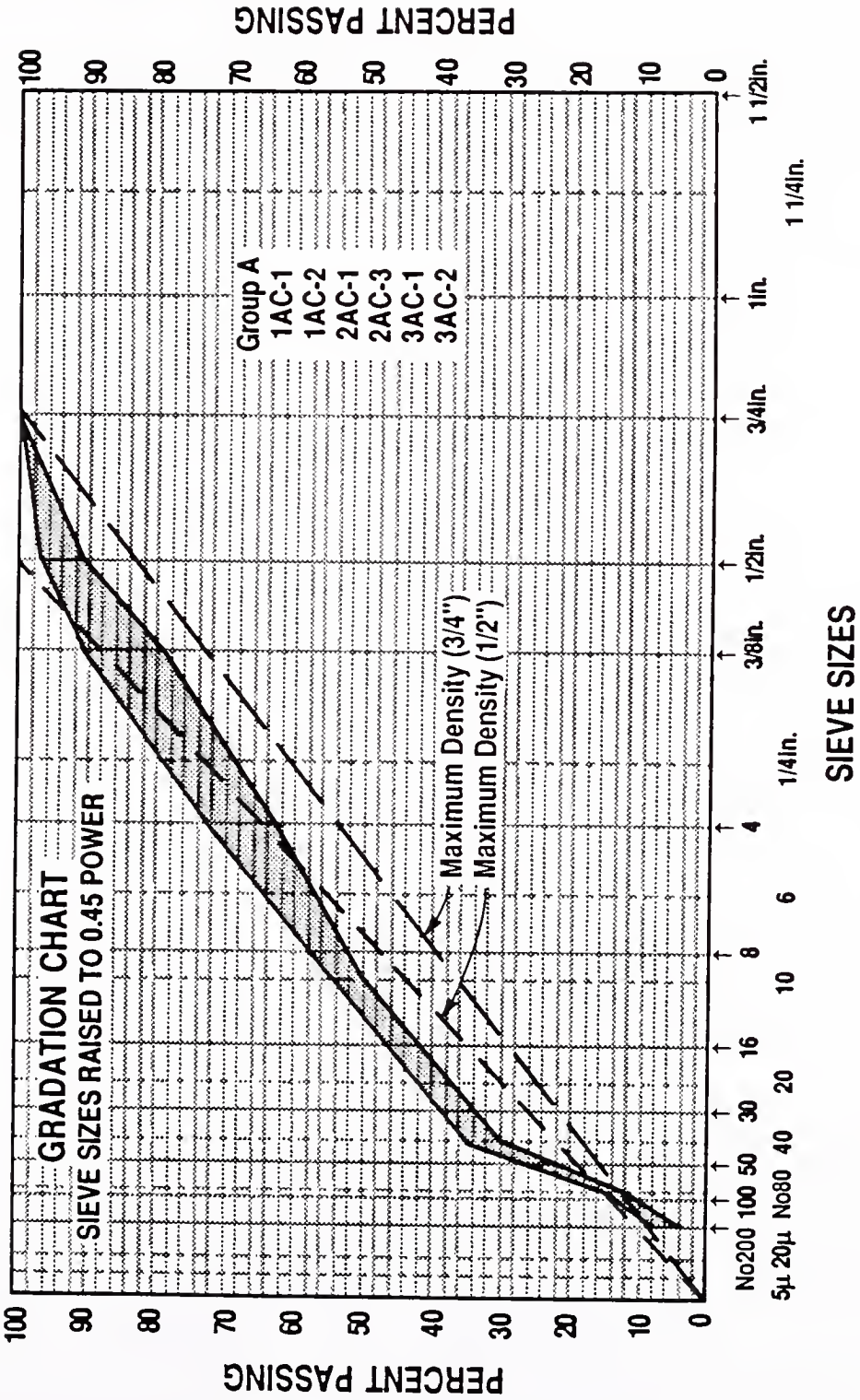


Figure 4.2 Gradation Range for Group A

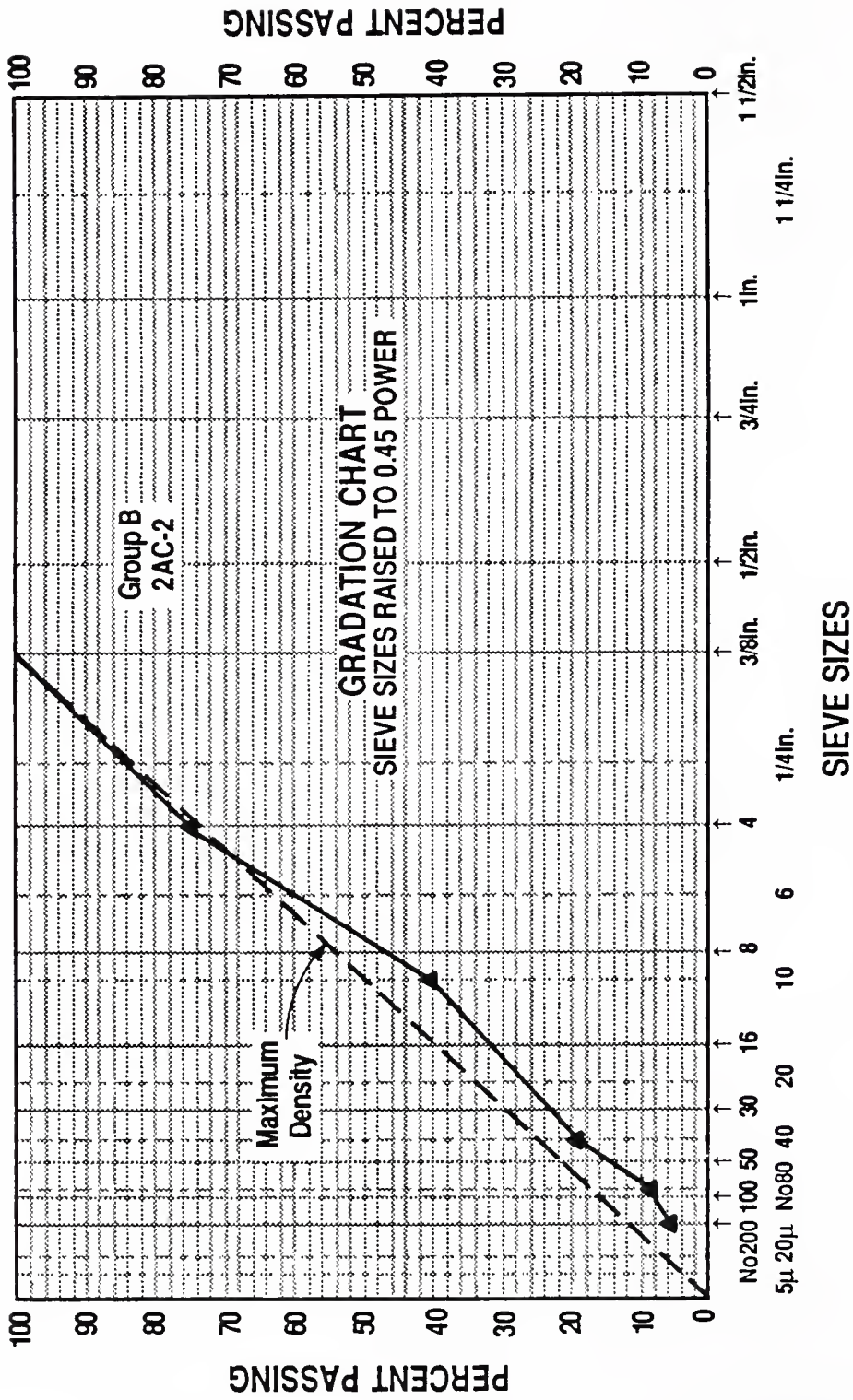


Figure 4.3 Gradation Range for Group B

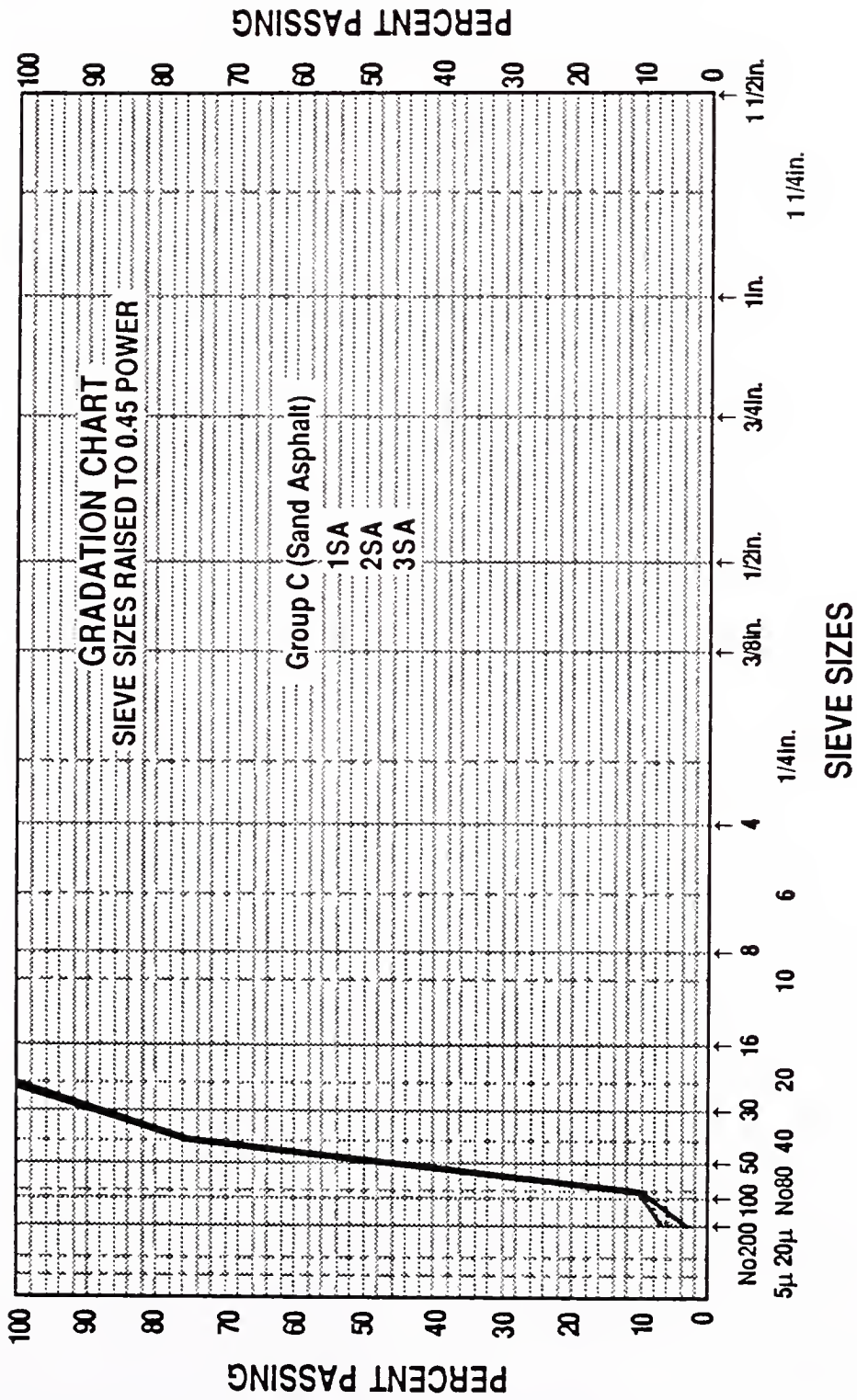


Figure 4.4 Gradation Range for Group C

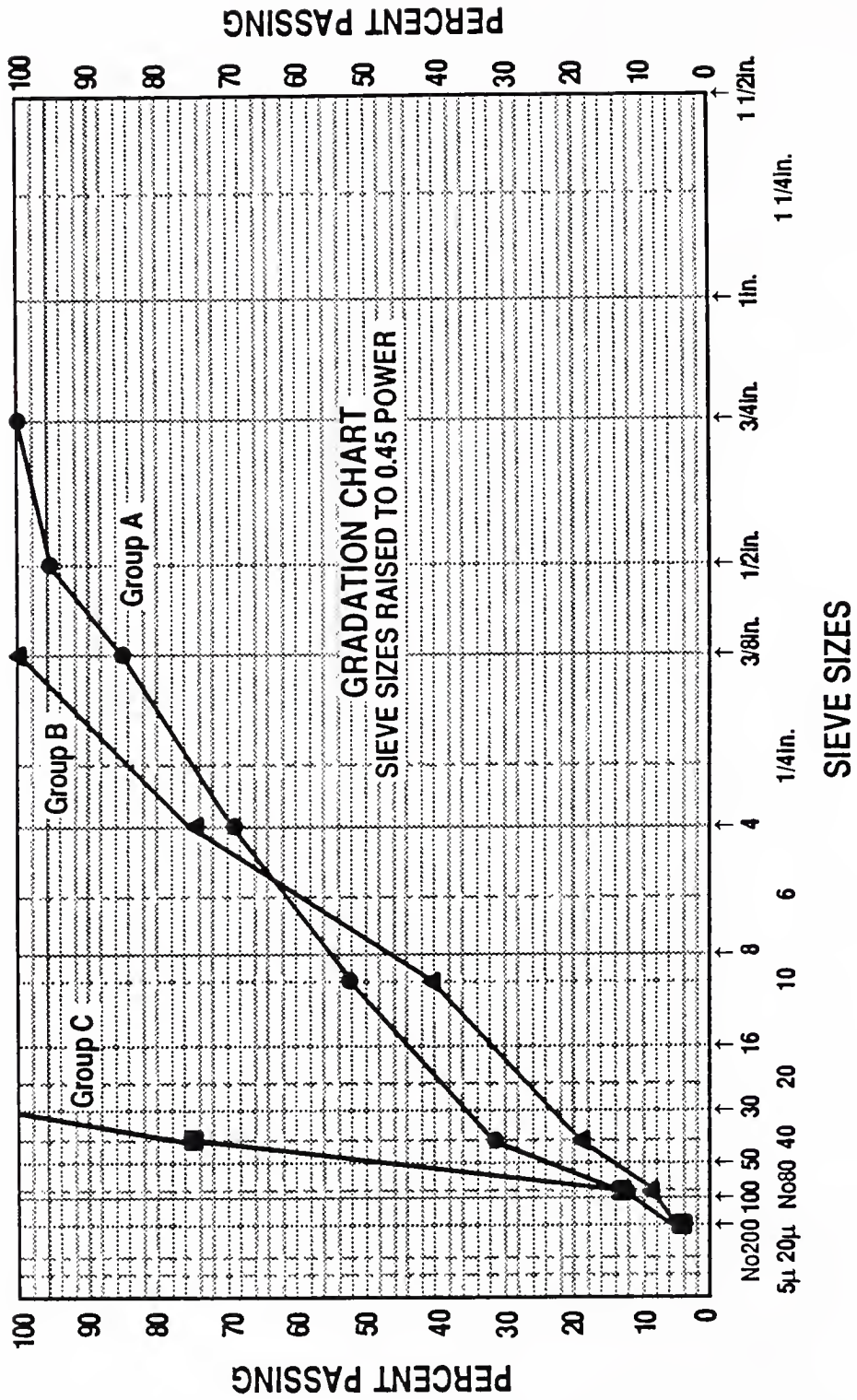


Figure 4.5 Gradation Comparison of All Groups

3.9 percent. Though, the asphalt contents for the asphalt concrete were close to normal limits (4 to 6 percent), the sand asphalt had values well below an established minimum of 6 percent (99).

4.6 Testing and Evaluation of Recovered Asphalts Using Penetration and Viscosity Measurements

The bitumen from eight asphalt concrete and six sand asphalt specimens was recovered to quantify its rheological properties. Tests were performed by the FDOT using the Abson procedure (AASHTO T 164-80 and T 170-82). These samples were representative of each bituminous layer at the three airfield sites. Since only a limited number of cores were obtained from these pavements, asphalts recovered from cores in the wheel path were chosen for testing. However, to study the effect of high air void content on hardening, through increased oxidation, a recovery of asphalt from cores outside the wheel path was performed at site 3.

Three separate tests were performed on the recovered asphalts. Two such tests, penetration and absolute viscosity, are discussed in this section. The third test was performed in the Schweyer rheometer and will be presented in section 4.7.

The penetration test (AASHTO T 49-80) is a highly empirical test still employed today to ensure that bituminous materials with undesirably low values at 25 C (77 F) are precluded from use (100). Occasionally, the penetration test is made at temperatures other than 25 C, usually at 4 C (39.2 F). Data from both test temperatures can be used to compute the penetration ratio and used to assess the temperature susceptibility of any asphalt cement. However, with the advent of more

theoretically sound methods, such as the Schweyer rheometer, this test will probably become obsolete.

Extremely low values ranging from 1 to 23 were recorded for the three sites giving an initial indication of the aged condition of these airfield pavements. Penetration values are given in Table 4.3.

The second test performed on the recovered samples was for absolute viscosity (AASHTO T 202-80). This test, normally performed at 60 C (140 F), made use of The Asphalt Institute vacuum viscometer. This viscometer allows the testing of a wide range of asphalt viscosities due to its various capillary sizes and multiple timing marks.

The data in Table 4.3 present a wide range of viscosities depicting various degrees of asphalt hardening. It is shown that four of the asphalts had estimated viscosities based on penetration values because the bitumen was too hard to flow in the viscometer. These estimates were determined from a data base developed by the FDOT for penetration values of 10 and lower. Estimations from the penetration values are highly empirical and should not be used solely to characterize the viscous properties of an asphalt.

Measured penetration at 25 C (77) were plotted against absolute viscosity at 60 C (140 F), and constant power viscosity at 25 C (77 F) and 15 C (59). In order to evaluate the penetration-viscosity relationships, the data base was expanded using outside sources. Penetration-viscosity data from Duke Field were combined with data from work by Ruth and Miller (101), Chari (102), and the Province of Canada and used in a regression analysis for each temperature. These plots are presented in Figures 4.6, 4.7, and 4.8, respectively. Equations 4.1 - 4.4 were developed from the analyses and can be used to predict viscosity from

Table 4.3 Penetration, Absolute Viscosity, and Air Void Content for Recovered
Asphalts Inside the Wheel Path

Layer Type-No.	Year Constructed	Site					
		1		2		3	
		Absolute Viscosity (% AV)	Pen ^(a) (% AV)	Absolute Viscosity (% AV)	Pen (% AV)	Absolute Viscosity (% AV)	Pen (% AV)
AC-1	1974	19 86,666 (6.5)	12 143,468 (5.7)	23 29,223 (6.7)			
Surface Course							
AC-2	1962 (sites 1,3) 1973 (site 2)	12 859,840 (7.9)	14 85,210 (11.9)	13/10 ^(c) 256,204/924,756 (3.4)/(7.5)			
AC-3	1962	NA	3 4,300,000 est ^(d) (8.4)	NA			
SA-1	1942-49	10 1,000,000 est ^(d) (29.0)	1 5,200,000 est ^(d) (24.8)	8 2,000,000 est ^(d) (26.3)			
Top half							
SA-2	1942-49	14 282,863 (27.8)	8 1,981,035 (28.8)	10 702,476 (21.0)			
Bottom half							

NOTE

(a) Penetration in units of 0.1 mm

(b) Absolute viscosity in poises

(c) Taken outside wheel path for comparison

(d) Absolute viscosity estimated on the basis of measured penetration relationships developed by FDOT

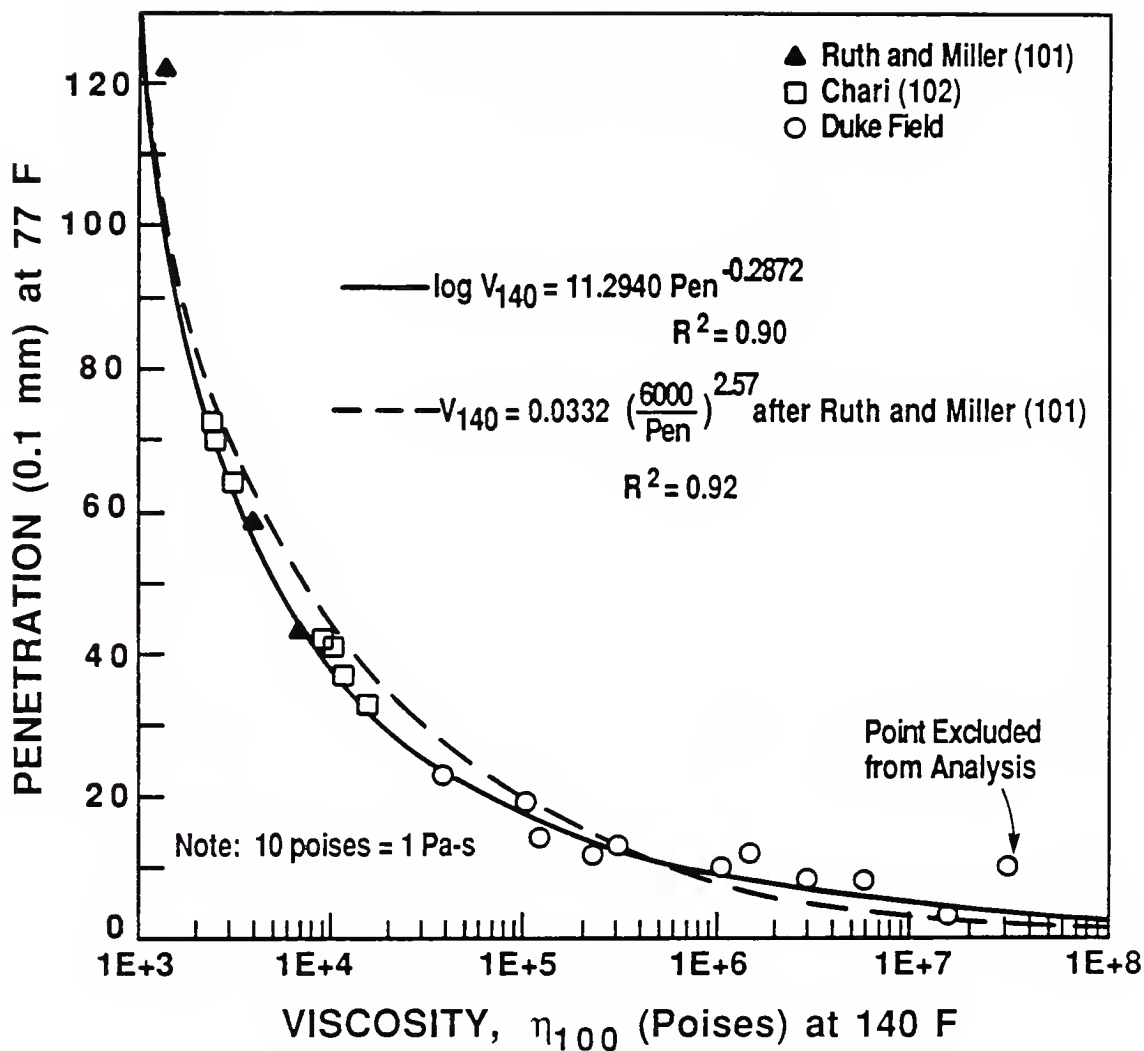


Figure 4.6 Relationship Between Penetration at 77 F and Absolute Viscosity at 140 F

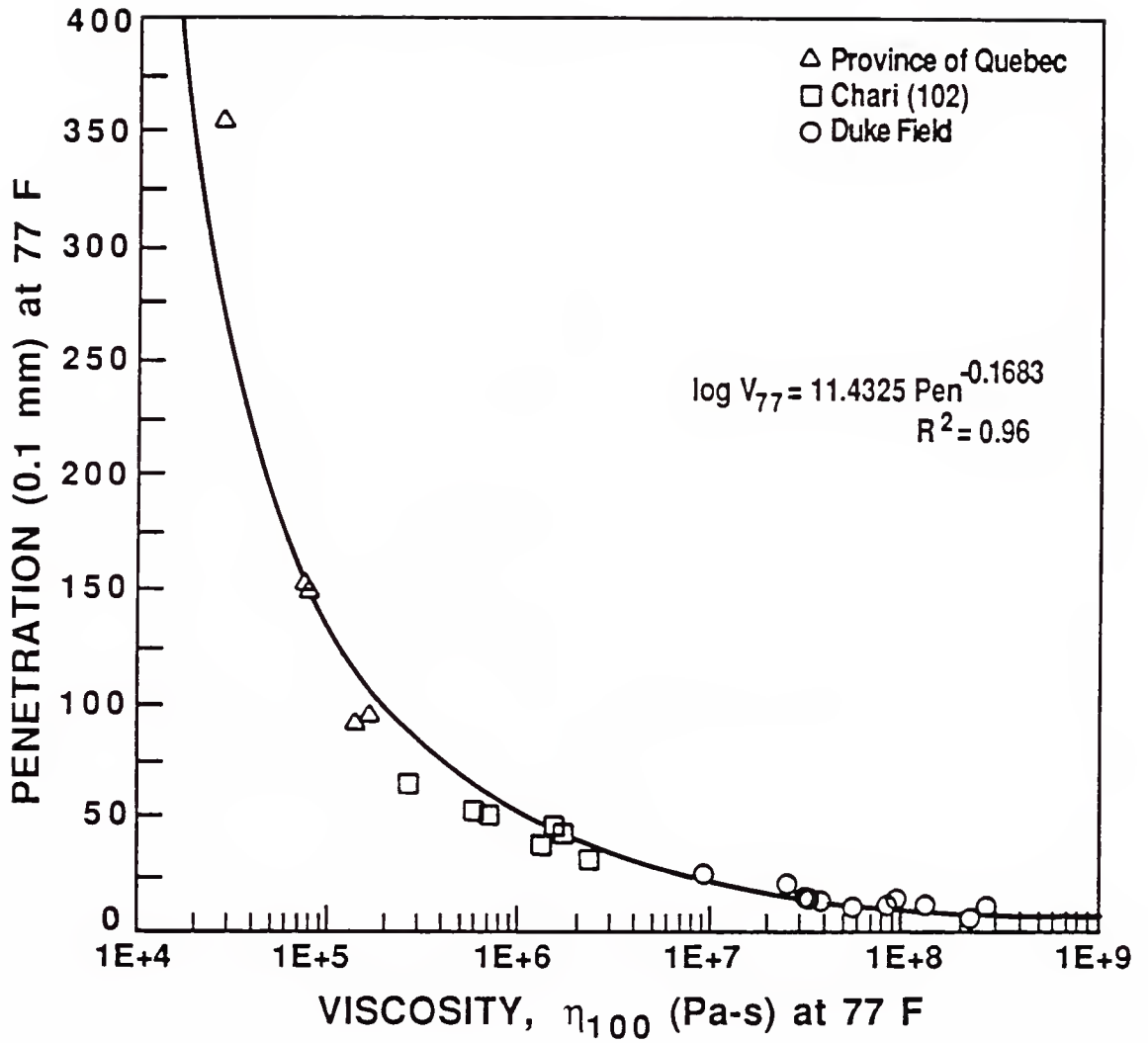


Figure 4.7 Relationship Between Penetration at 77 F and Constant Power Viscosity at 77 F

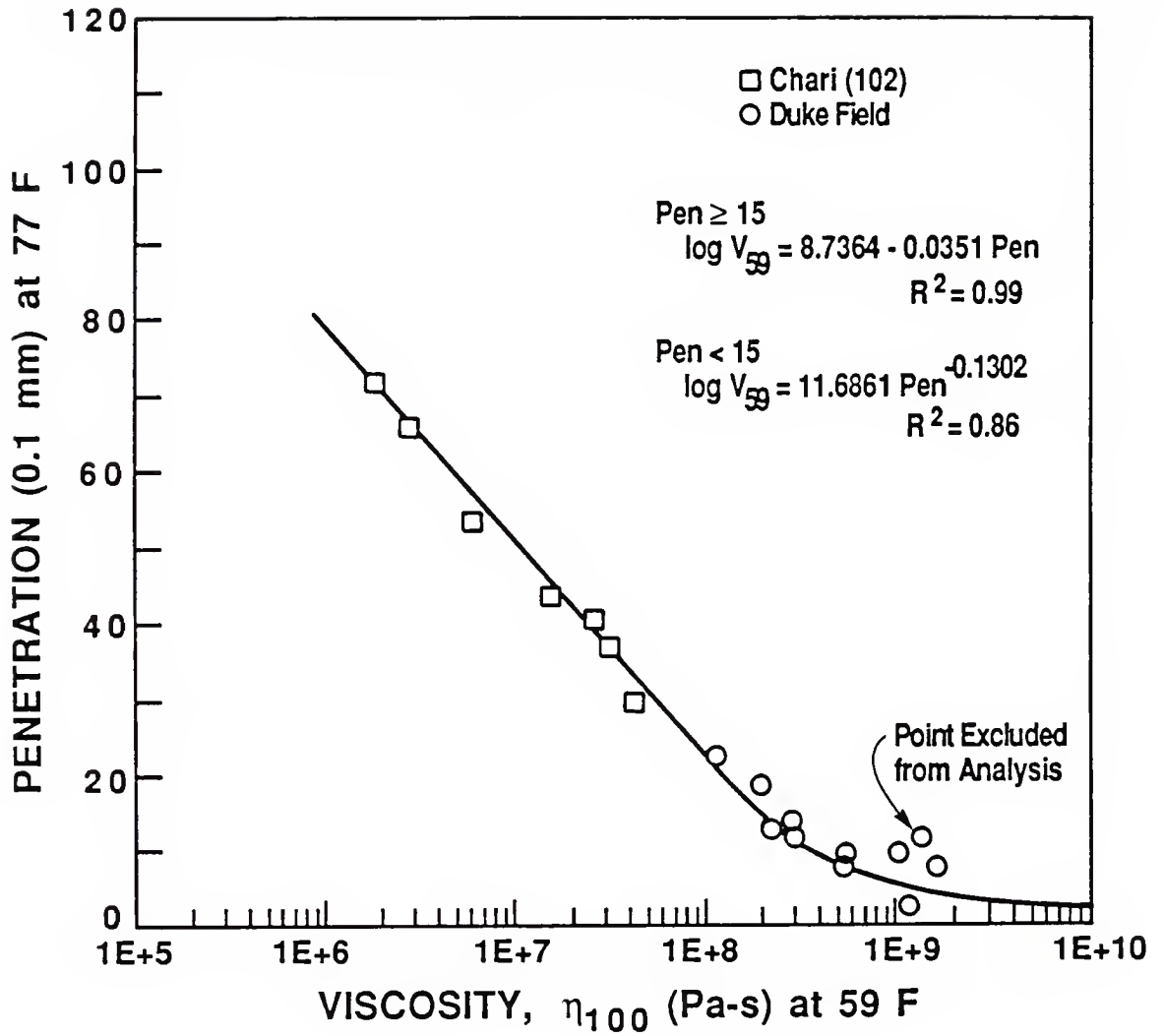


Figure 4.8 Relationship Between Penetration at 77 F and Constant Power Viscosity at 59 F

measured penetration. Measured and predicted values of viscosity are given in Appendix D.

At 60 C (140 F)

$$\log V_{140} = 11.2940 \text{ Pen}^{-0.2872}, \text{ poises} \quad (4.1)$$

$$(N = 20 \quad R^2 = 0.8950)$$

At 25 C (77 F)

$$\log V_{77} = 11.4325 \text{ Pen}^{-0.1683}, \text{ Pa-s} \quad (4.2)$$

$$(N = 23 \quad R^2 = 0.9550)$$

At 15 C (59 F) Pen > 15

$$\log V_{59} = 8.7364 - 0.0351 \text{ Pen}, \text{ Pa-s} \quad (4.3)$$

$$(N = 9 \quad R^2 = 0.9879)$$

At 15 C (59 F) Pen < 15

$$\log V_{59} = 11.6861 \text{ Pen}^{-0.1302}, \text{ Pa-s} \quad (4.4)$$

$$(N = 11 \quad R^2 = 0.8644)$$

Absolute viscosity data were also regressed using equation 4.5 developed by Ruth and Miller (101). The results of this analysis are shown as a dashed line in Figure 4.6. The computed R^2 value of 0.92 was near the value of 0.90 obtained by equation 4.1.

$$V_{140} = 0.0332 \left(\frac{6000}{\text{Pen}} \right)^{2.57}, \text{ poises} \quad (4.5)$$

$$(N = 20 \quad R^2 = 0.9178)$$

Estimated viscosities can be used in other predictive equations to obtain asphalt concrete properties such as the elastic modulus and fracture energy. Care must be taken, however, when using empirical correlations and estimated viscosities should be verified using a theoretical method (e.g., Schweyer rheometer).

The lack of information on the grade of asphalt cements used in constructing pavements at Duke Field made it necessary to assume the grade of asphalt for estimation of binder hardening. Historically, penetration graded asphalts around 50 to 60 pen and viscosity graded asphalts equal to an AC-20 (2,000 poises at 60 C (140 F)) are commonly specified for airport design (103). Assuming a five-fold increase in viscosity caused by plant hot-mix and construction operations, the initial in-service absolute viscosity would be around 10,000 poises. Based on these assumptions, absolute viscosities have increased from three to 200 times the assumed original values. In those instances where the absolute viscosity was estimated, increases in hardening were even greater.

Another indication as to the amount of hardening that has occurred is through the use of constant power viscosity at typical ambient temperatures. In Figure 4.9, constant power viscosity at 25 C (77 F) is plotted against exposure time. Exposure time is the amount of time the asphalt layer remains exposed to the surface. Two lines are shown representing the extreme maximum and minimum hardening rates which were taken from previous equations developed by Ruth et al. (81). These equations were used to back-project to the constant power viscosity values at the end of construction. Predicted viscosities ranging between 200,000 and 300,000 Pa-s corresponded to original values measured by Ruth et al. (81). The use of the prediction equations to compute the rate of hardening for the Duke Field asphalts appeared reasonable considering that no other information was available. From the data in Figure 4.9, two observations can be made: 1) binder hardening is time dependent, and 2) the rate of hardening increases with higher air void content.

How much effect air voids have on viscosity is difficult to say with the limited information given. The influence of exposure on asphalt hardening becomes apparent when comparing the second asphalt concrete layer at site 2 (2AC-2) with the top courses at all three sites in Table 4.3. It is interesting to note the relatively low absolute viscosity of this layer (85,210 poises) even though it shows the highest air void content (11.9 percent). The author attributes this phenomenon to the overlaying of this layer only one year after its placement, where its exposure to ultraviolet radiation and other environmental factors was limited. Given identical environmental conditions another comparison of age hardening was made involving layer

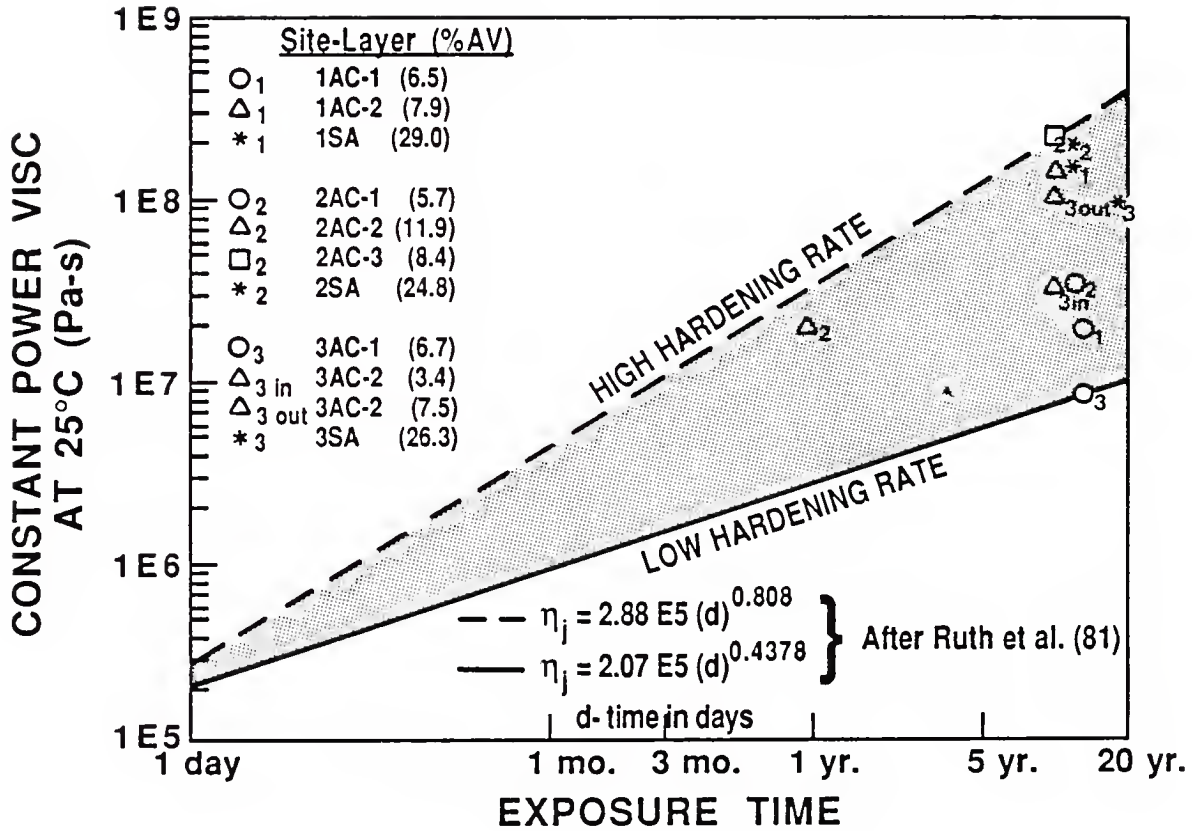


Figure 4.9 Range of Hardening for the Asphalt Cements

3AC-2. The binder outside the wheel path shows over 3.5 times the amount of hardening at 60 C (140 F) than does the material inside the wheel path. A plausible reason for this is that the air void content outside the wheel path is 7.5 percent while it is only 3.4 percent in the wheel path, thereby demonstrating the possible effects of oxidation on asphalt hardening.

4.7 Asphalt Viscosity Testing Using the Schweyer Constant Stress Rheometer for the Determination of Temperature and Shear Susceptibility

4.7.1 Background

The Schweyer Constant Stress Rheometer was designed to determine the low-temperature rheological properties of asphalt cements at shear rates approximating those encountered in the field. Traditional creep tests require much higher stresses or longer loading times to obtain results in a reasonable period of time. The use of higher stresses produces shear rates which may or may not be proportional to the imposed stress. This means that a bitumen may exhibit Newtonian-like flow or behave as a shear susceptible material (dilatant or pseudoplastic) depending on the stress imposed. Since asphalt cements normally behave pseudoplastically at low temperatures and strain rates, the use of such creep tests could produce significant errors in predicting rheological behavior, especially at low temperatures (< 25 C (77 F)). For a complete study of asphalt rheology and use of the Schweyer Constant Stress Rheometer, refer to Teng (63).

4.7.2 Equipment and Test Procedures

The Schweyer rheometer used in this study consisted of 1) a nitrogen operated gas cylinder which applied a specified force to the plunger

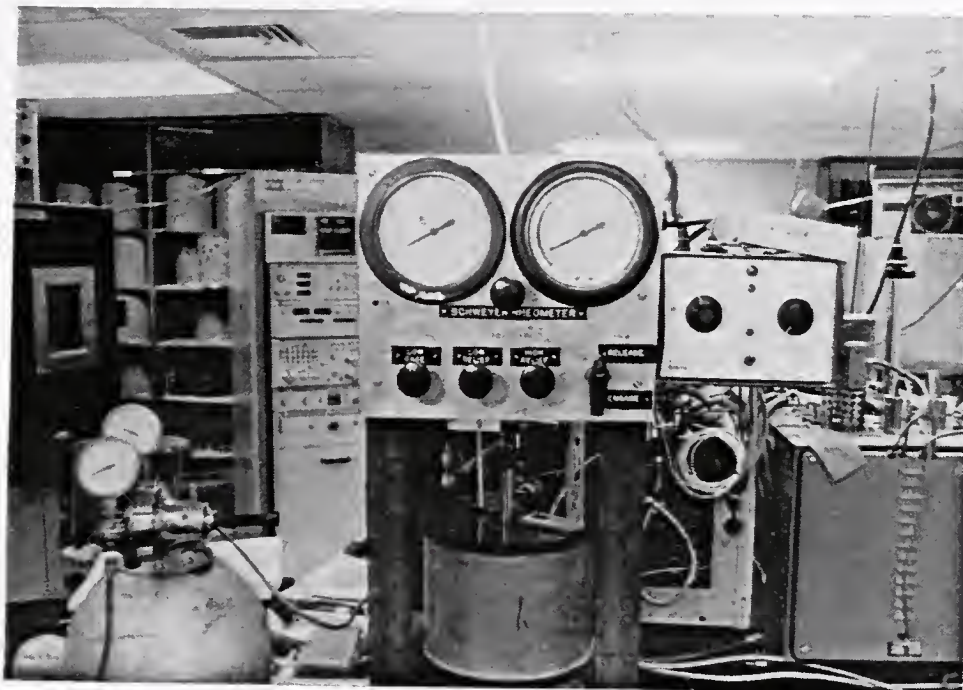
in the sample tube and 2) a LVDT (Linear Variable Differential Transducer) which measured the vertical displacement of the plunger. The LVDT was hooked up to a an IBM System 9000 personal computer for interpretation. The plunger force was set by adjusting the pressure of the nitrogen gas going into the pneumatic cylinder. Pressures were determined by one of two pressure gages. The low pressure gage was read for pressures below 15 psi while the high pressure gage was used for pressures above 15 psi.

The sample tubes were placed three at a time in the insulated aluminum block which was cooled by circulating coolant from a refrigeration unit. The desired test temperatures were maintained by an electrical core heater in the block which is controlled by presetting the electrical temperature control unit. Temperatures were read with a standard glass thermometer placed in the remaining sample hole. The entire system is pictured in Figure 4.10.

4.7.3 Data Acquisition and Analysis

Samples from every bituminous layer were tested in the Schweyer rheometer. Due to the tremendous range of binder hardness, a wide temperature band was selected for testing, namely, from 10 C (50 F) to 55 C (131 F) at 5 C increments. Five stress levels were used for each test with magnitudes depending on the relative hardness of the material. Gage pressures of 90, 70, 50, 30, and 20 psi were normally applied to the samples and when appropriate reduced to accommodate softer materials. Care was taken not to overstress the material and induce plug flow.

Two types of rheometer tubes (Figure 4.11) were used throughout the testing. The first type incorporated the use of a capillary while the



a) Schweyer Rheometer



b) IBM 9000 Computer

Figure 4.10 The Schweyer Rheometer Test System

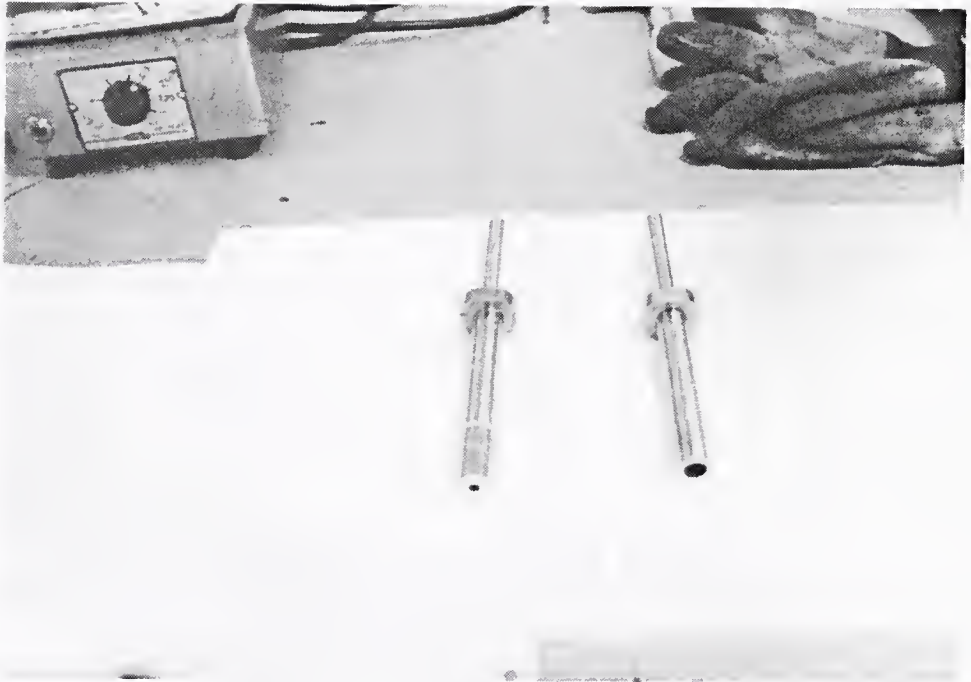


Figure 4.11 F-Tube (left) and G-Tube

second was a straight plug tube with a uniform diameter. The capillary tube chosen was an F-tube which had a capillary diameter of 4.78 mm. This tube which represented the largest diameter capillary available, was used at warmer temperatures when the asphalt cement displayed seemingly good flow characteristics. When flow became too minute to measure accurately (< 1 mm at 20 psi), the F-tube was replaced with the G-tube. The G-tube had a plug diameter of 9.53 mm. Testing stopped when flow in this tube became negligible at 5 C (41 F) for the softest asphalt.

As mentioned earlier, an IBM 9000 PC collected, stored, and graphically displayed the data received from the LVDT along with user inputs for test and tube designation, applied force, initial sample height, and test temperature. A computer program SCHWY3A developed by Dr. Mang Tia, University of Florida, stored the input information and graphically recorded the deformation-time plot on the screen immediately after each preset two-minute test interval. This allowed for the option of proceeding with the next stress level or redoing the last sequence if required.

The test data from the Schweyer rheometer were analyzed using another computer program SCHWY4A developed by Tia. This program called up the information from SCHWY3A and allowed for the insertion of slope data along with last minute load corrections. It then proceeded to plot the log of shear stress versus the log of shear rate. SCHWY4A also calculated the shear susceptibility (C) from the slope of the best fit line through the data points. The following regression equation was used to relate shear stress (τ) to shear rate ($\dot{\gamma}$).

$$\log \tau = A + C \log \dot{\gamma} \quad (4.6)$$

where

$$A = \log \eta_{1.0}$$

$\eta_{1.0}$ = apparent viscosity at shear rate $\dot{\gamma} = 1.0/\text{sec}$

The SCHWY4A program calculated the viscosity at shear rates equal to $\eta_{1.0}$ (1.0 sec^{-1}) and constant power viscosity η_j ($j=100 \text{ Watts/m}^3$). It also enabled the user to delete suspect data to improve correlations. Final plots and computations of viscosities were then printed out.

4.7.4 Relationship Between Viscosity and Temperature

The viscosity-temperature relationship of the asphalt cements was of primary importance for establishing binder viscosities corresponding to pavement temperatures measured during NDT. These viscosities were correlated to the resilient and fracture characteristics of the asphalt mixtures and used in subsequent pavement stress analysis.

Viscosity measurements at one temperature only are usually not sufficient to define the low temperature rheological behavior of bitumens. Therefore, it is often desirable to obtain test results at different temperatures by plotting the log of apparent viscosity with the log of temperature. The plot can be based on any desired shear rate although best results are achieved using constant power viscosity. The apparent viscosity at a constant power of 100 Watts/m^3 can be computed as

$$\eta_j = \eta_{1.0} \left(\frac{100}{\eta_{1.0}} \right)^{\frac{C-1}{C+1}}, \text{ Pa-s} \quad (4.7)$$

where

$$\begin{aligned}
 j &= \tau_j \dot{\gamma}_j = 100, \text{ constant power input, Watts/m}^3 \\
 \eta_j &= \eta_{100}, \text{ constant power viscosity, Pa-s} \\
 \eta_{1.0} &= \text{viscosity at } 1.0 \text{ sec}^{-1}, \text{ Pa-s} \\
 C &= \text{shear susceptibility (complex flow)}
 \end{aligned}$$

Regression analyses were performed to establish the linearity of the test data using equation 4.8.

$$\log \eta_{100} = b_0 + b \log K \quad (4.8)$$

A linear relationship was also established between $\log (\eta_{100})$ and degrees C using the above equation and is presented graphically in Figure 4.12 for each bituminous layer. The data shown are more dispersed at high temperatures because of the lower temperature susceptibility of some of the older layers. Most layers, however, exhibited similar temperature susceptibility, although relative viscosities at a specific temperature differed up to more than a factor of ten. Values of R^2 for the asphalt concrete layers ranged between 0.98 and 1.00 while for the sand asphalt values were between 0.92 and 1.00. All of the test data including measured viscosities, derived equations, R^2 values, and shear susceptibility factors are given in Appendix E.

Since the asphalts demonstrated linearity, predicted values were extrapolated down to 0 C (32 F). Extrapolation was required because direct measurements were impossible due to the extremely brittle nature of the recovered asphalts.

As previously stated in the literature review, the asphalt concrete mix resilient and creep properties appear dependent on viscosity values,

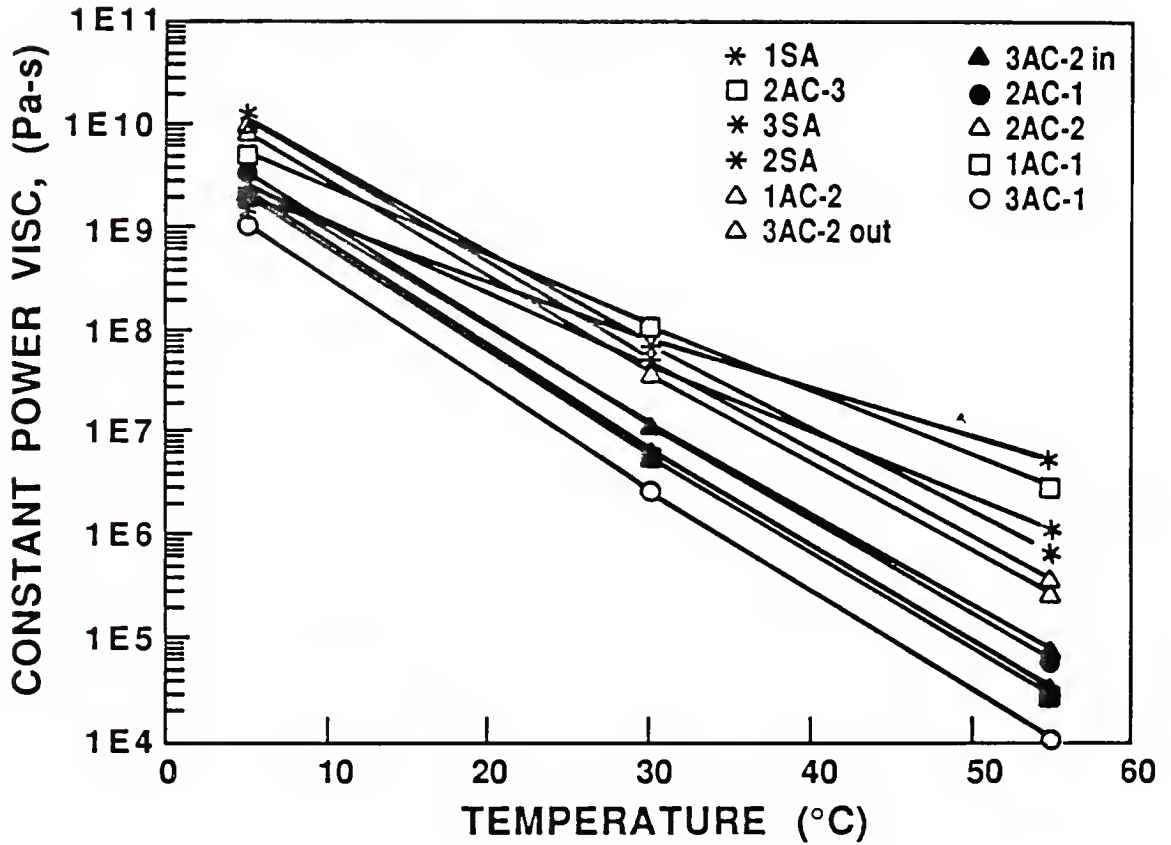


Figure 4.12 Temperature Susceptibility Curves for the Asphalt Cements

especially at low temperatures. Ruth et al. (36) offered the following equations which relate the dynamic resilient modulus ($E_{0.1}$) to constant power viscosity (η_{100}).

For $\eta_{100} < 9.19E+08$ Pa-s

$$\log E_{0.1} = 7.18659 + 0.30677 \log \eta_{100}, \text{ Pa} \quad (4.9)$$

For $\eta_{100} > 9.19E+08$ Pa-s

$$\log E_{0.1} = 9.51345 + 0.04716 \log \eta_{100}, \text{ Pa} \quad (4.10)$$

These equations were derived for dense-graded mixtures subjected to a haversine loading time of 0.1 sec.

4.8 Diametral Testing of Bituminous Field Samples

4.8.1 General

The diametral testing program included a thorough evaluation of asphalt concrete and sand asphalt mix properties. Three types of diametric tests were performed including 1) the dynamic resilient modulus test, 2) the indirect tensile test (quick), and 3) the static creep test for fracture energy. Test results are analyzed and presented in Chapter 5.

The resilient moduli tests were conducted to determine the elastic behavior of the core specimens and its relationship with viscosity and the air void content. Indirect tensile tests were used to acquire the maximum strength of the asphalt mixtures at 25 C (77 F). Static creep

tests were performed to assess the fracture energy characteristics of the asphalt concrete which included failure strain and creep rate. Moreover, these tests were done to developed the relationship between fracture energy, viscosity, and air void content.

4.8.2 Laboratory Equipment

Diametral nondestructive and destructive testing were conducted with the MTS (Materials Test System). Resilient modulus and static creep tests were performed using the newly commissioned MTS located at the University of Florida (UF) while the indirect tensile tests were accomplished at the FDOT. Although the UF system was newer, both devices had similar electrical consoles, loading capacities, and operating procedures.

The MTS consisted of four components: loading system, electronic control console, recording system, and temperature control system. The UF MTS is shown in Figure 4.13.

4.8.2.1 Loading System. The MTS loading system consisted of a load and support frame, an actuator operated by a servovalve, a 10 metric ton (22,000 lbs.) capacity load cell, and a diametral loading frame. The loading frame assembly is illustrated in Figure 4.14.

4.8.2.2 Electronic Control Console. The electronic control console (Figure 4.15) provided automatic control of the loading machine. It included a servo control unit, cycle counter, wave function generator and a pulse sequence for repetitive load applications, and transducer conditioners to monitor load magnitude and actuator position.

4.8.2.3 Recording System. Applied load, actuator stroke, and horizontal strain or displacement could be measured and recorded on the



Figure 4.13 Machine Test System (MTS)

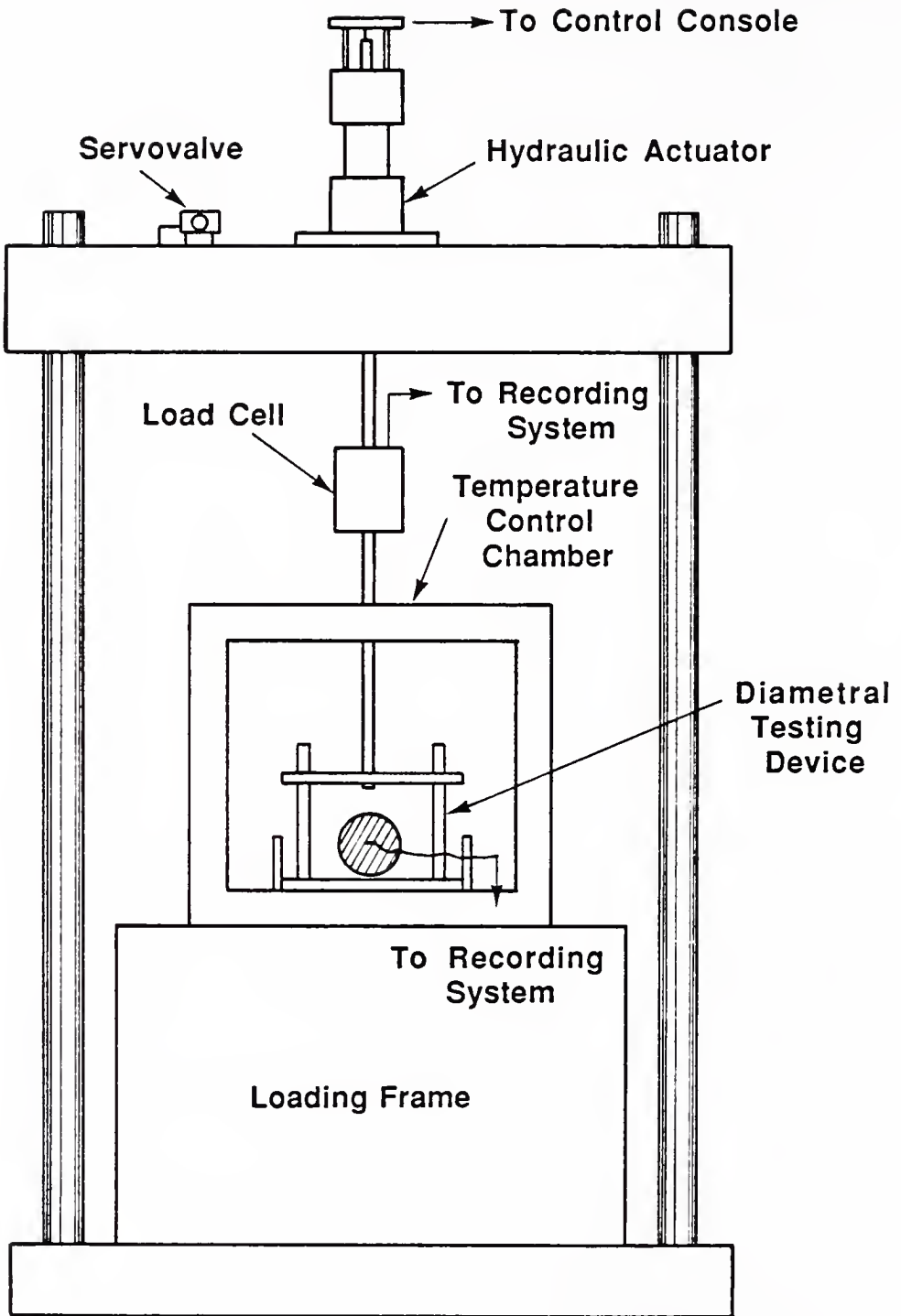


Figure 4.14 Loading System



Figure 4.15 Electronic Control Console

MTS X-Y plotter or external strip chart recorder. With the aid of an externally mounted signal conditioner, strains down to one micro strain (10^{-6} in./in.) could be detected. The recording system (Figure 4.16) was calibrated so that 1 mm of displacement on the chart equaled 4 micro strain from the specimen.

4.8.2.4 Temperature Control System. Tests were performed in a well-insulated chamber which allowed easy access for specimen placement and a clear view for inspection. Heat was provided by two open element heaters while cooling was done by liquid nitrogen which fed through a solenoid valve to regulate its flow. Air was circulated by means of an electric fan which ran continuously during testing. Temperature control of ± 1 F was accomplished through the use of a type J thermocouple placed inside the chamber which ran to a digital controller located on the electronic console. Internal core temperatures were measured with a Fluk T80-150 temperature probe placed inside the center of a dummy specimen. In this way, temperature equilibrium was assured before testing began. Figure 4.17 shows the temperature control chamber with external probe attached to the dummy sample.

4.8.3 Preparation of Test Specimens

Core samples initially required surface smoothing to eliminate protrusions of exposed aggregate. Once prepared, 0.5 in., 120 ohm strain gages were bonded on both sides of the core parallel to each other. This aided in revealing the possible effects of load eccentricities, inadequate bonding, and aggregate concentration at the core center. It also served to average the strains across the specimen. This is warranted due to the inherent experimental errors induced in conducting diametral tests.

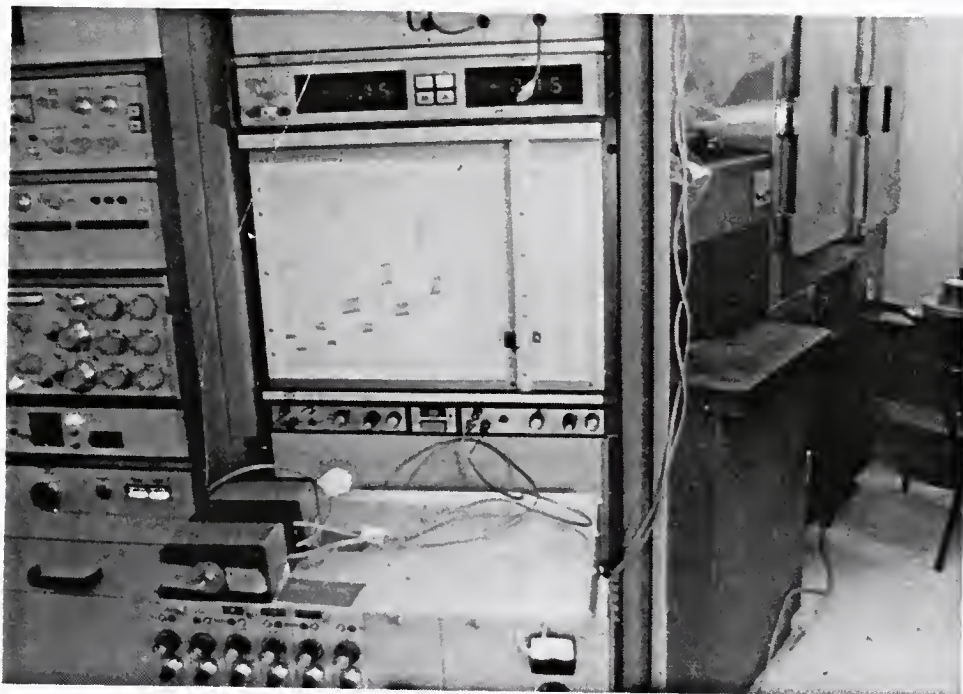


Figure 4.16 Recording System

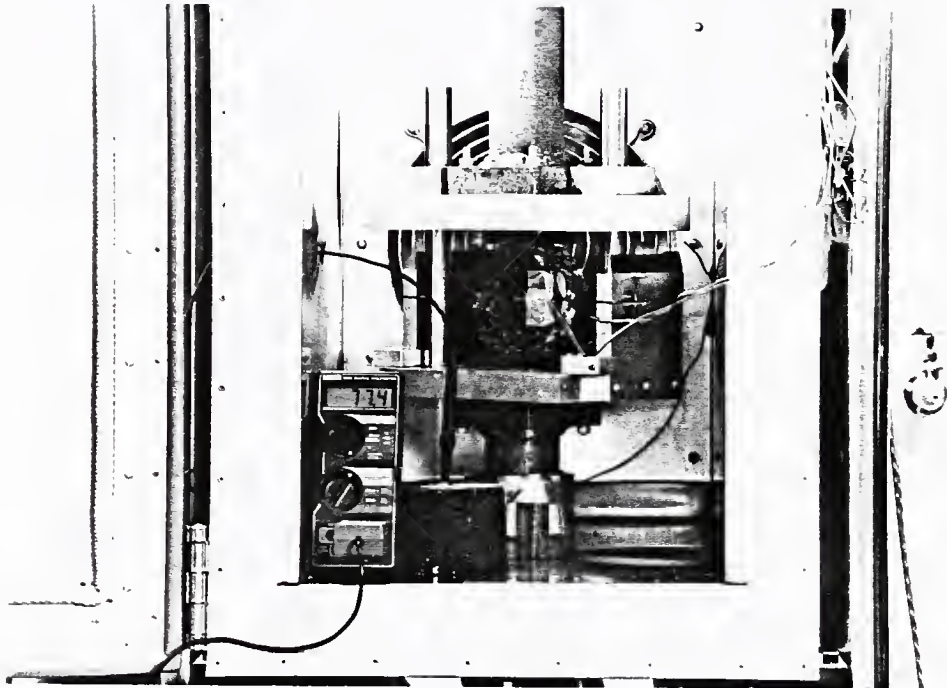


Figure 4.17 Temperature Control Chamber with Dummy Sample and Thermal Probe

Once the strain gages and wire leads were attached and bridge circuit connections made, the specimen was placed in the loading frame as illustrated in Figure 4.18. The strain gages were positioned horizontally, checked for alignment, then wired to the signal conditioner. The chamber temperature was then brought to the appropriate level and the specimen allowed to thermally stabilize. When equilibrium was achieved, the strain gages were calibrated using the signal conditioner in accordance with procedures set forth for a quarter bridge circuit (104). Once the calibration was done, testing commenced.

4.8.4 Preconditioning of Test Specimens

A small static preload (5-10 psi) was applied to each sample to eliminate errors caused by uneven contact on the loading strip which stemmed from surface irregularities. Temperatures chosen for preconditioning corresponded to η_{100} values of between 5 and 10 million Pa-s, as determined from the viscosity-modulus relationship given by equation 4.9.

Nonrecoverable creep of approximately 100 micro strain for the asphalt concrete and 40 micro strain for the sand asphalt was permitted. The preload was applied between 3 and 12 minutes depending on the creep rate. Preconditioning of the sand asphalt, however, was discontinued due to its extreme brittle nature that resulted in the failure of some samples.

The load was removed after the appropriate strain was achieved and the specimen was allowed to elastically recover before beginning the dynamic tests. A typical creep response curve is shown in Figure 4.19.

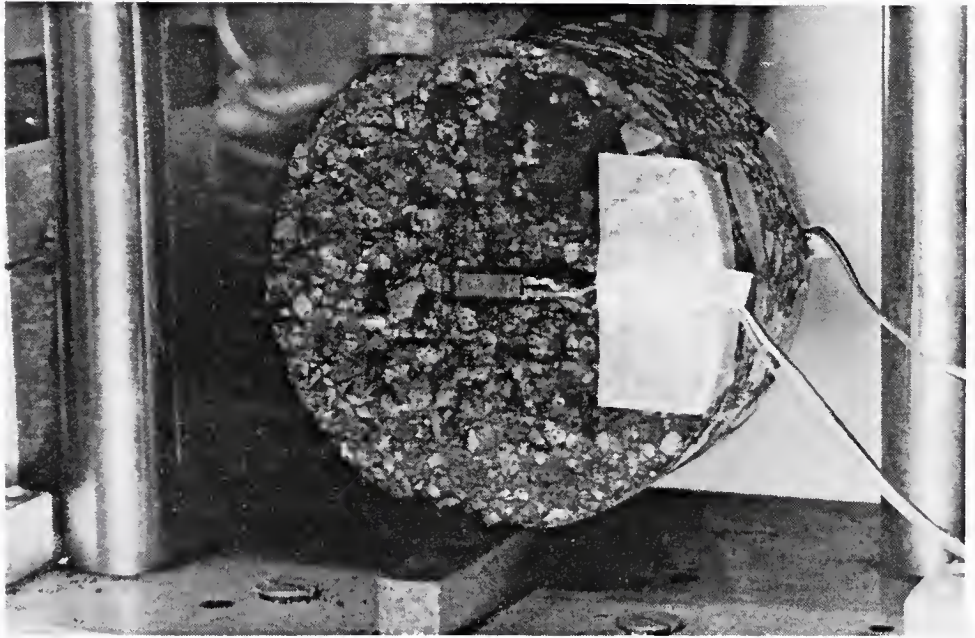


Figure 4.18 Strain Gaged Sample Ready for Indirect Tensile Testing

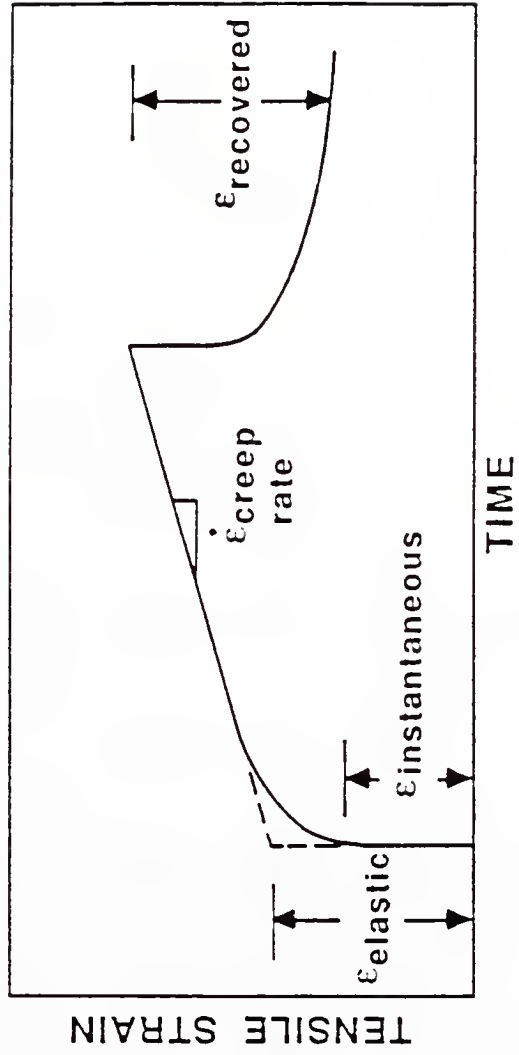


Figure 4.19 Typical Creep Response Curve for Asphalt Concrete

4.8.5 Dynamic Resilient Modulus Test

The resilient modulus is defined as the ratio of applied stress to resilient strain (recoverable strain). Essentially, it is the dynamic elastic modulus of a viscoelastic material, i.e., its stress-strain response is time dependent. Resilient testing described in this section is based on the fact that for short loading durations the response is mainly elastic (105). When incorporating strain gages to measure horizontal strains, an assumption of a line load condition exists and the resilient modulus can be obtained directly from the slope of the stress-strain curve.

Since a limited number of samples were available, it was first decided to conduct nondestructive testing to obtain the resilient properties of the bituminous mixtures. Because of this, certain assumptions were made regarding the maximum tensile strength of the asphalt concrete and the sand asphalt. A value of 200 psi at 25 C (77 F) was chosen for the asphalt concrete based on results obtained by Ruth et al. (106) for 1.5-in. thick field cores. For the sand asphalt, a maximum tensile strength of 50 psi was estimated from an inadvertent failure of a specimen during preloading. The maximum operating stresses for the resilient modulus test were selected as 30 percent of the maximum tensile strengths or 60 and 15 psi, respectively, for the asphalt concrete and sand asphalt. Stresses between 20 and 40 percent of the maximum can be used for testing without loss in linearity of the stress-strain data (106).

A repetitive stress-controlled compressive load was applied along the vertical diameter of the sample using a 0.1 sec on - 0.4 sec off haversine loading. Five stress levels were chosen, each about 40 cycles

in duration. Normally, three temperatures were selected for each specimen corresponding to predicted moduli values of 250,000, 500,000, and 1,000,000 psi as determined from the viscosity-temperature-modulus relationships presented in section 4.7 and Appendix E.

During testing, dynamic strains for the two gages were recorded on the MTS X-Y plotter by alternating between them via a toggle switch. This reciprocating procedure resulted in no loss of accuracy to the plotter. Total resilient strains were measured by the gages which included the delayed elastic recovery. Kennedy (107) described two measurements used to quantify elastic strain or deformation: instantaneous and total which yield instantaneous and total resilient moduli, respectively. Often times, it is difficult to distinguish the two, and therefore, the use of total values is preferred. Ruth et al. (106) discovered that little additional delayed recovery occurs after 0.4 sec relaxation for a 0.1 sec loading. Consequently, the use of a 1:4 load to relaxation ratio is adequate for the evaluation of total resilient moduli.

4.8.6 Indirect Tensile Test (Quick)

As traffic is applied to a pavement, the bottom of the asphalt layer is subjected to radial and tangential stresses. The indirect tensile test offers a quick, practical way to determine the ultimate stress the pavement can withstand during a nonrepetitive loading scenario. The theory of the test assumes an isotropic and homogeneous material behaving linear elastically (73). At a fast rate of loading (up to 2.68 in. per minute) a bituminous mixture shows a reasonable elastic response.

During this study, indirect tensile tests were conducted by the FDOT on eleven asphalt concrete and twelve sand asphalt specimens. A compressive load was applied at the constant rate of 2.0 in. per minute until failure. The strip chart recorder registered horizontal and vertical deformation, and applied load. The tensile strength (S_t) was calculated based on the following equation presented by Mamlouk (73):

$$S_t = \frac{2P_{max}}{\pi t d} \quad (4.11)$$

where

P_{max} = load at failure

t = thickness of specimen

d = diameter of specimen

Poisson's ratio was computed from the equation 4.12 (106).

$$\mu = 3.59 \frac{dh}{dv} - 0.27 \quad (4.12)$$

where

dh = horizontal deformation at failure

dv = vertical deformation at failure

4.8.7 Static Creep Test (Fracture Energy)

Indirect static creep tests were used to determine asphalt mixture parameters as fracture energy, failure creep strain, strain rate, and creep modulus. These parameters were evaluated and correlated with asphalt and mix properties such as viscosity and air void content.

Ruth et al. (46) inferred that fracture energy is perhaps the best approach in defining failure in asphalt concrete mixtures. Defined as the area under the stress-strain curve, fracture energy (F_E) is related to constant power viscosity using the following equation developed by the above researchers:

$$\log F_E = 6.3244 - 0.3277 \log \eta_{100}, \text{ Pa} \quad (4.13)$$

Tests were performed on 13 airfield specimens representing every asphalt concrete layer. Tests on sand asphalt proved unsuccessful because creep strains could not be developed at the low stresses required. Temperatures selected for testing ranged between -5 C (23 F) and 15 C (59 F) which related to η_{100} values between 10^8 and 10^{11} Pa-s. Difficulty arose in choosing the optimum stress at which to conduct the tests for the various asphalt types. Stresses were selected from estimated tensile strengths and from resilient moduli to allow 30 minutes of creep before the initiation of failure. Generally, a value around 60 percent of the anticipated maximum tensile strength is chosen to conduct such fracture tests.

CHAPTER 5 RESULTS AND ANALYSES OF DIAMETRAL TESTING

5.1 Introduction

Results obtained from diametral resilient modulus, indirect tensile, and static creep tests are presented and analyzed in this chapter. Results of the laboratory measured data are given in Appendix F. First discussed, is the dynamic elastic response of the in-service cores at various test temperatures. Correlations between modulus, viscosity, and air void content are then established. Next, maximum tensile strengths at 25 C (77 F) are tabulated and compared to determine the effects of viscosity and air void content. Finally, fracture energies from static creep tests are presented to provide additional insight into the failure characteristics of these pavements.

5.2 Dynamic Resilient Modulus

Resilient modulus ($E_{0.1}$) values were calculated from the tensile stress equation 4.11, modified to incorporate the horizontal strain (ϵ_x).

$$E_{0.1} = \frac{2P}{\pi t d \epsilon_x} \quad (5.1)$$

Strain response was essentially linear for each stress level. Slight increases, however, were noted in some samples as stresses approached 30 percent of the maximum anticipated strength. Dynamic response produced

considerable scatter between the two strain gages. Therefore, average strain values were used for moduli computations. This dispersion decreased somewhat at lower temperatures due possibly to the reduction in relative hardness between the binder and the aggregate. Slippage or loss of bond among strain gages was rarely observed during testing.

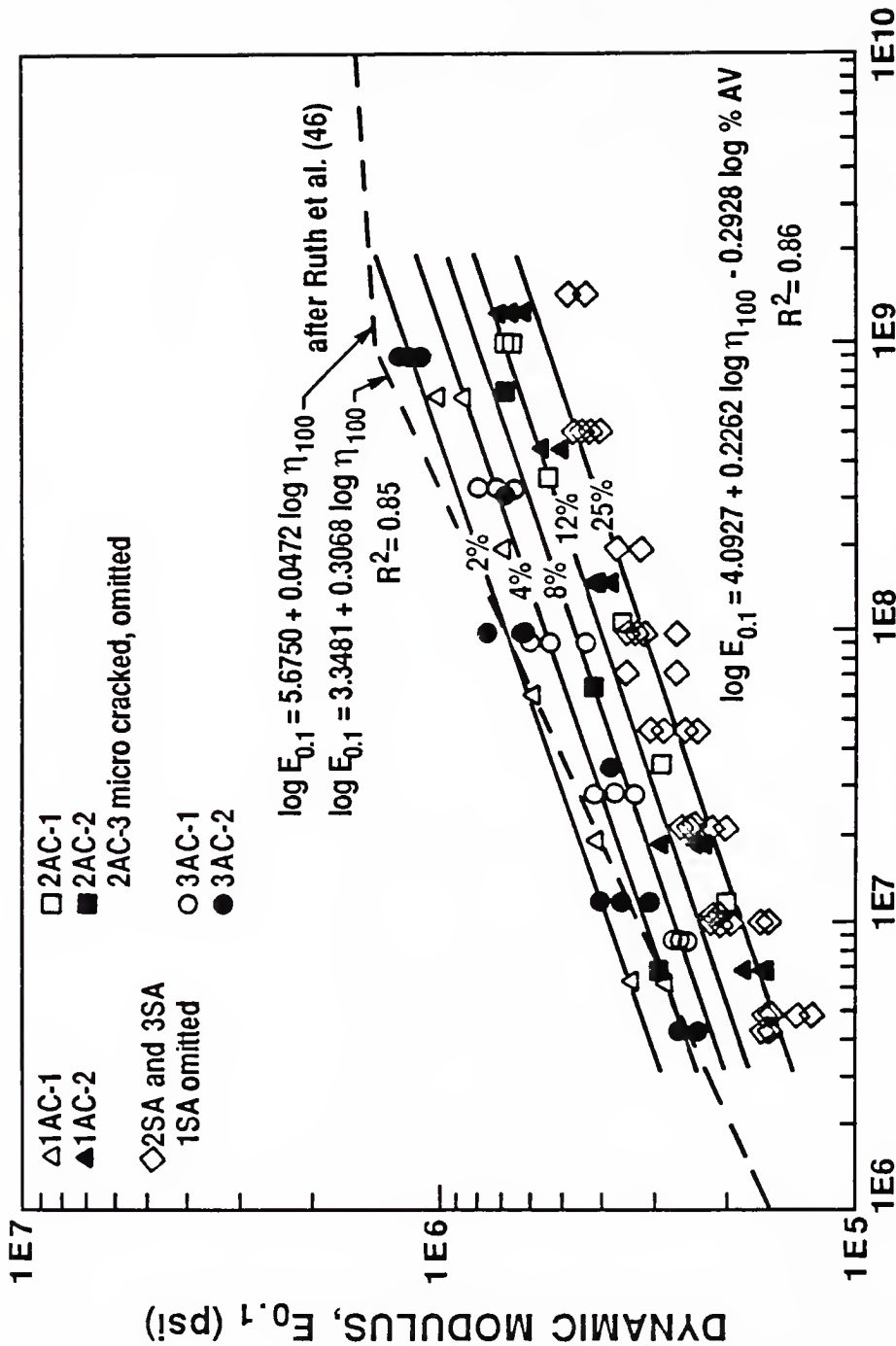
Moduli calculated from the average strain, were plotted against constant power viscosity (η_{100}) for all bituminous layers (Figure 5.1). A multiple regression analysis was performed to determine the correlation of measured moduli with variables as viscosity, and air void content. A suitable relationship between $E_{0.1}$, η_{100} , and % AV for the different mixtures was obtained by regression analysis and given by equation 5.2.

$$\log E_{0.1} = 4.0927 + 0.2262 \log \eta_{100} - 0.2928 \log \% \text{ AV, psi} \quad (5.2)$$

$$(N = 102 \quad R^2 = 0.8635)$$

The data appeared to flatten as η_{100} values rose above 7.0×10^8 Pa-s when compared to previous work done by Ruth et al. (46).

A second plot (Figure 5.2) was made, this time using the slopes from equations 4.9 and 4.10. The data were again regressed to compute new constants and to reestablish the correlation with air voids. Equations 5.3 and 5.4 were derived and used in all subsequent moduli calculations. Equation 5.4 was derived directly from equation 4.10 because so few data points existed above 1.0×10^9 Pa-s to establish a correlation.



CONSTANT POWER VISC, η_{100} (Pa-s)

Figure 5.1 Dynamic Resilient Modulus Test Results

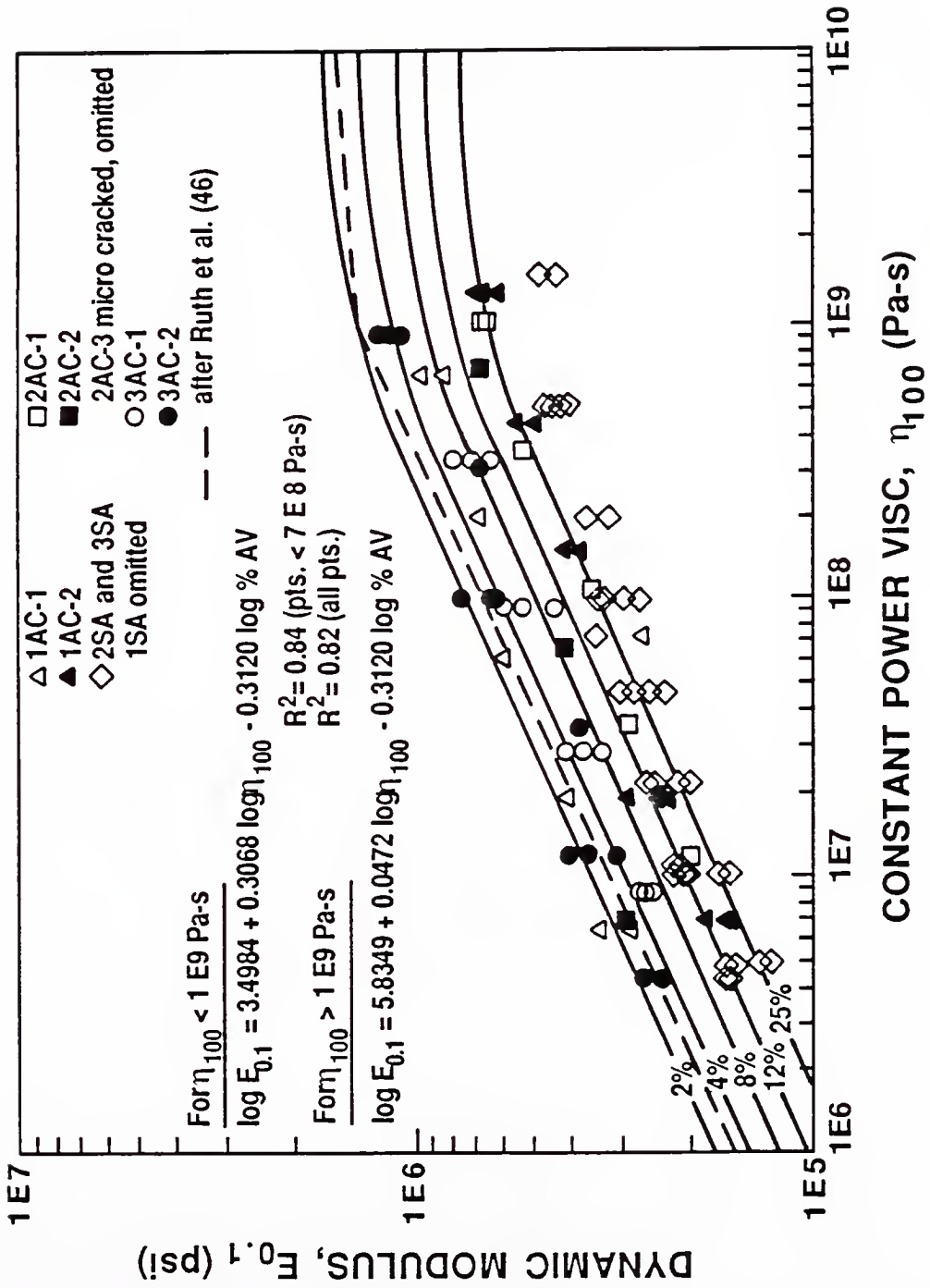


Figure 5.2 Dynamic Resilient Modulus Test Results Using Modified Equations

For $\eta_{100} < 1.0E+09$ Pa-s

$$\log E_{0.1} = 3.4984 + 0.30677 \log \eta_{100} - 0.3120 \log \% AV, \text{ psi} \quad (5.3)$$

(N = 91 R² = 0.8406)

For $\eta_{100} > 1.0E+09$ Pa-s

$$\log E_{0.1} = 5.8349 + 0.04716 \log \eta_{100} - 0.3120 \log \% AV, \text{ psi} \quad (5.4)$$

The upper limit of $E_{0.1}$ is approximately 2.9×10^6 psi for asphalt concrete.

A modulus ratio (MR) was computed for specimens above 4 percent air voids and is presented in Figure 5.3. The MR at a given viscosity is the ratio of the modulus at a particular air void content to the modulus of a dense-graded mixture of 4 percent air voids. Shown in Figure 5.3 are the modulus ratios computed from equation 5.5 and from previous work presented by Ruth et al. (76).

$$MR = 1.49 \% AV^{-0.2856} \quad (5.5)$$

(N = 6 R² = 1.00)

Results on asphalt concrete specimens taken from site 2, layer 3 were excluded from all analyses due to erroneously low moduli values. Values near 40,000 psi suggest that the fracturing of the material occurred prior to testing, and probably took place in the field. This is discussed more extensively in the next section.

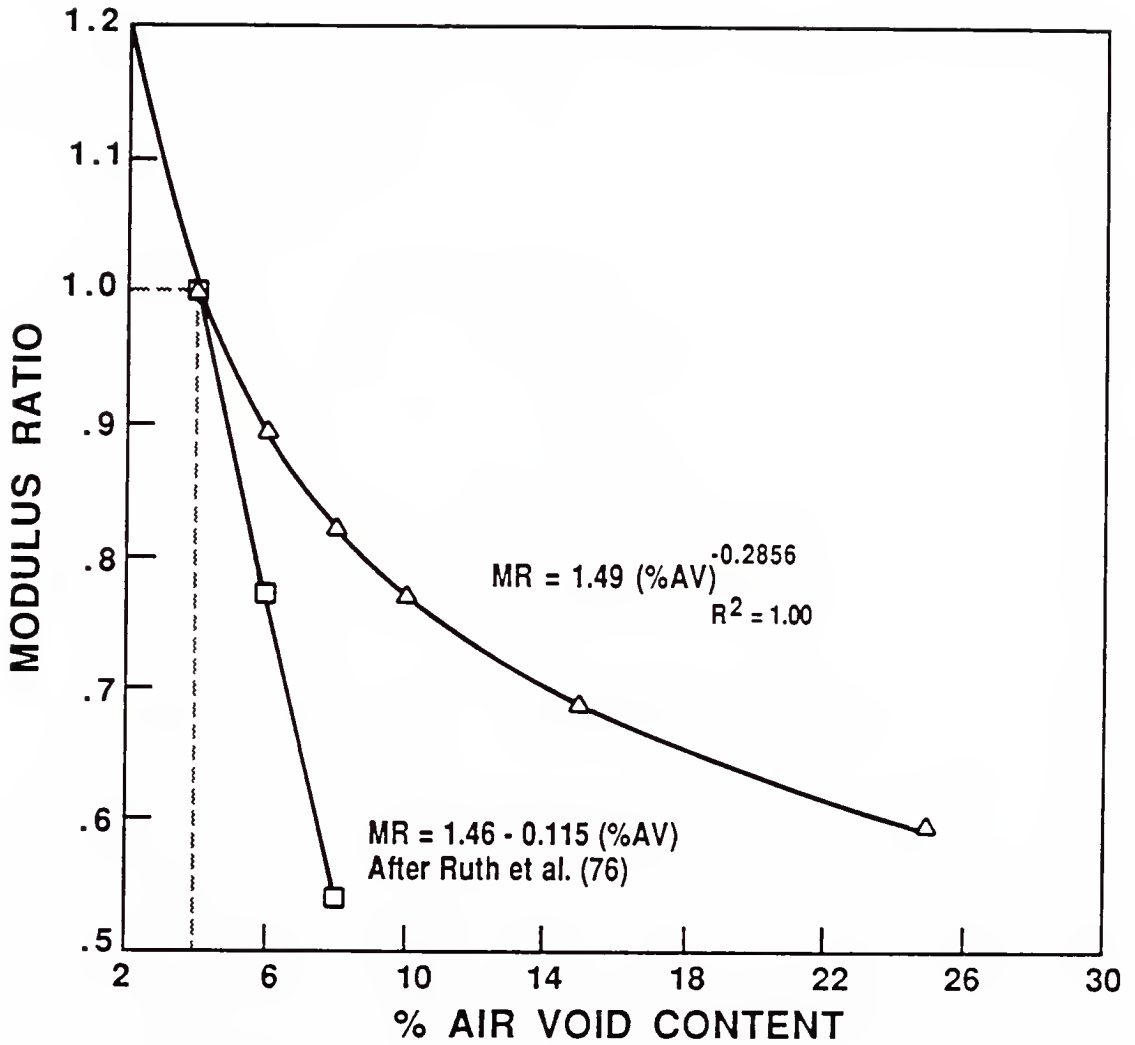


Figure 5.3 Modulus Ratios as a Function of Air Voids

5.3 Tensile Strength

Failure load and vertical and horizontal deformations at failure were measured at 25 C (77 F) using the indirect tensile device. The vertical and horizontal deformations were used to compute the Poisson's ratio. Results are presented in Table 5.1.

The average tensile strength of all asphalt concrete specimens, excluding those from site 2, layer 3, was 211.4 psi. This value approximated the value of 200 psi given by Ruth (106) chosen to compute the maximum allowable stress used in resilient testing. Extremely low strengths came from the bottom asphalt concrete layer at site 2 (2AC-3). The average value of 68.6 psi, along with an erroneously high Poisson's ratio (1.35) and a low resilient modulus, implied a highly compressible, fractured mixture. Paradoxically, layer 1AC-2 built at the same time and of the same mixture as 2AC-3 showed a significantly higher average strength of 201.9 psi, a Poisson's ratio of 0.38, and a higher modulus. The reason for this became clear upon visible inspection of the failed cores. Breakage occurred around the aggregate particles revealing the high presence of fines. Apparently, the loss of strength resulted from stripping action of the asphalt binder caused by water and fines entering the porous mixture. This action decreased the binder-aggregate bonds enough to dramatically reduce the strength of the cores. What made this perplexing was that more visible cracking was observed at site 1 than at site 2. Base officials cited that layer 2AC-3 was severely distressed before its initial overlay in 1973 and subsequent overlay in 1974. The first overlay has, in effect, acted like a buffer by delaying the propagation of reflective cracking to the

Table 5.1 Results From Indirect Tensile Test With Viscosity and Air Void Content at 25 C (77 F)

Site	Type Layer	Layer No.	Indirect Tensile Strength (psi)	Poisson's Ratio at Failure (μ)	Constant Power Viscosity (Pa-s)	Air Voids (percent)
1	AC	1	181.1	0.20 (a)	1.941 E7	7.7
	AC	2	201.9	0.38	1.506 E8	7.7
	SA	-	81.2	0.06	1.552 E8	28.6
2	AC	1	183.7	0.37	3.547 E7	4.5
	AC	2	177.5	0.22	2.109 E7	12.4
	AC	3	66.3	1.40	2.354 E8	8.9
	AC	3	70.8	1.29	2.354 E8	8.9
	SA	-	56.1	0.01	1.984 E8	23.5
	SA	-	57.5	0.09	1.984 E8	23.9
3	AC	1	200.8	0.40	8.683 E6	4.3
	AC	2	286.4	0.42	1.109 E8	4.6
	AC	2	248.7	0.45	1.109 E8	2.9
	SA	-	60.9	-0.05	1.009 E8	21.0
	SA	-	73.0	-0.05	1.009 E8	22.3
	SA	-	60.2	0.11	1.009 E8	21.0
	SA	-	61.9	-0.02	1.009 E8	21.8
	SA	-	54.4	-0.10	1.009 E8	25.9

NOTE

$$a) \mu = 3.59 \frac{dh}{dV} - 0.27$$

surface. Other locations on the airfield stand to suffer like degradation in the near future if restorative action is not soon taken.

Maximum strengths for a specific location were observed at site 3, averaging 245.3 psi. Not surprising, this site had the lowest air void contents and displayed the least amount of visible distress (e.g., cracking and rutting) when compared with the other two sites.

The maximum tensile strength for the sand asphalt averaged 63.2 psi at 25 C (77 F) for all three sites. Since the η_{100} values at this temperature were above 1.0×10^8 Pa-s, this strength was believed to have reached a plateau (106). This demonstrates the extremely brittle nature of the material and its high susceptibility to brittle fracture even at moderate Florida temperatures.

A multiple regression was performed on the data to determine the correlation of tensile strength with constant power viscosity and air void content. Equation 5.6 was developed from the analysis and the results plotted in Figure 5.4. Tensile strength correlated only slightly with viscosity but correlated highly with air voids. This was probably due to the leveling off of tensile strength experienced at constant power viscosities near 1.0×10^8 Pa-s. For example, at 4 percent air voids, the computed tensile strength increased only 14.5 percent between a viscosity of 1.0×10^6 and 1.0×10^9 Pa-s. However, at a viscosity equal to 1.0×10^8 Pa-s, the tensile strength decreased 34.7 percent between 2 and 6 percent air voids and 79.8 percent between 2 and 25 percent air voids.

$$S_t = 291.04 + 10.65 \log \eta_{100} - 224.27 \log \% AV, \text{ psi} \quad (5.6)$$

$$(N = 15 \quad R^2 = 0.8710)$$

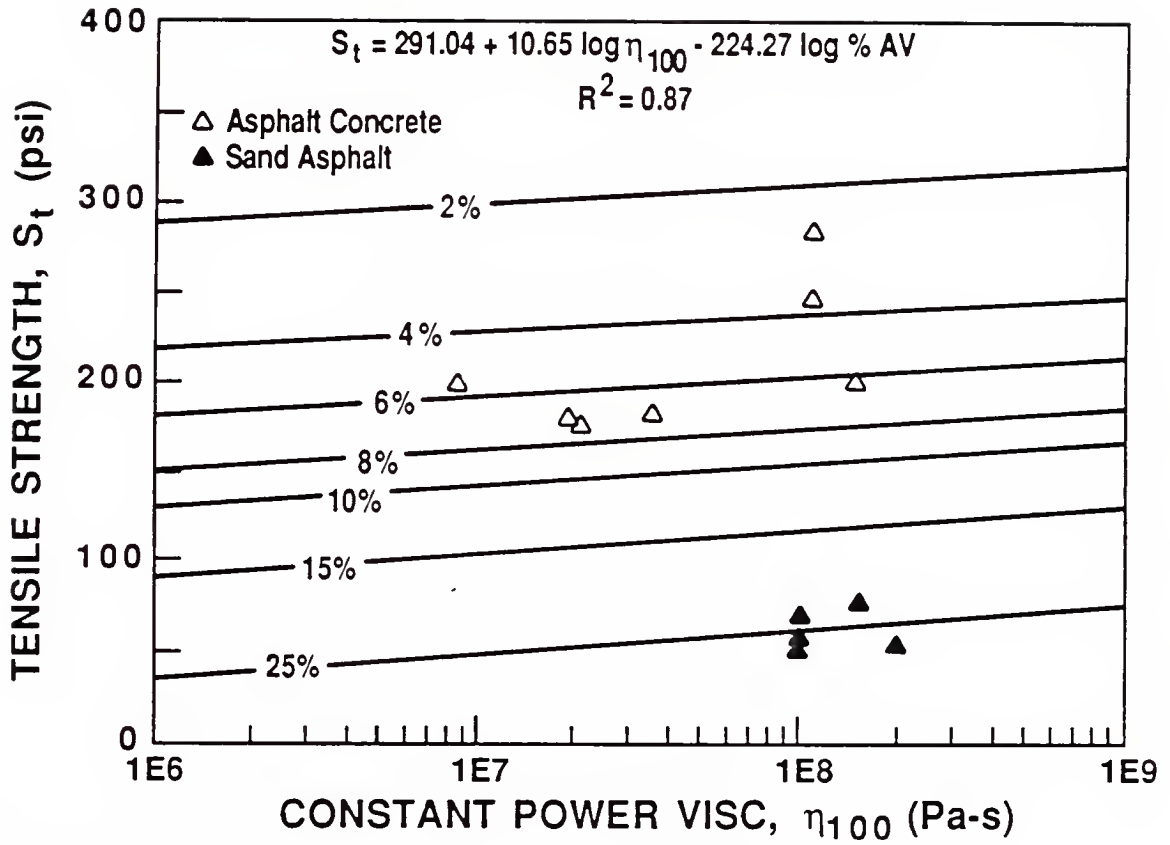


Figure 5.4 Tensile Strength Test Results

5.4 Indirect Static Creep

Static creep tests were performed at different temperatures and stresses to determine the fracture characteristics of the in-service asphalt concrete mixtures. Specimens were loaded under constant stress until failure with strain being recorded with time. From the strain-time curve the following parameters were obtained: initial elastic strain (y-intercept), creep strain rate (slope of curve), and failure strain.

Fracture energy (F_E) was calculated from the failure stress and strain using the trapezoidal formula:

$$F_E = 0.5 \sigma \epsilon_e + \sigma \epsilon_{cr} \quad (5.7)$$

where

σ = applied tensile stress, Pa

ϵ_e = elastic strain

ϵ_{cr} = creep strain (nonrecoverable)

A correlation between fracture energy and constant power viscosity resulted in a low R^2 value of 0.58, caused by appreciable data scatter. However, when inserting air void content into the regression model, the R^2 value increased to 0.76 (equation 5.8). Figure 5.5 shows the plot of $\log(F_E)$ versus $\log(\eta_{100})$ with corrections given for air void content. Also depicted is the fracture energy equation developed by Ruth et al. (46) for laboratory compacted samples.

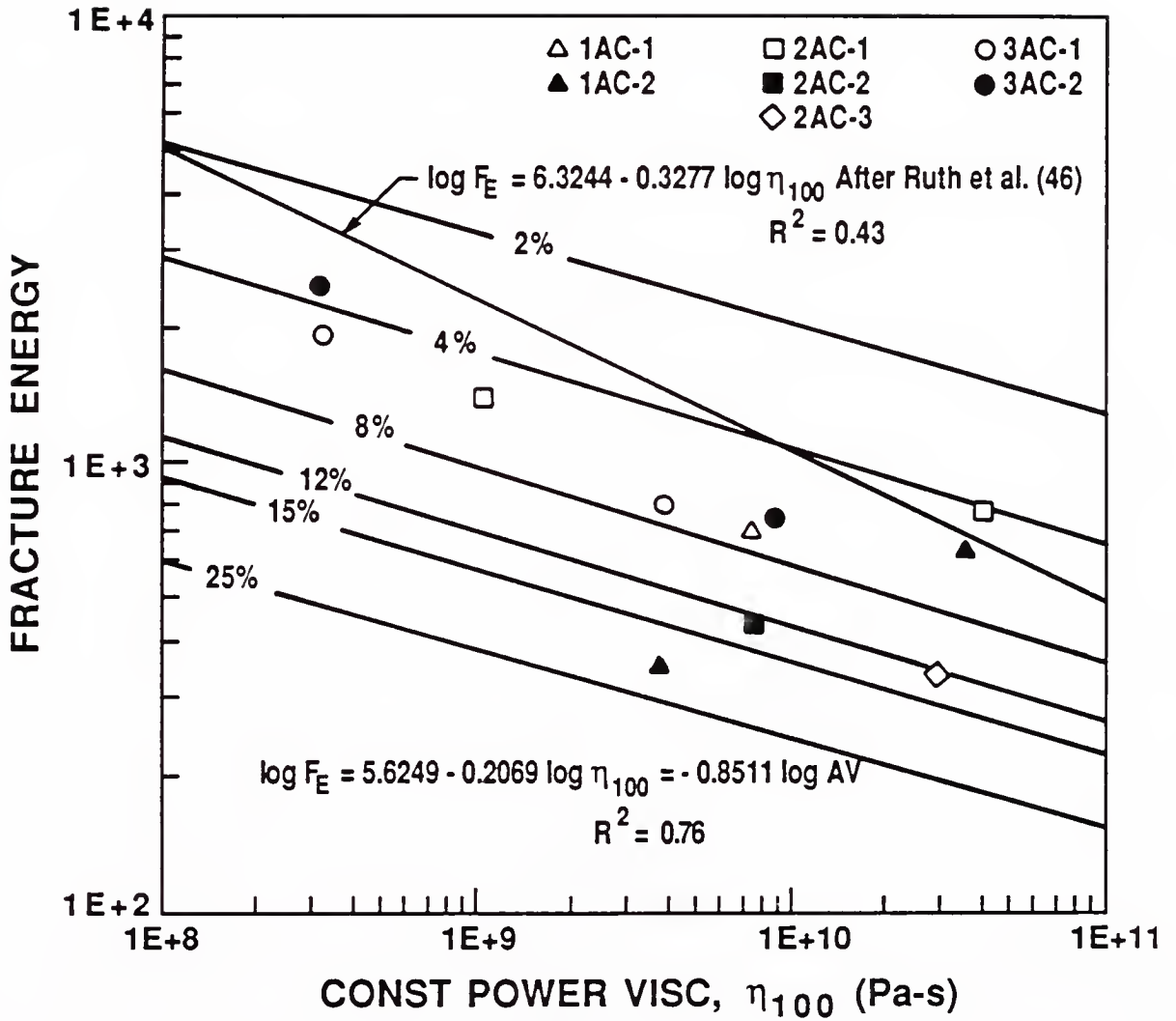


Figure 5.5 Results of Fracture Energy Tests

$$\log F_E = 5.6249 - 0.2069 \log \eta_{100} - 0.8511 \log \% AV, Pa \quad (5.8)$$

$$(N = 11 \quad R^2 = 0.7640)$$

As with the resilient modulus data, fracture energy was re-regressed (Figure 5.6) using the slope of the line given by Ruth et al. (46). The R^2 value fell only slightly from 0.76 to 0.73 indicating that the data and initial correlations were reasonable. The transformed equation is given as

$$\log F_E = 6.5879 - 0.3277 \log \eta_{100} - 0.6059 \log \% AV, Pa \quad (5.9)$$

$$(N = 11 \quad R^2 = 0.7252)$$

As shown, the energy required for fracture is less for the in-service than for the laboratory compacted cores. Factors such as strip-ping, weathering, and hardening can all result in lower fracture energy values through the development of micro cracking in the core material. For a given viscosity, specimens with higher air void contents generally displayed lower fracture energies. The role air voids play in the creep failure of bituminous mixtures can best be visualized by the arrangement of the binder-aggregate matrix. Given the looser arrangement of a higher air void mixture, less energy is required to cause separation or yielding. This energy is increased when mixtures are consolidated producing greater densities and lower air void contents.

Mix viscosities provide better correlations where shear rates become very small and can be used to predict the incremental stresses

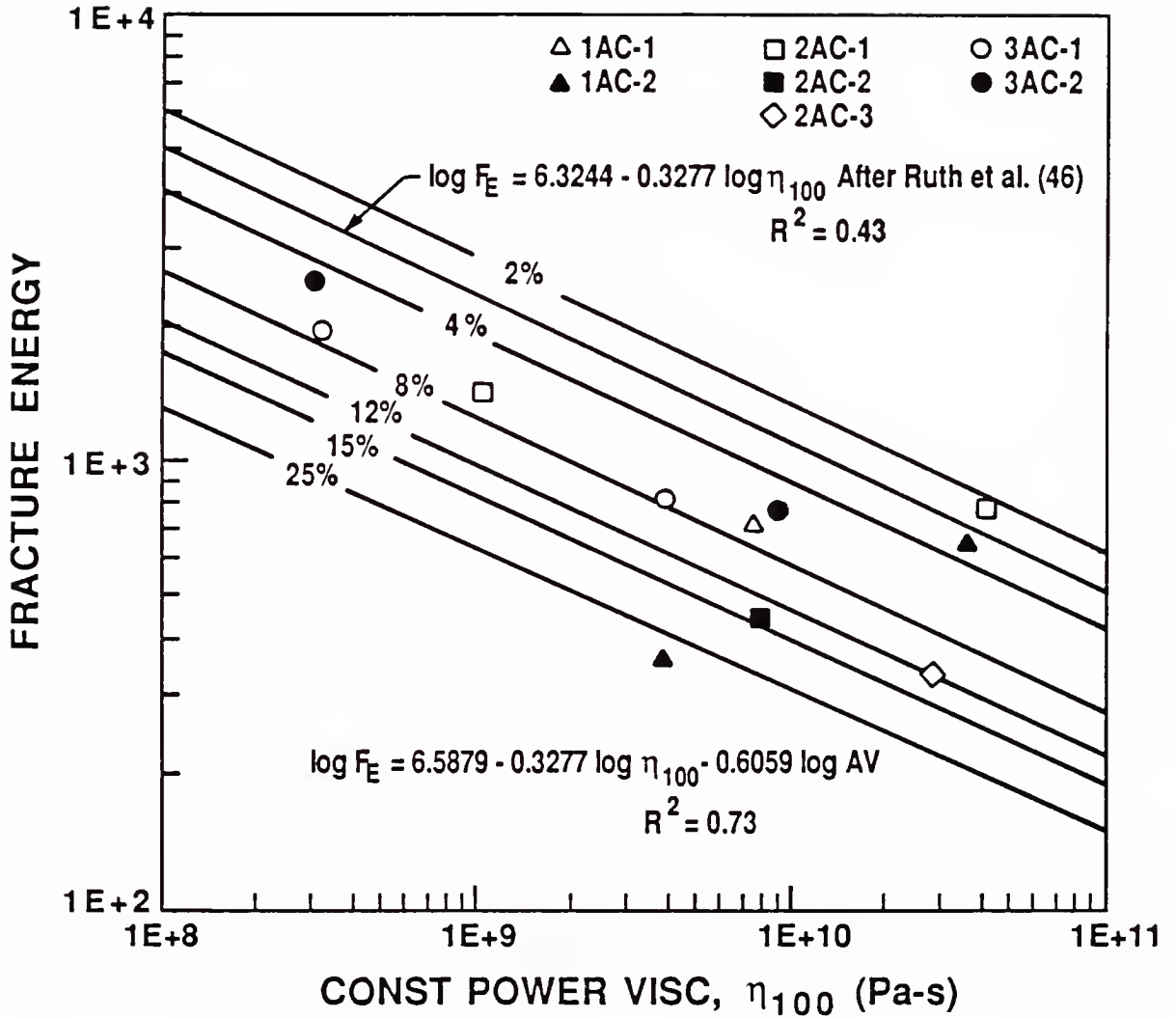


Figure 5.6 Results of Fracture Energy Tests Using Modified Equation

and strains used in thermal analysis. An attempt was made to compute mix viscosity ($\eta_{0.01}$) using values of failure stress and creep strain rate ($\dot{\epsilon}_{cr}$) with the expression:

$$\eta_{0.01} = \frac{\sigma}{\dot{\epsilon}_{cr}} \quad (5.10)$$

Relationships between $\eta_{0.01}$ and η_{100} were developed (equation 5.11) and illustrated in Figure 5.7. Appreciable scattering of the data is apparent, probably resulting from the wide range of air voids tested and the lack of control specimens available. Incorporating air voids into the regression analysis did not improve the correlation.

$$\log \eta_{0.01} = 5.5353 + 0.6410 \log \eta_{100}, \text{ Pa-s} \quad (5.11)$$

$$(N = 10 \quad R^2 = 0.7743)$$

5.5 Summary

From the analyses and discussion on the diametral tests performed in this study, the influence of viscosity and air void content on the resilient and creep behavior of asphalt mixtures is apparent. The results show that as viscosity increased the modulus increased, but the the energy required for fracture decreased. Also, as air voids increased, both the modulus and fracture energy decreased. It was hard to determine exactly how much effect viscosity and air voids have on the resilient and fracture response of asphalt mixtures. Other factors such as gradation and bitumen content also play an important role.

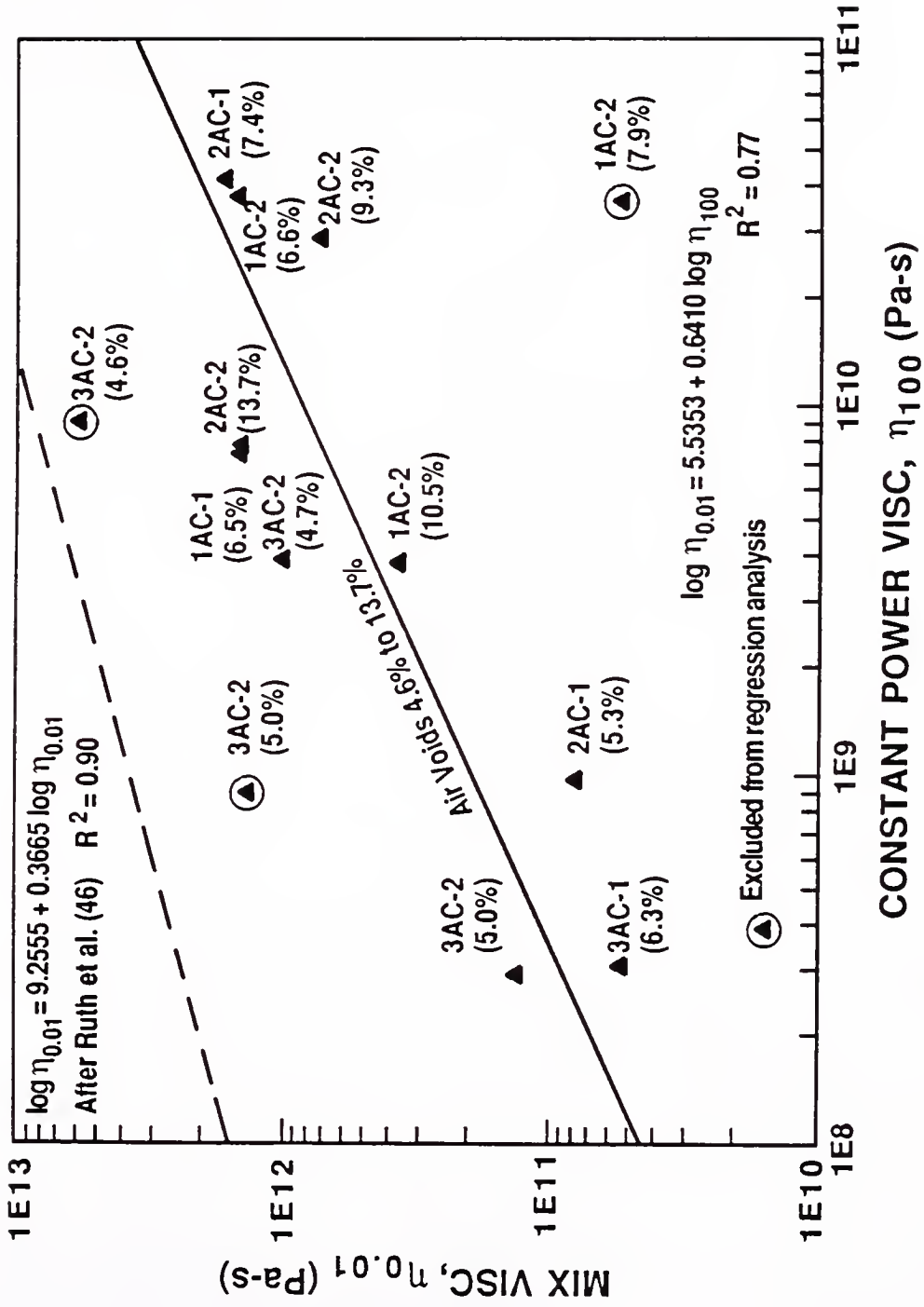


Figure 5.7 Correlation Between Mix Viscosity, $\eta_{0.01}$, and Constant Power Viscosity, η_{100}

CHAPTER 6 ANALYSES OF FIELD MEASURED FWD DATA

6.1 Introduction

This chapter presents the analyses of the field measured FWD data with respect to determining the elastic characteristics of the pavement materials at each test site. Field testing procedures along with a description of the FWD have been presented in Chapter 3. The results of the field measured FWD data are given in Appendix G.

The variable degree of pavement cracking from site to site posed a unique problem for interpreting the FWD data using the linear elastic computer program BISDEF. The underlying assumption in the theoretical analysis of these data was that each pavement layer acted as an isotropic, homogeneous, and linear elastic medium. After initial iterations, difficulty arose in accounting for the variability in pavement cracking. It became apparent that it was futile to analyze these cracked pavements strictly from predicted moduli derived from the analysis of uncracked laboratory samples. It was equally nonproductive letting BISDEF iterate for all layer moduli, as it was designed to do, since it either over or under predicted the moduli outside conceivable ranges. These aged pavements had to be analyzed from an unconventional but rational approach that included making logical assumptions to ensure that reasonable results could be achieved.

This chapter will focus on the separate evaluation of each test site. Comparisons among sites were done where applicable and are

presented. The analysis of site 3 was undertaken first because, of the three sites, it displayed the most uniform deflection response and exhibited the least amount of surface distress (e.g., cracking and rutting). Confidence in the results obtained at site 3 set the tone for analyses of sites 1 and 2. Since these two sites showed more severe forms of distress, certain assumptions regarding the treatment of each pavement layer had to be made.

For these analyses, the following general symbols will be used:

- E_1 weighted asphalt concrete modulus
- E_2 sand asphalt modulus
- E_4 subgrade modulus
- E_3 stabilized subbase - not used in the analyses

Site specific information will be given when required.

6.2 Computer Programs and Data Input

Four computer programs were used in the analyses of the FWD field data. The program MKFILE was first used to tabulate the raw data and make a BASIN-compatible data file. Then, the computer program BASIN was used to select representative deflection basins for each site by normalizing all the deflections and calculating the deflection basin areas. Once representative basins were selected (between four and six at each site and test temperature), BISDEF was used to compute moduli values that best described the input deflection basin. To calculate deflections, BISAR was used as a subroutine. The program BINPUT was used to build BISDEF-compatible data files. Instruction guides for the above programs are given in the Navy Airfield Pavement Evaluation Manual (5).

Each site consisted of three material types: 1) two or more layers of asphalt concrete, 2) a sand asphalt base, and 3) a sand subgrade. Stratigraphy data for all sites were presented in Chapter 3. For input into the BISDEF program, a maximum of three layers were used by combining the thicknesses of the asphalt concrete layers. During trial runs to compute the asphalt concrete modulus, BISDEF many times over predicted the modulus to values ranging from concrete to steel. This was especially true when BISDEF iterated for both the asphalt concrete and sand asphalt moduli. This was believed to be due, in part, to the thin asphalt thicknesses evaluated. Nevertheless, it was decided to combine the asphalt concrete layers and initially compute a weighted modulus value as determined from the prediction equations developed in Chapter 5. Deflection basins and moduli computed by BISDEF were identical whether using the weighted technique or inputting the moduli as separate layers. Also, assigning a fixed value for the asphalt concrete normally yielded reasonable moduli values for the underlying sand asphalt and subgrade. One drawback noted in using BISDEF was that no unique solution existed in reproducing the field measured deflection basin. Many combinations of moduli values produced similar results. It became obvious that matching deflection basins was only as important as the modulus values computed. This is why the study of flexible pavements over a wide temperature range is necessary to correctly interpret FWD data, especially if cracking exists.

6.3 Analysis of Site 3

The major focus of the analysis was on the stations inside the wheel path. FWD measurements were carried out at different load levels

to provide a means of checking the linearity of the load-deflection response and deciding the feasibility of using a linear elastic program such as BISDEF to model aged flexible airfield pavements. Two stations representing the best and worst load-deflection response are shown in Figure 6.1 and 6.2, respectively. Except for a slight stress stiffening (deflections decreasing with load) in Figure 6.2, measured deflections show strong linearity with applied load. Furthermore, the plots in both cases passed through the origin which suggests true linearity and good repeatability of the FWD load-deflection response. The linear elastic modeling of site 3 was therefore deemed appropriate. This supports the findings of Badu-Tweneboah (108) who reported that linearity is achieved at FWD loads beyond 6 kips and suggested that FWD deflections be measured at loads of at least 9 kips to minimize the effects of nonlinearity.

Site 3 was analyzed by BISDEF as a three layer system. BISDEF allowed layer moduli to be assigned (fixed) or computed through iteration. To start, E_1 and E_2 modulus values were calculated from prediction equations 5.3 and 5.4 and inputted as fixed values, while the subgrade modulus, E_4 was allowed to iterate. This arrangement assumed that the entire pavement structure was uncracked. After initial runs, it became apparent that this assumption was incorrect. Computed deflection basins indicated a substantially more rigid pavement than was measured by the FWD, especially at lower temperatures.

Based on available information, it was believed that there was extensive cracking in the sand asphalt layer. The next iterations were run, this time maintaining E_1 fixed and computing E_2 and E_4 . Here, computed deflections matched measured values within 5 percent, but

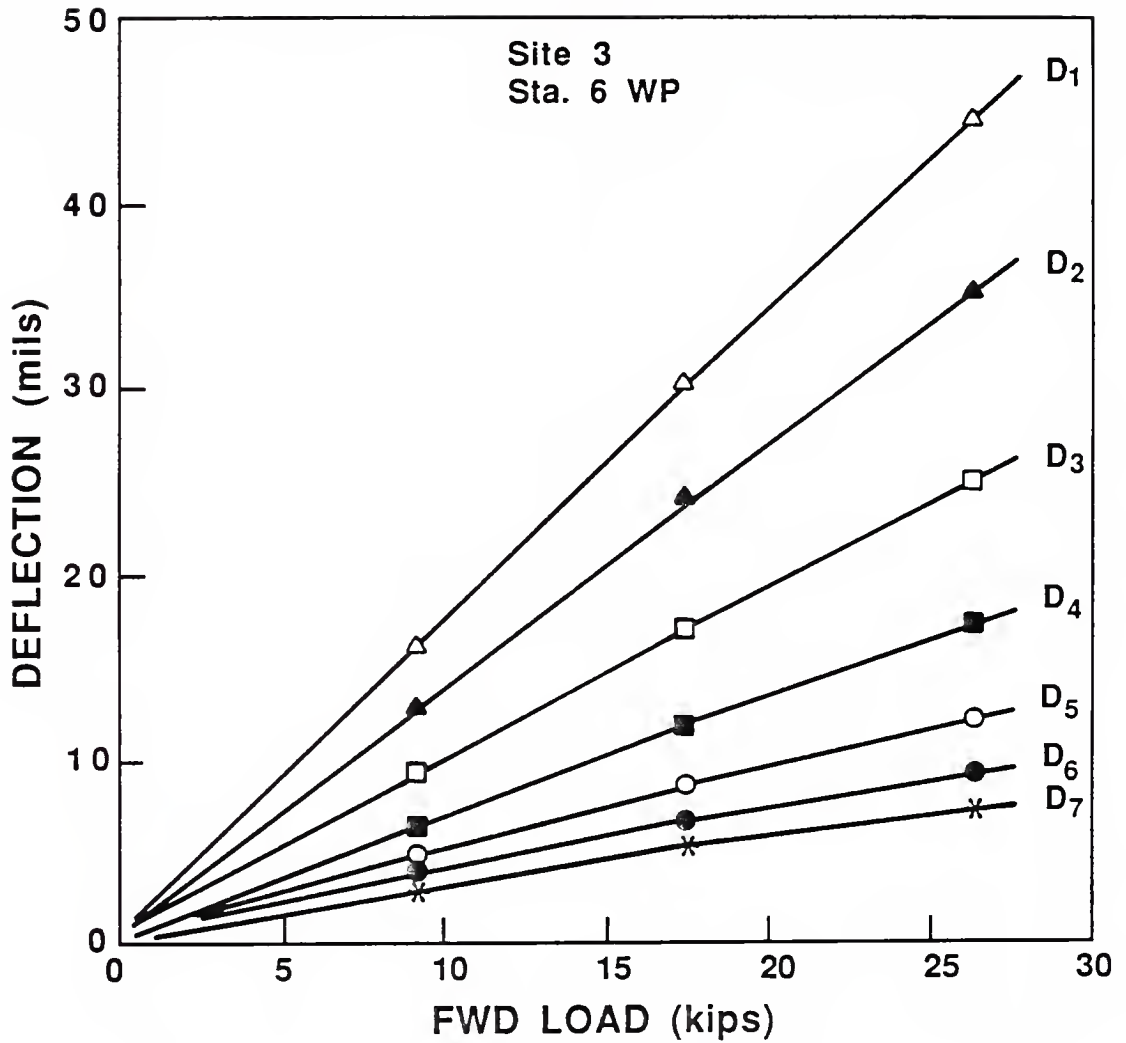


Figure 6.1 Surface Deflection as a Function of Load at Site 3
(Most Linear Response)

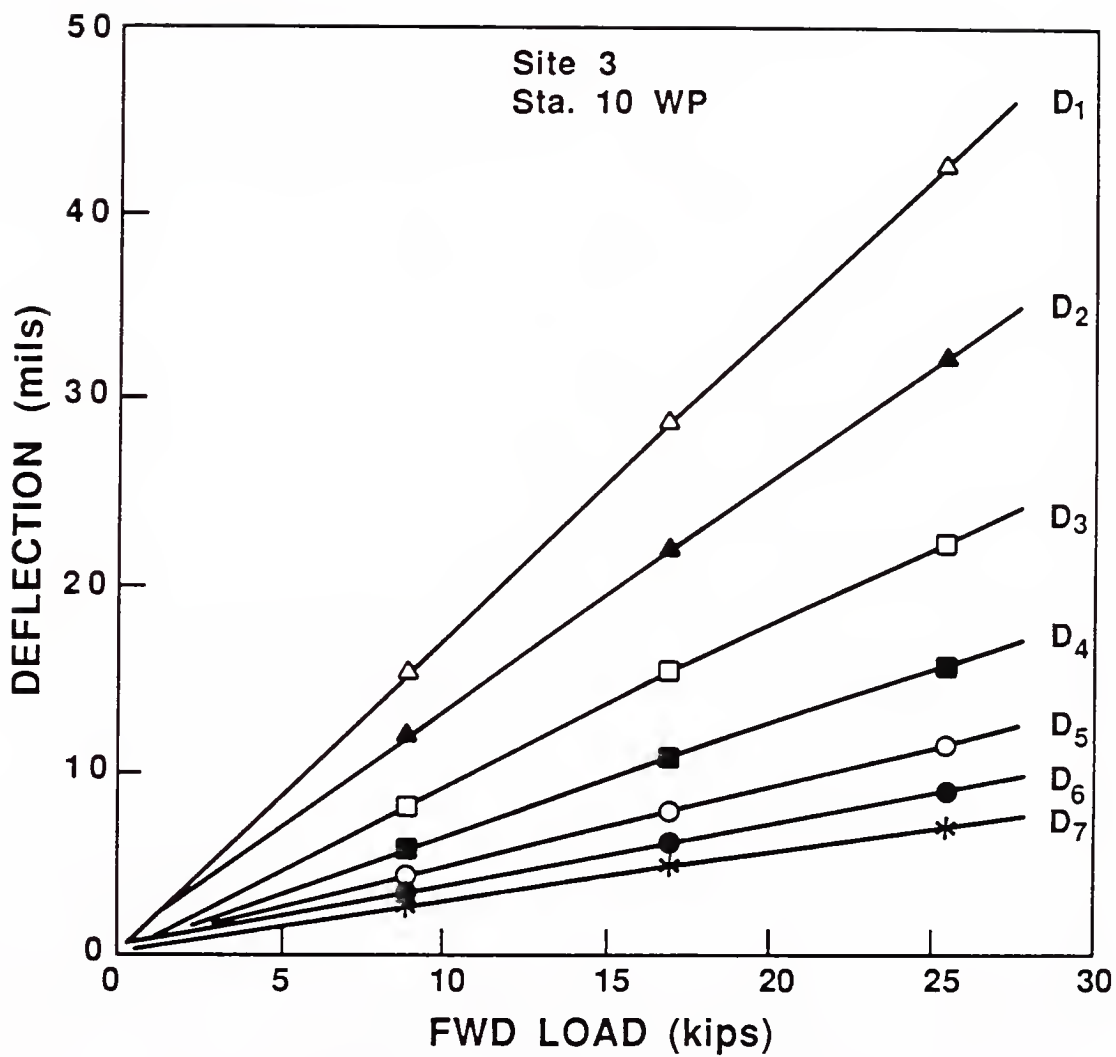


Figure 6.2 Surface Deflection as a Function of Load at Site 3 (Least Linear Response)

computed E_2 values were inconsistent with rheological behavior. Figure 6.3 illustrates the steady rise in E_2 values with temperature as predicted E_1 values decreased. Both values began to level off around 90 F. It was also around this temperature that the fixed and computed values of E_2 approached 200 ksi. Though it was entirely feasible for E_2 to be significantly cracked, it seemed impossible that E_2 values could decrease with decreasing temperature as shown.

Further refinements were necessary in the analytical procedure to accurately assess the pavement moduli. The next step was to assume that a certain degree of cracking at site 3 had been concealed by the lower viscosity of the wearing surface. From rheological data obtained for the asphalt layers it was shown that the second asphalt concrete layer was high enough in viscosity at low ambient temperatures to cause cracking. With aid of BISDEF, this rationale led to the development of a modulus formula for low severity cracking (equation 6.1).

$$E_1 = 30.8075 (\eta_{100})^{0.1375}, \text{ ksi} \quad (6.1)$$

$$(N = 40 \quad R^2 = 0.9466)$$

Iterations of BISDEF were run at all test temperatures substituting in reduced values of E_1 until consistent values of E_2 were achieved (Figures 6.3 and 6.4). A plot was then made of the computed E_1 values and η_{100} and shown in Figure 6.5. Comparing the modified E_1 values with that of an uncracked pavement shows around a 50 percent decrease in modulus at an η_{100} equal to 1.0×10^9 Pa-s. This percentage reduces as η_{100} decreases and the effect becomes negligible near 1.0×10^7 Pa-s. A

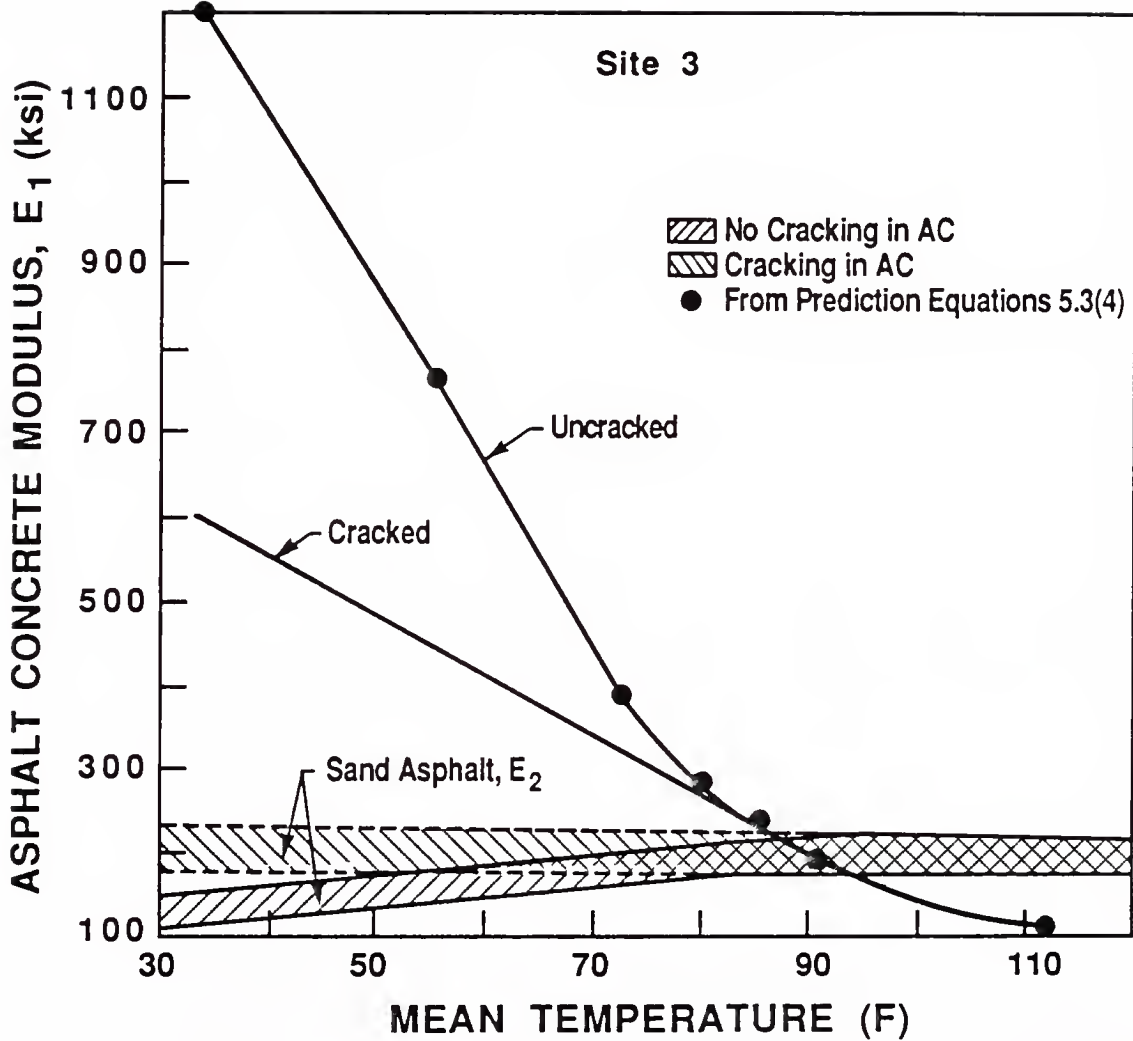


Figure 6.3 Change in E_1 and E_2 With Temperature for Cracked and Uncracked Pavement at Site 3

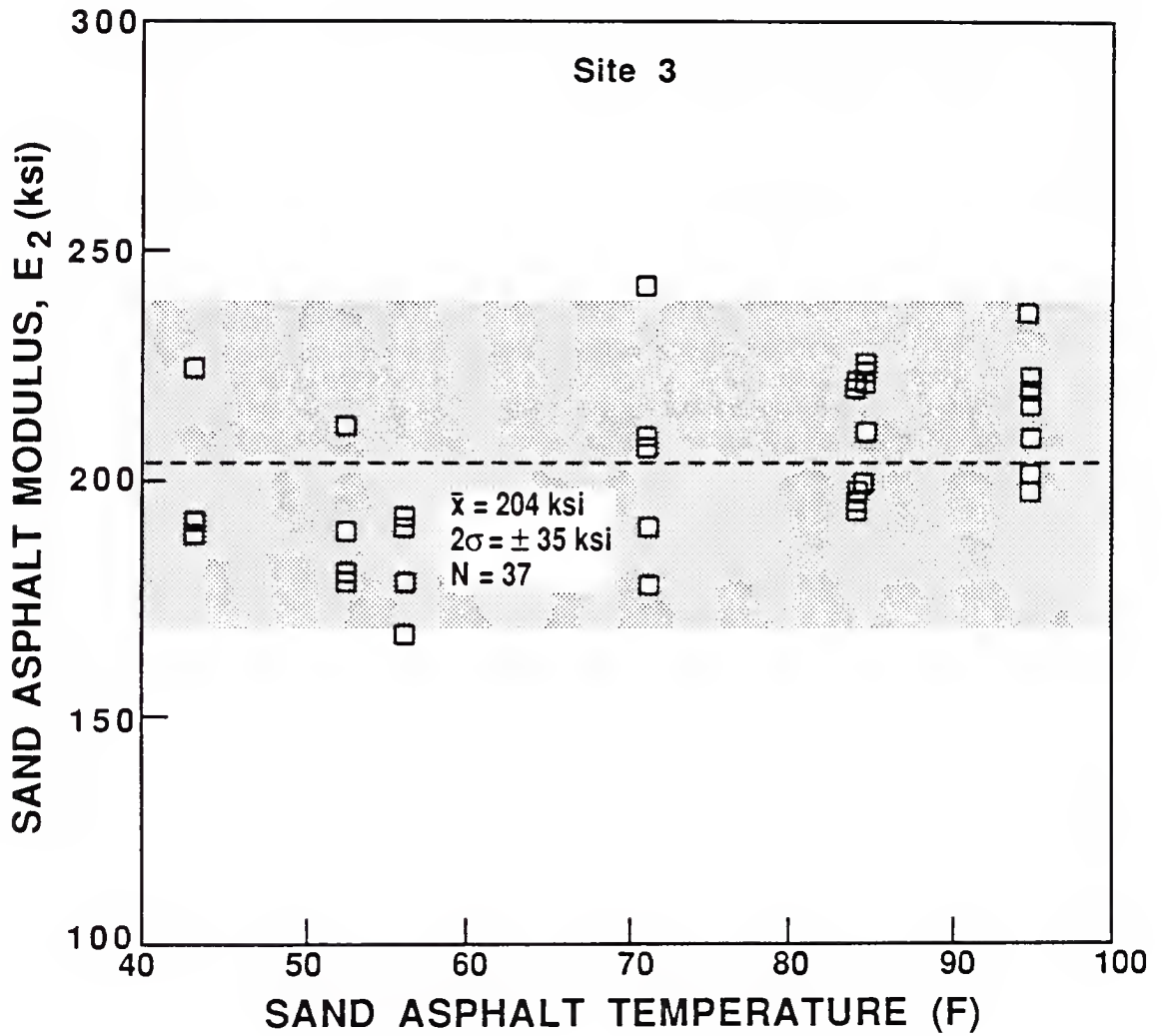


Figure 6.4 E_2 as a Function of Temperature at Site 3

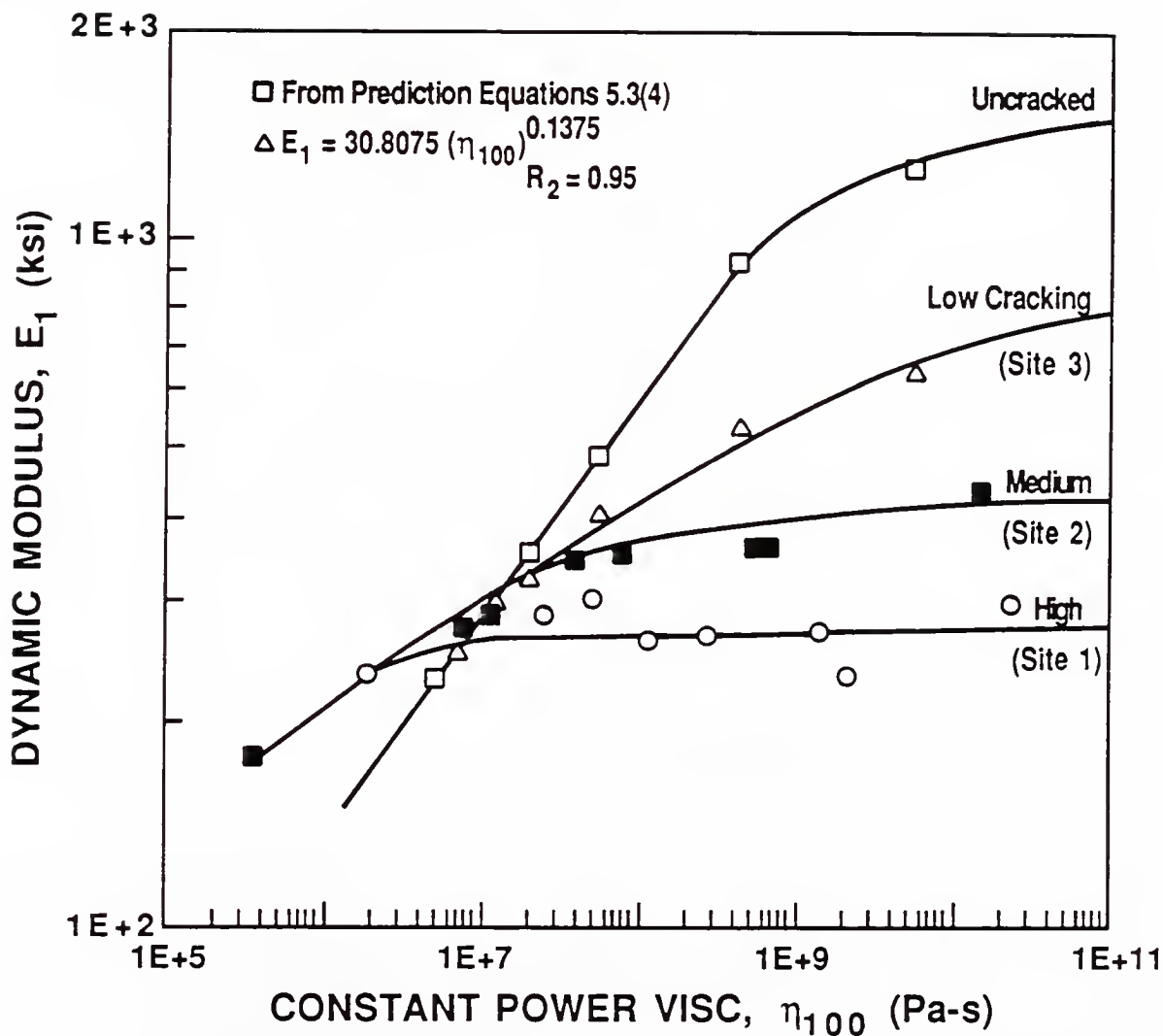


Figure 6.5 E_1 as a Function of η_{100} for Cracked and Un-cracked Pavements (All Sites)

second plot of E_2 values and n_{100} is presented Figure 6.6 and demonstrates the lack of correlation with viscosity. An average value of 204 ksi was obtained for E_2 .

During the iterative process to characterize the asphalt layers, E_4 values remained very consistent. Subgrade moduli computed using BISDEF were compared with the values predicted by equation 6.2 (108). Both methods predicted a tight band of values with a small amount of overlap. The average predicted E_4 value was 13.8 ksi while for BISDEF the value was slightly lower at 12.3 ksi, a difference of only 12 percent. The comparison of the two methods are plotted against pavement surface temperature and given in Figure 6.7. Consistency of the E_4 values verified the conclusions drawn in Chapter 3 on the negligible effects of moisture content on subgrade modulus values.

$$E_4 = 34.8891 (D_7)^{-0.97871}, \text{ ksi} \quad (6.2)$$

where

D_7 = the measured deflection at 72 in. normalized to a 9-kip load

To evaluate the effects of temperature, plots were made depicting the extreme temperature deflection response. Representative deflection basins at pavement surface temperatures of 31 F and 118 F are given in Figure 6.8. Also shown are the extreme deflection responses at both temperatures. Since both E_2 and E_4 have been shown to remain fairly constant throughout the temperature range, the difference in deflection response between the two temperatures was due primarily to the changing rheological properties of the asphalt concrete.

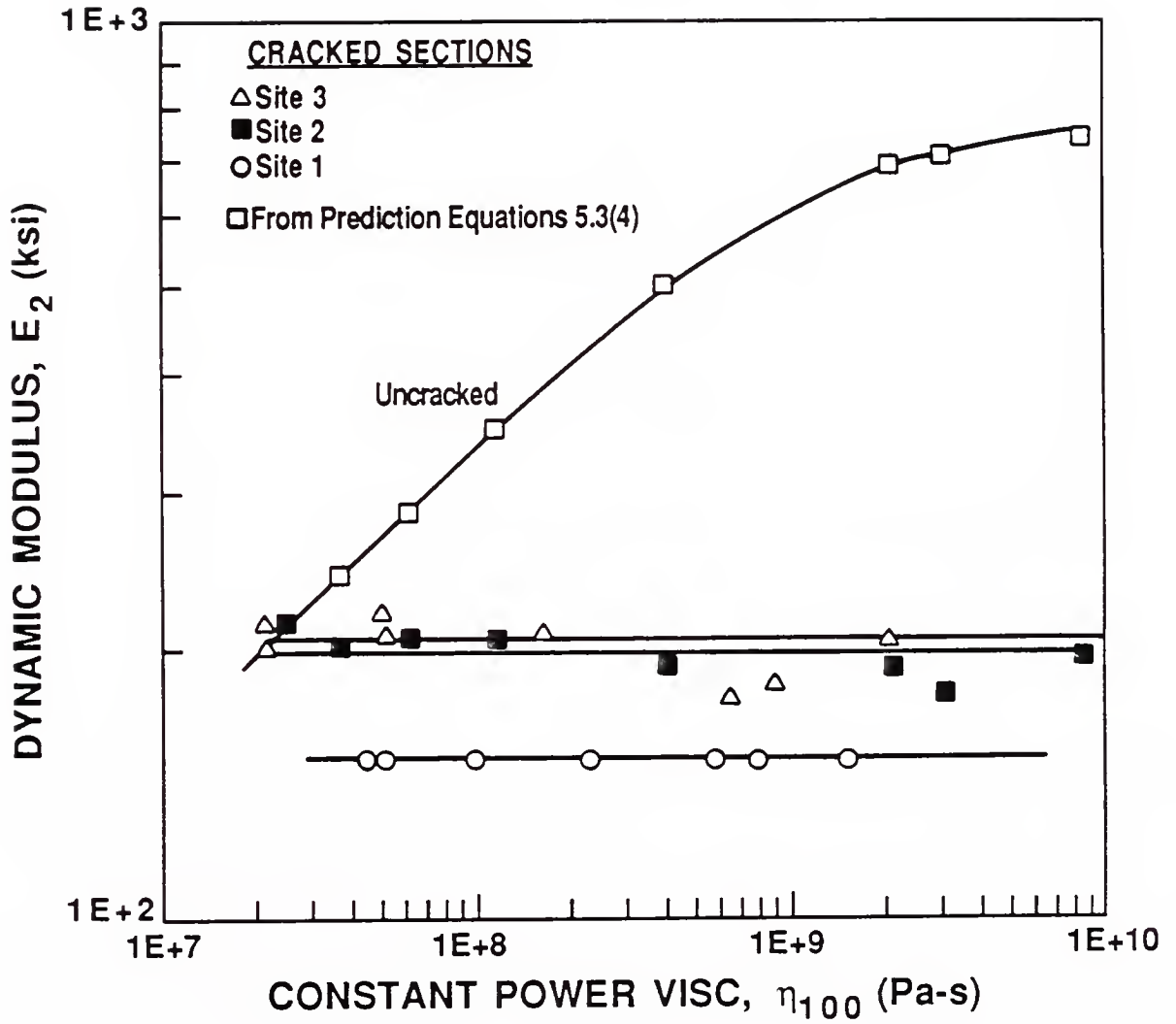


Figure 6.6 E_2 as a Function of η_{100} for Cracked and Uncracked Pavements (All Sites)

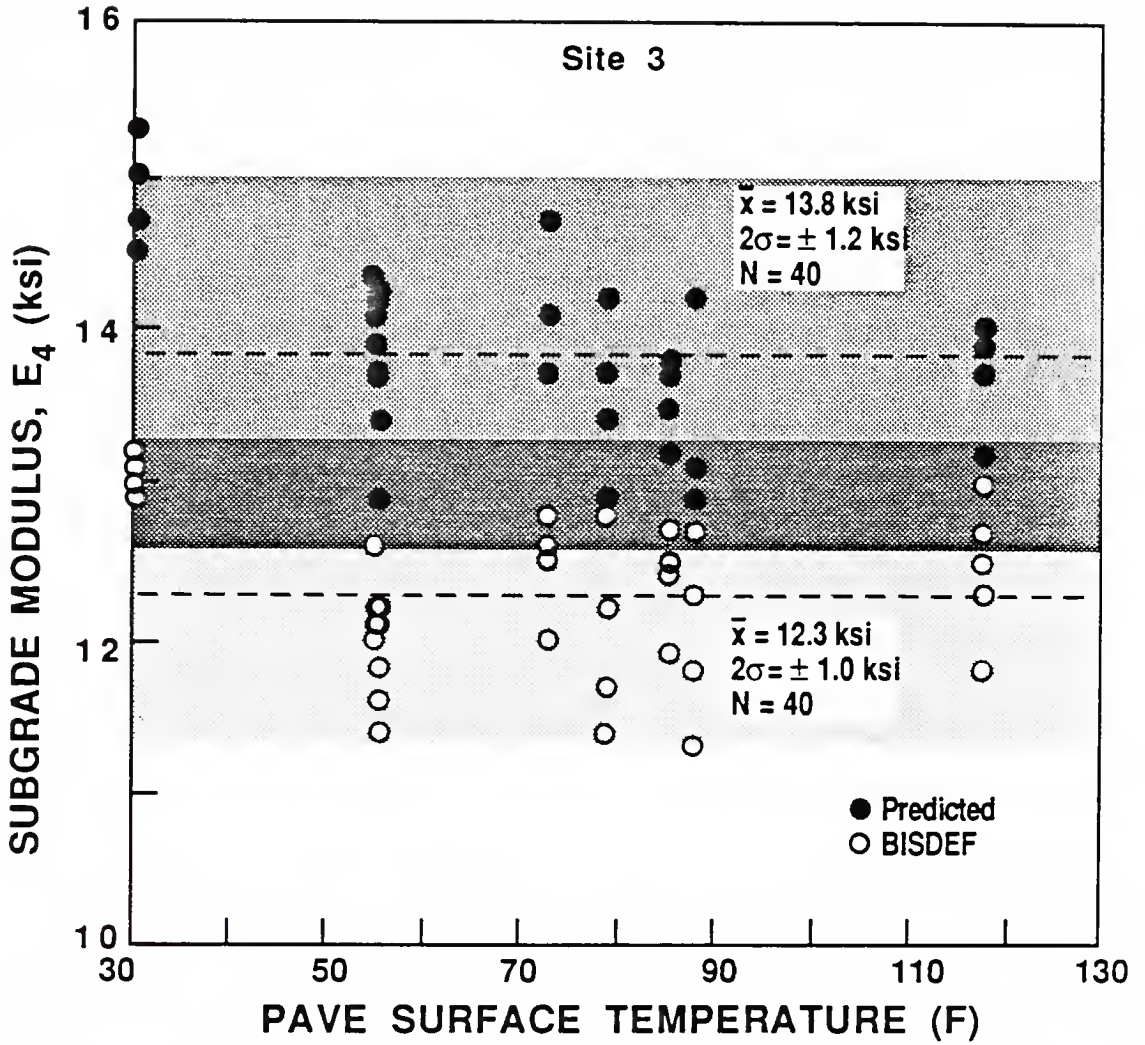


Figure 6.7 Comparison of E_4 Values as a Function of Temperature at Site 3

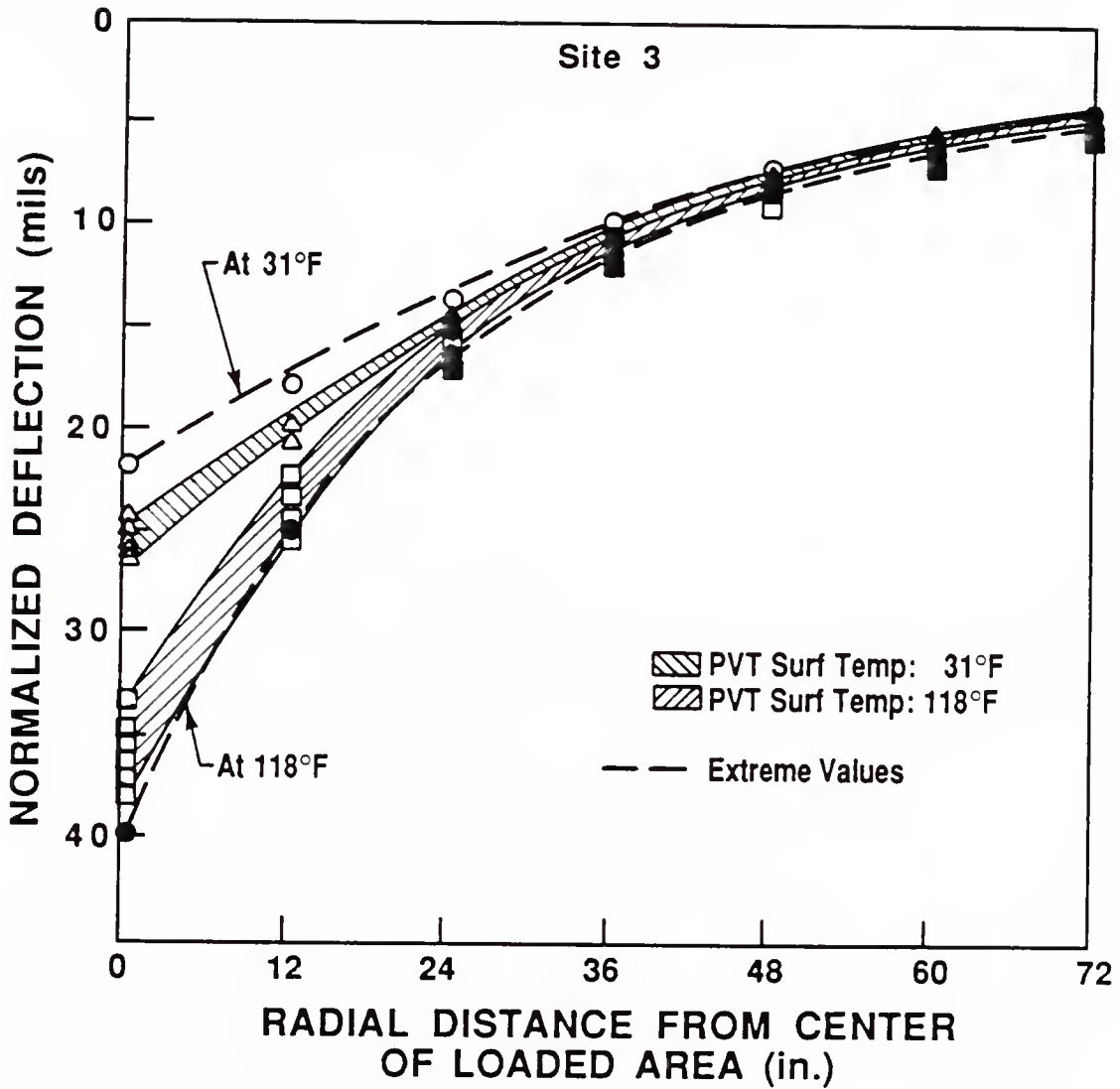


Figure 6.8 Extreme Temperature Deflection Response at Site 3
(Normalized to 18-kip Load)

Finally, the stiffest deflection responses both in and out of the wheel path were plotted over the temperature range (Figures 6.9 and 6.10). Shown is the ability of BISDEF to match the measured deflection basins by fixing E_1 (uncracked) and allowing E_2 and E_4 to iterate. Also presented are the deflection basins produced by fixing E_1 and E_2 using the uncracked moduli prediction equations and iterating for E_4 . At 31 F, a stiffer pavement was computed than was measured for both inside and outside the wheel path. Based on computed E_2 values, it was apparent that cracking in the sand asphalt was still evident in the wheel path and to a somewhat lesser degree outside it. At 118 F, measured and computed deflection basins matched very closely both in and out of the wheel path. This was because at this temperature cracked and uncracked moduli values were about equal.

6.4 Analysis of Site 2

Site 2 displayed similar responses and characteristics as site 3. Load-deflection response was again essentially linear with points passing near the origin (Figures 6.11 and 6.12). For input into BISDEF, identical procedures to site 3 were followed with one exception--the incorporation of a third asphalt concrete layer. Recall from Chapter 5, that this third layer was considered micro cracked by exhibiting low modulus and tensile strength values. Initial trials to obtain the modulus of this layer using BISDEF was discouraging as it computed values well beyond the normal range for bituminous mixtures. It was then decided to combine this layer with the sand asphalt since both layers were considered cracked. This allowed site 2 to be treated as three layer system.

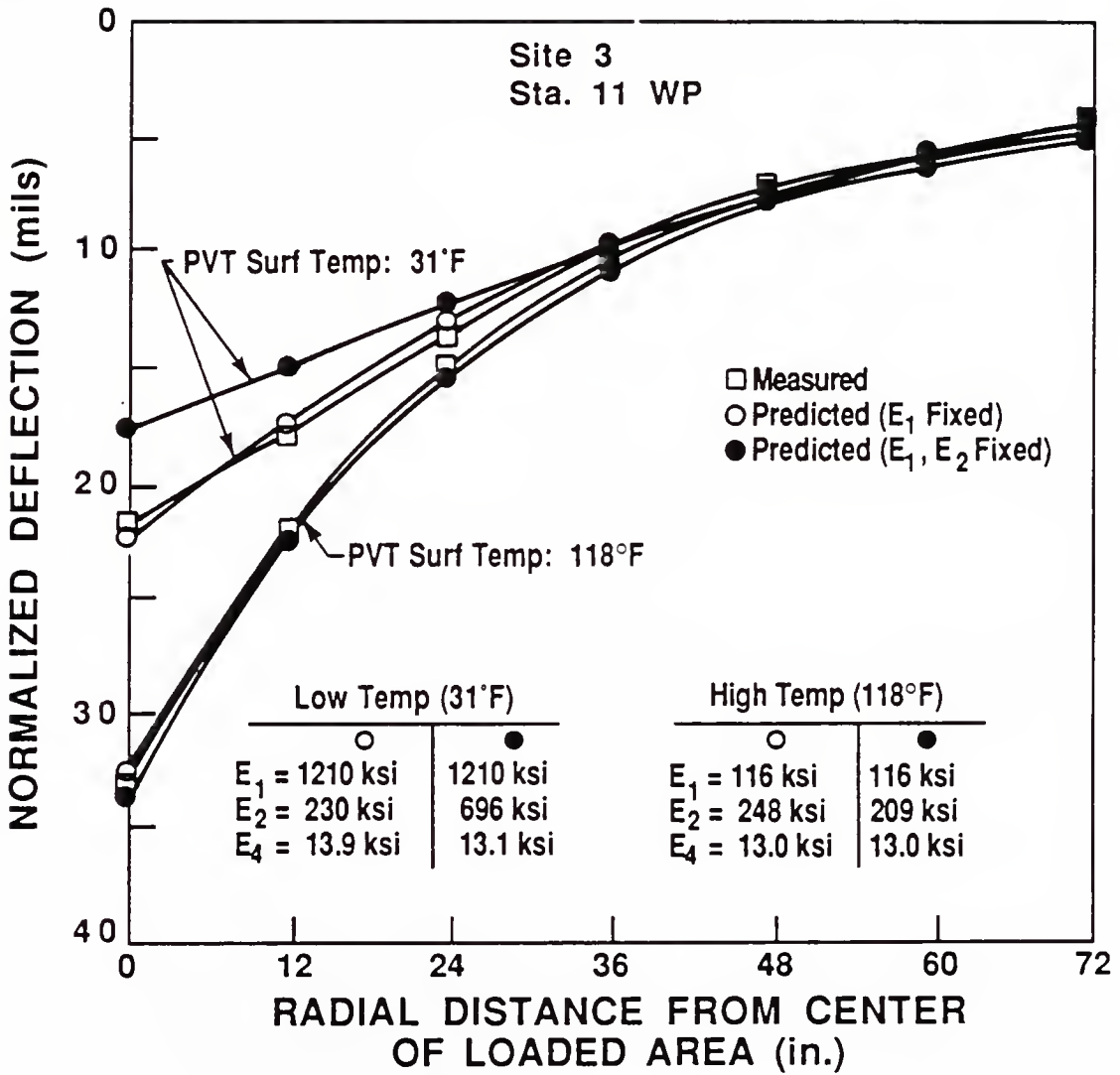


Figure 6.9 Measured and Predicted Deflection Basins in Wheel Path at Site 3 (Normalized to 18-kip Load)

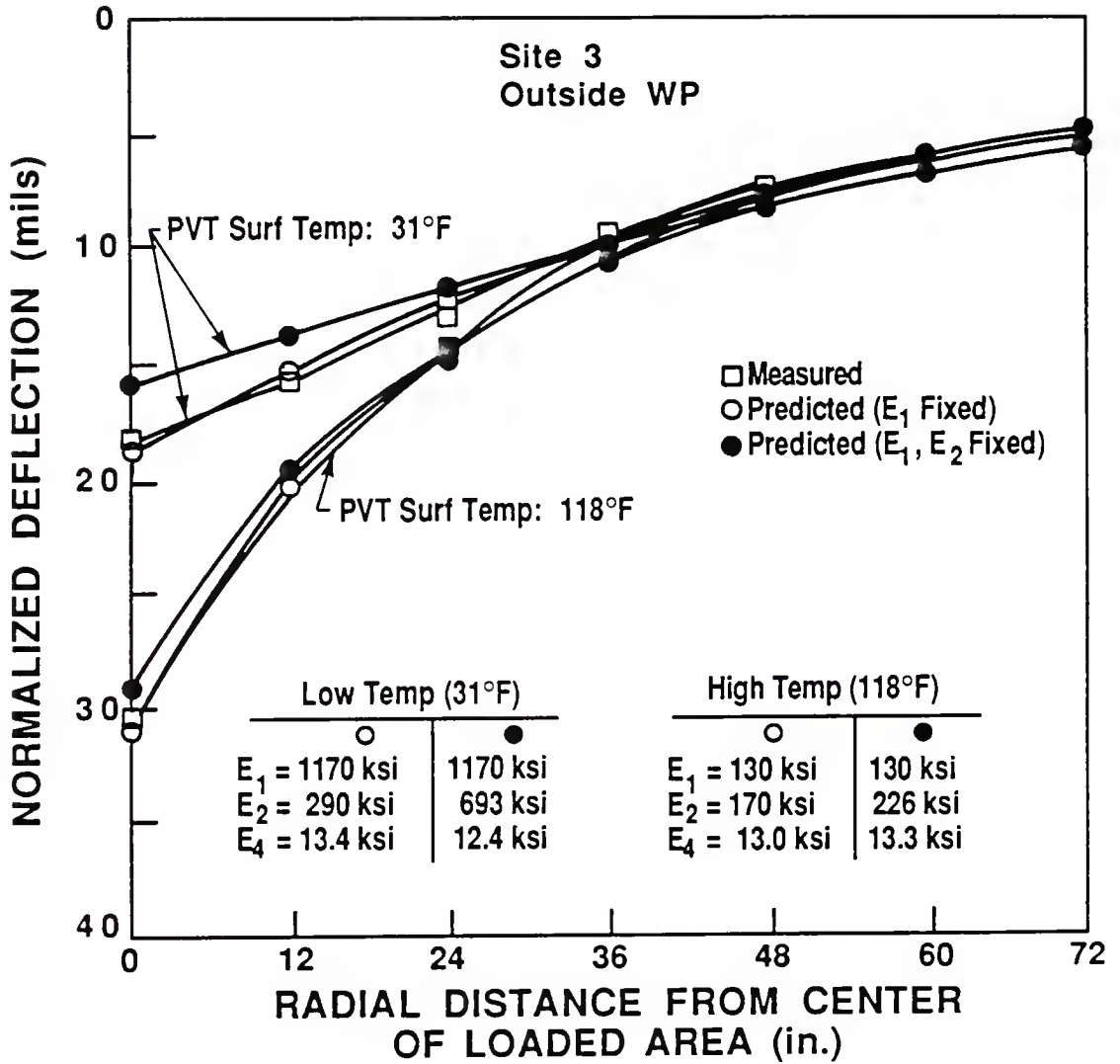


Figure 6.10 Measured and Predicted Deflection Basins Outside Wheel Path at Site 3 (Normalized to 18-kip Load)

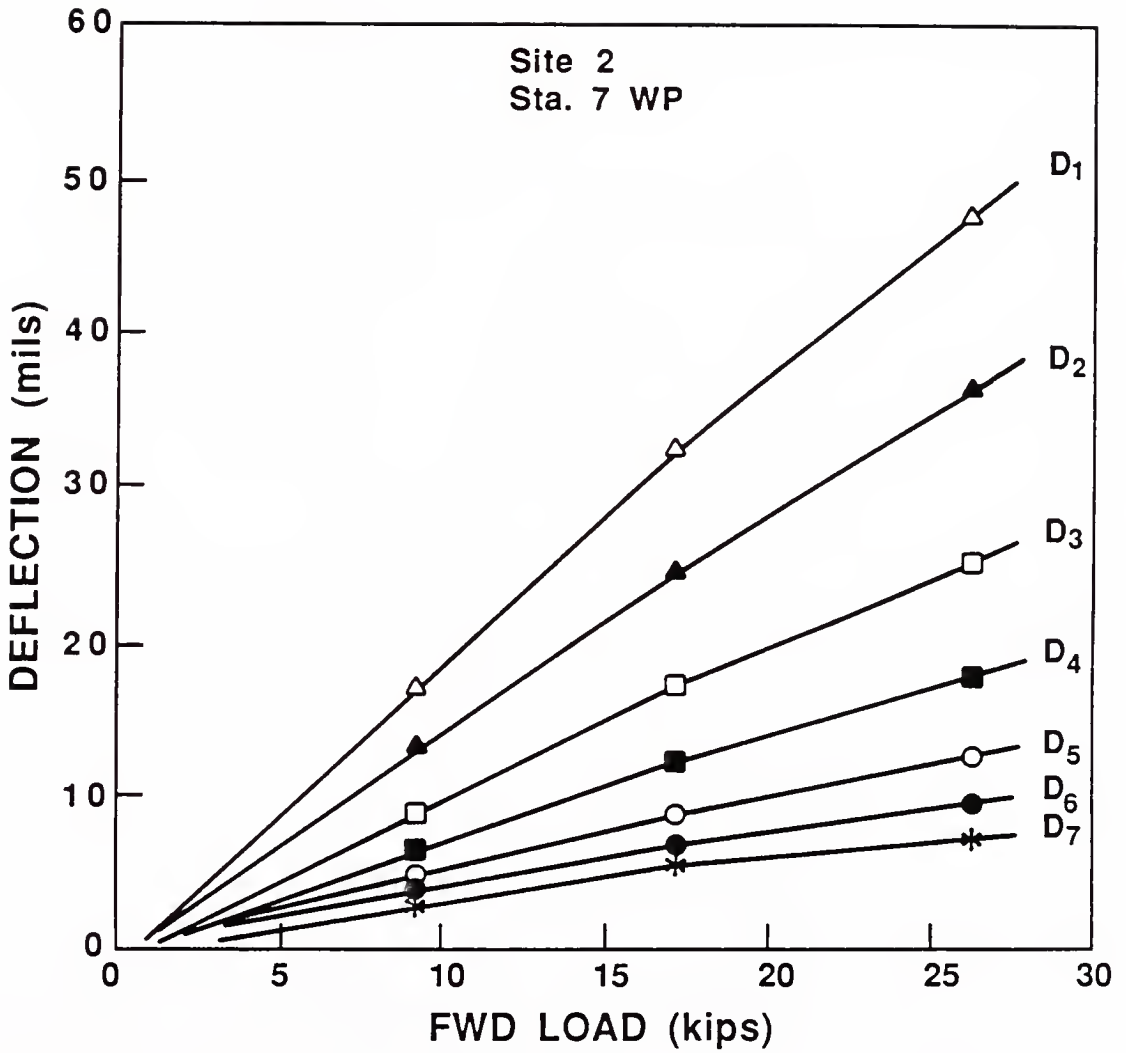


Figure 6.11 Surface Deflection as a Function of Load at Site 2
(Most Linear Response)

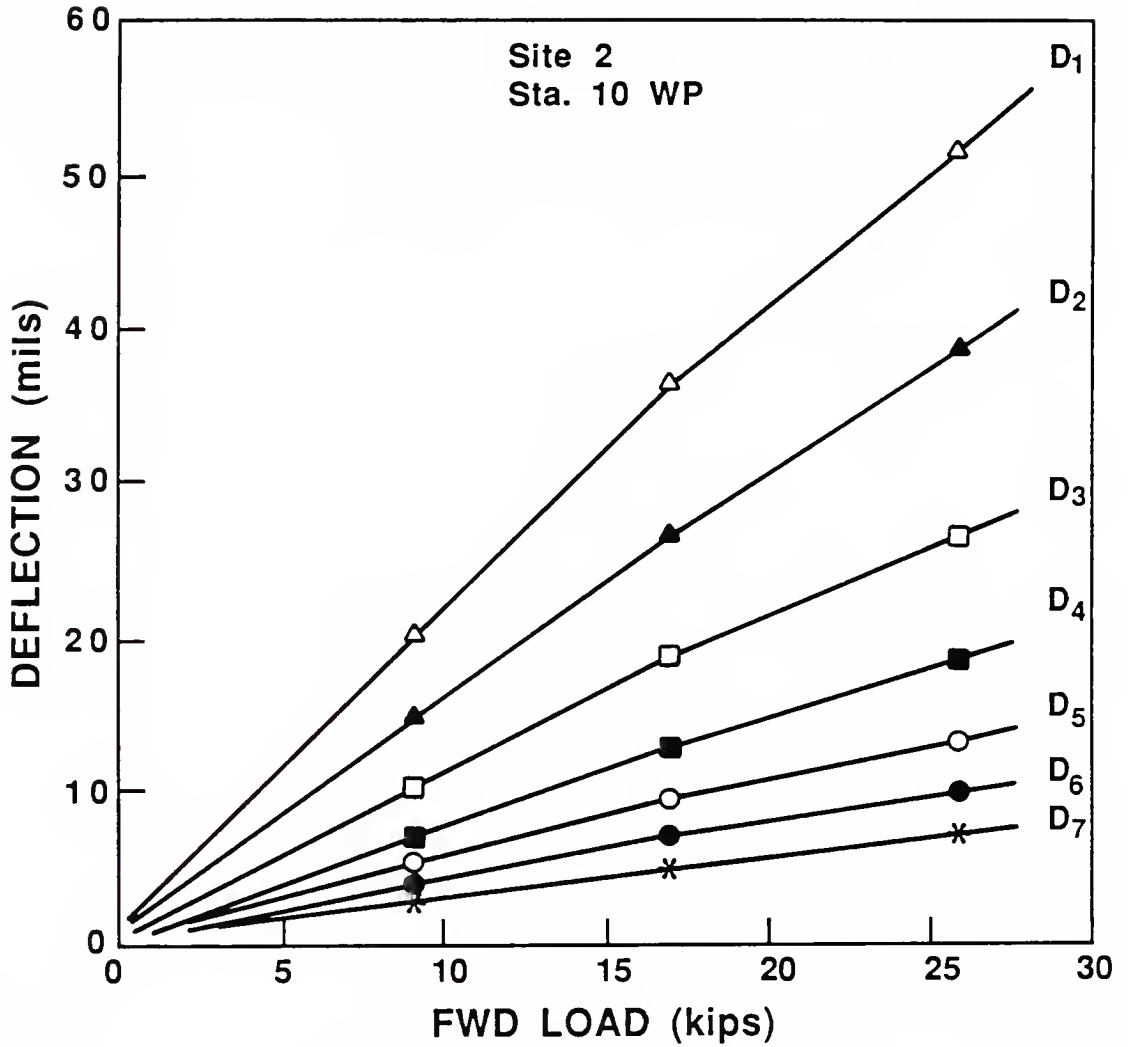


Figure 6.12 Surface Deflection as a Function of Load at Site 2
(Least Linear Response)

To begin the analysis, E_1 values were fixed using the equations for an uncracked pavement, while E_2 and E_4 were to be computed. A similar pattern developed as shown for site 3 in Figure 6.3. E_2 values were again lower at low temperature then rose to a plateau of approximately 200 ksi near 90 F. It seemed clear that like site 2, the sand asphalt was cracked and a adjustment to E_1 again had to be made. E_1 values computed from equation 6.1 for cracking at site 3 worked well for intermediate and high pavement temperatures (> 75 F) at site 2, but these values were too high at low pavement temperatures. This appeared logical since there was a greater degree of cracking present at this site. This increase in cracking was accounted for by reducing the high viscosity E_1 values (Figure 6.5). When the values obtained from Figure 6.5 for site 2 were fixed into the BISDEF program, consistent E_2 values resulted (Figure 6.13). The average value of 198 ksi was very close to the value of 204 ksi calculated for site 3.

Subgrade E_4 values remained fairly constant throughout the analysis. Computed E_4 values given in Figure 6.14 were again below those predicted by equation 6.2 but the difference was only 15 percent.

Measured deflection response was plotted (Figure 6.15) at the extreme temperatures to evaluate the effects of the change in E_1 values on the deflection basins. The deflection bands depicting representative basins at pavement temperatures of 28 F and 118 F did not deviate much at the nearer sensor positions and were indistinguishable at the further sensor locations. The extreme deflection basin at 28 F illustrated a very stiff basin with good stress transfer to the outer sensor positions.

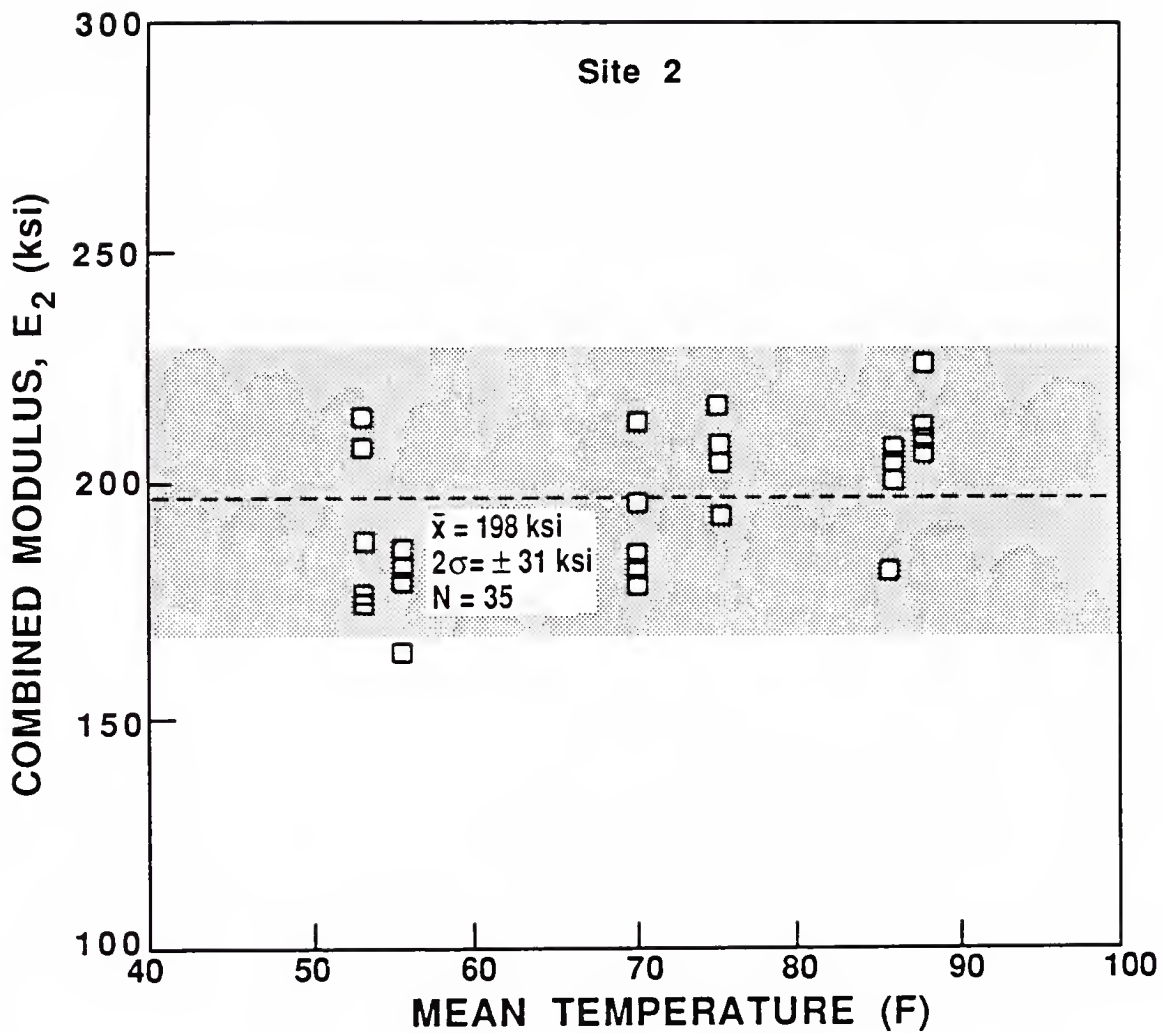


Figure 6.13 E_2 as a Function of Temperature at Site 2

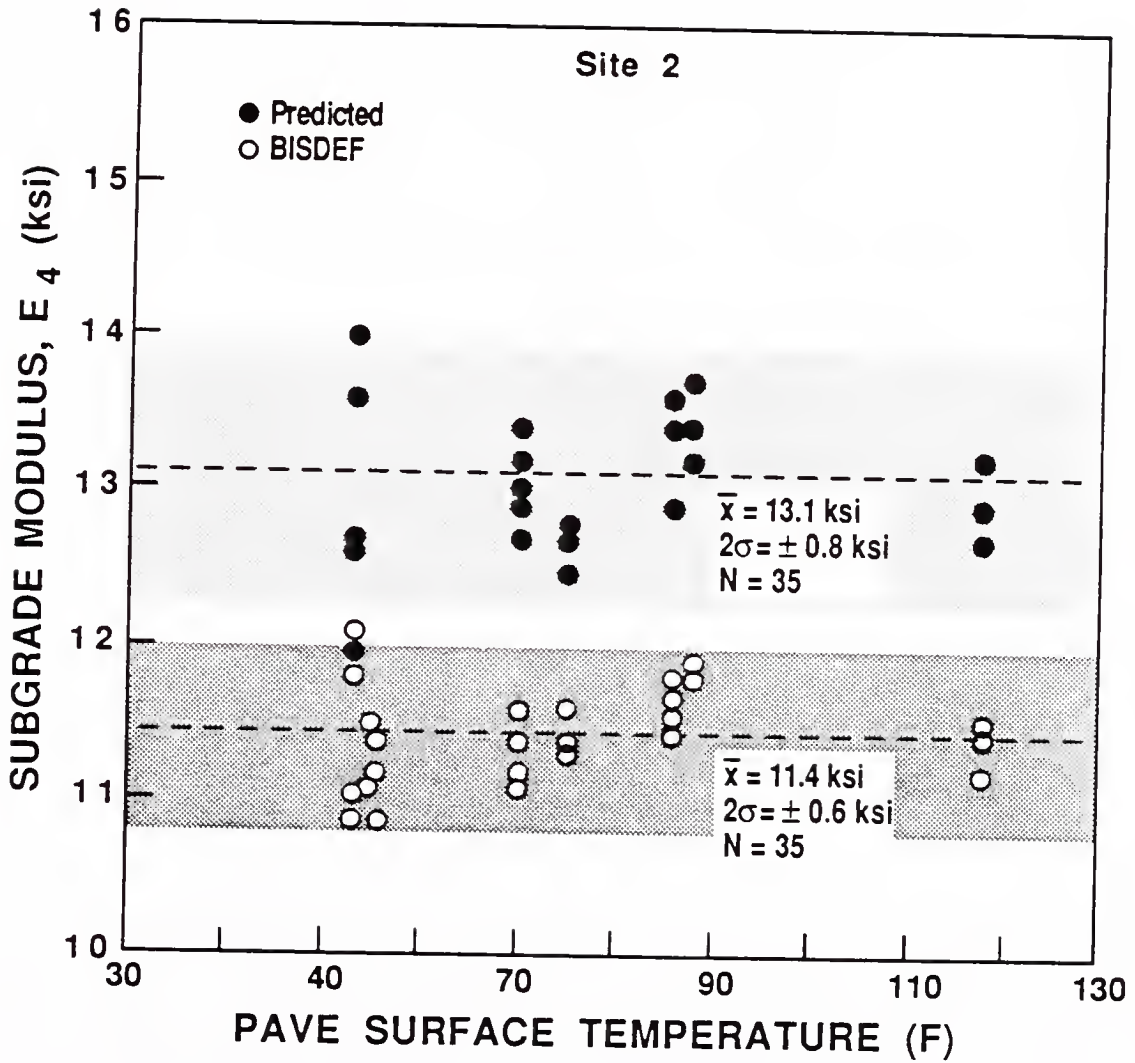


Figure 6.14 Comparison of E_4 Values as a Function of Temperature at Site 2

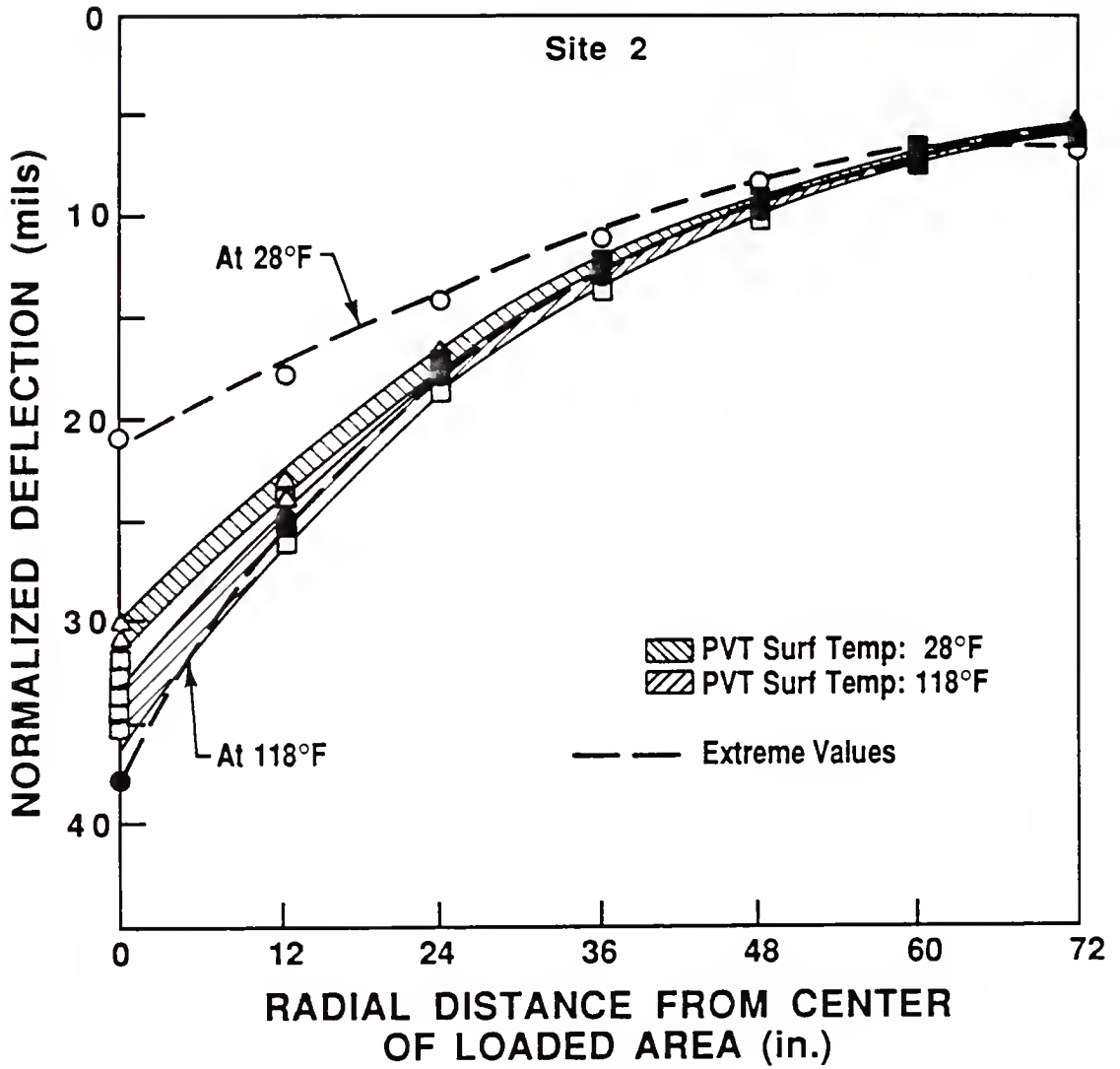


Figure 6.15 Extreme Temperature Deflection Response at Site 2
(Normalized to 18-kip Load)

Comparisons were made between site 2 and site 3 at both low and high pavement temperatures. At low temperature (Figure 6.16), representative deflections from site 3 were approximately 20 percent lower than site 2 at the inner sensor locations. This difference can be attributed primarily to the lower degree of cracking in the asphalt concrete at site 3 since E_2 and E_4 values were almost identical for both sites. At high temperature (Figure 6.17) the difference was less distinguishable. Furthermore, the lowest extreme values at low and high temperatures were virtually the same for both sites. This showed that as the degree of cracking in the asphalt concrete diminished, temperature extremes had little effect on the relative deflections between the two sites (Figures 6.16 and 6.17).

Lastly, at site 2, the stiffest deflection basins in and out of the wheel path were evaluated at the extreme temperatures. Inside the wheel path, E_1 values were computed for an uncracked pavement. Outside the wheel path, all three asphalt concrete layers were combined and E_1 values calculated using the weighted averaging technique. This was done on the assumption that the third asphalt concrete layer was not cracked outside the wheel path. In all cases, the computed deflection basins matched the measured basins very well (all within 5 percent). Shown in Figures 6.18 and 6.19, deflections outside the wheel path were 15 to 25 percent less than inside. The main reason for this difference was that E_4 values outside the wheel path were 30 percent higher than inside. Results achieved by the weighting technique were nearly identical to those produced by assigning a separate modulus value to each asphalt concrete layer.

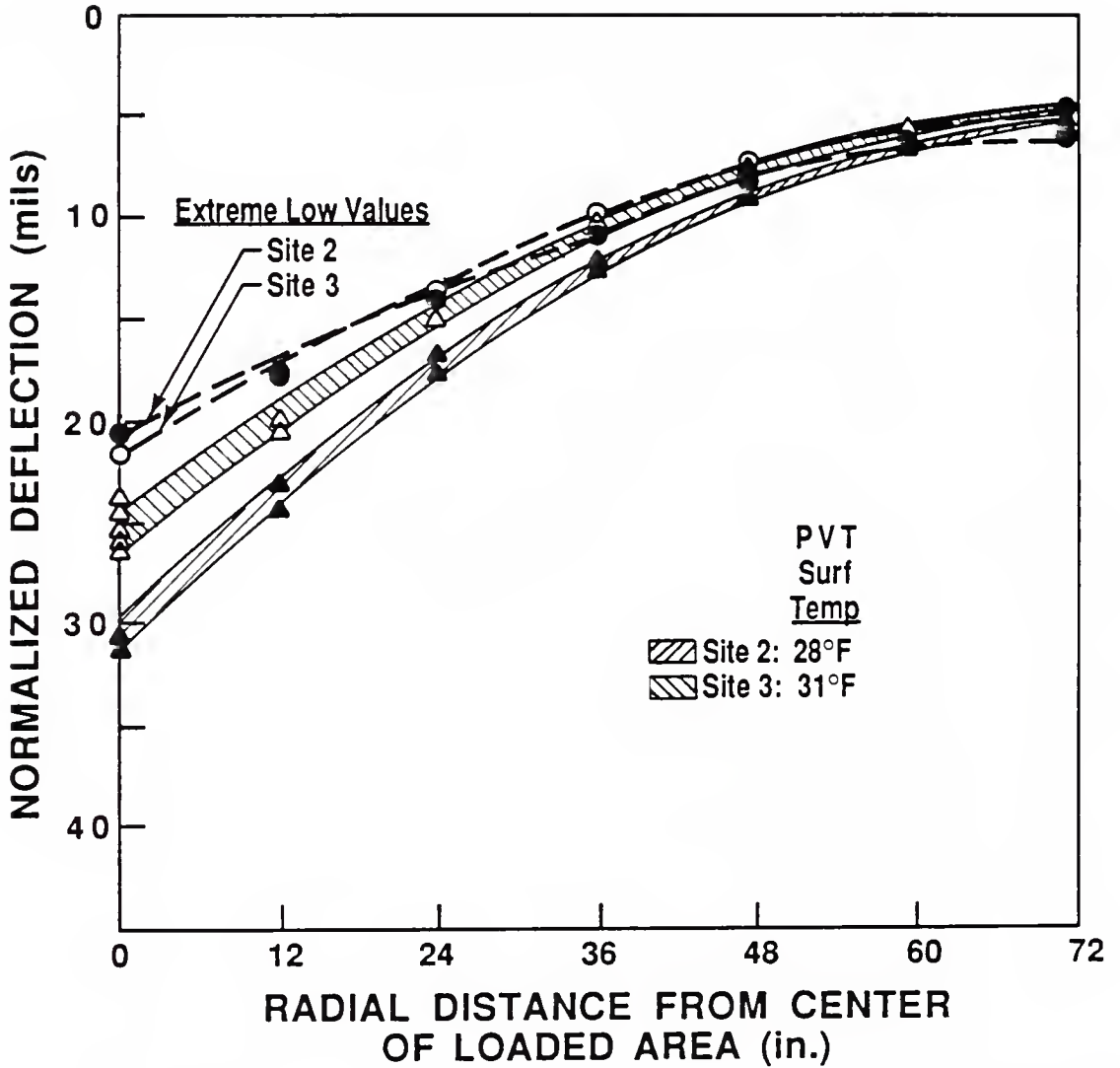


Figure 6.16 Comparison of Low Temperature Deflection Response Between Sites 2 and 3 (Normalized to 18-kip Load)

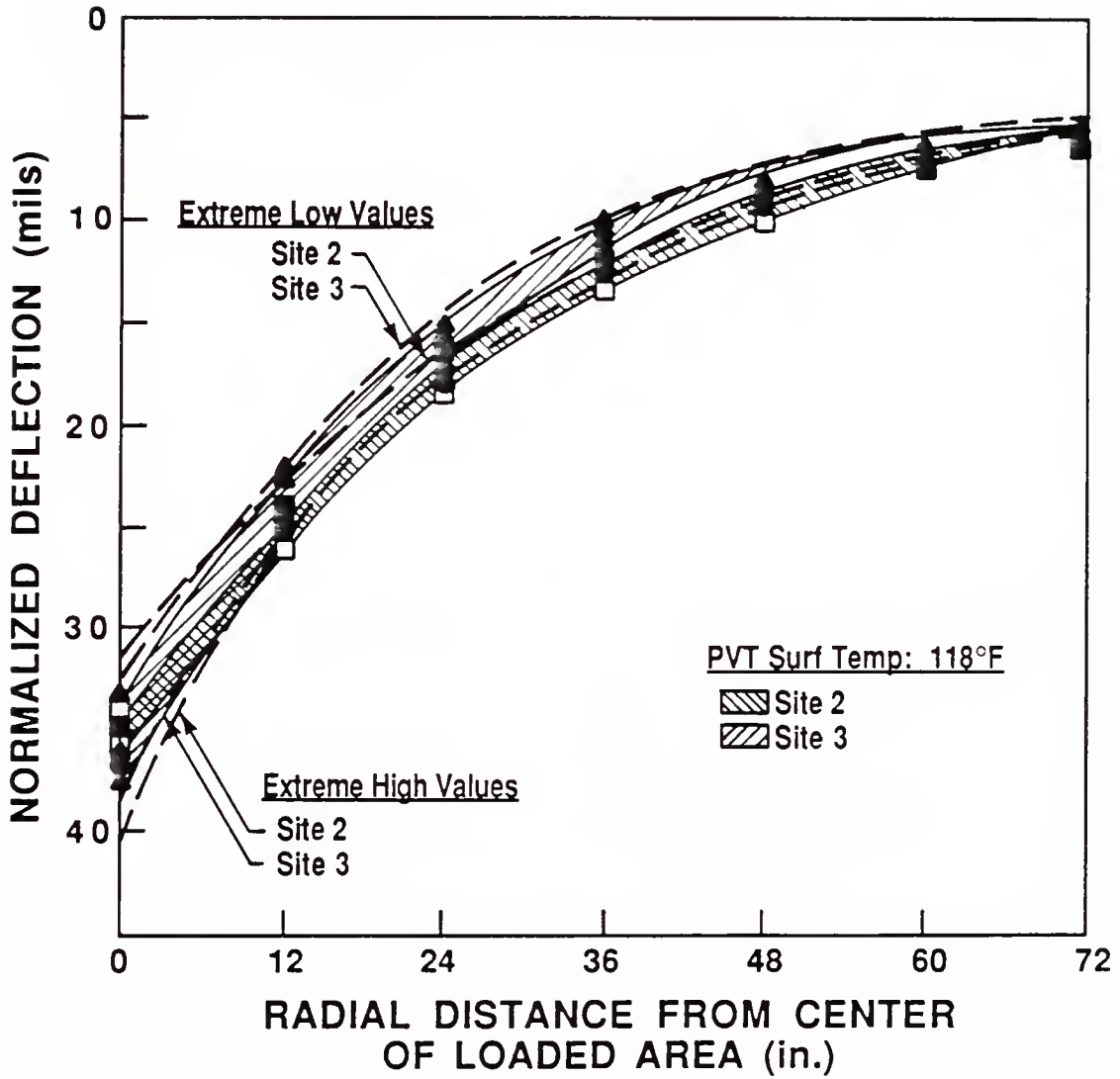


Figure 6.17 Comparison of High Temperature Deflection Response Between Sites 2 and 3 (Normalized to 18-kip Load)

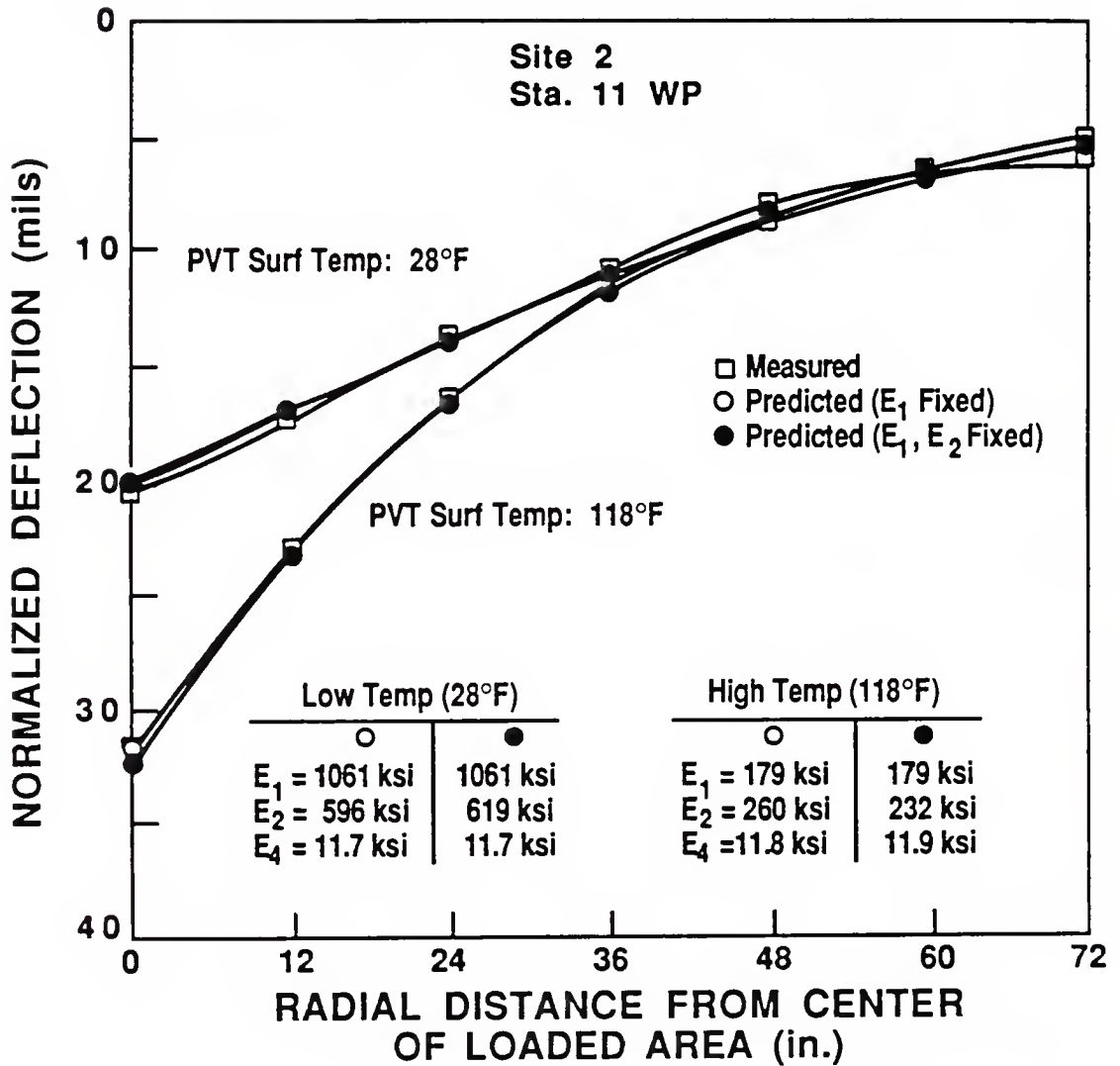


Figure 6.18 Measured and Predicted Deflection Basins in Wheel Path at Site 2 (Normalized to 18-kip Load)

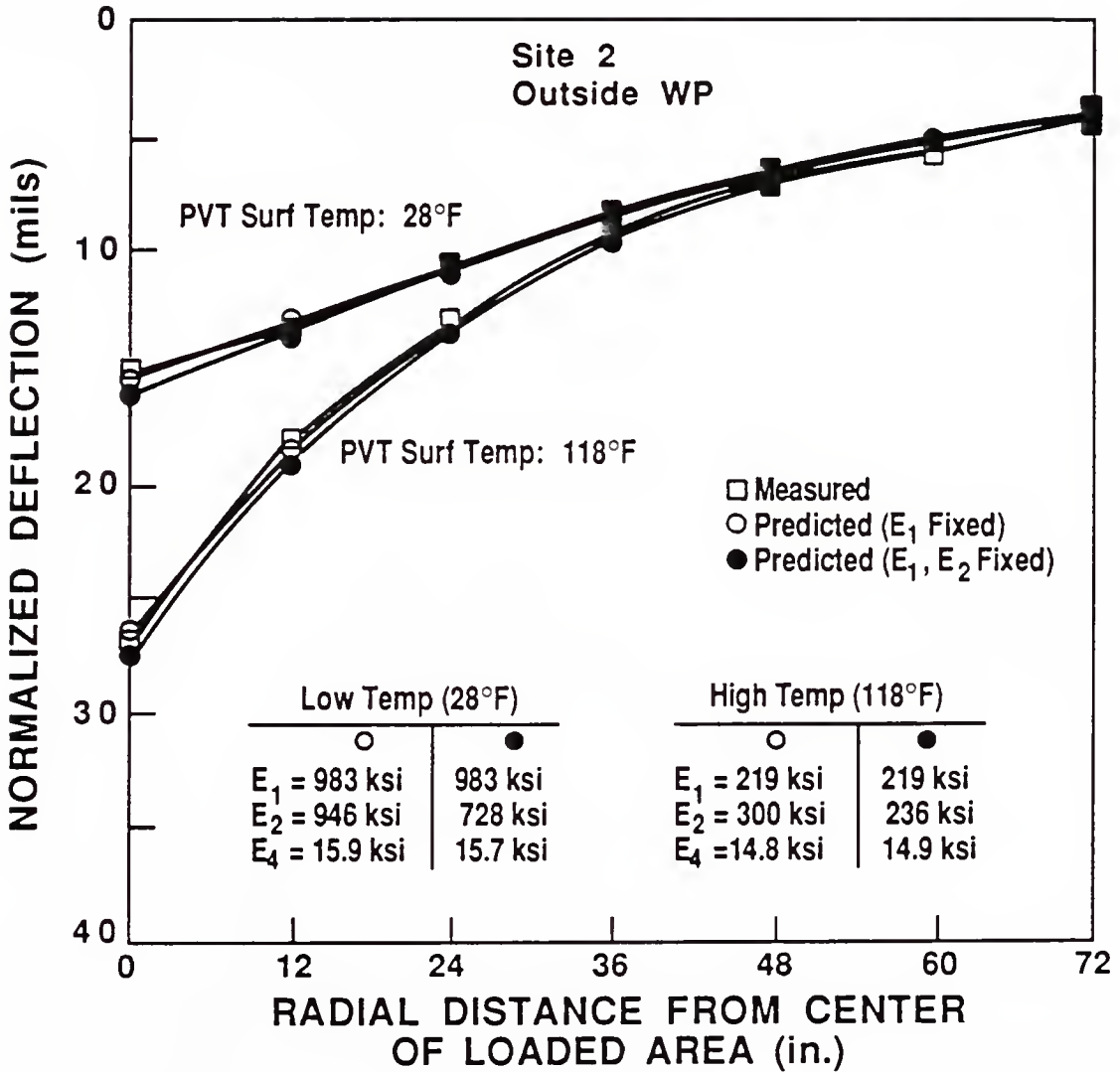


Figure 6.19 Measured and Predicted Deflection Basins Outside Wheel Path at Site 2 (Normalized to 18-kip Load)

6.5 Analysis of Site 1

Site 1 was the most perplexing to characterize. Severe block cracking riddled the pavement, often times running between the sensors positions. The load-deflection response shown in Figures 6.20 and 6.21 did not disclose any abnormalities from a stress dependency standpoint, although responses from the three outer sensors (D_5 , D_6 , and D_7) were grouped together and somewhat detached from the others. This would tend to indicate that the transfer of stresses to these sensors was poor when compared to the responses presented for sites 2 and 3.

Initial iterations using BISDEF suggested that neither the cracked or uncracked methods worked in computing E_1 values. Deflection basins matched poorly and E_2 values were atypically low. The only developing trend was the stabilizing of E_2 values close to 150 ksi at higher temperatures. It was then decided to solve for E_1 by fixing E_2 at 150 ksi. Though this value is below the values of 198 and 204 ksi calculated for sites 2 and 3 respectively, the condition of this pavement and its traffic history (heavily trafficked) made this assumption sound.

With E_2 held fixed, iterations were run to compute E_1 and E_4 over the range of temperatures. Temperature appeared to have little effect on computed E_1 values. In fact, from Figure 6.22, it is shown that E_1 remained constant over the entire temperature range. Computed E_1 values are plotted versus η_{100} and compared with E_1 relationships for sites 2 and 3 in Figure 6.5.

The representative deflection basins plotted in Figure 6.23 at the extreme temperatures appear incorrect. Representative basins at the lowest temperature show greater deflections than basins at the warmest temperature. This contradiction was brought to light when E_4 values

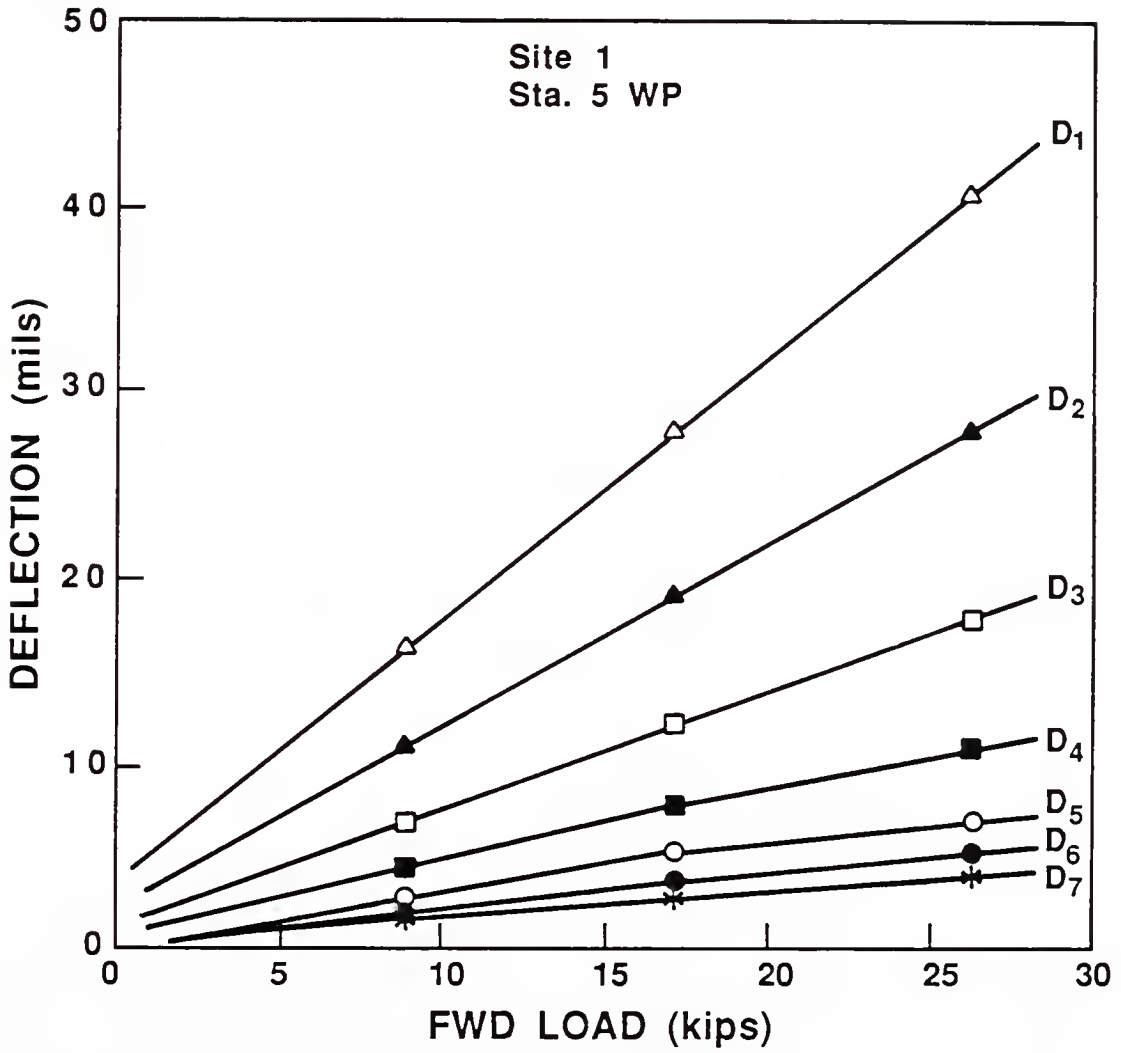


Figure 6.20 Surface Deflection as a Function of Load at Site 1 (Most Linear Response)

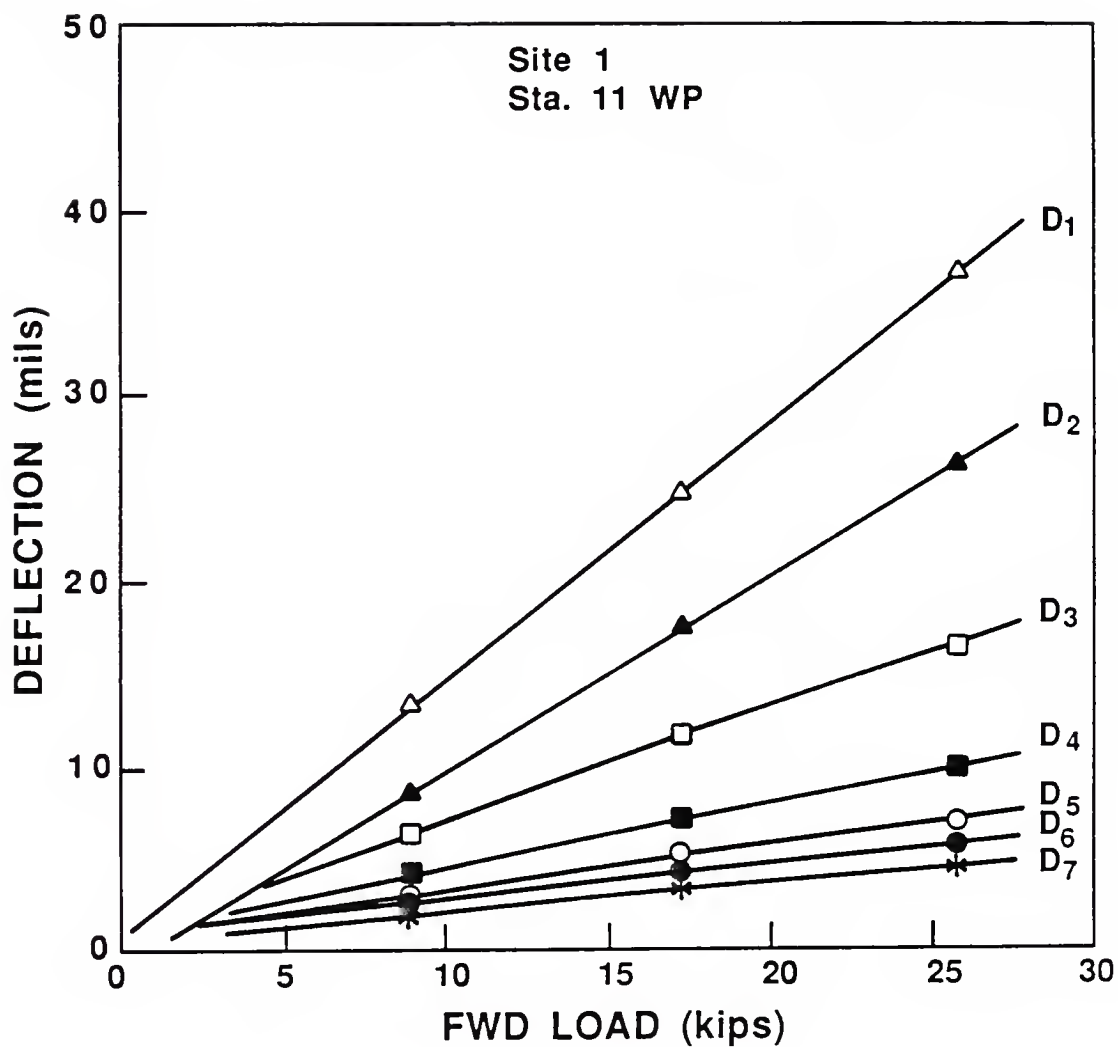


Figure 6.21 Surface Deflection as a Function of Load at Site 1 (Least Linear Response)

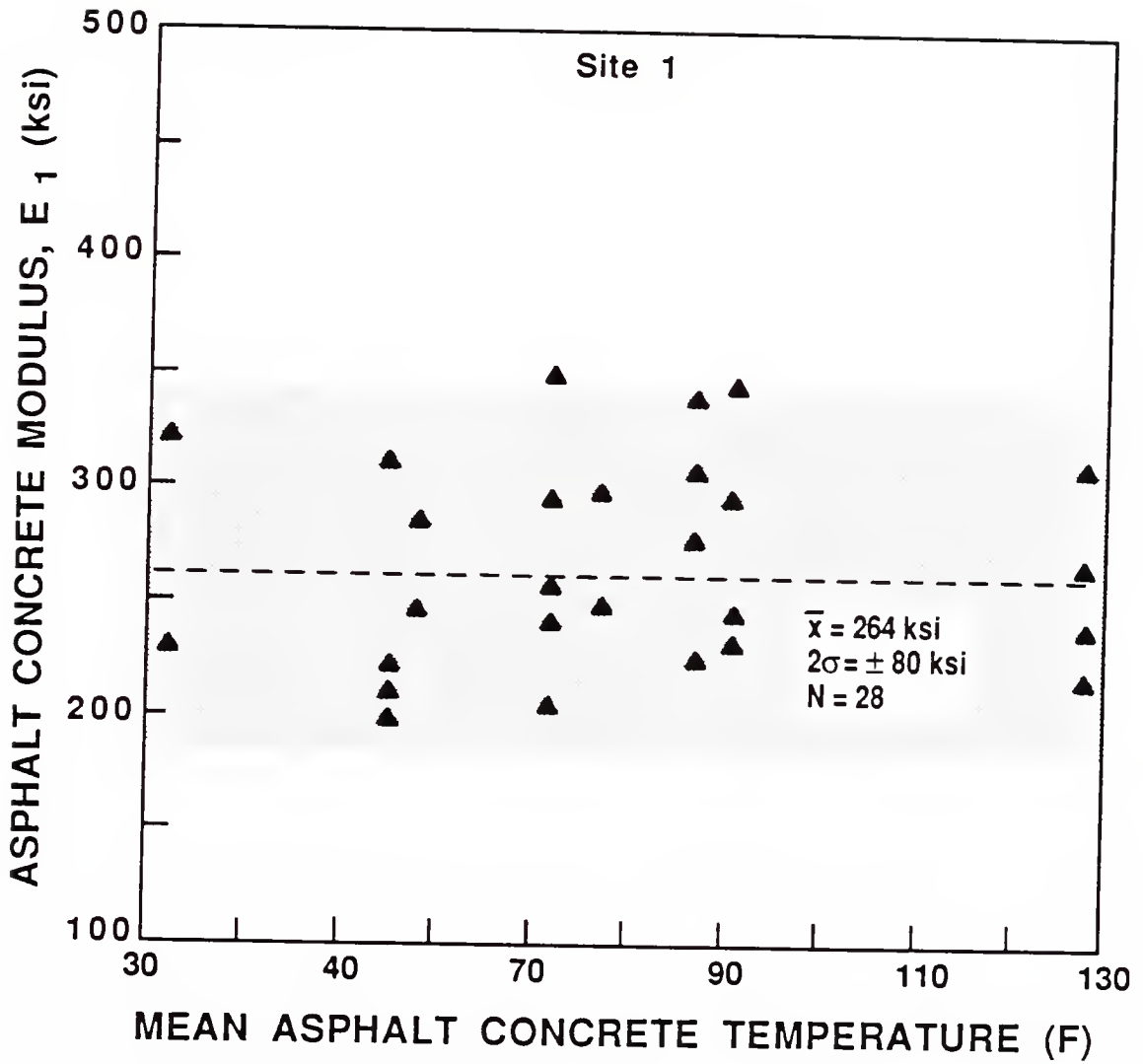


Figure 6.22 E_1 as a Function of Temperature at Site 1

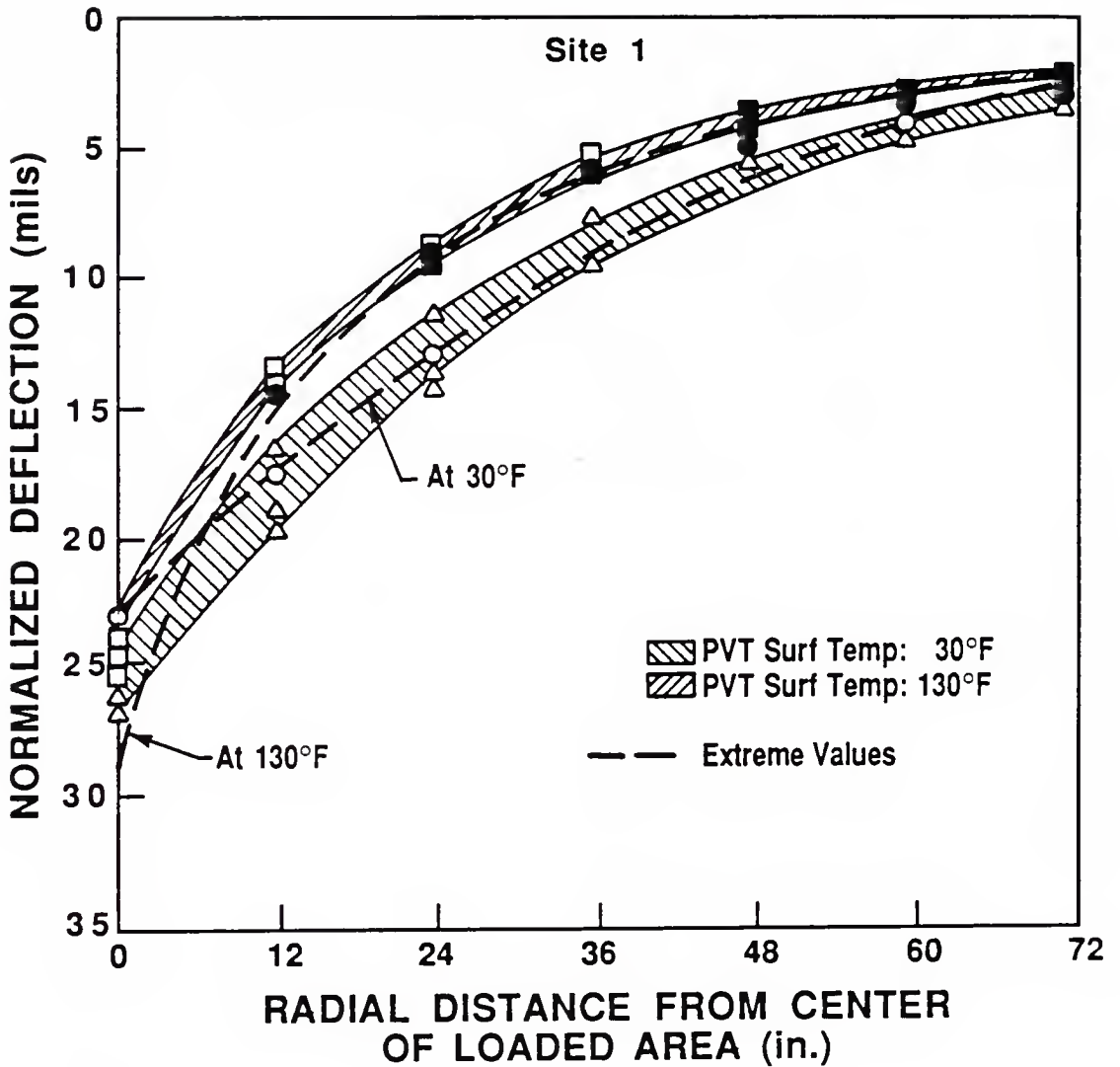


Figure 6.23 Extreme Temperature Deflection Response at Site 1 (Normalized to 18-kip Load)

were calculated and plotted in Figure 6.24. This illustrates that as the pavement temperatures rose, E_4 values went up. BISDEF computed values went from an average of around 18 ksi at 30 F to over 22 ksi at 130 F, an increase of 25 percent. Predicted values rose approximately 18 percent. While searching for possible explanations for this occurrence, questions arose concerning subgrade moisture conditions. These concerns, however, lessened when the following facts were revealed:

- 1) moisture contents taken with the nuclear moisture gauge at site 2 showed no change in moisture content over the period in question;
- 2) sites 2 and 3 showed no changes in E_4 values with temperature;
- 3) inconsistent rainfall amounts for the period did not coincide with steady increases in E_4 values with temperature; and,
- 4) the clean (< 1 percent fines), well-draining nature of the subgrade.

One plausible explanation for the increase in E_4 values was the decrease in the transfer of stress to the outer sensors as the pavement warmed. This was most likely caused by the severe degree of cracking at the pavement surface. This, in turn, resulted in slightly lower measured deflections and thus higher computed E_4 values. If this pavement was to be analyzed as uncracked, an average E_4 of 18.0 kips taken at the coldest temperature would be used.

Since uncracked sections of pavement could not be isolated at site 1, evaluations outside the wheel path were not done.

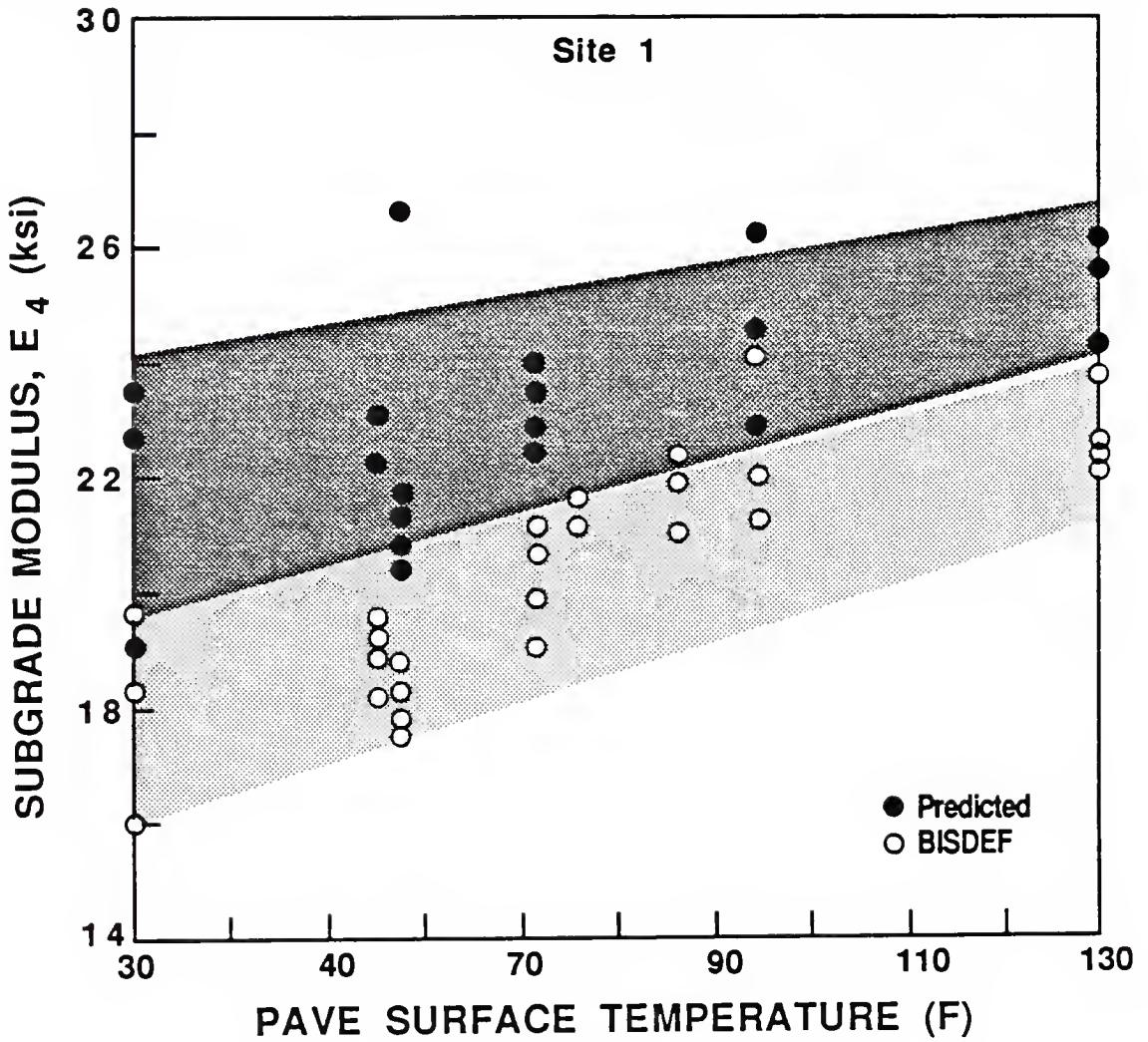


Figure 6.24 Comparison of E_4 Values as a Function of Temperature at Site 1

6.6 Summary

The analyses of these cracked pavements using the layered elastic program BISDEF were quite successful. Only when the pavement was severely cracked, as with site 1, did it present difficulty. Assumptions concerning the cracked nature of the asphalt concrete and sand asphalt layers proved to be reasonable ones. The relative degree of cracking in the asphalt concrete between sites was noticeable using measured deflections at low temperatures. This cracking, however, was more obscured at higher temperatures. Application of the prediction equations developed in Chapter 5 for the uncracked sections, worked reasonably well. The weighted averaging of the asphalt concrete layers did not effect the computed deflections nor the calculated values of E_2 and E_4 .

Overall, the BISDEF program faired best in computing E_4 values but was unsuccessful in calculating E_1 values with any consistency. It would be beneficial for the user to obtain the modulus of the asphalt concrete courses by other means for input into BISDEF. This can be done directly through resilient modulus testing or indirectly through viscosity-modulus relationships.

CHAPTER 7 STRESS ANALYSES FOR PAVEMENT REHABILITATION

7.1 Introduction

Defining failure often eludes the engineer in that many pavements, such as those at Duke Field, show extensive structural failure through cracking but still remain functional. Ullidtz and Stubstad (109) referred to structural and functional deterioration as cracking and rutting, respectively. The horizontal tensile stress or strain at the bottom of the asphalt layer and the vertical compressive stress and strain at the top of the subgrade are normally considered in the analyses of flexible pavements. These, respectively in effect, relate to the bearing capacity and riding quality of the pavement.

Many factors can result in the cracking of flexible pavements. Existing design methods consider cracking in the asphalt-bound layers caused by traffic-load-induced fatigue. The allowable stress or strain criterion is based on the number of repetitions or passes to arrive at the fatigue level. However, Ruth et al. (46) argued that cracking is a short-term phenomenon that results when the combined effects of load and thermal stresses exceed the tensile strength of the asphalt concrete. Work done by Roque (110) indicated that rapid cooling produces sufficient temperature gradients to cause the pavement to lift off from its base in a cyclic (rippling) pattern. Therefore, the stresses imposed by heavy wheel loads, especially on low trafficked pavements, can be high enough to cause cracking in the flexible layers.

The pavements evaluated at Duke Field have demonstrated appreciable deterioration through cracking and rutting and have far exceeded their expected life. Substandard conditions have existed there for a number of years without any long-term solution to correct original design deficiencies, other than infrequent surface treatments.

This chapter will evaluate the adequacy of the original pavement design to meet existing mission demands, then offer specific alternatives for rehabilitation. First presented, will be the analysis of the pavements using the as-constructed (original) design. Then, hypothetical cases for improvement will be given using the original design but substituting in softer, less temperature susceptible asphalts to see what effect it would have on pavement response. Finally, specific scenarios will be presented for rehabilitation of the existing pavement using both conventional overlay and recycling methods. The major thrust of the analyses will consider short-term loading with the effects of any long-term loading (thermal stresses) being neglected.

7.2 Stress Analysis on the As-Constructed Pavements

7.2.1 Input Parameters

The pavement systems were evaluated as they existed in 1970 when the change in mission brought the C-130 aircraft to Duke Field. This change also brought gross aircraft loads up from 8 to 175 kips with single-wheel loads approaching 42 kips. It was shortly after this time period that cracking developed in the asphalt concrete surface course. This subsequently prompted the overlay construction in the mid-seventies. Recall from Chapter 3, that the airfield was originally

constructed in the forties with 6 to 9 in. of sand asphalt. In the early sixties, a 2-in. binder course was added.

Modulus values for the asphalt layers were calculated for an uncracked pavement using the prediction equations developed in Chapter 5. The subgrade moduli were computed by BISDEF in Chapter 6 from FWD data. Evaluations were done on sites 1 and 3 only, since layer thicknesses and computed moduli were similar for sites 2 and 3. Temperatures chosen for analysis were 23 and 86 F which represented, respectively, extreme low winter and typical summer-night temperature conditions.

The BISAR elastic computer program was used to calculate the critical stresses and strains at the bottom of the sand asphalt and at the top of the subgrade. Also computed were the maximum deflection under the load and percent compression of each layer. The elliptical loaded contact area for a single wheel of a C-130 was represented by superpositioning two concentric circles of varying stress concentration. The circles had diameters of 17.0 and 22.0 in. which translated into an average contact stress of 110.5 psi. This contact stress approximated the value of 105 psi given for this type of aircraft (90). This representation was necessary to effectively simulate the elliptical shape of the tire's contact area. Since the gear configuration of the C-130 is characterized as a single-tandem, two loaded areas 60 in. apart were used in the analysis. Stresses and strains directly below one wheel for this tandem arrangement were initially computed. Graphical representations and tables depicting the characteristics of the C-130 were presented in Chapter 3.

7.2.2 Comparison of Pavement Response Using As-Constructed and Improved Material Design Methods

The results of the stress analyses for the two pavements are given in Tables 7.1 to 7.6. The critical response parameters are also summarized in Table 7.7. Tables 7.1 and 7.2 present the predicted response at the two extreme temperatures using the original asphalts. Modulus values were obtained from current rheology relationships. The assumption here, was that no further age-hardening occurred in the asphalt layers after being overlaid.

The results in Table 7.1 show that even at 86 F, tensile stresses at the bottom of the sand asphalt layer far exceeded the maximum tensile strength of 100 psi computed from equation 7.1 and demonstrated by previous laboratory testing. This modified equation was derived from an equation used to determine the modulus of elasticity of concrete from its compressive strength (111).

$$S_{tac} = \left(\frac{E}{k}\right)^2 = 400 \text{ psi} \quad (7.1)$$

therefore,

$$k = \frac{E_{ac} \text{ max}}{\sqrt{S_{tac}}} = \frac{1,400,000}{\sqrt{400}} = 70,000$$

using k and E_2

$$S_{t sa} = \left(\frac{700,000}{70,000}\right)^2 = 100 \text{ psi}$$

where

$S_{t sa}$ and S_{tac} = maximum tensile strength of the sand asphalt and asphalt concrete,

Table 7.1 Input Parameters and Results of Stress Analysis
at 86 F on Original Pavements

a) Input Parameters for Bisar

Layer	Description	Thickness (in.)	Poisson's Ratio	Modulus (psi) *	
				Site 1	Site 3
1	Asphalt Concrete	1.8	0.35	279,000	294,000
2	Sand Asphalt	7.5 (8.0)	0.35	257,000	207,000
3	Subgrade	semi- infinite	0.40	18,000	12,300

* Asphalt Concrete and Sand Asphalt Moduli computed from equation 5.3
Subgrade Modulus computed from BISDEF

b) Pavement Stress Analysis

Response Parameters **		Site 1	Site 3
Maximum Surface Deflection	(mils)	62.9	84.4
Radial Stress, Bottom of AC Layer	(psi)	-177.0	-192.0
Radial Strain, Bottom of AC Layer	(micro strain)	-256.0	-272.0
Radial Stress, Bottom of SA Layer	(psi)	194.0	195.0
Radial Strain, Bottom of SA Layer	(micro strain)	528.0	643.0
Percentage of Failure Stress ***	(percent)	194.0	195.0
Vertical Stress, Top of Subgrade	(psi)	-36.3	-30.2
Vertical Strain, Top of Subgrade	(micro strain)	-1690.0	-2080.0
Deflection in Asphalt Layers	(percent)	3.8	3.7
Deflection in Subgrade	(percent)	96.2	96.3

** Computed under single wheel for tandem wheel loading

*** Failure tensile stress of 100 psi

NOTE:

+ = tensile

- = compressive

Table 7.2 Input Parameters and Results of Stress Analysis
at 23 F on Original Pavements

a) Input Parameters for Bisar

Layer	Description	Thickness (in.)	Poisson's Ratio	Modulus (psi) *	
				Site 1	Site 3
1	Asphalt Concrete	1.8	0.35	1,180,000	1,340,000
2	Sand Asphalt	7.5 (8.0)	0.35	709,000	763,000
3	Subgrade	semi- infinite	0.40	18,000	12,300

* Asphalt Concrete and Sand Asphalt Moduli computed from equation 5.4
Subgrade Modulus computed from BISDEF

b) Pavement Stress Analysis

Response Parameters **		Site 1	Site 3
Maximum Surface Deflection	(mils)	48.1	61.1
Radial Stress, Bottom of AC Layer	(psi)	-251.0	-276.0
Radial Strain, Bottom of AC Layer	(micro strain)	-97.6	-95.4
Radial Stress, Bottom of SA Layer	(psi)	280.0	300.0
Radial Strain, Bottom of SA Layer	(micro strain)	254.0	246.0
Percentage of Failure Stress ***	(percent)	280.0	300.0
Vertical Stress, Top of Subgrade	(psi)	-20.5	-14.9
Vertical Strain, Top of Subgrade	(micro strain)	-913.0	-946.0
Deflection in Asphalt Layers	(percent)	2.1	1.6
Deflection in Subgrade	(percent)	97.9	98.4

** Computed under single wheel for tandem wheel loading

*** Failure tensile stress of 100 psi

NOTE:

+ = tensile

- = compressive

$$\begin{aligned} E_2 &= \text{maximum modulus of the sand asphalt} \\ &= 700,000 \text{ psi @ 23 percent air voids} \end{aligned}$$

Stresses in the bound asphalt wearing course were all in compression due to the thinness of the layer and relative stiffness of the sand asphalt. Vertical subgrade compressive stresses were generally high constituting around 30 percent of the average vertical stress of 110.5 psi applied by each wheel. This value is more than the limiting 10 percent level conventionally used with classical Boussinesq's solutions for a static loading (39). Subgrade deformation represented over 96 percent of the total deformation for both sites. Strain values at both sites exceeded the 2.6×10^{-4} in./in. subgrade strain criteria established by the Shell Oil Company for repetitive loadings (39). This criteria ensures that permanent strain in the subgrade will not lead to excessive rutting at the pavement surface. In low trafficked airfields, however, strain tolerances can be much higher, especially if comprised of granular material. Since it was shown that failure developed from cracking in the sand asphalt, it was likely that subgrade stresses were increased which led to excessive strains and deformations. This could explain, at least in part, the rutting observed at sites 1 and 2.

An analysis at 23 F was done to compare with the values predicted at 86 F. This comparison was done only to demonstrate the effects of temperature on pavement stiffness and resulted stresses and strains. In reality, these pavements systems were shown to have failed both structurally (cracking in the sand asphalt) and functionally (excessive subgrade strain) at higher ambient temperatures. From Table 7.2, tensile stresses at the bottom of the sand asphalt jumped over 40 percent to a high value of 300 psi at site 1. Failure stress ratios for the sand

asphalt were close to 200 percent at 86 F and 300 percent at 23 F. Subgrade strain values, though lower at 86 F, were still over 300 percent higher than the limit set by the Shell Oil Company.

The above evaluation indicated that the stresses produced by the C-130 aircraft were high enough to initiate failure in the pavements, even at above average temperatures. High tensile stresses in the asphalt-bound layers and high vertical compressive stresses (strains) in the subgrade indicated that these pavements were not designed to accommodate present aircraft loads. It can be shown from Tables 7.3 and 7.4, that even if the asphalt layers were constructed using a softer, lower temperature susceptible asphalt like the Texaco Air-Blown (TAB), the stresses and strains would still exceed failure limits. The temperature-modulus relationships for the Duke Field and TAB asphalts are compared in Figure 7.1. Using the TAB asphalt, stresses in the sand asphalt were still high. Even with a stiffer subgrade at site 1, the failure stress ratio in the sand asphalt at 86 F was near 70 percent. At 23 F, this value rose to 274 percent, again demonstrating the inability of the pavement to withstand the loads imposed.

Finally, a study was undertaken to determine what positive effects on pavement performance would have resulted if, during initial construction, quality materials and tighter controls were used. Essentially, the only difference in construction technique in this case was replacing the sand asphalt with a full-depth asphalt concrete layer. Below are listed the assumptions and criteria used in the analysis:

- 1) The full-depth layer was placed in 1950 using the TAB asphalt and compacted to 7 percent air voids.

Table 7.3 Input Parameters and Results of Stress Analysis at 86 F on Original Pavements Using the Texaco Air-Blown Asphalt

a) Input Parameters for Bisar

Layer	Description	Thickness (in.)	Poisson's Ratio	Modulus (psi) *	
				Site 1	Site 3
1	Asphalt Concrete	1.8	0.35	96,200	96,200
2	Sand Asphalt	7.5 (8.0)	0.35	66,300	66,300
3	Subgrade	semi- infinite	0.40	18,000	12,300

* Asphalt Concrete and Sand Asphalt Moduli computed from equation 5.3 (no age-hardening assumed)
Subgrade Modulus computed from BISDEF

b) Pavement Stress Analysis

Response Parameters **		Site 1	Site 3
Maximum Surface Deflection	(mils)	86.7	112.0
Radial Stress, Bottom of AC Layer	(psi)	-120.0	-136.0
Radial Strain, Bottom of AC Layer	(micro strain)	-367.0	-471.0
Radial Stress, Bottom of SA Layer	(psi)	69.7	97.9
Radial Strain, Bottom of SA Layer	(micro strain)	1000.0	1210.0
Percentage of Failure Stress ***	(percent)	69.7	97.9
Vertical Stress, Top of Subgrade	(psi)	-60.9	-50.2
Vertical Strain, Top of Subgrade	(micro strain)	-2960.0	-3590.0
Deflection in Asphalt Layers	(percent)	11.4	8.9
Deflection in Subgrade	(percent)	88.6	91.1

** Computed under single wheel for tandem wheel loading

*** Failure tensile stress of 100 psi

NOTE:

+ = tensile

- = compressive

Table 7.4 Input Parameters and Results of Stress Analysis at 23 F
on Original Pavements Using the Texaco Air-Blown Asphalt

a) Input Parameters for Bisar

Layer	Description	Thickness (in.)	Poisson's Ratio	Modulus (psi) *	
				Site 1	Site 3
1	Asphalt Concrete	1.8	0.35	926,000	926,000
2	Sand Asphalt	7.5 (8.0)	0.35	639,000	639,000
3	Subgrade	semi- infinite	0.40	18,000	12,300

* Asphalt Concrete and Sand Asphalt Moduli computed from equation 5.3
(no age-hardening assumed)
Subgrade Modulus computed from BISDEF

b) Pavement Stress Analysis

Response Parameters **		Site 1	Site 3
Maximum Surface Deflection	(mils)	49.8	64.6
Radial Stress, Bottom of AC Layer	(psi)	-239.0	-255.0
Radial Strain, Bottom of AC Layer	(micro strain)	-117.0	-126.0
Radial Stress, Bottom of SA Layer	(psi)	274.0	291.0
Radial Strain, Bottom of SA Layer	(micro strain)	278.0	287.0
Percentage of Failure Stress ***	(percent)	274.0	291.0
Vertical Stress, Top of Subgrade	(psi)	-22.1	-16.9
Vertical Strain, Top of Subgrade	(micro strain)	-988.0	-1680.0
Deflection in Asphalt Layers	(percent)	2.0	1.7
Deflection in Subgrade	(percent)	98.0	98.3

** Computed under single wheel for tandem wheel loading

*** Failure tensile stress of 100 psi

NOTE:

+ = tensile

- = compressive

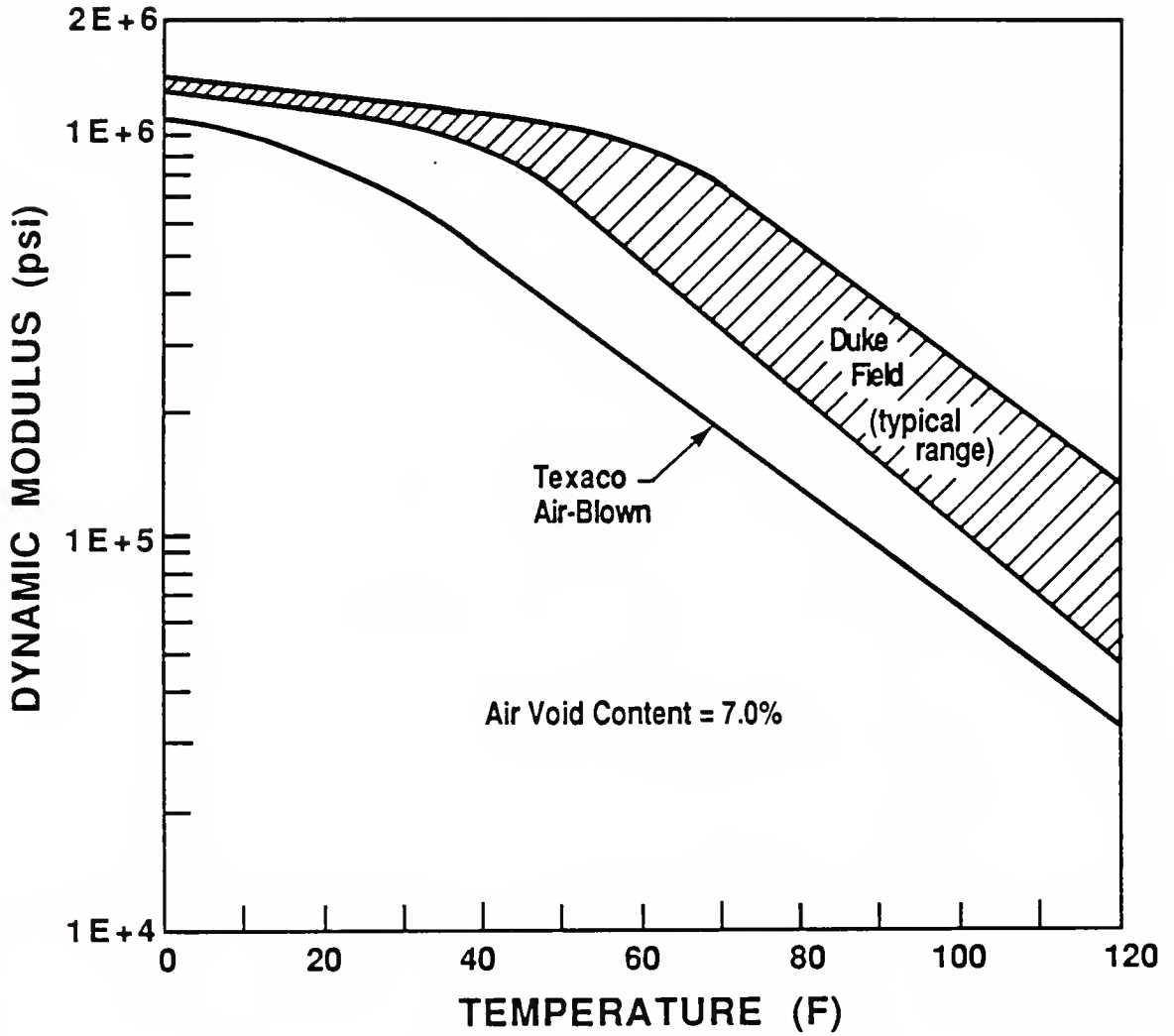


Figure 7.1 Comparison of Modulus-Temperature Relationships Between the Duke Field and Texaco Air-Blown Asphalts

- 2) The asphalt age-hardened for twenty years at a low hardening rate while the air void content reduced to 5 percent through traffic compaction.
- 3) After twenty years, a thin surface course was added using the same asphalt cement and compacted to 7 percent air voids.

The analysis, presented Tables 7.5 and 7.6, showed that the stresses and strains produced by the C-130 were still somewhat high at elevated ambient temperatures. At 86 F, the tensile stresses at the bottom of the full-depth asphalt concrete were 247 and 274 psi for sites 1 and 3, respectively. The small difference being attributed to the stiffer subgrade at site 1. Using a maximum tensile strength of 400 psi given for asphalt concrete, the stress ratios were between 60 and 70 percent. From the standpoint of load-induced stresses, 50 percent is considered high, especially at 86 F. Vertical compressive stresses to the subgrade at both sites were still high with values of 36.2 psi computed for site 1 and 28.0 psi for site 3.

Results at 23 F were less encouraging. Tensile stress ratios in the asphalt concrete climbed to over 90 percent. At this value, failure due to fatigue (repeated loadings) alone would be anticipated under relatively few load applications. Compressive stresses in the subgrade at 23 F began to approach normal limits and at site 3 reached a low of 14.9 psi.

The prior analyses confirmed that the pavements could not have handled the increased loads brought on by the C-130 aircraft under the original design conditions. The sand asphalt was too weak and brittle to hold up against existing subgrade support. Even in the full-depth

Table 7.5 Input Parameters and Results of Stress Analysis at 86 F on Full-Depth Asphalt Concrete Pavements Using the Texaco Air-Blown Asphalt

a) Input Parameters for Bisar

Layer	Description	Thickness (in.)	Poisson's Ratio	Modulus (psi) *	
				Site 1	Site 3
1	Asphalt Concrete	1.8	0.35	96,200	96,200
2	Asphalt Concrete	7.5 (8.0)	0.35	353,000	353,000
3	Subgrade	semi- infinite	0.40	18,000	12,300

* Asphalt Concrete Moduli computed from equation 5.3
(layer 2 age-hardened for 20 years at low hardening rate
from Chapter 4)
Subgrade Modulus computed from BISDEF

b) Pavement Stress Analysis

Response Parameters **		Site 1	Site 3
Maximum Surface Deflection	(mils)	63.2	81.8
Radial Stress, Bottom of AC Layer 1	(psi)	-121.0	-126.0
Radial Strain, Bottom of AC Layer 1	(micro strain)	-370.0	-398.0
Radial Stress, Bottom of AC Layer 2	(psi)	247.0	274.0
Radial Strain, Bottom of AC Layer 2	(micro strain)	481.0	515.0
Percentage of AC Failure Stress ***	(percent)	61.8	68.5
Vertical Stress, Top of Subgrade	(psi)	-36.2	-28.0
Vertical Strain, Top of Subgrade	(micro strain)	-1630.0	-1810.0
Deflection in Asphalt Layers	(percent)	3.3	2.7
Deflection in Subgrade	(percent)	96.7	97.3

** Computed under single wheel for tandem wheel loading

*** Failure tensile stress of 400 psi

NOTE:

+ = tensile

- = compressive

Table 7.6 Input Parameters and Results of Stress Analysis at 23 F on Full-Depth Asphalt Concrete Pavements Using the Texaco Air-Blown Asphalt

a) Input Parameters for Bisar

Layer	Description	Thickness (in.)	Poisson's Ratio	Modulus (psi) *	
				Site 1	Site 3
1	Asphalt Concrete	1.8	0.35	926,000	926,000
2	Asphalt Concrete	7.5 (8.0)	0.35	1,310,000	1,310,000
3	Subgrade	semi- infinite	0.40	18,000	12,300

* Asphalt Concrete Moduli computed from equation 5.3 (4)
(layer 2 age-hardened for 20 years at low hardening rate
from Chapter 4)
Subgrade Modulus computed from BISDEF

b) Pavement Stress Analysis

Response Parameters **		Site 1	Site 3
Maximum Surface Deflection	(mils)	44.5	57.7
Radial Stress, Bottom of AC Layer 1	(psi)	-229.0	-238.0
Radial Strain, Bottom of AC Layer 1	(micro strain)	-109.0	-113.0
Radial Stress, Bottom of AC Layer 2	(psi)	368.0	382.0
Radial Strain, Bottom of AC Layer 2	(micro strain)	177.0	180.0
Percentage of AC Failure Stress ***	(percent)	92.0	95.5
Vertical Stress, Top of Subgrade	(psi)	-17.1	-13.0
Vertical Strain, Top of Subgrade	(micro strain)	-713.0	-774.0
Deflection in Asphalt Layers	(percent)	1.1	0.9
Deflection in Subgrade	(percent)	98.9	99.1

** Computed under single wheel for tandem wheel loading

*** Failure tensile stress of 400 psi

NOTE:

+ = tensile

- = compressive

Table 7.7 Summary of Critical Response Parameters for the As-Constructed Design Using Original and Texaco Air-Blown Asphalts

Asphalt Type	Evaluated Temp. (F)	Maximum Surf. Defl. (mils)	Radial Stress Bottom Asphalt Layer (psi)	Failure Stress Ratio (percent)	Vertical Strain Top of Subgrade (x10E-6)	Subgrade Compression (percent)
Original						
Site 1	86	62.9	194	194	1690	96.2
Site 3		84.4	195	195	2080	96.3
Site 1	23	48.1	280	280	913	97.9
Site 3		61.1	300	300	946	98.4
Texaco Air-Blown (TAB)						
Site 1	86	86.7	70	70	2960	88.6
Site 3		112.0	98	98	3590	91.1
Site 1	23	49.8	274	274	988	98.0
Site 3		64.6	291	291	1680	98.3
Full-Depth (TAB)						
Site 1	86 (aged)	63.2	247	62	1630	96.7
Site 3		81.8	274	69	1810	97.3
Site 1	23 (aged)	44.5	368	92	713	98.9
Site 3		57.7	382	96	774	99.1

asphalt case, the subgrade modulus would of needed to be over 50,000 psi to reduce the stresses to desirable levels.

7.3 Rehabilitation of Existing Pavements

The pavements evaluated at Duke Field have deteriorated to where operational hazards could soon pose a threat to existing air traffic. Signs of weathering and ravelling present the risk of foreign object damage (FOD) that could impair aircraft wheels and engines. The current condition of the pavement clearly demonstrates inadequate design and maintenance. Since the early seventies, overlay construction projects were undertaken to cover up the cracking and rutting that had resulted from excessive binder viscosities (low fracture energy) and aircraft loads. High air void contents in the asphalt layers also contributed to failure, especially in the sand asphalt where its strength was severely degraded. In order to correct the deficiencies that exist and alleviate the potential for operational hazards and restrictions, restorative measures should be taken. A specific rehabilitation scenario will be offered for each site which will take into account existing layer properties and surface distress conditions.

7.3.1 Rehabilitation of Site 3

Overlay construction is warranted as long as the pavement presents no riding difficulties which would indicate a serious sublayer condition. Since the pavement at site 3 showed minimal distress it was selected first for restoration. Applying overlay methodology here, for all practical purposes, concedes the cracking already present in the underlying layers. The aim here is to 1) provide a rideable wearing surface resistant to reflective cracking and 2) prevent further cracking

in the existing system by maintaining stresses either at or below current levels. Certain construction measures, however, should be taken to minimize the rate and degree of reflective cracking. They are listed below:

- 1) Clean and grout all existing cracks.
- 2) After tack coat, place 3-in. minimum of high quality course aggregate mix with 1-in. top size aggregate. Compact to 7 percent air void content or less. Used as a stress relief layer.
- 3) Place 2 in. of high quality structural mix similar to FDOT Type S-1, with 3/4-in. top size aggregate. Compact to 7 percent or less.

Large maximum aggregate sizes are used to bridge the cracks and provide stress relief to minimize reflective cracking to the surface. Drawbacks to this method are the additional considerations for changing grade and drainage requirements.

A stress analysis was done on the system to predict its performance, first at 86 F (present day) and then at 23 F after 20 years of in-service hardening using the TAB asphalt. Stresses and strains were computed using BISAR at various locations under and away from the wheel load (Figure 7.2). Results presented in Table 7.8 indicate that at 86 F a maximum tensile stress of 111 psi occurred at the bottom of the sand asphalt layer directly under the wheel load. This value, though, was reduced from 195 psi computed for the original pavement. Subgrade vertical stresses were also reduced from 30.2 to 16.9 psi. Maximum tensile stresses at the top of the overlay measured 6.8 psi and occurred 45 in. out from the center of the loaded area in the wheel path. At

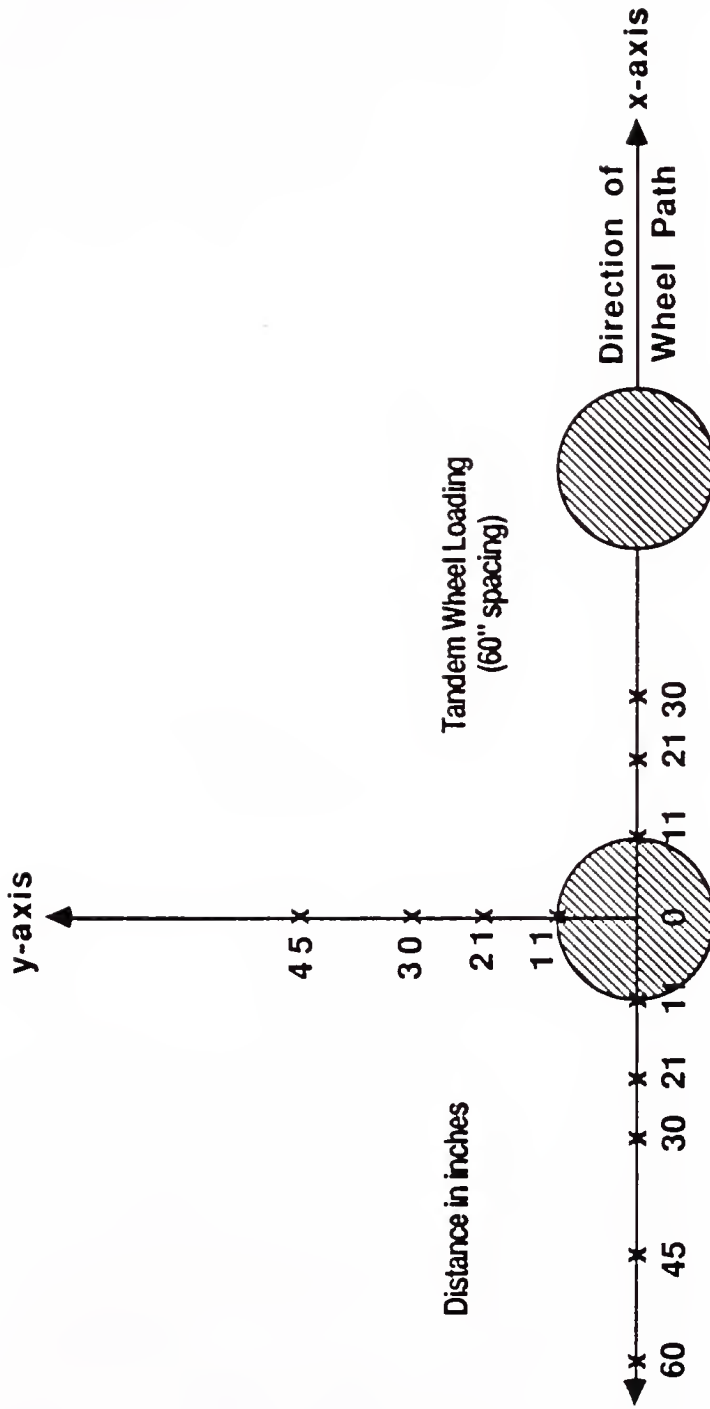


Figure 7.2 Radial Distances Used in Pavement Stress Analyses

Table 7.8 Input Parameters and Results of Stress Analysis for Overlay Rehabilitation at Site 3

a) Input Parameters for Bisar

Layer	Description	Thickness (in.)	Poisson's Ratio	Modulus (psi) *	
				86 F	23 F
1	Asphalt Concrete (OL)	5.0	0.35	96,200	1,310,000
2	Asphalt Concrete	3.5	0.35	294,000	700,000
3	Sand Asphalt	8.0	0.35	204,000	204,000
4	Subgrade	semi- infinite	0.40	12,300	12,300

* AC Overlay Moduli computed from equation 5.3 (4)
(at 23 F, OL age-hardened for 20 years at low hardening rate)
Layers 2 and 3 analyzed as cracked (no further age-hardening assumed)
Subgrade Modulus computed from BISDEF

b) Pavement Stress Analysis

Response Parameters **		86 F	23 F
Maximum Surface Deflection	(mils)	68.7	51.5
Radial Stress, Top of Overlay	(psi)	6.8	25.7
Radial Strain, Top of Overlay	(micro strain)	97.7	25.7
Radial Stress, Bottom of Overlay	(psi)	-77.0	35.2
Radial Strain, Bottom of Overlay	(micro strain)	-119.0	38.7
Percentage of Failure Stress ***	(percent)	--	8.8
Radial Stress, Bottom of Layer 2	(psi)	-8.0	125.0
Radial Strain, Bottom of Layer 2	(micro strain)	76.0	130.0
Radial Stress, Bottom of Layer 3	(psi)	111.0	70.3
Radial Strain, Bottom of Layer 3	(micro strain)	361.0	220.0
Vertical Stress, Top of Subgrade	(psi)	-16.9	-9.9
Vertical Strain, Top of Subgrade	(micro strain)	-1190.0	-725.0

** Maximum computed values for tandem wheel loading

*** Failure tensile stress of 400 psi

NOTE: + = tensile
- = compressive

23 F (after aging) stresses in the overlay increased as expected but were still within desirable ranges. Table 7.8 revealed a maximum tensile stress of 70.3 psi in the sand asphalt which was reduced from 300 psi, originally. A tensile stress of 125 psi predicted at the bottom of the cracked asphalt concrete layers was also tolerable. At the top of the overlay, the maximum tensile stress developed was 25.7 psi and occurred 60 in. away from the loaded area in the wheel path. At neither temperature did tensile stresses develop at the top of the overlay between the two wheel loads. This implied that this area was entirely in compression with no reverse bending occurring.

This overlay design appeared to perform well under analysis. Load-induced stresses appeared low enough to allow for the added effects of thermal stresses, even after 20 years.

7.3.2 Rehabilitation of Site 2

Site 2 was analyzed from overlay, recycling and reconstruction perspectives. It was found that removing the original asphalt concrete and replacing it with a recycled mixture greatly increased the tensile stresses in the pavement at 23 F. This occurred because of the high increase in stiffness in the new asphalt layer relative to the degraded increase in stiffness in the cracked layers of the original pavement. This was even more apparent when reconstructing the entire pavement. For this design, 6 in. of sand subgrade was excavated and replaced with 12 in. of crushed limestone, then overlaid with 5 in. of new asphalt. Maximum tensile stresses in the asphalt concrete at 23 F after 20 years were extremely high at 378 psi. Again, the reduced stiffness in the limestone base ($E = 85,000$ psi) as compared with the original sand asphalt and asphalt concrete layers concentrated the tensile stresses in

the reconstructed asphalt concrete layer. The limestone base did, however, help reduce the vertical stress to the subgrade to 12.8 psi.

The best method to reduce stresses to the subgrade while decreasing the tensile stresses in the bound layers was to overlay the existing pavement. Following construction procedures for site 3, 5 in. of new asphalt was added to the existing pavement. Using this approach, stresses were greatly diminished (Table 7.9). At 86 F, the highest tensile stress in the sand asphalt was reduced from 195 psi for the original pavement to 132 psi. Therefore, no further cracking would be expected in this layer. The maximum tensile stress predicted at the top of the asphalt concrete was 7.5 psi which occurred 45 in. from the center loaded area in the wheel path. Subgrade compressive stresses were dropped from 30 to 17 psi. After the 20 year aging period, stresses at 23 F remained low. A maximum tensile stress of 99.0 psi was computed at the bottom of the overlay under the wheel load. The highest tensile stress predicted at the top of the pavement was 26.8 psi and developed 60 in. from the center of the loaded area in the wheel path. Subgrade stresses also reached a very low value of 10.4 psi due to the thickness and relative stiffness of the upper layers.

7.3.3 Rehabilitation of Site 1

Site 1 was a prime candidate for recycling of the asphalt concrete courses. Profuse block cracking would make this site more difficult to effectively overlay than site 3. However, a stiff subgrade here helped to reduce the stresses in the upper material and therefore, additional asphalt layers were not required. Below outlines the recycling construction procedures for site 1:

Table 7.9 Input Parameters and Results of Stress Analysis for Overlay Rehabilitation at Site 2

a) Input Parameters for Bisar

Layer	Description	Thickness (in.)	Poisson's Ratio	Modulus (psi) *	
				86 F	23 F
1	Asphalt Concrete (OL)	5.0	0.35	96,200	1,310,000
2	Asphalt Concrete	2.9	0.35	289,000	450,000
3	Sand Asphalt	8.0	0.35	198,000	198,000
4	Subgrade	semi- infinite	0.40	11,400	11,400

* AC Overlay Moduli computed from equations 5.3 (4)
(at 23 F, OL age-hardened for 20 years at low hardening rate)
Layers 2 and 3 analyzed as cracked (no further age-hardening assumed)
Subgrade Modulus computed from BISDEF

b) Pavement Stress Analysis

Response Parameters **		86 F	23 F
Maximum Surface Deflection	(mils)	74.1	56.8
Radial Stress, Top of Overlay	(psi)	7.5	26.8
Radial Strain, Top of Overlay	(micro strain)	105.0	26.6
Radial Stress, Bottom of Overlay	(psi)	-77.5	99.0
Radial Strain, Bottom of Overlay	(micro strain)	-117.0	70.9
Percentage of Failure Stress ***	(percent)	--	24.8
Radial Stress, Bottom of Layer 2	(psi)	-173.0	87.3
Radial Strain, Bottom of Layer 2	(micro strain)	61.8	171.0
Radial Stress, Bottom of Layer 3	(psi)	132.0	92.1
Radial Strain, Bottom of Layer 3	(micro strain)	489.0	345.0
Vertical Stress, Top of Subgrade	(psi)	-17.2	-10.4
Vertical Strain, Top of Subgrade	(micro strain)	-1300.0	-827.0

** Maximum computed values for tandem wheel loading

*** Failure tensile stress of 400 psi

NOTE: + = tensile
- = compressive

- 1) Mill off asphalt concrete to 1/2 in. above sand asphalt.
- 2) Smooth milled surface and grout obvious cracks.
- 3) Place 3.0 in. of high quality structural mix with 1-in. top size aggregate. Compact to 7 percent air void content or less.

Similar analytical procedures to sites 2 and 3 were followed for site 1. Results of the analysis in Table 7.10 indicated that the stresses were reduced 37 percent in the sand asphalt layer at 86 F and 66 percent at 23 F (after aging). Compressive stresses at the top of the subgrade, though, remained about the same. Tensile stresses in the recycled surface course at 86 F remained low, as expected. These stresses, however, were elevated after 20 years. Analysis at 23 F showed that the maximum tensile stresses at the top and bottom of the recycled layer were 11.1 and 215 psi, respectively. The high load-induced stress computed for the bottom of the asphalt concrete could, in combination with thermally-applied stresses, precipitate failure. How soon failure would occur would depend on many factors including 1) rate of binder hardening and 2) critical temperature and rate of cooling relative to binder viscosity.

7.4 Summary

The evaluated pavements at Duke Field failed because they were underdesigned to adequately handle the increased loads brought on by the C-130 mission. Analyses demonstrated that tensile stresses in the weak, brittle sand asphalt were 200 to 300 percent higher than its fracture strength. Subgrade stresses at warmer temperature were also high. Reconstruction techniques offered considerably less stiffness to the underlying system and tended to concentrate higher stresses in the upper

Table 7.10 Input Parameters and Results of Stress Analysis for Recycling Rehabilitation at Site 1

a) Input Parameters for Bisar

Layer	Description	Thickness (in.)	Poisson's Ratio	Modulus (psi) *	
				86 F	23 F
1	Asphalt Concrete (OL)	3.5	0.35	96,200	1,310,000
2	Asphalt Concrete	0.5	0.35	264,000	264,000
3	Sand Asphalt	7.5	0.35	150,000	150,000
4	Subgrade	semi- infinite	0.40	18,000	18,000

* AC Overlay Moduli computed from equations 5.3 (4)
(at 23 F, OL age-hardened for 20 years at low hardening rate)
Layers 2 and 3 analyzed as cracked (no further age-hardening assumed)
Subgrade Modulus computed from BISDEF

b) Pavement Stress Analysis

Response Parameters **		86 F	23 F
Maximum Surface Deflection	(mils)	66.9	54.3
Radial Stress, Top of Overlay	(psi)	11.1	41.6
Radial Strain, Top of Overlay	(micro strain)	156.0	48.5
Radial Stress, Bottom of Overlay	(psi)	-88.0	215.0
Radial Strain, Bottom of Overlay	(micro strain)	-180.0	130.9
Percentage of Failure Stress ***	(percent)	--	53.8
Radial Stress, Bottom of Layer 2	(psi)	-107.0	23.2
Radial Strain, Bottom of Layer 2	(micro strain)	-113.8	167.0
Radial Stress, Bottom of Layer 3	(psi)	122.0	94.1
Radial Strain, Bottom of Layer 3	(micro strain)	604.0	447.0
Vertical Stress, Top of Subgrade	(psi)	-37.8	-25.2
Vertical Strain, Top of Subgrade	(micro strain)	-1840.0	-1310.0

** Maximum computed values for tandem wheel loading

*** Failure tensile stress of 400 psi

NOTE: + = tensile
- = compressive

asphalt layers. Rehabilitation efforts generally focused on the overlaying of the existing pavement to reduce stresses down to desirable levels. The main emphasis here was to provide a high quality top course using large aggregate sizes that can minimize the rate and amount of reflective cracking to the surface. Also, it was important to maintain low stresses near the top of the pavement where age-hardening is expected to be the greatest due to damaging environmental factors such as wind, sunlight, and heat.

CHAPTER 8 CONCLUSIONS AND RECOMMENDATIONS

8.1 Conclusions

A study was conducted to evaluate FWD deflection response on an aged flexible airfield pavement at ambient temperature conditions. The chosen site, Duke Field, Florida offered a variety of pavement surface distresses and a wide range of pavement temperatures. Based on the results obtained from the analysis of the field and laboratory data, the following general conclusions were drawn pertaining to the structural adequacy of the pavement:

1. The Duke airfield was underdesigned and poorly maintained to meet current mission requirements. Stress analysis conducted on the original airfield pavements clearly demonstrated that failure was initiated by a combination of excessive loads and high binder viscosities. These conditions led to exceedingly high stresses in the sand asphalt base.
2. The distressed conditions at each site may be reasonably explained. The severe block cracking observed at site 1 resulted primarily from the extremely high asphalt viscosity of its binder course at low-temperatures. This resulted in an increase in stiffness (higher stresses) and a reduction in available fracture energy. Cracks then developed and reflected to the surface. Site 2 had a binder course that was also extremely brittle and fragmented resulting from a high asphalt viscosity and what appeared to be stripping of the asphalt

binder. The surface condition at site 2 would resemble that of site 1 if an intermediate wearing course of lower asphalt viscosity had not been applied. Site 3 showed the least amount of surface distress, although it had sublayer properties similar to that observed at site 2. Well-compacted asphalt concrete at site 3 (air voids less than 7 percent) aided in retarding age-hardening which kept viscosities low and reduced the potential for thermal cracking. Also, rutting was minimized because this taxiway allowed for greater aircraft wander (lateral wheel gear displacement) which increased the pass-to-coverage ratio.

3. The collection of FWD field data over a wide temperature range was required to accurately assess the moduli of the cracked asphalt-bound layers. Modulus values were tuned over this wide temperature range until consistent results were achieved. This was not possible at one temperature. Despite the rational procedure followed, the severe cracking at site 1 made it very difficult to determine layer moduli. Cracks running between sensor positions gave erroneous deflection values, especially at warmer temperatures where subgrade moduli were computed higher than at lower temperatures.
4. The BISDEF layered elastic computer program performed well when predicting the moduli of lower layers, especially that of the subgrade, but did a poor job in assessing the moduli of the asphalt concrete. Assigning a correct modulus value for the asphalt concrete aided the BISDEF program to predict supporting layer moduli and match deflection basins with good reliability. The relative stiffness of these pavements at high temperatures (over 100 F)

resulted in a good match of predicted and measured deflections at inner sensor positions with minimal rigid plate effects.

5. The BASIN computer program performed adequately in selecting representative basins for analysis. The normalization of the FWD data helped to show the effects of load and degree of cracking on the linearity of the deflection response. Load-deflection response was essentially linear at all sites. Differences arose, however, in the absolute values of deflections from station to station within a site. This was primarily attributed to the degree of cracking present. Because of the cracking at all three sites, many basins were required to truly represent existing pavement conditions.
6. Modulus-viscosity-air void relationships derived from rheology and resilient modulus testing worked quite well in matching deflection basins using BISDEF for the uncracked pavement sections. Reduction in modulus values were obtained for the cracked sections and correlated primarily with the degree of cracking present. When comparing pavements with similar base and subgrade moduli, the difference in measured deflections appeared to be dependent on the degree of cracking in the asphalt concrete. This was more noticeable at colder temperatures since the cracked and uncracked moduli at warmer temperatures were almost identical due to the increased effects of aggregate gradation on the stiffness of asphalt concrete.
7. Stress analyses indicated the only viable rehabilitative approach to effectively reduce critical stresses in the pavement was to use an overlay of at least 3 to 5 in. on top of the existing pavement. The overlay material should be of high quality, show good stability, and demonstrate adequate stress relief to bridge underlying cracks.

Further degradation of these pavements could lead to accelerated spalling and ravelling if restorative action is not soon taken.

The following conclusions specifically address the pavement material properties derived from laboratory and field measurements:

8. Air void content was shown to influence the resilient and creep properties of asphalt cores in the laboratory along with constant power viscosity. Indirect tensile tests indicated that for a given viscosity, resilient modulus values were reduced 20 percent between 4 and 8 percent air voids and almost 45 percent between 4 and 25 percent. The effects on fracture energy were even more dramatic. Fracture energy was reduced 35 percent between 4 and 8 percent air void content and close to 70 percent between 4 and 25 percent air voids. Limited test data, however, found no correlation between mix-viscosity and air voids, although it is believed to exist.
9. The Schwyer rheometer was used to determine the low-temperature flow (viscosity) characteristics of the recovered asphalts. Due to the brittle nature of the age-hardened material at low temperature, reliable results were not achieved below 15 C (59 F). However, good viscosity-temperature correlations were obtained and used in predicting the resilient modulus of the asphalt mixtures in the pavement analyses. Excessive age-hardening rates of the binder were observed and probably resulted from the combined effects of excessive plant-mix temperatures and poor field compaction.
10. Penetration-viscosity relationships were developed at 140, 77, and 59 F and provided a quick means to determine viscosity-related asphalt mix properties such as resilient modulus and fracture

energy. However, the empirical nature of using penetration data to predict asphalt properties is not considered to be reliable.

11. Subgrade moisture values held essentially constant ranging between 5 and 6 percent throughout the testing phase. Also, the consistent subgrade modulus values computed for sites 2 and 3 using BISDEF indicated no appreciable change in moisture conditions. Higher modulus values outside the wheel path near the edge of the taxiway at site 2, could be attributed to the combined effects of soil density and moisture content differences. At site 1 a decrease in deflection response from the outer sensors demonstrated a slight increase in subgrade moduli with increasing pavement temperature. This response was probably due to both extensive cracking and temperature which decreased the transfer of stress to the outer sensor positions.
12. Thermocouples installed in the pavement gave accurate accounts of pavement temperature profiles during field testing. They were especially useful where temperature gradients existed. The Southgate and Deen 5-day model compared favorably for uniform pavement temperatures. However, under non-uniform, high gradient, temperature conditions the model underpredicted temperatures during periods of thermal heating and overpredicted temperatures during periods of thermal cooling.

8.2 Recommendations

The goal of this research was to offer a rational approach to evaluate flexible airfield pavements, especially aged pavements, using the FWD. Older asphalt pavements are beset by a unique set of problems that

require both the understanding and application of rheological and elastic concepts. The following are recommendations for further study or consideration and are provided based on the results obtained in this investigation:

1. Careful attention should be paid to the present condition of the airfield at Duke since further degradation could occur very rapidly and present operational hazards caused by pavement spalling and ravelling.
2. The evaluation of cracked asphalt concrete pavements using the FWD should include as a minimum: 1) obtaining field data at extreme ambient temperatures to observe trends in deflection response and computed moduli; 2) acquiring the elastic properties of the asphalt layers through either resilient modulus testing or modulus-viscosity relationships; 3) assessing the cracked nature of the pavement and using, through the modulus prediction equations, the computed values as fixed inputs into an elastic computer program such as BISDEF; and 4) pavement stress analysis computing the critical stresses and strains to determine the condition of the pavement before and after rehabilitation. Included should be projections for age-hardening of the asphalt.
3. In severely cracked pavements, 12-in. dynamic plate load tests should be performed on the subgrade to verify the computed subgrade modulus. Tests should be conducted at different stress levels not to exceed 35 psi.
4. Efforts should be made to quantify the current condition of airfield pavements and determine how they would hold up against system

alterations such as the use of radial tires, higher tire pressures, and greater loads.

5. Further work on the effects of age-hardening is required to assess long-term pavement performance. In addition, stress analyses using the combined effects of load and thermal-induced stresses should be performed to establish relationships between pavement performance (stress-strain response) and material properties.

APPENDIX A
SUBGRADE MOISTURE PROFILES

Table A.1 Results of Gravimetric and Volumetric Moisture Contents Measured in the Field

Depth (ft.)	Month												
	January		February		March		April		May		June		
	% w(a)		% θ		% θ		% θ		% θ		% θ		
	Cen	Edge	Cen	Edge	Cen	Edge	Cen	Edge	Cen	Edge	Cen	Edge(b)	
2	6.8	6.0	15.9	16.5	13.1	11.8	12.8	11.9	13.1	12.3	13.3	16.2	
3	5.3	4.8	15.6	14.2	12.9	12.0	12.8	12.2	Did Not	12.9	11.8	12.7	14.3
4	5.0	4.8	12.8	12.0	12.5	11.7	12.6	11.9	Test	12.7	11.2	12.8	12.8
5	5.2	4.2	12.3	10.9	11.9	10.3	12.3	10.5		12.5	10.4	12.4	11.9
6	5.3	4.5	11.4	10.7	11.2	10.4	11.1	10.3		11.3	10.2	11.2	-

NOTE:

(a) Gravimetric samples recovered one day before volumetric readings taken

(b) Higher values caused by water infiltration from broken moisture seal

APPENDIX B
FIELD THERMAL PROFILES

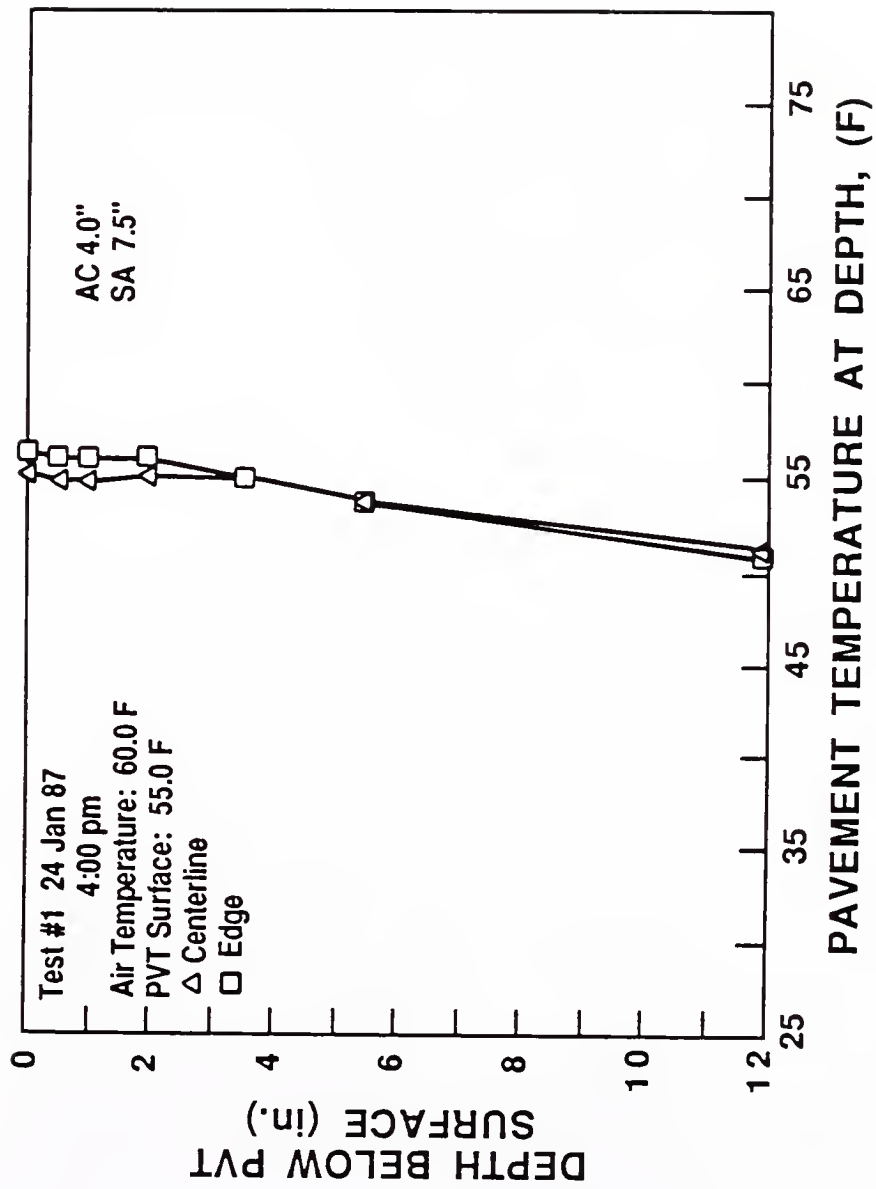


Figure B.1 Temperature Profile (Test 1)

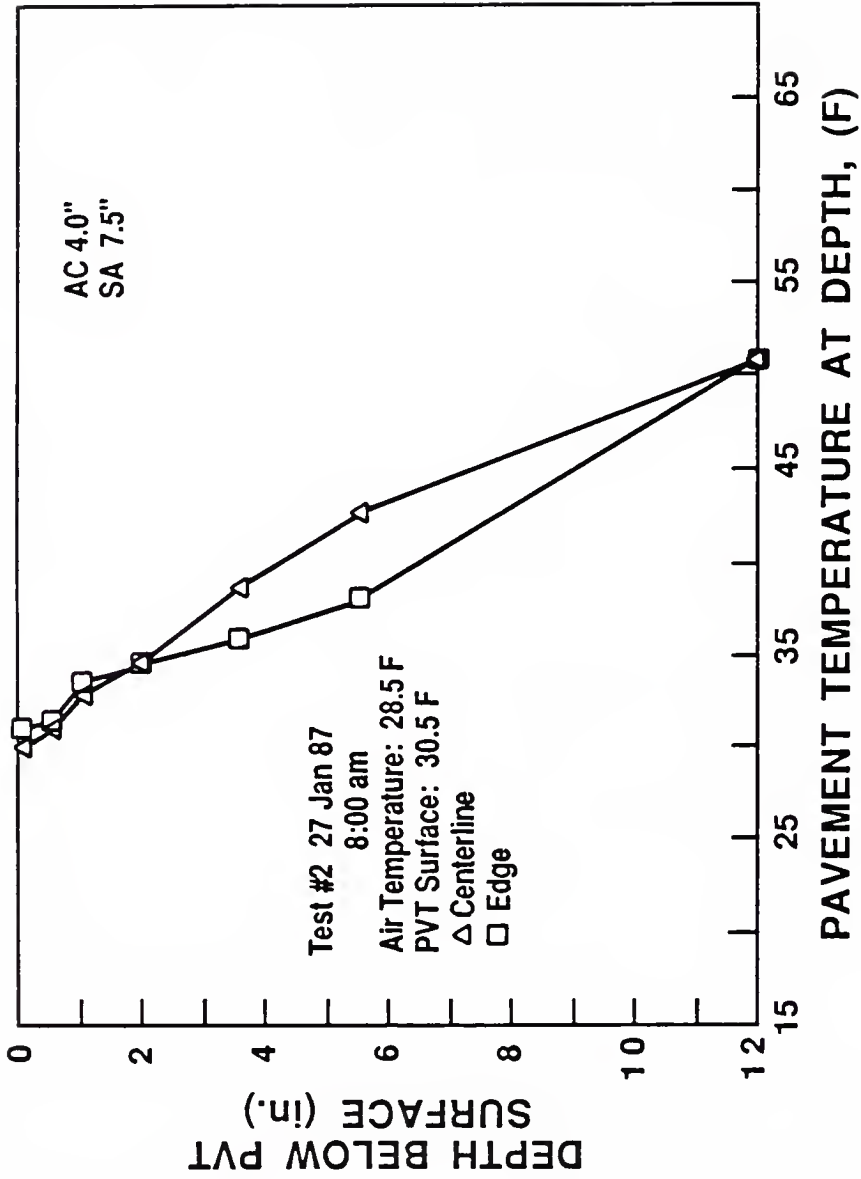


Figure B.2 Temperature Profile (Test 2)

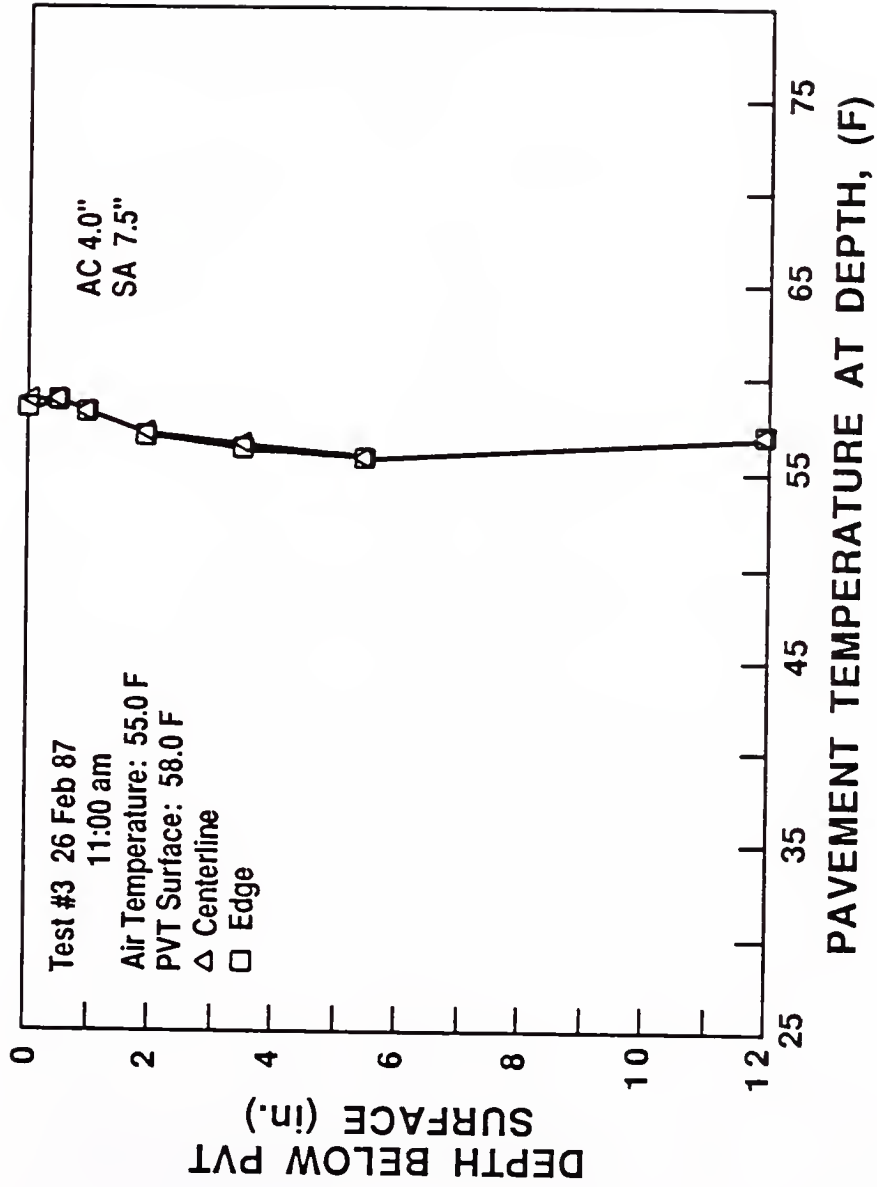


Figure B.3 Temperature Profile (Test 3)

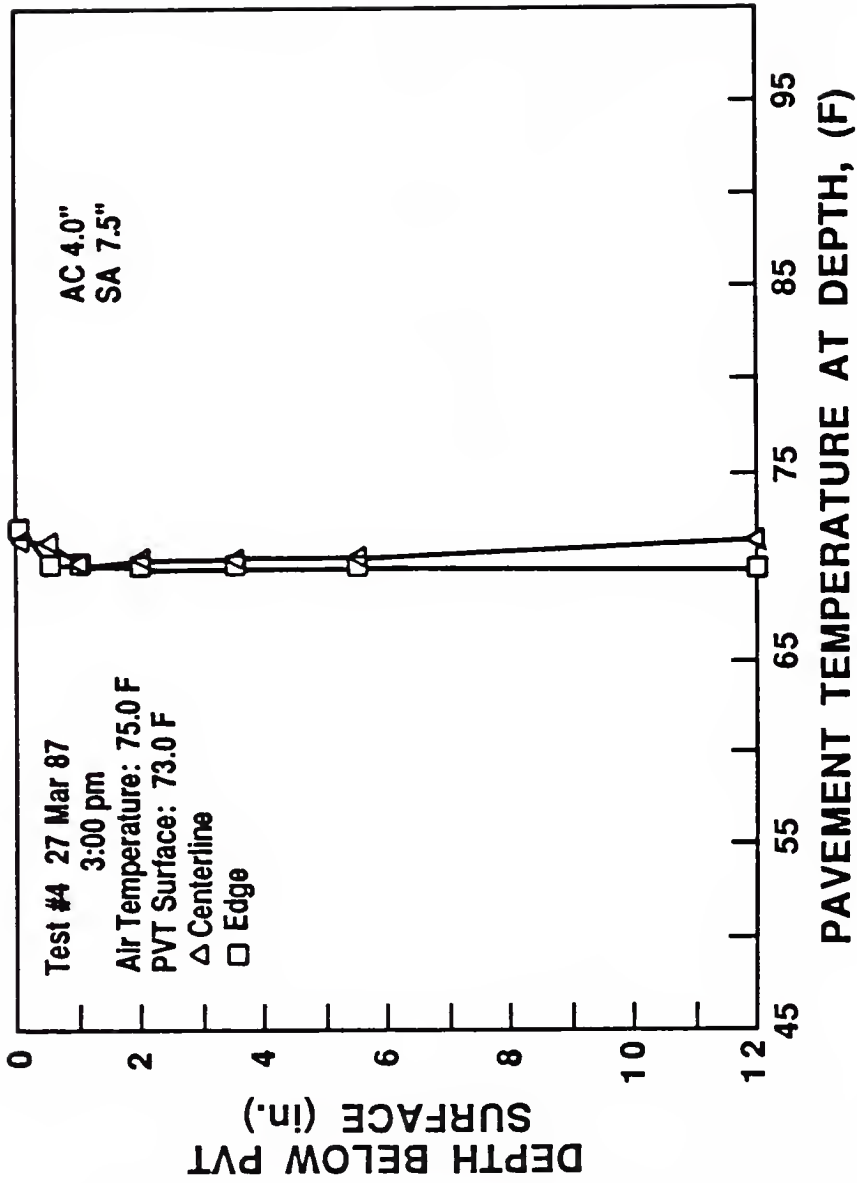


Figure B.4 Temperature Profile (Test 4)

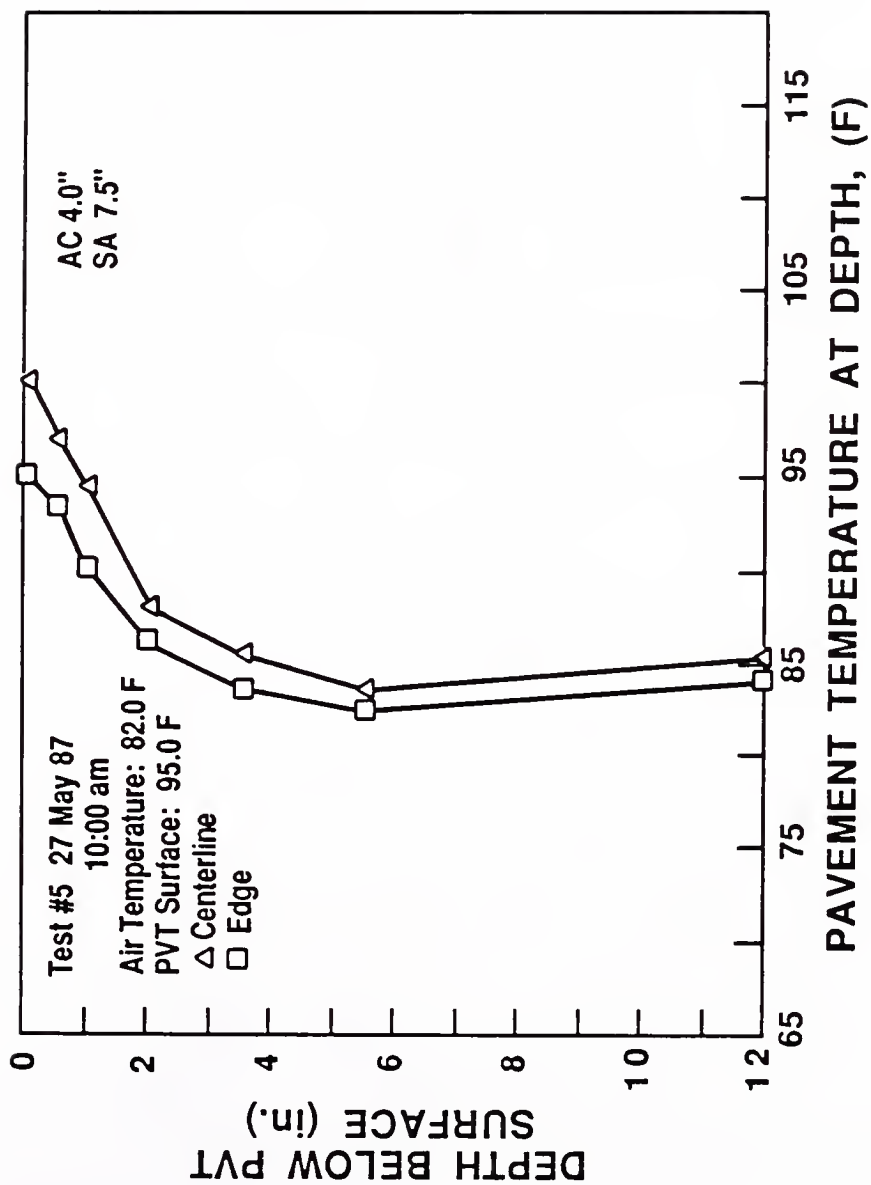


Figure B.5 Temperature Profile (Test 5)

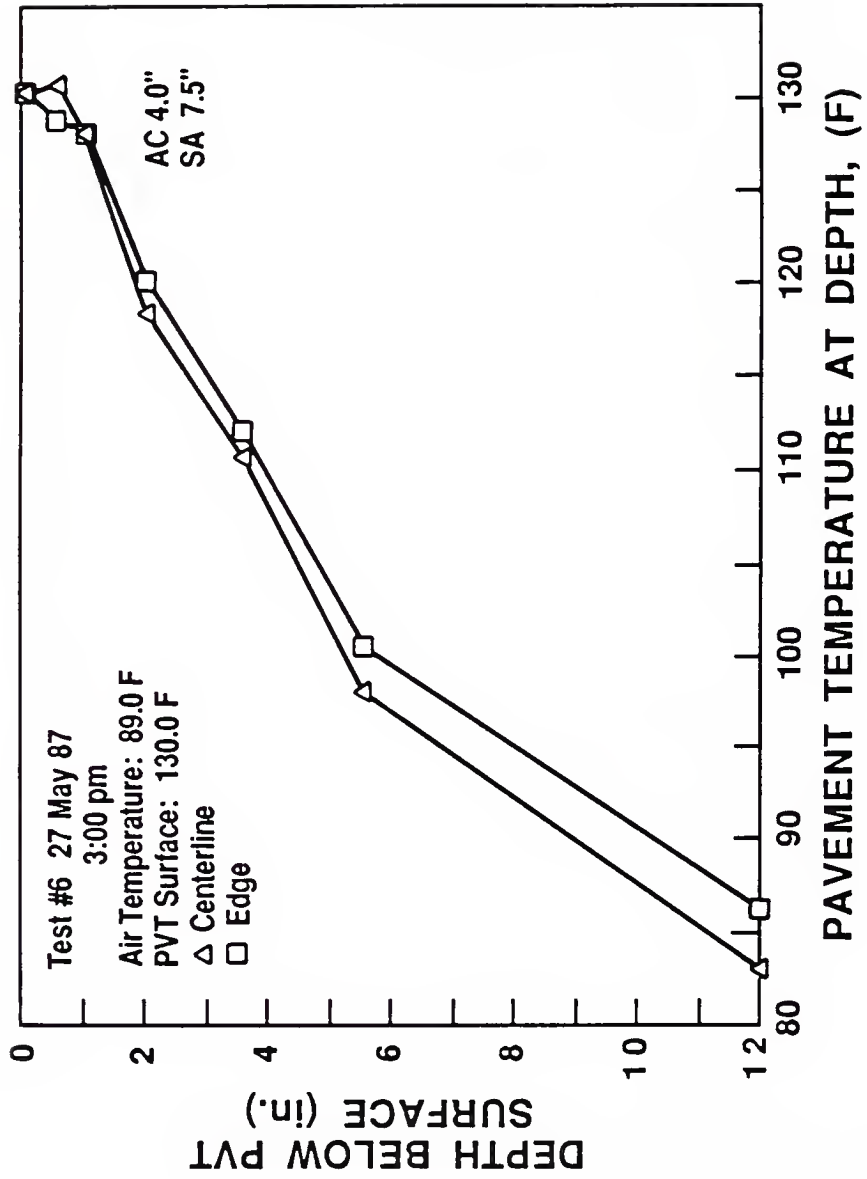


Figure B.6 Temperature Profile (Test 6)

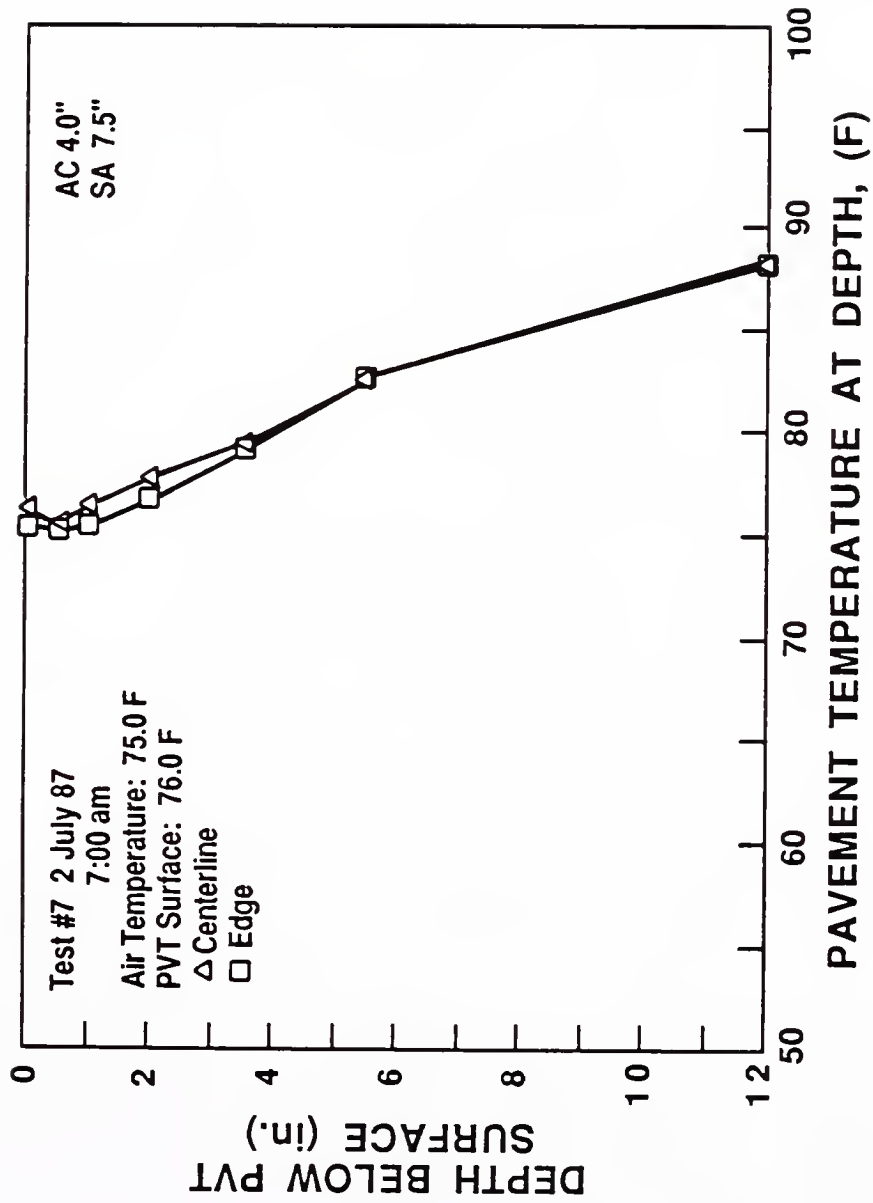


Figure B.7 Temperature Profile (Test 7)

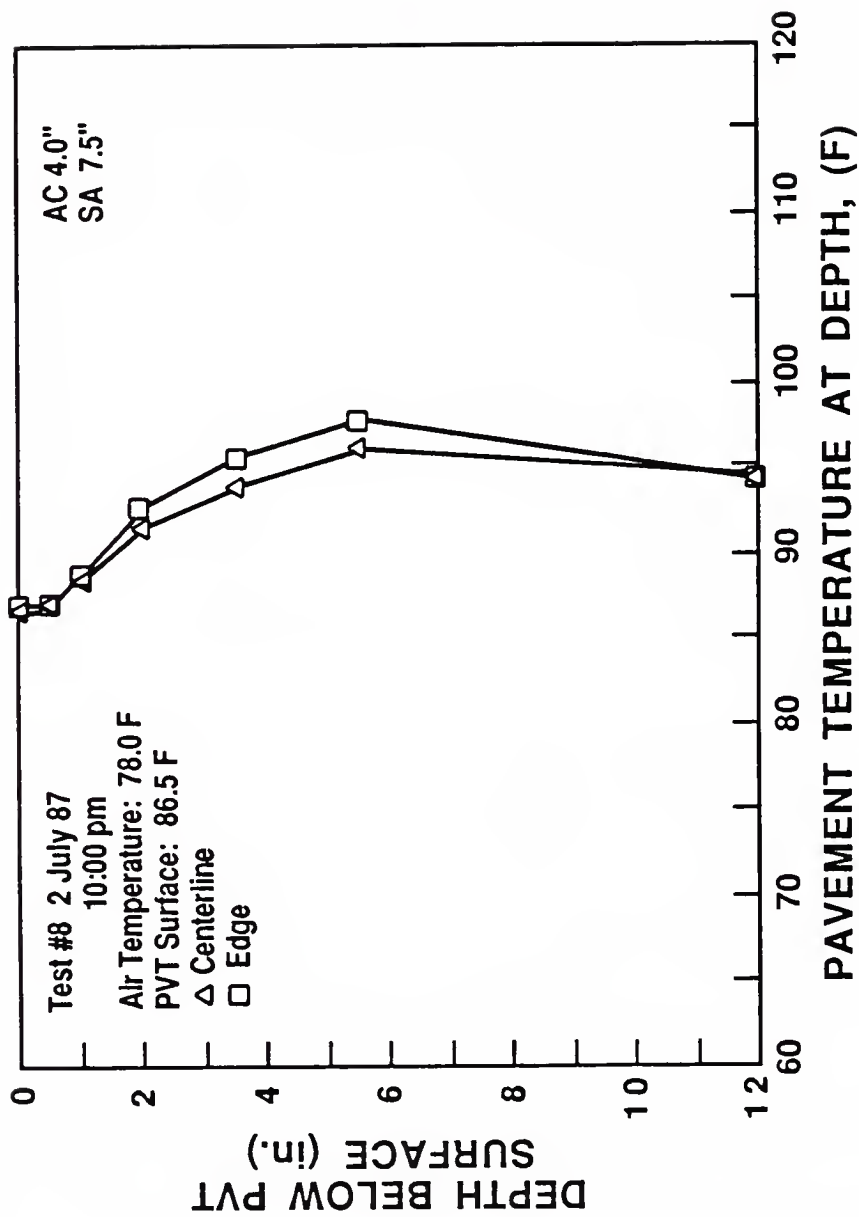


Figure B.8 Temperature Profile (Test 8)

APPENDIX C
GRADATION TEST RESULTS

Table C.1 Gradation and Asphalt Content of Bituminous Layers

Sieve Size	% Passing										
	1AC-1	1AC-2	1SA	2AC-1	2AC-2	2AC-3	2SA	3AC-1	3AC-2	3SA	
1"						100					
3/4"	100	100		100		99		100	100		
1/2"	91	93		93	100	93		97	90		
3/8"	84	85		88	100	84		90	79		
No. 4	65	73		69	75	73		71	63		
No. 10	50	53	100	54	40	51	100	53	52	100	
No. 40	30	35	74	32	19	31	75	30	30	71	
No. 80	12	13	9	13	8	12	13	12	13	10	
No. 200	5.5	4.1	2.6	6.5	5.0	4.4	6.2	5.9	4.4	4.5	
Asphalt Content	5.2	6.4	3.6	5.2	4.8	6.1	3.6	5.4	6.0	3.9	

APPENDIX D
PENETRATION-VISCOSITY CORRELATIONS

Table D.1 Correlation Between Penetration and Viscosity

Site-Layer	Penetration @ 77 F (0.1 mm)	Absolute Viscosity @ 140 F (poises) ^(a)	Const. Power Viscosity @ 77 F (Pa-s)	Const. Power Viscosity @ 59 F (Pa-s)
Duke Field				
1AC-1	19	1.02 E5 7.05 E4	2.42 E7 9.23 E6	1.86 E8 1.17 E8
1AC-2	12	1.42 E6 3.41 E5	9.13 E7 3.35 E7	1.28 E9 2.86 E8
1SA	10	3.14 E7 ^(c) 6.76 E5	1.38 E8 5.75 E7	5.15 E8 ^(c) 4.56 E8
2AC-1	12	2.20 E5 3.41 E5	3.61 E7 3.35 E7	2.77 E8 2.86 E8
2AC-2	14	1.18 E5 1.96 E5	2.93 E7 2.15 E7	2.67 E8 1.94 E8
2AC-3	3	1.55 E7 1.73 E8	2.13 E8 3.18 E9	1.10 E9 1.34 E10
2SA	8	2.82 E6 1.64 E6	2.66 E8 1.14 E8	1.53 E9 8.21 E8
3AC-1	23	3.75 E4 3.89 E4	8.87 E6 5.56 E6	1.07 E8 8.49 E7

Table D.1--continued

3AC-2 (inside)	13	Measured Predicted	2.99 E5 2.55 E5	3.04 E7 2.66 E7	2.09 E8 2.33 E8
3AC-2 (outside)	10	Measured Predicted	1.04 E6 6.76 E5	7.89 E7 5.75 E7	9.73 E8 4.56 E8
3SA	8	Measured Predicted	5.59 E6 1.64 E6	1.01 E8 1.14 E8	4.98 E8 8.21 E8
Province of Quebec	352	Measured Predicted		2.77 E4 1.83 E4	
	150	Measured Predicted		6.99 E4 8.30 E4	
	146	Measured Predicted		7.64 E4 8.74 E4	
	92	Measured Predicted		1.59 E5 2.19 E5	
	88	Measured Predicted		1.34 E5 2.41 E5	
Chari (102)	72	Measured Predicted	2.39 E3 2.03 E3		1.74 E6 1.62 E6
	70	Measured Predicted	2.49 E3 2.16 E3		
	66	Measured Predicted			2.65 E6 2.63 E6

Table D.1--continued

64	Measured Predicted	3.09 E3 2.63 E3	2.54 E5 4.76 E5	
54	Measured Predicted		5.64 E6 6.93 E6	
52	Measured Predicted		5.47 E5 7.58 E5	
50	Measured Predicted		7.59 E5 8.29 E5	
44	Measured Predicted		1.46 E6 1.11 E6	1.47 E7 1.56 E7
42	Measured Predicted	8.93 E3 7.25 E3		
41	Measured Predicted	1.02 E4 7.72 E3	1.63 E6 1.32 E6	2.46 E7 1.98 E7
37	Measured Predicted	1.15 E4 1.01 E4	1.25 E6 1.68 E6	2.94 E7 2.74 E7
33	Measured Predicted	1.52 E4 1.37 E4		
30	Measured Predicted		2.25 E6 2.82 E6	3.98 E7 4.82 E7
20	Measured Predicted			9.61 E7 1.08 E8

Table D.1--continued

Ruth and Miller (101)	122	Measured	1.43 E3
		Predicted	6.95 E2
	58	Measured	3.92 E3
		Predicted	3.30 E3
	43	Measured	6.70 E3
		Predicted	6.83 E3

NOTE:

- (a) Extrapolated from viscosity-temperature relationships derived from Schwyer rheometer tests
- (b) 1 Pa-s = 10 poises
- (c) Excluded from regression analysis

APPENDIX E
SCHWEYER RHEOMETER TEST RESULTS ON RECOVERED FIELD CORES

Table E.1 Schwyer Rheometer Test Results on Asphalts Recovered From Site 1

Temp		Site 1 AC Layer 1 Visc, η_{100} (Pa-s)		Complex		Remarks
C	K	Measured	Predicted ^(a)	Flow Factor	R ²	
0	273	-	7.504E+09	-	-	
5	278	-	2.185E+09	-	-	
10	283	4.612E+08	6.502E+08	0.4320	0.9883	G tube
15	288	1.855E+08	1.977E+08	0.4616	0.9982	"
20	293	9.946E+07	6.133E+07	0.5812	0.9963	"
20	293	6.111E+07	6.133E+07	0.5500	0.9970	F tube
25	298	2.422E+07	1.941E+07	0.5415	0.9983	"
30	303	9.695E+06	6.262E+06	0.5160	0.9993	"
35	308	-	2.058E+06	-	-	
40	313	-	6.886E+05	-	-	
45	318	-	2.344E+05	-	-	
50	323	-	8.116E+04	-	-	
55	328	-	2.856E+04	-	-	
60	333	8.667E+03	1.021E+04	-	-	absolute viscosity

(a) $\log \eta_{100} = 175.51 - 67.99 \log K$ R² = 0.9927

Temp		Site 1 AC Layer 2 Visc, η_{100} (Pa-s)		Complex		Remarks
C	K	Measured	Predicted ^(a)	Flow Factor	R ²	
0	273	-	3.674E+10	-	-	
5	278	-	1.177E+10	-	-	
10	283	-	3.845E+09	-	-	
15	288	-	1.282E+09	-	-	
20	293	4.692E+08	4.352E+08	0.3946	0.9940	G tube
25	298	9.125E+07	1.506E+08	0.5173	0.9933	F tube
30	303	4.798E+07	5.300E+07	0.4905	0.9987	"
35	308	2.096E+07	1.898E+07	0.5015	0.9982	"
40	313	8.634E+06	6.911E+06	0.5148	0.9993	"
45	318	4.911E+06	2.557E+06	0.4404	0.9970	"
50	323	-	9.608E+05	-	-	
55	328	-	3.665E+05	-	-	
60	333	8.598E+04	1.419E+05	-	-	absolute viscosity

(a) $\log \eta_{100} = 163.41 - 62.74 \log K$ R² = 0.9776

Table E.1--continued

Temp		Visc, η_{100}		Site 1 Sand Asphalt (Pa-s)	Complex	R ²	Remarks
C	K	Measured	Predicted ^(a)	Flow Factor			
0	273	-	3.370E+09	-	-	-	
5	278	-	1.781E+09	-	-	-	
10	283	-	9.522E+08	-	-	-	
15	288	-	5.147E+08	-	-	-	
20	293	-	2.812E+08	-	-	-	
25	298	1.380E+08	1.552E+08	0.5975	0.9931	-	F tube
30	303	1.154E+08	8.648E+07	0.5396	0.9997	-	"
30	303	7.353E+07	8.648E+07	0.6529	0.9634	-	"
35	308	5.482E+07	4.867E+07	0.4658	0.9958	-	"
40	313	2.457E+07	2.763E+07	0.4269	0.9961	-	"
45	318	-	1.584E+07	-	-	-	
50	323	-	9.156E+06	-	-	-	
55	328	-	5.338E+06	-	-	-	
60	333	1.000E+05	3.137E+06	-	-	-	est @ pen=10 ^(b)

(a) $\log \eta_{100} = 95.11 - 35.13 \log K$

R² = 0.9190

(b) excluded from regression analysis

Table E.2 Schwyer Rheometer Test Results on Asphalts Recovered From Site 2

Temp		Site 2 AC Layer 1 Visc, n_{100} (Pa-s)		Complex		Remarks
C	K	Measured	Predicted ^(a)	Flow Factor	R ²	
0	273	-	1.205E+10	-	-	
5	278	-	3.602E+09	-	-	
10	283	8.226E+08	1.001E+09	0.5524	0.9980	G tube
15	288	2.767E+08	3.434E+08	0.4776	0.9915	"
20	293	1.024E+08	1.093E+08	0.5328	0.9898	F tube
25	298	3.612E+07	3.547E+07	0.5425	0.9932	"
30	303	1.487E+07	1.173E+07	0.5431	0.9894	"
35	308	6.979E+06	3.949E+06	0.4869	0.9965	"
40	313	-	1.353E+06	-	-	
45	318	-	4.716E+05	-	-	
50	323	-	1.671E+05	-	-	
55	328	-	6.015E+04	-	-	
60	333	1.430E+04	2.199E+04	-	-	absolute viscosity

$$(a) \log n_{100} = 172.11 - 66.51 \log K$$

Temp		Site 2 AC Layer 2 Visc, n_{100} (Pa-s)		Complex		Remarks
C	K	Measured	Predicted ^(a)	Flow Factor	R ²	
0	273	-	7.777E+09	-	-	
5	278	-	2.287E+09	-	-	
10	283	4.765E+08	6.871E+08	0.5961	0.8378	G tube
15	288	2.666E+08	2.109E+08	0.3959	0.9882	"
15	288	1.346E+08	2.109E+08	0.6297	0.9995	F tube
20	293	6.149E+07	6.604E+07	0.5449	0.9901	"
25	298	2.933E+07	2.109E+07	0.5252	0.9985	"
30	303	1.153E+07	6.866E+06	0.4984	0.9942	"
35	308	-	2.276E+06	-	-	
40	313	-	7.683E+05	-	-	
45	318	-	2.638E+05	-	-	
50	323	-	9.211E+04	-	-	
55	328	-	3.268E+04	-	-	
60	333	8.521E+03	1.178E+04	-	-	absolute viscosity

$$(a) \log n_{100} = 174.21 - 67.45 \log K$$

$$R^2 = 0.9894$$

Table E.2--continued

Temp		Site 2 AC Layer 3 (Pa-s)		Complex		Remarks
C	K	Visc, η_{100} Measured	Predicted ^(a)	Flow Factor	R ²	
0	273	-	1.241E+10	-	-	
5	278	-	5.457E+09	-	-	
10	283	-	2.436E+09	-	-	
15	288	-	1.103E+09	-	-	
20	293	5.749E+08	5.061E+08	0.3153	0.9921	G tube
25	298	2.130E+08	2.354E+08	0.3592	0.9980	"
30	303	1.179E+08	1.109E+08	0.3658	0.9975	F tube
35	308	4.728E+07	5.285E+07	0.3979	0.9911	"
40	313	2.727E+07	2.551E+07	0.4008	0.9965	"
45	318	1.329E+07	1.245E+07	0.3914	0.9967	"
50	323	-	6.146E+06	-	-	
55	328	-	3.067E+06	-	-	
60	333	4.300E+05	1.547E+05	-	-	est @ pen=3 ^(b)

(a) $\log \eta_{100} = 120.33 - 45.25 \log K$ R² = 0.9949

(b) excluded from regression

Temp		Site 2 Sand Asphalt (Pa-s)		Complex		Remarks
C	K	Visc, η_{100} Measured	Predicted ^(a)	Flow Factor	R ²	
0	273	-	3.504E+10	-	-	
5	278	-	1.200E+10	-	-	
10	283	-	4.188E+09	-	-	
15	288	1.528E+09	1.489E+09	0.4410	0.9486	G tube
20	293	4.710E+08	5.389E+08	0.3898	0.9974	"
25	298	2.656E+08	1.984E+08	0.3587	0.9836	"
30	303	5.908E+07	7.427E+07	0.5596	0.9933	F tube
35	308	3.323E+07	2.825E+07	0.4394	0.9993	"
40	313	1.019E+07	1.092E+07	0.5482	0.9993	"
45	318	-	4.282E+06	-	-	
50	323	-	1.704E+06	-	-	
55	328	-	6.881E+05	-	-	
60	333	1.981E+05	2.816E+05	-	-	absolute viscosity

(a) $\log \eta_{100} = 154.40 - 59.05 \log K$ R² = 0.9958

Table E.3 Schwyer Rheometer Test Results on Asphalts Recovered From Site 3

Temp		Site 3 AC Layer 1 Visc, η_{100} (Pa-s)		Complex		Remarks
C	K	Measured	Predicted ^(a)	Flow Factor	R ²	
0	273	-	3.920E+09	-	-	
5	278	-	1.105E+09	-	-	
10	283	2.792E+08	3.187E+08	0.5541	0.9786	G tube
15	288	1.066E+08	9.393E+07	0.5851	0.9993	"
15	288	5.625E+07	9.393E+07	0.6912	0.9973	F tube
20	293	2.840E+07	2.827E+07	0.5920	0.9983	"
25	298	8.886E+06	8.683E+06	0.5865	0.9972	"
30	303	4.419E+06	2.720E+06	0.5560	0.9983	"
35	308	-	8.684E+05	-	-	
40	313	-	2.824E+05	-	-	
45	318	-	9.347E+04	-	-	
50	323	-	3.148E+04	-	-	
55	328	-	1.078E+04	-	-	
60	333	2.922E+03	3.752E+03	-	-	absolute viscosity

$$(a) \log \eta_{100} = 179.54 - 69.76 \log K \quad R^2 = 0.9933$$

Temp		Site 3 AC Layer 2 (inside) Visc, η_{100} (Pa-s)		Complex		Remarks
C	K	Measured	Predicted ^(a)	Flow Factor	R ²	
0	273	-	8.962E+09	-	-	
5	278	-	2.832E+09	-	-	
10	283	-	9.133E+08	-	-	
15	288	2.089E+08	3.004E+08	0.8539	0.8532	G tube
20	293	1.468E+08	1.008E+08	0.5714	0.9910	"
20	293	1.006E+08	1.008E+08	0.7788	0.9956	F tube
25	298	3.039E+07	3.442E+07	0.8253	0.9899	"
30	303	1.349E+07	1.197E+07	0.6579	0.9993	"
35	308	6.025E+06	4.235E+06	0.6332	0.9983	"
40	313	-	1.524E+06	-	-	
45	318	-	5.571E+05	-	-	
50	323	-	2.069E+05	-	-	
55	328	-	7.804E+04	-	-	
60	333	2.562E+04	2.987E+04	-	-	absolute viscosity

$$(a) \log \eta_{100} = 164.60 - 63.48 \log K \quad R^2 = 0.9923$$

Table E.3--continued

Temp		Site 3 AC Layer 2 (outside) (Pa-s)		Complex		Remarks
C	K	Visc, η_{100} Measured	Predicted ^(a)	Flow Factor	R ²	
0	273	-	2.728E+10	-	-	
5	278	-	8.723E+09	-	-	
10	283	-	2.846E+09	-	-	
15	288	9.732E+08	9.470E+08	0.4610	0.9929	G tube
20	293	3.672E+08	3.212E+08	0.5200	0.9979	"
25	298	7.889E+07	1.109E+08	0.7293	0.9962	F tube
30	303	3.927E+07	3.899E+07	0.6668	0.9816	"
35	308	1.492E+07	1.394E+07	0.6092	0.9990	"
40	313	6.874E+06	5.069E+06	0.5964	0.9990	"
45	318	-	1.873E+06	-	-	
50	323	-	7.028E+05	-	-	
55	328	-	2.677E+05	-	-	
60	333	9.248E+04	1.035E+05	-	-	absolute viscosity

$$(a) \log \eta_{100} = 163.50 - 62.83 \log K$$

$$R^2 = 0.9956$$

Temp		Site 3 Sand Asphalt (Pa-s)		Complex		Remarks
C	K	Visc, η_{100} Measured	Predicted ^(a)	Flow Factor	R ²	
0	273	-	6.082E+09	-	-	
5	278	4.674E+09	2.602E+09	0.2469	0.9636	G tube
10	283	8.203E+08	1.130E+09	0.5005	0.9967	"
15	288	-	4.981E+08	-	-	
20	293	-	2.227E+08	-	-	
25	298	5.308E+07	1.009E+08	0.4812	0.9951	F tube
30	303	-	4.633E+07	-	-	
35	308	1.987E+07	2.154E+07	0.4316	0.9977	F tube
40	313	-	1.014E+07	-	-	
45	318	8.150E+06	4.832E+06	0.3630	0.9963	E tube
50	323	-	2.329E+06	-	-	
55	328	-	1.135E+06	-	-	
60	333	5.246E+05	5.594E+05	-	-	absolute viscosity

$$(a) \log \eta_{100} = 123.75 - 46.78 \log K$$

$$R^2 = 0.9786$$

APPENDIX F
DIAMETRAL TEST RESULTS ON FIELD CORES

Table F.1 Dynamic Resilient Modulus Test Results on 1AC-1

Temp C (F)	Specimen Height (in.)	Stress σ (psi)	Elastic Strain		$E_{0.1}$ ave ^(a) (psi)	Data Points Used
			ϵ_1 ($\times 10^{-6}$)	ϵ_2 ($\times 10^{-6}$)		
30 (86)	2.06	4.64	9	20	318,000	All
		7.88	17	37	292,000	
		12.67	30	61	278,000	
		17.31	43	84	272,000	
		20.55	50	100	274,000	
25 (77)	2.06	5.25	9	16	423,000	All
		7.42	13	20	447,000	
		10.04	17	29	437,000	
		12.83	22	40	417,000	
		16.69	28	56	399,000	
		19.78	32	67	400,000	
15 (59)	2.06	9.58	9	16	773,000	All
		20.86	19	37	745,000	
		30.44	28	58	708,000	
		39.87	36	80	687,000	
		51.61	48	112	647,000	
10 (50)	2.06	10.66	4	20	888,000	All
		20.40	8	37	903,000	
		30.75	16	52	904,000	
		40.79	25	69	872,000	
		52.07	31	88	874,000	
30 (86)	1.92	5.13	11	16	377,000	All
		9.95	20	34	366,000	
		15.25	31	58	343,000	
		20.56	44	76	342,000	
		26.03	58	100	329,000	
20 (68)	1.92	9.45	11	18	665,000	All
		20.39	27	40	610,000	
		30.50	39	64	593,000	
		40.29	52	90	569,000	
		50.23	65	116	556,000	
10 (50)	1.92	9.62	8	12	962,000	All
		20.23	16	23	1,043,000	
		30.67	24	36	1,022,000	
		40.62	32	50	996,000	
		51.39	42	63	981,000	

NOTE: (a) $E_{0.1}$ ave computed using average strain $\frac{\epsilon_1 + \epsilon_2}{2}$

Table F.2 Dynamic Resilient Modulus Test Results on IAC-2

Temp C (F)	Specimen Height (in.)	Stress σ (psi)	Elastic Strain ϵ_1 ϵ_2 ($\times 10^{-6}$) ($\times 10^{-6}$)		$E_{0.1}$ ave ^(a) (psi)	Data Points Used
40 (104)	1.69	4.33	-	18	240,000	All(b)
		6.97	-	45	156,000	
		11.30	-	73	154,000	
		15.26	-	104	147,000	
		19.02	-	140	136,000	
25 (77)	1.69	11.30	12	26	441,000	All(b)
		14.13	16	33	431,000	
		15.07	19	36	419,000	
		18.83	24	44	424,000	
		20.72	25	52	399,000	
15 (59)	1.69	10.17	6	13	795,000	All(b)
		20.72	14	28	740,000	
		29.95	24	43	700,000	
		40.68	32	58	697,000	
		55.56	52	84	661,000	
40 (104)	1.32	3.86	9	12	371,000	Last 4
		8.68	36	44	217,000	
		12.54	57	68	201,000	
		17.60	88	110	178,000	
		22.67	120	162	161,000	
35 (95)	1.32	8.44	29	20	343,000	All
		12.78	44	36	318,000	
		17.12	61	49	310,000	
		23.87	98	75	276,000	
		29.42	140	110	236,000	
25 (77)	1.32	5.31	9	8	632,000	Last 5
		10.37	22	16	552,000	
		14.95	32	27	509,000	
		23.87	64	52	412,000	
		34.24	108	82	360,000	
		41.96	148	108	328,000	
20 (68)	1.32	6.27	8	9	746,000	All
		12.06	20	19	622,000	
		19.29	38	32	554,000	
		25.56	56	48	492,000	
		34.72	84	70	451,000	

Table F.2--continued

Temp C (F)	Specimen Height (in.)	Stress σ (psi)	Elastic Strain ϵ_1 ($\times 10^{-6}$)	Elastic Strain ϵ_2 ($\times 10^{-6}$)	$E_{0.1}$ ave ^(a) (psi)	Data Points Used
15 (59)	1.32	6.99	8	8	852,000	All
		16.64	24	22	723,000	
		23.39	36	32	688,000	
		34.24	62	52	599,000	
		41.96	84	68	552,000	
		48.71	108	84	507,000	
40 (104)	1.51	4.64	24	20	211,000	All
		7.17	47	36	172,000	
		11.59	92	60	153,000	
		15.18	132	83	141,000	
		19.60	180	112	134,000	
35 (95)	1.51	5.06	21	12	301,000	All
		8.43	44	26	241,000	
		13.91	79	48	219,000	
		18.13	110	68	204,000	
		23.19	150	88	195,000	
25 (77)	1.51	5.90	16	8	484,000	All
		12.23	40	20	408,000	
		18.76	68	36	361,000	
		25.51	96	52	345,000	
		31.62	132	68	316,000	
20 (68)	1.51	6.32	12	8	632,000	All
		12.23	28	18	532,000	
		17.07	40	26	517,000	
		22.34	60	38	458,000	
		30.14	88	54	425,000	
15 (59)	1.51	6.11	4	4	1,528,000	Last 5
		12.44	19	16	707,000	
		20.03	36	26	655,000	
		26.56	49	35	632,000	
		33.09	66	44	602,000	
		40.89	88	55	571,000	
40 (104)	1.99	5.28	12	48	176,000	All
		7.36	18	70	167,000	
		10.56	36	92	165,000	
		12.96	56	100	166,000	
		16.15	90	112	160,000	

Table F.2--continued

Temp C (F)	Specimen Height (in.)	Stress σ (psi)	Elastic Strain ϵ_1 ϵ_2 ($\times 10^{-6}$) ($\times 10^{-6}$)		$E_{0.1}$ ave ^(a) (psi)	Data Points Used
25 (77)	1.99	5.92	10	8	673,000	Last 4
		10.24	22	28	406,000	
		15.36	36	40	404,000	
		21.59	56	56	386,000	
		26.71	76	67	373,000	
20 (68)	1.99	5.12	6	13	533,000	All
		10.88	16	24	544,000	
		15.83	30	32	507,000	
		21.91	46	41	503,000	
		28.47	64	56	473,000	
		34.71	82	68	464,000	
15 (59)	1.99	4.80	4	8	774,000	All
		11.84	15	22	630,000	
		15.83	20	28	660,000	
		21.75	29	37	659,000	
		29.91	46	52	610,000	
		39.35	64	67	600,000	

NOTE: (a) $E_{0.1}$ ave computed using average strain $\frac{\epsilon_1 + \epsilon_2}{2}$

(b) moduli calculated from gage 2 (gage 1 bad)

Table F.3 Dynamic Resilient Modulus Test Results on 1SA

Temp	Specimen	Stress	Elastic Strain		$E_{0.1}$	$ave^{(a)}$	Data
C (F)	Height (in.)	σ (psi)	ϵ_1 ($\times 10^{-6}$)	ϵ_2 ($\times 10^{-6}$)	(psi)		Points Used
55 (131)	1.96	2.44	4	9	370,000		Last 4
		3.57	8	15	308,000		
		4.55	10	19	312,000		
		6.01	13	26	307,000		
		7.63	16	32	313,000		
45 (113)	1.96	2.76	5	8	406,000		All
		4.06	10	12	363,000		
		5.36	14	18	335,000		
		7.63	20	27	326,000		
		9.58	24	34	328,000		
40 (104)	1.96	3.25	4	12	406,000		All
		4.87	8	17	393,000		
		6.49	10	23	391,000		
		8.12	14	28	383,000		
		9.74	18	33	380,000		
35 (95)	1.96	3.08	6	8	440,000		All
		4.87	9	12	459,000		
		6.66	12	16	469,000		
		8.12	14	20	472,000		
		10.07	18	27	450,000		
30 (86)	1.96	3.25	4	8	524,000		All
		4.71	7	10	548,000		
		6.33	9	16	510,000		
		7.96	11	20	510,000		
		9.58	13	24	521,000		
55 (131)	2.37	2.15	14	4	234,000		All
		2.95	24	5	208,000		
		3.63	29	8	197,000		
		5.24	47	9	186,000		
		6.45	56	14	184,000		
45 (113)	2.37	2.28	20	4	190,000		All
		3.09	28	4	191,000		
		4.30	43	6	175,000		
		6.18	50	9	210,000		
		6.85	63	14	178,000		
40 (104)	2.37	2.15	12	3	291,000		All
		3.49	20	6	264,000		
		4.84	30	8	255,000		
		6.58	38	10	270,000		
		7.79	45	12	274,000		

Table F.3--continued

Temp C (F)	Specimen Height (in.)	Stress σ (psi)	Elastic Strain		$E_{0.1}$ ave ^(a) (psi)	Data Points Used
			ϵ_1 ($\times 10^{-6}$)	ϵ_2 ($\times 10^{-6}$)		
35 (95)	2.37	2.69	8	4	420,000	All
		3.63	14	5	386,000	
		4.57	21	6	341,000	
		5.78	25	8	352,000	
		6.85	36	8	309,000	
30 (86)	2.37	2.42	8	4	403,000	All
		4.03	15	6	380,000	
		5.24	20	8	385,000	
		6.31	24	8	399,000	
		8.33	32	9	408,000	
55 (131)	2.41	1.67	10	6	214,000	All
		2.93	18	10	209,000	
		3.77	24	12	205,000	
		4.89	32	18	196,000	
		6.56	45	23	192,000	
45 (113)	2.41	2.51	12	8	246,000	All
		4.19	24	12	235,000	
		5.59	32	14	245,000	
		6.70	40	19	228,000	
		8.67	46	24	251,000	
40 (104)	2.41	2.09	11	6	243,000	All
		3.77	16	9	299,000	
		4.61	22	13	265,000	
		6.98	33	17	279,000	
		8.66	41	22	278,000	
35 (95)	2.41	2.79	12	5	332,000	All
		4.05	18	8	312,000	
		5.86	26	12	305,000	
		7.12	31	16	304,000	
		8.52	37	18	313,000	
30 (86)	2.41	2.93	10	6	376,000	All
		4.33	16	9	349,000	
		5.73	20	12	358,000	
		6.98	24	13	375,000	
		8.24	31	18	338,000	
55 (131)	2.11	2.41	7	8	311,000	All
		3.62	9	9	411,000	
		4.53	12	12	371,000	
		5.58	16	20	314,000	
		6.49	20	24	297,000	

Table F.3--continued

Temp C (F)	Specimen Height (in.)	Stress σ (psi)	Elastic Strain ϵ_1 ($\times 10^{-6}$)	Elastic Strain ϵ_2 ($\times 10^{-6}$)	$E_{0.1}$ ave ^(a) (psi)	Data Points Used
45 (113)	2.11	2.11	8	4	352,000	All
		3.32	16	8	277,000	
		5.28	24	13	287,000	
		7.24	28	20	302,000	
		9.05	31	25	326,000	
40 (104)	2.11	2.26	7	3	538,000	All
		3.62	10	6	464,000	
		5.28	16	10	406,000	
		7.84	20	16	431,000	
		10.26	24	21	454,000	
35 (95)	2.11	2.26	7	2	514,000	All
		3.92	10	7	456,000	
		6.18	16	11	461,000	
		8.15	21	15	458,000	
		10.26	24	20	466,000	
30 (86)	2.11	3.17	8	4	528,000	All
		4.68	9	8	564,000	
		8.00	16	12	571,000	
		10.11	19	16	581,000	
		12.52	24	20	574,000	

NOTE: (a) $E_{0.1}$ ave computed using average strain $\frac{\epsilon_1 + \epsilon_2}{2}$

Table F.4 Dynamic Resilient Modulus Test Results on 2AC-1

Temp C (F)	Specimen Height (in.)	Stress σ (psi)	Elastic Strain ϵ_1 ϵ_2 ($\times 10^{-6}$) ($\times 10^{-6}$)		$E_{0.1}$ ave ^(a) (psi)	Data Points Used
25 (77)	1.57	5.27	4	28	325,000	All
		8.11	8	52	272,000	
		10.14	11	36	285,000	
		13.38	20	76	279,000	
		16.83	28	90	285,000	
15 (59)	1.57	9.12	5	24	625,000	All
		19.87	19	52	558,000	
		29.60	34	76	540,000	
		39.53	51	102	516,000	
		50.68	72	160	437,000	
10 (50)	1.57	10.34	8	24	646,000	All
		20.48	12	46	706,000	
		31.42	26	65	692,000	
		41.36	40	84	667,000	
		54.74	63	108	642,000	
30 (86)	1.82	2.97	9	17	232,000	All
		5.07	16	36	200,000	
		7.00	24	48	194,000	
		9.62	32	67	195,000	
		11.54	40	85	185,000	
20 (68)	1.82	9.62	14	35	391,000	All
		18.89	31	70	375,000	
		25.89	45	102	351,000	
		34.63	64	140	338,000	
		43.38	86	188	317,000	
10 (50)	1.82	9.79	12	14	765,000	All
		18.19	20	29	745,000	
		26.76	30	48	683,000	
		36.90	40	75	643,000	
		46.35	50	104	604,000	
30 (86)	1.39	4.12	8	16	349,000	All
		5.72	12	20	358,000	
		8.01	18	31	328,000	
		12.14	28	48	319,000	
		15.34	41	59	308,000	
		21.07	70	76	289,000	

Table F.4--continued

Temp C (F)	Specimen Height (in.)	Stress σ (psi)	Elastic Strain ϵ_1 ϵ_2 ($\times 10^{-6}$) ($\times 10^{-6}$)		$E_{0.1}$ ave ^(a) (psi)	Data Points Used
20 (68)	1.39	9.62	12	20	594,000	All
		19.46	29	36	597,000	
		31.37	60	61	519,000	
		39.39	84	77	490,000	
		51.29	118	101	470,000	
10 (50)	1.39	9.39	12	8	939,000	All
		22.21	28	20	918,000	
		33.43	41	34	889,000	
		44.88	56	48	866,000	
		55.19	72	58	849,000	

NOTE: (a) $E_{0.1}$ ave computed using average strain $\frac{\epsilon_1 + \epsilon_2}{2}$

Table F.5 Dynamic Resilient Modulus Test Results on 2AC-2

Temp C (F)	Specimen Height (in.)	Stress σ (psi)	Elastic Strain		$E_{0.1}$ ave ^(a) (psi)	Data Points Used
			ϵ_1 ($\times 10^{-6}$)	ϵ_2 ($\times 10^{-6}$)		
30 (86)	1.39	4.58	9	12	432,000	All
		11.91	26	40	361,000	
		16.72	44	58	328,000	
		23.13	56	88	318,000	
		30.00	72	148	273,000	
25 (77)	1.39	11.45	24	24	477,000	All
		13.74	24	28	520,000	
		14.88	30	29	503,000	
		17.17	37	34	485,000	
		19.46	40	43	470,000	
15 (59)	1.39	9.62	12	16	697,000	All
		20.15	26	32	700,000	
		29.31	44	47	646,000	
		41.45	71	64	615,000	
		57.71	109	87	588,000	
10 (50)	1.39	11.45	12	14	881,000	All
		23.36	28	31	789,000	
		33.89	40	42	823,000	
		44.42	64	58	726,000	
		60.45	93	76	715,000	
30 (86)	1.16	4.39	12	9	414,000	Last 5
		5.49	17	13	371,000	
		12.35	40	40	309,000	
		14.00	47	45	304,000	
		19.76	74	80	257,000	
		27.99	113	128	232,000	
20 (68)	1.16	10.98	16	16	686,000	Last 4
		21.95	45	46	486,000	
		31.83	71	74	441,000	
		41.44	97	104	413,000	
		55.16	144	163	359,000	
10 (50)	1.16	9.60	11	12	842,000	Last 4
		20.86	28	29	735,000	
		34.30	48	52	686,000	
		41.44	60	64	666,000	
		52.69	76	86	650,000	

NOTE: (a) $E_{0.1}$ ave computed using average strain $\frac{\epsilon_1 + \epsilon_2}{2}$

Table F.6 Dynamic Resilient Modulus Test Results on 2AC-3

Temp C (F)	Specimen Height (in.)	Stress σ (psi)	Elastic Strain ϵ_1 ($\times 10^{-6}$)	Strain ϵ_2 ($\times 10^{-6}$)	$E_{0.1}$ ave ^(a) (psi)	Data Points Used
25 (77)	2.10	7.58	67	63	117,000	None ^(b)
		9.85	84	80	120,000	
		12.13	106	104	115,000	
		14.40	113	117	125,000	
		16.67	152	144	113,000	
45 (113)	1.63	2.54	52	40	55,000	None ^(b)
		5.08	84	112	52,000	
		8.20	144	196	48,000	
		10.15	244	236	42,000	
		13.86	400	-	-	
40 (104)	1.63	5.08	72	65	74,000	None ^(b)
		7.23	124	120	59,000	
		8.98	188	196	47,000	
		13.86	268	280	51,000	
		17.18	376	388	45,000	
25 (77)	1.51	10.75	25	44	309,000	None ^(b)
		12.65	32	56	289,000	
		16.23	45	74	272,000	
		19.39	59	89	263,000	
		23.19	80	109	246,000	
		30.56	130	156	214,000	
15 (59)	1.51	9.70	26	9	551,000	None ^(b)
		18.13	52	32	434,000	
		28.46	74	74	385,000	
		39.21	108	132	326,000	
		49.11	181	190	265,000	
10 (50)	1.51	9.49	20	20	470,000	None ^(b)
		20.24	45	59	388,000	
		31.83	80	108	339,000	
		41.53	132	150	295,000	
		51.86	216	187	257,000	

NOTE: (a) $E_{0.1}$ ave computed using average strain $\frac{\epsilon_1 + \epsilon_2}{2}$

(b) Samples excluded from analyses because of low moduli values due to micro cracking

Table F.7 Dynamic Resilient Modulus Test Results on 2SA

Temp C (F)	Specimen Height (in.)	Stress σ (psi)	Elastic Strain ϵ_1 ($\times 10^{-6}$)	Elastic Strain ϵ_2 ($\times 10^{-6}$)	$E_{0.1}$ ave ^(a) (psi)	Data Points Used
45 (113)	1.86	2.91	17	14	191,000	All
		3.77	27	22	153,000	
		6.34	49	36	159,000	
		8.39	54	48	165,000	
		10.62	67	60	166,000	
40 (104)	1.86	3.60	16	12	254,000	All
		5.31	25	26	209,000	
		7.88	38	36	213,000	
		9.93	44	48	216,000	
		12.33	46	56	240,000	
35 (95)	1.86	2.05	10	16	158,000	All
		3.60	17	25	173,000	
		6.00	22	36	208,000	
		8.56	31	50	211,000	
		10.45	38	67	199,000	
30 (86)	1.86	2.74	10	5	370,000	All
		4.45	15	9	365,000	
		6.68	21	18	344,000	
		8.56	25	20	379,000	
		11.13	32	33	339,000	
25 (77)	1.86	3.25	8	9	378,000	All
		4.97	12	13	401,000	
		6.51	16	19	374,000	
		8.22	20	23	381,000	
		9.93	24	30	371,000	
15 (59)	1.86	3.25	5	8	492,000	All
		4.62	7	11	513,000	
		6.51	11	16	486,000	
		7.71	14	18	494,000	
		9.59	18	22	480,000	
45 (113)	1.80	2.65	13	16	184,000	All
		4.24	21	25	186,000	
		6.37	38	48	147,000	
		8.13	46	64	147,000	
		9.90	56	78	148,000	
40 (104)	1.80	2.65	8	10	294,000	All
		4.07	15	20	231,000	
		7.25	32	43	194,000	
		9.55	40	59	193,000	
		12.38	48	81	192,000	
35 (95)	1.80	3.18	7	8	418,000	Last 4
		5.13	12	15	377,000	
		6.90	22	24	297,000	
		9.37	28	32	308,000	
		11.67	35	40	312,000	

Table F.7--continued

Temp C (F)	Specimen Height (in.)	Stress σ (psi)	Elastic Strain ϵ_1 ϵ_2 ($\times 10^{-6}$) ($\times 10^{-6}$)		$E_{0.1}$ ave ^(a) (psi)	Data Points Used
30 (86)	1.80	3.71	4	15	386,000	Last 4
		5.84	16	25	286,000	
		8.13	21	37	282,000	
		10.43	28	50	267,000	
		13.26	36	65	263,000	
25 (77)	1.80	3.36	8	10	373,000	All
		5.13	14	18	325,000	
		7.07	18	25	327,000	
		8.31	22	32	306,000	
		10.08	25	40	313,000	
15 (59)	1.80	3.36	5	9	480,000	All
		4.95	8	14	450,000	
		6.01	12	17	423,000	
		8.13	15	23	428,000	

NOTE: (a) $E_{0.1}$ ave computed using average strain $\frac{\epsilon_1 + \epsilon_2}{2}$

Table F.8 Dynamic Resilient Modulus Test Results on 3AC-1

Temp C (F)	Specimen Height (in.)	Stress σ (psi)	Elastic Strain ϵ_1 ϵ_2 ($\times 10^{-6}$) ($\times 10^{-6}$)		$E_{0.1}$ ave ^(a) (psi)	Data Points Used
25 (77)	1.61	1.38	5	2	406,000	Last 5
		2.57	12	4	321,000	
		5.34	29	8	290,000	
		8.11	51	12	258,000	
		10.28	70	13	248,000	
		14.04	81	28	256,000	
20 (68)	1.61	7.32	27	5	458,000	All
		15.42	45	25	443,000	
		19.18	56	36	419,000	
		24.32	72	52	394,000	
		32.23	84	78	399,000	
15 (59)	1.61	5.14	12	4	627,000	All
		11.47	24	12	637,000	
		18.19	36	24	602,000	
		25.11	48	39	573,000	
		30.45	58	52	554,000	
		36.77	68	64	557,000	
10 (50)	1.61	8.70	16	16	530,000	Last 4
		18.78	8	38	817,000	
		27.68	13	56	809,000	
		32.03	24	60	763,000	
		43.69	42	68	797,000	
25 (77)	1.58	4.63	16	16	286,000	All
		7.66	31	27	264,000	
		12.09	49	44	259,000	
		16.92	70	66	248,000	
		22.16	90	92	244,000	
20 (68)	1.58	4.84	12	12	403,000	All
		8.06	22	19	391,000	
		14.30	39	34	389,000	
		19.74	55	55	360,000	
		30.62	84	86	360,000	
15 (59)	1.58	10.28	16	20	571,000	All
		20.55	36	40	541,000	
		32.84	60	62	538,000	
		40.90	76	76	538,000	
		54.20	103	108	502,000	

Table F.8--continued

Temp C (F)	Specimen Height (in.)	Stress σ (psi)	Elastic Strain ϵ_1 ($\times 10^{-6}$)	Strain ϵ_2 ($\times 10^{-6}$)	$E_{0.1}$ ave ^(a) (psi)	Data Points Used
10 (50)	1.58	10.47	15	15	707,000	All
		20.75	28	28	736,000	
		31.83	45	43	723,000	
		40.90	58	56	718,000	
		51.98	74	75	695,000	
5 (77)	1.38	3.69	13	11	313,000	All
		6.00	26	19	268,000	
		8.07	36	29	248,000	
		11.99	56	50	225,000	
		15.68	75	74	211,000	
20 (68)	1.38	5.77	13	16	390,000	All
		12.46	30	44	335,000	
		16.84	40	63	328,000	
		22.83	56	88	317,000	
		27.45	68	112	306,000	
15 (59)	1.38	6.00	9	9	682,000	Last 4
		14.53	22	40	469,000	
		22.37	40	60	447,000	
		28.37	50	82	430,000	
		35.52	60	100	444,000	
10 (50)	1.38	8.53	11	15	646,000	All
		19.84	24	36	661,000	
		28.14	34	54	640,000	
		35.98	44	68	643,000	
		45.90	54	92	630,000	

NOTE: (a) $E_{0.1}$ ave computed using average strain $\frac{\epsilon_1 + \epsilon_2}{2}$

Table F.9 Dynamic Resilient Modulus Test Results on 3AC-2

Temp C (F)	Specimen Height (in.)	Stress σ (psi)	Elastic Strain		$E_{0.1}$ ave ^(a) (psi)	Data Points Used
			ϵ_1 ($\times 10^{-6}$)	ϵ_2 ($\times 10^{-6}$)		
35 (95)	1.62	4.32	14	-	308,000	All ^(b)
		7.27	26	-	280,000	
		11.00	42	-	262,000	
		15.72	66	-	240,000	
		24.56	108	-	227,000	
25 (77)	1.62	9.82	19	32	384,000	All
		12.77	40	26	387,000	
		16.70	49	32	409,000	
		17.68	54	36	391,000	
		19.65	64	40	378,000	
15 (59)	1.62	10.41	8	20	754,000	All
		20.43	21	36	714,000	
		30.45	36	53	683,000	
		39.69	48	72	662,000	
		54.03	64	104	643,000	
35 (95)	1.65	6.95	20	40	232,000	All
		9.65	30	51	238,000	
		11.96	42	60	234,000	
		14.11	50	68	238,000	
		16.78	65	79	234,000	
30 (86)	1.65	5.02	9	9	571,000	Last 4
		9.06	21	24	408,000	
		12.54	32	36	369,000	
		17.17	44	52	358,000	
		21.22	58	68	335,000	
20 (68)	1.65	10.22	12	16	720,000	Last 4
		19.48	28	32	649,000	
		29.32	43	48	646,000	
		38.97	59	64	631,000	
		50.35	76	84	629,000	
10 (50)	1.65	9.45	8	7	1,277,000	All
		18.71	20	16	1,051,000	
		29.71	29	28	1,046,000	
		39.36	40	36	1,036,000	
		50.16	50	48	1,020,000	
30 (86)	1.76	4.88	4	27	317,000	All
		8.50	7	48	306,000	
		10.67	8	60	312,000	
		13.75	14	78	300,000	
		18.99	16	100	326,000	
20 (68)	1.76	8.50	4	24	620,000	All
		17.72	10	51	587,000	
		26.23	15	72	604,000	
		34.00	22	89	612,000	
		44.49	30	111	634,000	

Table F.9--continued

Temp C (F)	Specimen Height (in.)	Stress σ (psi)	Elastic Strain ϵ_1 ($\times 10^{-6}$)	Elastic Strain ϵ_2 ($\times 10^{-6}$)	$E_{0.1}$ ave ^(a) (psi)	Data Points Used
10 (50)	1.76	9.04	4	10	1,256,000	All
		20.44	9	28	1,099,000	
		27.67	12	36	1,143,000	
		36.53	18	46	1,149,000	
35 (95)	1.46	46.12	22	60	1,119,000	All
		5.45	23	15	287,000	
		8.72	40	26	264,000	
		12.43	60	36	259,000	
30 (86)	1.46	15.26	72	44	263,000	All
		19.40	92	53	268,000	
		5.45	12	12	447,000	
		9.81	28	21	405,000	
20 (68)	1.46	13.74	38	29	409,000	All
		18.97	56	40	395,000	
		25.29	76	51	399,000	
		9.81	18	5	861,000	
10 (50)	1.46	20.71	36	18	779,000	All
		31.61	53	32	746,000	
		42.52	72	44	733,000	
		53.42	94	60	696,000	
10 (50)	1.46	10.90	12	5	1,267,000	All
		20.28	20	12	1,252,000	
		28.13	28	16	1,267,000	
		37.07	39	24	1,181,000	
		53.42	54	36	1,192,000	

NOTE: (a) $E_{0.1}$ ave computed using average strain $\frac{\epsilon_1 + \epsilon_2}{2}$

(b) Moduli calculated from gage 1

Table F.10 Dynamic Resilient Modulus Test Results on 3SA

Temp C (F)	Specimen Height (in.)	Stress σ (psi)	Elastic Strain		$E_{0.1}$ ave ^(a) (psi)	Data Points Used
			ϵ_1 ($\times 10^{-6}$)	ϵ_2 ($\times 10^{-6}$)		
45 (113)	2.05	2.95	14	22	166,000	A11
		3.73	24	31	135,000	
		6.21	40	55	131,000	
		7.61	51	70	126,000	
		10.25	61	93	133,000	
40 (104)	2.05	2.95	12	12	242,000	First 4 ^(b)
		4.35	16	22	229,000	
		5.90	24	40	184,000	
		6.99	32	64	146,000	
		10.09	-	68	-	
45 (113)	1.93	2.97	12	22	177,000	A11
		4.29	18	34	166,000	
		5.61	26	44	160,000	
		7.92	36	64	158,000	
		9.57	36	70	181,000	
40 (104)	1.93	2.47	6	13	257,000	A11
		3.46	11	20	225,000	
		5.28	16	34	213,000	
		6.60	20	40	220,000	
		7.75	24	46	221,000	
35 (95)	1.93	2.31	6	12	269,000	A11
		3.63	8	18	275,000	
		4.62	11	24	266,000	
		6.60	16	36	252,000	
		8.58	20	48	252,000	
30 (86)	1.93	2.64	5	10	347,000	A11
		4.12	8	16	343,000	
		5.77	12	26	307,000	
		7.42	16	35	292,000	
		9.57	24	46	272,000	
25 (77)	1.93	2.64	8	7	357,000	A11
		4.12	10	13	361,000	
		5.77	12	18	380,000	
		7.26	14	27	356,000	
		8.74	16	36	336,000	
15 (59)	1.93	3.96	4	14	450,000	A11
		4.78	4	17	451,000	
		6.76	6	24	451,000	
		8.41	10	30	425,000	
		10.06	12	33	445,000	

Table F.10--continued

Temp C (F)	Specimen Height (in.)	Stress σ (psi)	Elastic Strain		$E_{0.1}$ ave ^(a) (psi)	Data Points Used
			ϵ_1 ($\times 10^{-6}$)	ϵ_2 ($\times 10^{-6}$)		
45 (113)	1.65	2.51	16	7	216,000	None ^(b)
		4.44	28	14	209,000	
		5.40	32	13	239,000	
		6.17	38	24	200,000	
		7.12	36	30	216,000	
45 (113)	1.94	3.28	18	19	178,000	All
		5.25	32	32	164,000	
		7.88	50	55	150,000	
		11.49	75	80	148,000	
		13.45	80	89	159,000	
40 (104)	1.94	2.46	11	8	262,000	All
		5.09	22	22	229,000	
		6.73	32	32	210,000	
		8.86	36	47	213,000	
		12.30	52	70	202,000	
35 (95)	1.94	2.62	11	7	298,000	All
		4.59	20	15	261,000	
		6.56	26	26	248,000	
		8.70	34	40	236,000	
		11.16	45	56	221,000	
30 (86)	1.94	2.95	7	12	314,000	All
		4.10	10	16	311,000	
		6.73	20	27	288,000	
		8.86	24	33	312,000	
		10.67	31	44	338,000	
25 (77)	1.94	2.63	7	9	337,000	All
		4.27	11	16	319,000	
		5.74	13	21	338,000	
		7.71	21	28	313,000	
		9.19	25	32	319,000	
15 (59)	1.94	3.28	6	8	482,000	All
		4.76	9	10	496,000	
		6.40	12	14	492,000	
		8.04	14	20	479,000	
		9.35	18	22	468,000	
45 (113)	1.89	3.03	16	17	183,000	All
		4.38	24	31	159,000	
		5.73	34	40	156,000	
		7.07	43	52	140,000	
		8.76	52	60	156,000	

Table F.10--continued

Temp C (F)	Specimen Height (in.)	Stress σ (psi)	Elastic Strain ϵ_1 ($\times 10^{-6}$)	Elastic Strain ϵ_2 ($\times 10^{-6}$)	$E_{0.1}$ ave ^(a) (psi)	Data Points Used
40 (104)	1.89	3.37	13	17	225,000	All
		5.05	21	28	207,000	
		6.40	29	34	204,000	
		7.92	36	41	206,000	
		9.94	48	51	200,000	
35 (95)	1.89	3.37	12	12	272,000	All
		5.05	20	20	250,000	
		7.24	28	31	246,000	
		8.42	34	38	234,000	
		9.77	40	44	233,000	
30 (86)	1.89	3.54	13	12	290,000	All
		4.88	16	16	305,000	
		6.23	22	20	291,000	
		7.75	26	28	289,000	
		9.26	32	34	279,000	
25 (77)	1.89	2.86	8	7	376,000	All
		4.55	14	13	335,000	
		6.06	20	18	319,000	
		7.75	24	24	326,000	
		9.26	29	29	317,000	
15 (59)	1.89	3.03	3	10	473,000	All
		4.72	6	14	482,000	
		6.91	12	18	467,000	
		7.75	15	22	421,000	
		9.43	17	24	458,000	
45 (113)	2.44	2.61	16	13	179,000	All
		3.91	30	26	142,000	
		5.09	44	36	128,000	
		6.39	52	48	128,000	
		7.96	68	60	124,000	
40 (104)	2.44	2.61	16	13	179,000	All
		4.04	24	21	180,000	
		5.22	32	30	168,000	
		6.26	40	37	163,000	
		7.82	50	42	170,000	
35 (95)	2.44	1.83	8	7	241,000	All
		3.91	16	16	241,000	
		5.22	25	23	216,000	
		6.65	33	32	204,000	
		7.56	40	36	199,000	

Table F.10--continued

Temp C (F)	Specimen Height (in.)	Stress σ (psi)	Elastic Strain		$E_{0.1}$ ave ^(a) (psi)	Data Points Used
			ϵ_1 ($\times 10^{-6}$)	ϵ_2 ($\times 10^{-6}$)		
30 (86)	2.44	2.74	11	8	280,000	All
		3.91	16	14	257,000	
		5.09	20	19	260,000	
		6.91	28	28	249,000	
		8.09	36	33	234,000	
25 (77)	2.44	3.00	8	10	341,000	All
		4.56	14	16	304,000	
		5.87	20	20	296,000	
		7.30	24	24	299,000	
		8.87	33	30	282,000	
15 (59)	2.44	2.48	7	6	421,000	All
		3.91	10	8	444,000	
		5.61	13	10	475,000	
		6.78	18	15	408,000	
		7.96	20	18	415,000	
45 (113)	2.32	2.06	12	19	134,000	All
		4.12	29	32	135,000	
		5.35	40	44	127,000	
		6.86	56	56	123,000	
		8.09	70	64	121,000	
40 (104)	2.32	2.20	10	14	183,000	All
		3.16	20	20	156,000	
		4.80	30	30	161,000	
		6.17	40	38	157,000	
		7.68	53	47	154,000	
35 (95)	2.32	2.47	10	12	225,000	All
		4.00	17	20	214,000	
		5.10	27	26	194,000	
		6.95	38	31	200,000	
		8.23	48	40	187,000	
30 (86)	2.32	2.61	9	12	256,000	All
		4.20	16	16	255,000	
		5.49	24	22	239,000	
		6.72	31	28	227,000	
		8.23	40	36	219,000	
25 (77)	2.32	2.88	8	12	282,000	All
		5.08	16	18	299,000	
		6.45	24	24	269,000	
		7.82	31	29	262,000	
		9.06	38	34	253,000	

Table F.10--continued

Temp C (F)	Specimen Height (in.)	Stress σ (psi)	Elastic Strain ϵ_1 ($\times 10^{-6}$)	Elastic Strain ϵ_2 ($\times 10^{-6}$)	$E_{0.1}$ ave ^(a) (psi)	Data Points Used
15 (59)	2.32	2.61	4	8	435,000	All
		4.12	8	12	412,000	
		5.63	10	16	420,000	
		6.59	13	21	388,000	
		7.82	18	23	380,000	
45 (113)	1.85	2.75	13	12	222,000	All
		4.13	24	18	197,000	
		6.02	34	25	203,000	
		7.23	44	32	189,000	
		8.77	53	40	189,000	
40 (104)	1.85	3.27	12	12	273,000	All
		4.99	21	18	260,000	
		6.54	28	22	260,000	
		7.74	36	26	242,000	
		9.46	44	35	239,000	
35 (95)	1.85	3.44	12	8	331,000	All
		5.16	20	16	290,000	
		6.54	24	20	297,000	
		8.26	30	25	304,000	
		10.32	40	32	287,000	
30 (86)	1.85	3.44	8	8	420,000	All
		4.82	12	12	402,000	
		6.37	17	17	379,000	
		8.26	24	22	356,000	
		9.81	31	27	338,000	
25 (77)	1.85	3.61	8	9	420,000	All
		4.82	11	11	430,000	
		6.71	16	16	425,000	
		8.43	23	20	394,000	
		9.98	28	22	399,000	
15 (59)	1.85	2.93	5	5	598,000	All
		5.68	10	10	557,000	
		8.26	16	14	558,000	
		10.15	20	18	540,000	

NOTE: (a) $E_{0.1}$ ave computed using average strain $\frac{\epsilon_1 + \epsilon_2}{2}$

(b) Specimen failed during testing

Table F.11 Indirect Tensile Test Results

Site	Layer Type	Layer No.	Sample Height (in.)	Failure Load (lbs.)	Vertical Deformation (in.)	Horizontal Deformation (in.)
1	AC	1	2.06	2,344	0.060	0.0078
	AC	2	1.69	2,144	0.036	0.0065
	SA	-	1.96	1,000	0.025	0.0015
2	AC	1	1.57	1,813	0.048	0.0085
	AC	2	1.39	1,550	0.044	0.0060
	AC	3	2.10	875	0.030	0.0140
	AC	3	1.63	725	0.030	0.0130
	SA	-	1.86	655	0.051	0.0040
	SA	-	1.80	650	0.032	0.0032
3	AC	1	1.61	2,031	0.070	0.0130
	AC	2	1.65	2,969	0.039	0.0075
	AC	2	1.76	2,750	0.044	0.0088
	SA	-	2.44	1,120	0.050	0.0030
	SA	-	2.32	888	0.053	0.0032
	SA	-	1.89	715	0.048	0.0050
	SA	-	1.85	720	0.042	0.0029
SA	-	1.93	660	0.054	0.0026	

NOTE: All tests conducted at 25 C (77 F)

Table F.12 Fracture Energy Parameters and Creep Test Data

Site	Layer No.	Temp (C)	Fracture Energy	Const. Power Viscosity (Pa-s)	Mix Viscosity (Pa-s)	AV (%)	Measurements				
							Creep Stress psi (Pa)	Failure Strain (xE-6)	Elastic Strain (xE-6)	Creep Rate (xE-6/sec)	
1	1	0	730	7.50 E9	1.56 E12	6.5	117.7 (811,542)	980	160	0.52	
	2	0	665	3.67 E10	6.00 E10	7.9	133.9 (923,241)	960	480	15.40	
	2	0	367	3.67 E10	1.62E 12	6.6	108.0 (744,666)	600	215	0.46	
	2	10	364	3.85 E9	4.06 E11	10.5	51.8 (357,161)	1,120	120	0.88	
2	1	-5	791	4.12 E10	1.85 E12	7.4	171.7 (1,183,000)	770	203	0.64	
	1	10	1,388	1.00 E9	8.75 E10	5.3	99.7 (687,432)	2,200	360	7.86	
	2	0	444	7.78 E9	1.55 E12	13.7	91.9 (633,651)	795	190	0.41	
	3	-5	342	2.86 E10	7.97 E11	9.3	60.1 (414,390)	850	50	0.52	

Table F.12--continued

Site	Layer No.	Temp (C)	Fracture Energy	Const. Power Viscosity (Pa-s)	Mix Viscosity (Pa-s)	AV (%)	Measurements				
							Creep Stress (psi)	Failure Strain (xE-6)	Elastic Strain (xE-6)	Creep Rate (xE-6/sec)	
	1	0	831	3.92 E9	1.08 E12	4.7	104.8 (722,596)	1,280	260	0.67	
	1	10	1,913	3.19 E8	5.70 E10	6.3	131.3 (906,693)	2,260	300	15.90	
	3	2	0	771	8.96 E9	6.44 E12	4.6	121.5 (837,743)	1,000	160	0.13
	2	10	751	9.13 E8	1.41 E12	5.0	51.1 (352,335)	2,440	220	0.29	
	2	15	2,467	3.00 E8	1.39 E11	5.0	114.5 (789,478)	3,495	740	5.70	

NOTE: (a) Excluded from Regression Analysis for Fracture Energy

APPENDIX G
FIELD FWD TEST RESULTS

Table G.1 Results of FWD Tests on Site 1 (Test 1)

Temperature (F): Air = 60 Pvmt. Surf. = 55

Station No.	Applied Load (lbs.)	Measured Deflections (mils)						
		D ₁ (a)	D ₂	D ₃	D ₄	D ₅	D ₆	D ₇
		0 (b)	12	24	36	48	60	72
1	17496	28.2	17.1	11.0	6.9	4.3	3.2	2.8
	17624	26.4	15.9	10.3	6.8	4.6	3.6	3.0
	17568	31.6	15.4	10.2	6.6	4.4	3.5	2.9
2	17496	25.1	18.8	12.2	7.7	5.2	3.7	2.9
	17664	23.6	17.5	11.6	7.6	5.3	3.9	3.1
	17648	22.8	17.2	11.5	7.5	5.3	3.9	3.1
3	17576	24.0	18.4	12.9	6.2	4.6	3.6	2.6
	17688	22.6	17.3	12.4	6.3	4.7	3.6	2.7
	17664	22.6	17.1	12.3	6.3	4.7	3.7	2.6
4	17536	24.1	17.9	11.6	7.0	4.8	3.8	3.0
	17572	22.9	16.9	11.2	7.1	4.9	4.0	3.2
	17532	22.7	16.5	11.2	7.1	5.0	4.0	3.1
5	17592	25.1	17.9	11.7	7.6	5.2	3.6	3.1
	17608	26.3	17.3	11.4	7.4	5.0	3.3	3.1
	17536	25.0	17.0	11.2	7.3	4.9	3.3	3.0
6	17496	25.8	23.0	8.6	6.2	4.4	3.5	2.8
	17568	24.8	21.7	8.6	6.4	4.6	3.6	2.9
	17568	23.5	21.6	8.6	6.3	4.6	3.7	2.8
7	17440	25.5	18.1	11.8	6.8	4.4	3.6	2.9
	17536	24.3	17.4	11.6	7.0	4.6	3.8	3.3
	17584	26.1	16.8	11.4	7.0	4.8	3.9	3.2
8	17512	23.2	17.5	11.6	6.9	4.4	3.5	2.7
	17608	22.3	16.9	11.3	7.3	4.8	3.8	3.0
	17528	22.1	16.5	11.4	7.0	4.8	3.9	2.9
9	17456	23.0	16.6	11.0	7.2	5.1	3.5	2.3
	17528	22.1	15.9	10.6	7.3	5.3	3.9	2.8
	17592	22.6	15.6	10.6	7.2	5.3	3.9	2.7
10	17432	22.9	17.3	11.4	7.0	4.6	3.7	3.0
	17488	29.9	16.5	11.2	7.2	5.0	4.0	3.3
	17576	21.9	16.2	11.1	7.1	4.9	4.0	3.3

Table G.1--continued

Station No.	Applied Load (lbs.)	Measured Deflections (mils)						
		D_1 (a)	D_2	D_3	D_4	D_5	D_6	D_7
		0 (b)	12	24	36	48	60	72
11	17552	25.5	17.7	11.8	6.5	5.2	4.0	3.2
	17648	24.5	17.2	11.7	6.8	5.4	4.3	3.3
	17584	24.3	17.0	11.6	6.9	5.5	4.3	3.3
1 (OWP)	17632	22.4	18.2	11.3	7.9	5.5	3.8	2.9
	17664	23.9	16.8	10.6	7.5	5.3	3.8	3.0
	17656	21.5	16.5	10.4	7.4	5.2	3.7	2.8
2 (OWP)	17776	23.0	18.6	9.1	6.8	4.8	3.6	2.7
	17696	22.7	18.0	8.9	6.6	4.8	3.6	2.8
	17672	22.9	17.9	8.8	6.5	4.7	3.6	2.8

(a) Sensor No. (b) Radial Distance in Inches From Center of FWD Load

Table G.2 Results of FWD Tests on Site 1 (Test 2)

Temperature (F): Air = 29 Pvmt. Surf. = 30

Station No.	Applied Load (lbs.)	Measured Deflections (mils)						
		D ₁ (a)	D ₂	D ₃	D ₄	D ₅	D ₆	D ₇
		0 (b)	12	24	36	48	60	72
1	17920	25.5	17.8	12.2	8.1	4.9	3.1	2.5
	17992	24.6	16.9	11.8	8.0	4.9	3.4	2.9
	18016	24.5	16.6	11.6	7.9	5.0	3.4	3.0
2	17736	32.1	24.4	17.2	11.7	8.0	5.8	4.0
	17840	30.5	23.2	16.3	11.4	7.9	5.7	4.2
	17856	30.1	22.8	16.1	11.3	7.8	5.7	4.2
3	17888	22.5	19.0	9.0	6.9	5.3	4.3	2.6
	17944	22.4	18.9	9.0	6.9	5.3	4.3	2.7
	17880	22.3	18.8	8.9	6.9	5.3	4.3	2.7
4	17984	23.9	18.5	13.6	10.0	4.6	3.9	3.2
	18000	22.9	17.6	13.2	9.7	4.9	4.2	3.3
	17992	22.7	17.5	13.1	9.6	5.0	4.3	3.3
5	17600	35.9	23.3	14.4	7.8	3.5	1.1	1.6
	17584	34.5	22.3	14.0	7.8	3.7	1.5	2.3
	17672	34.1	22.0	13.8	7.8	3.9	1.9	2.5
6	17864	27.0	41.5	9.4	7.1	5.2	3.9	3.0
	17928	25.9	26.0	9.1	7.1	5.2	4.0	3.3
	17888	25.5	25.6	9.0	7.0	5.2	4.0	3.3
7	17816	27.6	20.5	14.4	9.3	3.9	3.2	2.6
	17912	26.4	19.7	14.2	9.5	4.2	3.6	3.1
	17856	26.1	19.5	14.0	9.5	4.2	3.6	3.0
8	17896	24.6	20.4	15.8	11.8	5.9	4.7	3.7
	17928	23.8	19.7	15.3	11.4	6.1	4.9	3.9
	17928	23.8	19.6	15.2	11.4	6.2	5.0	3.9
9	17728	26.5	18.7	12.4	7.1	3.9	2.3	0.5
	17896	25.2	17.8	11.9	7.2	4.3	2.9	1.5
	17904	25.0	17.5	11.8	7.0	4.3	3.1	1.7
10	17896	23.7	19.9	15.3	7.0	5.6	4.5	3.6
	17920	22.8	18.8	14.4	7.0	5.7	4.6	3.7
	17960	22.7	18.8	14.2	6.9	5.7	4.7	3.8

Table G.2--continued

Station No.	Applied Load (lbs.)	Measured Deflections (mils)						
		D_1 (a)	D_2	D_3	D_4	D_5	D_6	D_7
		0 (b)	12	24	36	48	60	72
11	17808	27.2	19.5	14.2	9.5	5.4	4.5	3.5
	17832	25.8	18.9	13.6	9.6	5.7	4.7	3.7
	17824	25.5	18.8	13.5	9.6	5.7	4.7	3.7
1 (OWP)	18048	26.6	22.4	18.0	13.1	6.7	9.6	3.5
	18152	25.6	21.2	17.1	12.7	6.7	9.4	3.6
	18072	25.4	20.8	16.7	12.5	6.8	9.3	3.6
2 (OWP)	18120	25.3	22.2	9.0	6.7	4.8	3.5	3.3
	18208	24.7	21.3	8.9	6.7	4.8	3.6	3.4
	18104	24.6	21.3	8.9	6.7	4.8	3.6	3.4

(a) Sensor No. (b) Radial Distance in Inches From Center of FWD Load

Table G.3 Results of FWD Tests on Site 1 (Test 3)

Temperature (F): Air = 55 Pvm. Surf. = 58

Station No.	Applied Load (lbs.)	Measured Deflections (mils)						
		D ₁ (a)	D ₂	D ₃	D ₄	D ₅	D ₆	D ₇
		0 (b)	12	24	36	48	60	72
1	26524	40.6	25.8	16.3	10.4	6.5	4.9	4.2
	17448	29.3	17.0	11.2	7.4	4.8	3.8	3.1
	9176	16.7	8.9	5.8	3.8	2.5	2.0	1.5
2	26592	32.9	24.0	16.5	10.7	7.1	5.3	4.4
	17344	22.5	16.7	11.3	7.4	5.2	3.9	3.0
	8952	12.1	9.2	6.3	4.1	2.8	2.1	1.7
3	26384	33.3	25.1	17.3	9.2	6.7	5.3	4.0
	17376	22.6	17.3	12.2	6.4	4.8	3.8	2.6
	9040	11.9	9.4	6.9	3.4	2.5	2.0	1.5
4	26440	33.7	24.7	16.3	9.8	6.6	5.4	4.3
	17312	22.6	16.6	11.4	7.1	4.1	3.9	3.1
	9072	11.9	8.9	6.0	3.9	2.6	2.1	1.7
5	26360	40.2	27.5	17.6	10.6	6.7	5.0	3.8
	17152	27.5	18.9	12.0	7.7	5.1	3.6	2.5
	8904	16.1	10.7	6.7	4.3	2.7	1.9	1.5
6	26176	40.2	36.7	14.3	10.0	6.7	4.9	3.8
	17208	24.9	22.8	9.2	6.8	4.9	3.9	3.1
	8872	13.8	13.3	4.8	3.6	2.6	2.2	1.7
7	26208	35.6	25.8	16.8	10.1	6.4	5.3	4.3
	17224	24.1	17.8	11.8	7.2	7.6	3.9	3.1
	8856	13.2	9.6	6.3	4.0	2.5	2.1	1.7
8	26088	33.9	25.6	16.9	10.2	6.8	5.7	4.4
	17200	22.9	17.6	12.0	7.6	5.1	4.3	3.2
	8832	12.3	9.7	6.6	4.3	2.8	2.3	1.8
9	26192	37.5	24.2	16.0	10.6	7.3	5.6	4.2
	17192	22.2	16.4	10.8	7.5	5.3	3.9	2.7
	8792	12.1	8.7	5.7	4.0	2.7	2.0	1.3
10	25920	32.6	26.6	17.3	8.6	7.1	5.7	4.7
	17192	22.0	17.3	12.2	6.2	5.2	4.2	3.4
	8880	11.6	9.3	6.6	3.4	2.8	2.3	1.9

Table G.3--continued

Station No.	Applied Load (lbs.)	Measured Deflections (mils)						
		D_1 (a)	D_2	D_3	D_4	D_5	D_6	D_7
		0 (b)	12	24	36	48	60	72
11	25832	36.3	26.1	16.5	9.8	7.1	5.8	4.5
	17152	24.4	17.3	11.6	7.1	5.2	4.3	3.2
	8848	12.9	8.3	6.2	3.8	2.8	2.3	1.8
1 (OWP)	25760	34.2	25.6	15.5	11.0	7.7	5.5	4.1
	17232	21.8	16.1	9.9	7.4	5.4	4.1	3.0
	8880	11.2	8.4	5.1	3.9	2.9	2.3	1.7
2 (OWP)	25760	38.3	27.7	16.7	19.2	6.8	5.2	4.0
	17232	24.9	18.2	11.1	6.4	4.8	3.7	2.8
	8880	12.9	9.5	5.8	3.5	2.6	2.0	1.5

(a) Sensor No. (b) Radial Distance in Inches From Center of FWD Load

Table G.4 Results of FWD Tests on Site 1 (Test 4)

Temperature (F): Air = 69 Pvm. Surf. = 72

Station No.	Applied Load (lbs.)	Measured Deflections (mils)						
		D ₁ ^(a)	D ₂	D ₃	D ₄	D ₅	D ₆	D ₇
		0 ^(b)	12	24	36	48	60	72
1	25736	50.1	20.9	13.5	8.9	6.2	4.9	4.0
	17000	22.7	13.8	9.1	6.1	4.4	3.5	2.8
	8536	12.1	6.7	4.5	3.1	2.3	1.8	1.4
2	25376	30.6	21.3	14.1	9.2	6.3	4.9	4.0
	16976	20.8	14.6	9.7	6.3	4.4	3.4	2.7
	8536	11.0	7.7	5.1	3.3	2.3	1.8	1.5
3	25328	32.7	22.0	14.5	8.2	6.2	4.9	3.8
	17048	20.3	14.9	10.1	5.7	4.3	3.4	2.6
	8736	10.6	7.8	5.4	2.9	2.2	1.8	1.4
4	25656	30.6	22.1	14.5	9.0	6.2	5.1	4.2
	17024	20.6	15.0	9.9	6.4	4.3	3.5	2.8
	8648	10.6	7.8	5.1	3.3	2.2	1.8	1.4
5	25160	38.2	24.2	14.9	9.3	6.3	4.6	3.1
	16928	26.6	16.6	10.3	6.6	4.6	3.3	2.2
	8480	14.4	8.9	5.4	3.4	2.3	1.6	1.0
6	25200	33.1	20.1	15.1	9.2	6.5	5.1	4.0
	16968	22.3	12.8	9.1	6.3	4.6	3.6	2.8
	8576	11.9	6.1	4.5	3.2	2.3	1.9	1.4
7	25280	34.7	23.2	15.3	9.2	6.3	5.2	4.2
	16888	21.6	15.8	10.6	6.5	4.4	3.7	3.0
	8512	11.5	8.3	5.6	3.4	2.3	1.9	1.5
8	25696	29.2	21.3	14.3	9.2	6.4	5.0	4.1
	17024	19.8	14.6	10.0	6.6	4.5	3.6	2.8
	8672	10.3	7.6	5.3	3.4	2.4	1.9	1.5
9	25448	29.4	21.3	14.1	9.6	6.8	4.9	3.8
	17096	19.8	14.2	9.6	6.6	4.7	3.4	2.7
	8592	10.4	7.4	4.9	3.4	2.3	1.7	1.3
10	25304	31.5	23.5	15.9	9.1	7.2	5.6	4.5
	16952	21.5	16.1	11.1	6.4	5.1	4.0	3.2
	8456	11.3	8.6	6.1	3.4	2.7	2.0	1.7

Table G.4--continued

Station No.	Applied Load (lbs.)	Measured Deflections (mils)						
		D_1 (a)	D_2	D_3	D_4	D_5	D_6	D_7
		0 (b)	12	24	36	48	60	72
11	25184	32.8	22.8	14.9	9.2	5.7	5.1	4.3
	16888	22.0	15.3	10.3	6.5	4.3	3.6	3.0
	8392	11.2	8.1	5.3	3.4	2.3	1.9	1.5
1 (OWP)	25048	30.5	21.9	13.3	9.5	6.8	4.9	4.1
	16872	20.1	14.3	8.7	6.5	4.7	3.4	2.9
	8512	10.0	7.2	4.3	3.3	2.4	1.7	1.4
2 (OWP)	24984	35.0	23.5	14.5	8.2	6.2	4.7	3.6
	16872	22.3	15.4	9.9	5.6	4.3	3.3	2.5
	8512	11.1	7.8	5.2	2.9	2.2	1.7	1.2

(a) Sensor No. (b) Radial Distance in Inches From Center of FWD Load

Table G.5 Results of FWD Tests on Site 1 (Test 5)

Temperature (F): Air = 82 Pvmnt. Surf. = 75

Station No.	Applied Load (lbs.)	Measured Deflections (mils)						
		D_1 (a)	D_2	D_3	D_4	D_5	D_6	D_7
		0 (b)	12	24	36	48	60	72
1	25936	37.0	21.0	13.1	8.0	5.8	5.2	4.0
	11920	18.2	10.0	6.2	4.1	3.0	2.5	1.9
	8168	13.0	6.7	4.3	2.7	2.1	1.7	1.3
2	26216	30.3	19.4	12.8	8.2	5.7	4.9	3.8
	11952	14.2	9.2	6.2	4.2	3.0	2.3	1.9
	8192	9.8	6.3	4.2	2.8	2.0	1.6	1.3
3	26168	30.8	20.7	13.8	7.7	5.7	4.7	3.8
	11912	14.4	10.1	6.9	3.8	2.9	2.3	1.9
	8152	9.9	7.0	4.9	2.7	2.0	1.5	1.3
4	26184	31.3	20.8	13.1	8.1	5.6	4.8	3.6
	11960	14.7	9.9	6.5	4.3	2.9	2.3	1.8
	8152	10.1	6.6	4.7	3.0	1.8	1.7	1.4
5	26016	34.8	21.7	13.6	8.5	5.5	4.4	3.9
	11944	16.4	10.5	6.7	4.1	3.1	2.4	1.9
	8192	11.7	7.2	4.5	3.2	1.9	1.5	1.4
6	26112	32.8	23.4	12.9	8.4	6.0	4.6	3.2
	11912	15.3	12.0	6.0	4.1	3.0	2.3	1.7
	8104	10.6	8.3	4.0	3.0	2.2	1.7	1.2
7	26188	32.3	21.1	13.6	8.3	5.3	4.6	3.9
	11984	15.2	9.9	6.6	4.3	2.9	2.4	1.9
	8168	10.6	6.9	4.4	2.9	2.0	1.6	1.3
8	26344	31.6	21.0	13.6	8.4	5.9	4.7	3.7
	11880	14.8	10.0	6.7	4.4	3.1	2.4	1.9
	8088	10.2	6.9	4.6	3.1	2.1	1.6	1.3
9	26376	30.4	20.3	13.4	8.8	6.1	4.7	3.9
	11968	14.0	9.4	6.3	4.3	3.0	2.4	1.9
	8208	9.6	6.5	4.4	3.0	2.0	1.6	1.3
10	26304	30.6	20.9	13.9	8.2	6.3	4.8	4.0
	11888	14.2	9.9	6.8	4.1	3.1	2.4	1.9
	8144	9.8	6.8	4.6	2.8	2.2	1.7	1.4

Table G.5--continued

Station No.	Applied Load (lbs.)	Measured Deflections (mils)						
		D ₁ (a)	D ₂	D ₃	D ₄	D ₅	D ₆	D ₇
		0 (b)	12	24	36	48	60	72
11	26288	34.1	21.8	14.1	8.8	6.1	5.0	4.2
	11920	15.8	10.3	6.8	4.4	3.1	2.4	1.9
	8152	11.0	7.1	4.6	3.0	2.1	1.7	1.3
1 (OWP)	26184	30.7	20.2	12.0	8.3	5.9	4.6	3.7
	11792	13.8	9.1	5.6	3.8	2.9	2.1	1.7
	8040	9.3	6.2	3.8	2.9	2.0	1.5	1.2
2 (OWP)	26096	36.5	22.0	10.6	7.5	5.5	4.3	3.2
	11832	16.0	10.1	5.1	3.8	2.8	2.1	1.6
	8040	10.9	6.9	3.6	2.6	1.9	1.4	1.1

(a) Sensor No. (b) Radial Distance in Inches From Center of FWD Load

Table G.6 Results of FWD Tests on Site 1 (Test 6)

Temperature (F): Air = 91 Pvmnt. Surf. = 130

Station No.	Applied Load (lbs.)	Measured Deflections (mils)						
		D_1 (a)	D_2	D_3	D_4	D_5	D_6	D_7
		D_0 (b)	12	24	36	48	60	72
1	25800	40.9	20.4	12.6	8.2	6.0	4.6	3.7
	11760	18.5	9.5	5.9	3.9	2.9	2.2	1.7
	7960	12.8	6.5	4.1	2.7	1.9	1.5	1.2
2	26216	34.2	19.3	12.7	8.6	6.1	4.6	3.8
	11760	15.3	8.9	6.0	4.1	3.0	2.2	1.8
	8064	10.3	6.1	4.0	2.7	2.0	1.5	1.1
3	26144	34.7	20.3	13.0	8.3	6.1	4.7	3.8
	11768	15.7	9.4	6.1	3.9	2.9	2.3	1.8
	8048	10.6	6.5	4.2	2.7	2.0	1.5	1.2
4	25984	35.4	20.6	13.0	8.1	5.6	4.6	4.0
	11792	15.9	9.4	6.1	4.1	2.8	2.2	1.8
	8152	10.8	6.5	4.2	2.7	1.9	1.4	1.2
5	25864	37.6	21.3	13.1	8.3	5.9	4.7	3.7
	11856	16.9	9.9	6.2	4.0	2.9	2.2	1.8
	8104	11.6	6.7	4.2	2.7	1.9	1.5	1.2
6	26104	27.2	21.2	12.3	8.1	6.1	4.8	3.6
	11848	16.8	9.8	5.8	3.9	2.9	2.2	1.7
	8016	8.3	6.6	3.9	2.6	2.0	1.5	1.1
7	25976	35.3	20.6	13.1	8.4	5.8	4.7	3.8
	11832	15.8	9.4	6.2	4.1	2.9	2.3	1.9
	8120	10.7	6.4	4.1	2.7	2.0	1.5	1.2
8	26088	34.3	20.7	13.2	8.1	5.9	5.2	4.0
	11848	15.6	9.5	6.2	4.0	2.9	2.3	1.9
	8096	10.5	6.4	4.2	2.7	2.0	1.6	1.2
9	26160	33.9	20.7	13.2	8.7	6.1	5.0	4.0
	11944	15.0	9.2	6.2	4.1	3.0	2.3	1.9
	8120	10.2	6.3	4.2	2.8	2.0	1.5	1.2
10	26160	34.0	20.6	13.4	8.3	6.4	4.9	3.9
	11704	15.5	9.6	6.3	4.1	3.0	2.3	1.9
	8032	10.4	6.5	4.2	2.8	2.1	1.6	1.2

Table G.6--continued

Station No.	Applied Load (lbs.)	Measured Deflections (mils)						
		D ₁ (a)	D ₂	D ₃	D ₄	D ₅	D ₆	D ₇
		0 (b)	12	24	36	48	60	72
11	26040	35.3	21.2	13.9	8.7	6.5	4.9	4.1
	11728	16.0	9.8	6.5	4.3	3.0	2.3	1.9
	8024	10.8	6.5	4.6	3.0	2.1	1.6	1.2
1 (OWP)	26056	35.3	21.0	12.0	8.1	5.6	4.2	3.8
	11640	15.6	9.5	5.6	3.9	2.8	2.1	1.7
	7864	10.4	6.4	3.8	2.7	1.9	1.4	1.1
2 (OWP)	25768	43.7	22.0	11.4	7.4	5.4	4.2	3.2
	11656	19.2	10.0	5.3	3.7	2.7	2.1	1.7
	7896	13.0	6.9	3.6	2.5	1.8	1.4	1.1

(a) Sensor No. (b) Radial Distance in Inches From Center of FWD Load

Table G.7 Results of FWD Tests on Site 1 (Test 7)

Temperature (F): Air = 76 Pvmnt. Surf. = 76

Station No.	Applied Load (lbs.)	Measured Deflections (mils)						
		D_1 (a)	D_2	D_3	D_4	D_5	D_6	D_7
		0 (b)	12	24	36	48	60	72
1	17448	23.9	14.1	8.9	5.5	3.7	3.3	2.5
	12184	17.0	9.9	6.2	3.8	2.5	2.4	1.7
	8208	11.9	6.6	4.2	2.7	1.8	1.6	1.1
2	17336	20.6	14.0	9.4	6.2	4.4	3.3	2.7
	12128	14.8	10.1	6.8	4.4	3.1	2.3	1.9
	8224	10.4	7.2	4.8	3.1	2.2	1.7	1.4
3	17344	20.7	14.8	10.2	5.5	4.0	3.1	2.5
	12144	14.7	10.6	7.5	3.9	2.9	2.3	1.8
	8264	10.1	7.4	5.4	2.7	1.9	1.5	1.2
4	17344	21.3	14.6	9.4	5.9	3.7	3.3	2.7
	12048	15.1	10.2	6.6	4.3	2.7	2.3	1.9
	8200	10.5	7.0	4.5	2.9	1.9	1.5	1.3
5	17328	26.3	15.2	9.5	6.0	4.3	3.0	2.3
	12040	18.0	10.9	6.8	4.2	3.1	2.0	1.6
	8144	13.0	7.8	4.9	3.2	1.9	1.7	1.2
6	17312	21.6	17.7	8.4	5.7	4.0	3.1	2.4
	12008	15.4	13.2	5.7	3.9	2.8	2.2	1.7
	8080	10.7	9.7	3.0	2.7	2.0	1.5	1.1
7	17344	21.9	14.8	9.4	5.9	3.8	3.2	2.5
	12048	15.7	10.5	6.7	4.2	2.8	2.3	1.9
	8148	10.9	7.2	4.5	2.8	1.8	1.5	1.2
8	17296	20.3	14.3	9.6	6.1	4.1	3.4	2.6
	12032	14.3	10.1	6.8	4.4	3.0	2.5	1.8
	8160	9.8	7.0	4.8	3.1	2.1	1.8	1.3
9	17336	19.5	13.4	9.1	6.0	4.4	3.1	2.5
	11984	13.8	9.4	6.4	4.3	3.1	2.2	1.8
	8104	9.4	6.4	4.3	2.9	2.1	1.5	1.2
10	17184	19.6	14.3	10.1	5.9	4.5	3.6	2.8
	11856	13.9	10.2	7.3	4.2	3.3	2.6	2.0
	8032	9.6	7.1	5.1	2.9	2.2	1.8	1.4

Table G.7--continued

Station No.	Applied Load (lbs.)	Measured Deflections (mils)						
		D_1 (a)	D_2	D_3	D_4	D_5	D_6	D_7
		0 (b)	12	24	36	48	60	72
11	17160	21.9	14.9	9.7	6.1	4.3	3.4	2.8
	11856	15.4	10.5	6.9	4.4	3.1	2.5	2.0
	7968	10.6	7.2	4.8	3.1	2.2	1.7	1.4
1 (OWP)	17312	18.6	13.1	7.8	6.0	4.3	3.6	2.5
	11904	12.9	8.9	5.6	4.0	3.2	2.4	1.7
	8056	8.6	6.3	3.6	3.1	2.0	1.9	1.2
2 (OWP)	17376	23.0	15.1	6.8	5.0	3.7	2.9	2.1
	11944	15.9	10.7	4.8	3.6	2.7	2.1	1.5
	8072	10.8	7.4	3.3	2.5	1.9	1.4	1.0

(a) Sensor No. (b) Radial Distance in Inches From Center of FWD Load

Table G.8 Results of FWD Tests on Site 1 (Test 8)

Temperature (F): Air = 78 Pvm. Surf. = 88

Station No.	Applied Load (lbs.)	Measured Deflections (mils)						
		D ₁ (a)	D ₂	D ₃	D ₄	D ₅	D ₆	D ₇
		0 (b)	12	24	36	48	60	72
1	17192	24.6	13.9	8.6	5.6	4.1	3.2	2.4
	11880	17.4	9.8	6.0	4.0	2.9	2.3	1.7
	7976	11.7	6.5	4.0	2.7	2.0	1.5	1.1
2	17280	20.8	13.3	8.9	6.0	4.3	3.2	2.5
	11968	14.6	9.5	6.4	4.3	3.1	2.4	1.8
	8064	9.8	6.5	4.4	3.0	2.2	1.7	1.3
3	17144	21.0	13.8	9.3	5.4	4.0	3.1	2.5
	11808	14.7	9.8	6.8	3.8	2.9	2.3	1.8
	8024	9.8	6.6	4.6	2.6	2.0	1.5	1.1
4	17176	21.4	13.8	8.8	5.8	3.8	3.1	2.4
	11896	15.0	9.7	6.4	4.2	2.8	2.2	1.8
	8024	9.9	6.5	4.2	2.7	1.8	1.3	1.1
5	17216	23.2	14.4	9.2	5.9	4.0	3.5	2.8
	11904	16.5	10.1	6.4	4.2	3.0	2.5	1.8
	8008	11.2	7.1	4.7	3.0	1.9	1.7	1.4
6	17232	21.2	14.6	8.2	5.8	3.9	3.3	2.5
	11904	14.7	10.4	5.7	4.1	2.9	2.3	1.8
	7976	9.8	7.1	3.8	2.7	1.9	1.5	1.2
7	17200	21.7	14.1	9.2	5.9	3.6	3.2	2.5
	11920	15.3	10.0	6.4	4.2	2.6	2.2	1.7
	9784	10.3	6.8	4.3	2.9	1.8	1.5	1.1
8	17144	20.8	13.9	9.2	5.9	3.9	3.2	2.6
	11856	14.5	9.8	6.5	4.3	2.8	2.3	1.9
	7968	9.6	6.6	4.4	2.9	1.9	1.5	1.2
9	17168	19.9	13.1	8.8	5.9	4.1	3.0	2.5
	11864	13.9	9.2	6.1	4.2	3.0	2.2	1.8
	8016	9.3	6.2	4.2	2.9	2.0	1.6	1.3
10	17216	20.2	13.6	9.3	5.8	4.4	3.7	2.9
	11816	13.9	9.5	6.5	4.1	3.1	2.4	1.9
	7928	9.2	6.3	4.4	2.7	2.0	1.6	1.3

Table G.8--continued

Station No.	Applied Load (lbs.)	Measured Deflections (mils)						
		D_1 (a)	D_2	D_3	D_4	D_5	D_6	D_7
		0 (b)	12	24	36	48	60	72
11	17160	21.9	14.4	9.6	6.1	4.4	3.4	2.2
	11872	15.2	10.1	6.6	4.3	3.1	2.4	1.9
	7880	10.1	6.8	4.5	3.0	2.1	1.7	1.3
1 (OWP)	17360	19.2	12.8	7.8	5.6	4.1	3.1	2.4
	11896	13.2	8.9	5.5	3.9	2.9	2.1	1.6
	7872	8.7	5.8	3.7	2.7	2.0	1.6	1.2
2 (OWP)	17224	23.7	14.6	7.0	5.0	3.7	2.9	2.3
	11896	16.4	10.3	5.0	3.6	2.7	2.1	1.6
	7888	10.8	7.0	3.4	2.5	1.8	1.4	1.1

(a) Sensor No. (b) Radial Distance in Inches From Center of FWD Load

Table G.9 Results of FWD Tests on Site 2 (Test 1)

Temperature (F): Air = 60 Pvmt. Surf. = 55

Station No.	Applied Load (lbs.)	Measured Deflections (mils)						
		D ₁ (a)	D ₂	D ₃	D ₄	D ₅	D ₆	D ₇
		0(b)	12	24	36	48	60	72
1	17528	30.7	24.4	18.2	13.1	9.6	7.0	4.8
	17616	30.5	24.4	18.1	13.1	9.5	7.1	4.9
	17600	28.5	23.8	18.0	13.0	9.4	6.6	4.7
2	17552	34.0	26.6	18.4	12.1	8.5	6.3	4.8
	17576	29.9	25.0	17.5	11.8	8.4	6.4	5.0
	17560	29.0	24.5	17.4	12.1	8.7	6.0	4.9
3	17480	34.1	27.4	18.7	12.6	8.6	5.7	4.6
	17504	32.2	25.7	17.7	12.2	8.8	5.9	4.9
	17600	29.5	25.3	17.4	12.1	8.7	6.0	4.9
4	17440	33.8	27.0	18.7	13.1	9.3	6.9	5.3
	17560	32.4	25.3	17.8	12.4	9.0	6.8	5.2
	17520	29.9	24.9	17.6	12.4	9.1	6.9	5.3
5	17584	31.3	25.0	17.5	12.2	9.0	6.9	5.4
	17552	31.5	24.6	17.4	12.2	8.9	6.8	5.4
	17576	30.1	24.1	17.1	12.0	8.8	6.8	5.3
6	17368	35.4	27.4	18.7	12.3	7.6	6.1	4.8
	17496	33.8	25.5	17.6	12.1	7.8	6.3	5.0
	17480	30.9	25.0	17.4	12.1	7.8	6.3	5.1
7	17440	35.1	26.8	18.7	12.7	9.0	6.7	5.1
	17456	33.4	24.7	17.5	12.3	8.8	6.6	5.1
	17440	29.1	24.4	17.2	12.1	8.0	6.7	5.2
8	17384	35.6	27.7	19.1	12.9	9.4	7.0	5.4
	17488	32.3	25.7	18.0	12.6	9.2	7.0	5.6
	17456	31.5	25.2	17.7	12.4	9.2	6.9	5.5
9	17344	40.2	28.4	20.4	14.4	10.2	7.5	5.5
	17400	35.2	28.1	20.2	14.3	10.2	7.5	5.6
	17416	41.0	27.8	20.1	14.2	10.1	7.4	5.5
10	17200	37.7	28.1	18.8	12.5	8.8	6.5	4.7
	17320	35.9	26.2	17.8	12.2	8.8	6.7	5.1
	17400	32.8	25.9	17.8	12.2	8.9	6.7	5.1

Table G.9--continued

Station No.	Applied Load (lbs.)	Measured Deflections (mils)						
		D_1 (a)	D_2	D_3	D_4	D_5	D_6	D_7
		0 (b)	12	24	36	48	60	72
11	17592	23.9	20.6	16.0	11.6	8.4	6.3	5.1
	17664	23.2	19.8	15.4	11.3	8.4	6.4	5.3
	17656	20.9	19.5	15.4	11.0	8.3	6.3	5.3
1 (OWP)	17856	21.0	18.2	14.5	10.6	8.0	6.1	4.6
	17880	20.2	17.3	13.6	10.1	7.7	5.9	4.5
	17816	20.1	17.0	13.6	10.1	7.6	5.9	4.5
2 (OWP)	17400	35.6	26.7	18.7	13.3	9.4	6.8	5.2
	17456	34.5	25.2	17.8	12.8	9.2	6.9	5.4
	17432	34.8	24.7	17.6	12.6	9.0	6.7	5.3

(a) Sensor No. (b) Radial Distance in Inches From Center of FWD Load

Table G.10 Results of FWD Tests on Site 2 (Test 2)

Temperature (F): Air = 31 Pvm. Surf. = 28

Station No.	Applied Load (lbs.)	Measured Deflections (mils)						
		D_1 (a)	D_2	D_3	D_4	D_5	D_6	D_7
		0 (b)	12	24	36	48	60	72
1	17888	28.6	23.7	18.6	14.4	11.6	10.0	4.0
	17896	28.5	23.7	18.6	14.5	11.8	10.2	4.0
	17848	28.5	23.6	18.6	14.5	11.8	10.2	4.0
2	17784	30.9	24.1	17.3	12.1	8.6	6.5	4.8
	17840	30.5	23.7	17.1	12.0	8.6	6.4	4.9
	17776	26.0	23.5	17.0	11.8	8.6	6.4	4.9
3	17752	29.9	25.5	19.5	15.4	13.0	4.0	3.5
	17792	29.2	24.7	19.0	15.3	12.9	4.0	3.4
	17816	27.6	24.4	18.7	15.0	12.8	3.9	3.4
4	17776	29.2	23.6	17.5	12.7	9.4	6.9	5.1
	17856	28.7	23.2	17.3	12.7	9.4	7.1	5.4
	17832	28.6	23.2	17.2	12.7	9.4	7.1	5.4
5	17656	29.3	24.0	17.6	12.5	9.1	7.0	5.4
	17656	28.2	23.1	16.8	12.1	8.9	6.9	5.4
	17656	28.1	23.0	16.8	12.2	9.0	7.0	5.5
6	17496	34.4	30.0	25.1	22.2	5.0	4.2	3.7
	17672	33.0	28.3	23.6	20.8	5.2	4.4	4.0
	17680	32.8	28.1	23.3	20.6	5.3	4.6	4.0
7	17680	30.4	23.9	17.4	12.4	9.2	6.9	5.2
	17792	29.3	22.9	16.8	12.2	9.2	7.0	5.5
	17736	24.9	22.8	16.8	12.2	9.2	7.1	5.6
8	17600	33.2	27.9	21.3	16.4	13.2	10.5	8.3
	17744	31.9	26.7	20.4	15.9	12.7	10.2	8.6
	17768	31.6	26.4	20.2	15.8	12.6	10.1	8.1
9	17336	51.2	40.5	30.8	22.5	16.4	12.0	8.8
	17408	41.9	37.9	29.0	21.4	15.6	11.6	8.8
	17408	39.7	37.1	28.6	21.1	15.4	11.4	8.7
10	17472	36.9	29.4	21.4	15.7	11.1	7.7	5.1
	17600	35.9	28.2	20.9	15.2	10.9	7.8	5.3
	17520	33.1	27.9	20.7	15.0	10.8	7.7	5.3

Table G.10--continued

Station No.	Applied Load (lbs.)	Measured Deflections (mils)						
		D ₁ (a)	D ₂	D ₃	D ₄	D ₅	D ₆	D ₇
		0 (b)	12	24	36	48	60	72
11	17752	21.3	18.2	14.3	10.9	8.2	6.6	6.2
	17840	20.6	17.4	14.0	10.7	8.3	6.9	6.6
	17800	20.5	17.4	13.8	10.7	8.2	6.8	6.6
1 (OWP)	18056	15.7	13.6	11.0	8.6	6.8	5.5	4.3
	18128	15.6	13.6	10.9	8.6	6.8	5.4	4.4
	18176	15.6	13.6	10.9	8.6	6.8	5.5	4.4
2 (OWP)	17880	20.8	20.6	12.6	9.7	7.6	5.8	4.5
	18016	19.6	16.1	12.3	9.6	7.4	5.9	4.7
	18024	19.5	16.0	12.3	9.6	7.5	5.9	4.7

(a) Sensor No. (b) Radial Distance in Inches From Center of FWD Load

Table G.11 Results of FWD Tests on Site 2 (Test 3)

Temperature (F): Air = 54 Pvmt. Surf. = 53

Station No.	Applied Load (lbs.)	Measured Deflections (mils)						
		D ₁ (a)	D ₂	D ₃	D ₄	D ₅	D ₆	D ₇
		0(b)	12	24	36	48	60	72
1	27592	44.0	35.8	26.7	19.5	14.4	11.0	6.5
	17944	31.1	24.9	18.7	13.8	10.4	8.0	4.8
	9688	16.5	13.2	19.6	7.2	5.4	4.4	2.7
2	26984	46.7	38.5	25.0	16.7	11.8	8.9	6.8
	17320	33.0	25.2	17.6	12.0	8.5	6.4	5.0
	9472	17.6	13.3	9.4	6.3	4.6	3.6	2.8
3	27072	55.4	36.8	25.5	18.4	14.1	7.4	6.2
	17624	31.5	25.3	17.8	13.2	10.2	5.7	4.8
	9464	16.6	13.3	9.4	7.0	5.4	3.2	2.6
4	26752	43.5	35.1	25.2	18.2	13.0	9.9	7.8
	17424	31.0	23.7	17.5	12.7	9.3	7.0	5.4
	9392	16.4	12.4	9.3	6.8	4.9	3.8	3.1
5	26928	44.8	36.0	25.0	17.4	12.7	9.8	7.6
	17528	31.2	24.7	17.4	12.2	9.0	7.0	5.5
	9344	16.7	13.0	9.2	6.5	4.9	3.8	3.0
6	26536	51.1	37.9	26.3	19.2	10.2	8.4	6.8
	17176	33.7	26.0	18.6	14.0	17.5	16.3	5.1
	9240	18.1	14.0	10.1	7.7	4.3	3.6	2.9
7	26376	47.3	35.8	25.0	17.6	12.5	9.6	7.3
	17176	32.1	24.4	17.2	12.2	8.9	6.9	5.4
	9192	16.8	12.8	8.9	6.4	4.7	3.7	2.9
8	26296	53.3	38.0	26.1	20.0	14.2	11.0	7.9
	17184	33.8	25.9	18.1	13.8	9.9	7.7	5.6
	9184	17.9	14.1	9.4	7.4	5.3	4.2	3.1
9	26416	50.7	39.3	29.5	22.1	16.6	12.9	9.8
	17232	35.9	27.6	21.0	16.0	12.3	9.5	7.3
	9152	20.1	15.4	11.7	9.2	7.3	5.6	4.4
10	25936	51.6	38.6	26.6	18.7	13.5	10.0	7.2
	16880	36.3	26.6	18.9	13.1	9.7	7.2	5.2
	8952	20.2	14.8	10.5	7.3	5.4	4.1	3.0

Table G.11--continued

Station No.	Applied Load (lbs.)	Measured Deflections (mils)						
		D ₁ (a)	D ₂	D ₃	D ₄	D ₅	D ₆	D ₇
		0 (b)	12	24	36	48	60	72
11	26648	33.3	28.4	22.2	16.3	12.2	9.7	8.1
	17368	22.9	19.5	15.2	11.2	8.7	7.0	5.8
	9264	12.0	10.4	7.9	6.0	4.7	3.9	3.3
1 (OWP)	26328	29.2	24.5	18.9	14.2	11.0	8.6	6.5
	17536	19.9	16.6	13.0	9.8	7.6	5.9	4.6
	9224	10.3	8.8	6.8	5.2	4.0	3.2	2.5
2 (OWP)	25544	57.4	35.7	25.6	18.3	12.9	9.8	7.8
	17104	38.4	25.0	18.3	12.7	9.2	7.0	5.5
	8848	21.2	13.6	9.7	6.8	4.9	3.8	3.0

(a) Sensor No. (b) Radial Distance in Inches From Center of FWD Load

Table G.12 Results of FWD Tests on Site 2 (Test 4)

Temperature (F): Air = 69 Pvmnt. Surf. = 73

Station No.	Applied Load (lbs.)	Measured Deflections (mils)						
		D_1 (a)	D_2	D_3	D_4	D_5	D_6	D_7
		D_0 (b)	12	24	36	48	60	72
1	25320	42.2	33.1	24.8	17.9	13.1	9.6	6.8
	16968	29.0	22.8	17.0	12.4	9.1	6.7	4.8
	8640	14.7	11.6	8.6	6.2	4.7	3.5	2.6
2	24920	42.9	33.1	23.3	16.1	11.6	8.9	7.1
	16936	29.4	22.6	16.0	11.2	8.1	6.1	5.0
	8648	15.2	11.6	8.2	5.8	4.3	3.3	2.7
3	24936	43.3	33.4	23.3	16.4	11.9	8.3	6.8
	16896	29.5	22.8	15.9	11.4	8.3	5.9	4.9
	8504	15.0	11.6	8.0	5.8	4.4	3.2	2.6
4	25096	42.5	32.9	23.2	16.7	12.2	9.3	7.3
	16912	29.4	22.5	15.9	11.4	8.4	6.5	5.1
	8512	15.1	11.5	8.0	5.8	4.4	3.4	2.7
5	24952	42.4	33.4	23.4	16.6	12.2	9.2	7.2
	16800	29.1	22.8	16.0	11.4	8.4	6.5	5.1
	8464	14.8	11.6	8.0	5.8	4.3	3.4	2.7
6	24986	45.1	33.4	23.4	16.3	11.2	8.7	6.9
	16832	30.6	22.8	15.9	11.4	7.9	6.2	5.0
	8456	15.6	11.5	8.0	5.9	4.1	3.3	2.6
7	24904	43.3	32.8	23.5	16.8	12.4	9.4	7.4
	16792	29.6	22.4	16.0	11.6	8.6	6.7	5.3
	8448	15.1	11.3	8.1	5.9	4.5	3.5	2.8
8	24976	44.0	33.2	23.6	17.8	12.9	10.0	7.7
	16816	30.1	22.7	16.3	12.2	9.1	7.0	5.5
	8504	15.5	11.6	8.3	6.2	4.8	3.7	3.0
9	25304	49.0	32.4	23.6	17.3	13.2	9.4	7.4
	16992	29.6	22.2	16.2	12.0	9.1	6.8	5.3
	8592	15.4	11.6	8.5	6.3	4.8	3.7	2.9
10	24792	45.7	32.8	22.4	16.3	12.3	9.3	7.0
	16728	31.6	22.4	15.5	11.2	8.7	6.5	4.8
	8456	16.4	11.4	7.9	5.7	4.5	3.5	2.6

Table G.12--continued

Station No.	Applied Load (lbs.)	Measured Deflections (mils)						
		D ₁ (a)	D ₂	D ₃	D ₄	D ₅	D ₆	D ₇
		0 (b)	12	24	36	48	60	72
11	25360	32.6	26.7	20.7	15.8	11.9	9.2	7.2
	16944	22.3	18.4	14.2	10.9	8.3	6.4	5.1
	8656	11.2	9.4	7.2	5.5	4.3	3.3	2.6
1 (OWP)	25152	29.9	24.3	18.4	13.8	10.6	8.2	6.4
	17040	20.1	16.4	12.4	9.4	7.3	5.7	4.5
	8488	9.9	8.2	6.2	4.8	3.8	2.9	2.3
2 (OWP)	24664	42.7	31.6	22.7	16.8	12.5	9.3	7.2
	16784	29.0	21.7	15.5	11.5	8.7	6.6	5.2
	8400	14.6	11.2	8.0	5.9	4.5	3.5	2.7

(a) Sensor No. (b) Radial Distance in Inches From Center of FWD Load

Table G.13 Results of FWD Tests on Site 2 (Test 5)

Temperature (F): Air = 71 Pvm. Surf. = 75

Station No.	Applied Load (lbs.)	Measured Deflections (mils)						
		D ₁ (a)	D ₂	D ₃	D ₄	D ₅	D ₆	D ₇
		0(b)	12	24	36	48	60	72
1	25984	43.3	33.0	24.4	17.7	12.7	9.6	6.8
	12136	20.8	15.9	11.8	8.6	6.3	4.6	3.5
	8368	13.9	10.5	7.9	5.8	4.3	3.2	2.5
2	25984	42.5	32.5	23.4	16.1	11.6	8.9	7.5
	12080	20.6	15.6	11.2	7.9	5.9	4.5	3.6
	8280	13.9	10.4	7.5	5.5	4.0	3.1	2.5
3	26024	42.6	32.8	23.6	26.6	12.1	8.2	6.8
	12024	20.5	15.8	11.1	8.1	6.0	4.3	3.5
	8256	13.8	10.5	7.4	5.5	4.2	3.0	2.4
4	25840	59.0	31.9	23.4	16.8	12.4	9.2	7.2
	11920	20.4	15.4	11.2	8.2	6.1	4.7	3.7
	8296	13.7	10.2	7.8	5.9	4.3	3.2	2.8
5	25744	45.4	33.2	23.5	16.6	12.0	9.1	7.1
	11752	21.6	15.8	11.2	8.1	5.9	4.6	3.7
	8184	14.6	10.5	7.6	5.5	4.1	3.2	2.6
6	25856	44.3	33.1	23.1	15.7	11.2	8.8	6.9
	11904	21.3	15.6	11.2	7.9	5.8	4.5	3.6
	8240	14.3	10.4	7.6	5.5	4.0	3.2	2.6
7	25808	42.9	32.0	23.5	16.9	12.8	9.6	7.4
	11880	20.6	15.6	11.2	7.9	5.9	4.8	3.7
	8144	13.9	10.0	7.7	5.9	4.5	3.2	2.6
8	25744	44.1	32.4	23.5	17.4	13.2	11.0	8.3
	11920	21.1	15.5	11.3	8.4	6.5	5.2	4.1
	8128	14.3	10.6	7.7	5.8	4.5	3.6	2.9
9	25584	47.8	34.2	24.8	18.3	13.3	10.0	7.7
	11848	24.3	16.8	12.5	9.2	6.8	5.1	4.0
	8184	17.1	11.6	8.6	6.4	4.6	3.6	2.8
10	25720	45.6	32.1	22.7	16.4	12.3	9.4	6.8
	11808	22.2	15.5	11.0	7.9	6.0	4.6	3.5
	8024	15.1	10.4	7.4	5.6	4.2	3.2	2.4

Table G.13--continued

Station No.	Applied Load (lbs.)	Measured Deflections (mils)						
		D ₁ (a)	D ₂	D ₃	D ₄	D ₅	D ₆	D ₇
		0 (b)	12	24	36	48	60	72
11	26248	34.0	27.0	21.2	15.9	11.8	9.4	7.1
	11984	16.2	13.1	10.2	7.8	6.0	4.6	3.5
	8264	10.9	8.8	6.9	5.2	4.1	3.2	2.5
1 (OWP)	26344	29.5	23.1	17.2	12.9	10.1	8.2	6.3
	12080	13.5	10.8	8.2	6.3	4.9	4.0	3.1
	8112	9.0	7.1	5.3	4.2	3.4	2.7	2.1
2 (OWP)	25616	47.7	30.7	22.3	16.2	11.9	9.6	7.3
	11968	23.1	15.0	10.9	8.0	6.1	4.6	3.7
	7936	15.9	10.1	7.4	5.5	4.1	3.2	2.5

(a) Sensor No. (b) Radial Distance in Inches From Center of FWD Load

Table G.14 Results of FWD Tests on Site 2 (Test 6)

Temperature (F): Air = 91 Pvm. Surf. = 118

Station No.	Applied Load (lbs.)	Measured Deflections (mils)						
		D ₁ (a)	D ₂	D ₃	D ₄	D ₅	D ₆	D ₇
		0(b)	12	24	36	48	60	72
1	25648	47.9	35.2	25.2	17.7	12.7	9.5	7.2
	11648	22.7	16.7	12.2	8.6	6.3	4.7	3.7
	8016	15.1	11.2	8.1	5.8	4.3	3.2	2.5
2	25744	45.8	33.6	23.9	16.7	11.9	9.1	6.9
	11616	21.6	15.9	11.4	8.0	5.9	4.5	3.5
	8024	14.6	10.8	7.8	5.5	4.0	3.0	2.4
3	25800	46.3	33.5	23.6	16.4	11.5	8.8	7.4
	11680	21.8	15.8	11.2	8.0	5.8	4.4	3.6
	8008	14.7	10.6	7.6	5.3	4.1	2.9	2.3
4	25776	46.3	34.2	24.2	16.8	12.0	10.1	8.1
	11672	21.9	16.3	11.7	8.3	6.1	4.7	3.6
	8056	14.8	11.0	7.9	5.6	4.2	3.1	2.5
5	25704	47.7	34.6	24.4	16.6	12.1	9.5	7.9
	11632	22.5	16.6	11.8	8.1	6.0	4.6	3.5
	8040	15.4	11.0	7.0	5.6	4.1	3.1	2.7
6	25760	48.7	34.0	23.5	15.9	11.4	8.8	7.1
	11736	23.0	16.2	11.4	8.0	5.9	4.5	3.5
	8016	15.6	11.0	7.8	5.5	4.0	3.1	2.5
7	25736	45.6	33.1	23.8	16.9	12.7	9.6	7.5
	11616	21.7	15.7	11.6	7.9	5.8	4.7	3.7
	7984	14.7	10.8	7.6	6.1	4.6	3.1	2.3
8	25872	47.7	34.0	24.0	16.5	12.4	10.5	7.5
	11680	22.5	16.2	11.6	8.4	6.3	4.9	3.7
	7992	15.1	10.9	7.8	5.7	4.3	3.4	2.5
9	25624	48.4	34.1	24.1	16.7	12.4	9.7	7.2
	11776	23.2	16.1	11.6	8.5	6.3	4.7	3.7
	8024	15.6	10.6	7.8	5.9	4.2	3.3	2.7
10	25552	49.9	33.7	23.4	16.5	12.4	9.4	7.2
	11584	24.0	16.2	11.3	8.0	6.0	4.6	3.6
	7928	16.4	11.0	7.7	5.4	4.1	3.2	2.5

Table G.14--continued

Station No.	Applied Load (lbs.)	Measured Deflections (mils)						
		D ₁ (a)	D ₂	D ₃	D ₄	D ₅	D ₆	D ₇
		0 (b)	12	24	36	48	60	72
11	26336	39.5	30.6	22.6	16.6	12.4	9.6	7.3
	11840	18.5	14.3	10.8	8.0	6.1	4.6	3.6
	8234	12.6	9.7	7.4	5.4	4.1	3.2	2.6
1 (OWP)	26168	39.5	26.9	19.3	13.5	10.2	8.4	6.0
	11608	17.7	12.5	9.0	6.6	4.9	3.8	3.0
	8000	11.9	8.2	6.0	4.5	3.4	2.8	2.1
2 (OWP)	25448	56.4	31.7	22.5	15.8	11.8	9.3	7.1
	11536	26.0	14.8	10.6	7.6	5.8	4.5	3.5
	7712	17.2	9.7	7.2	5.2	4.0	3.0	2.3

(a) Sensor No. (b) Radial Distance in Inches From Center of FWD Load

Table G.15 Results of FWD Tests on Site 2 (Test 7)

Temperature (F): Air = 82 Pvm. Surf. = 86

Station No.	Applied Load (lbs.)	Measured Deflections (mils)						
		D ₁ (a)	D ₂	D ₃	D ₄	D ₅	D ₆	D ₇
		0 (b)	12	24	36	48	60	72
1	17200	29.0	22.1	16.4	12.0	8.7	6.4	4.8
	11840	20.3	15.5	11.5	8.4	6.2	4.6	3.5
	7960	13.5	10.4	7.8	5.6	4.2	3.1	2.4
2	17104	28.8	22.0	15.8	11.0	8.1	6.3	5.0
	11760	20.1	15.3	11.0	7.7	5.8	4.4	3.5
	7912	13.4	10.4	7.5	5.2	3.7	3.2	2.5
3	17128	29.6	22.5	15.7	11.3	8.2	5.9	4.8
	11760	20.6	15.6	10.9	7.8	5.7	4.2	3.4
	7856	13.6	10.4	7.3	5.3	3.9	2.9	2.4
4	17216	29.5	22.3	15.8	11.2	8.2	6.4	5.0
	11784	20.5	15.4	11.0	7.8	5.7	4.5	3.5
	8048	13.7	10.3	7.2	5.2	3.8	3.0	2.3
5	17032	29.5	22.5	16.0	11.2	7.9	6.3	5.0
	11624	20.5	15.5	10.6	7.7	5.9	4.6	3.6
	7856	13.6	10.5	7.8	5.4	3.6	3.0	2.4
6	17048	30.5	22.1	15.6	10.9	7.8	6.2	4.8
	11816	21.3	15.4	11.0	7.8	5.5	4.5	3.5
	7904	14.3	10.2	7.2	5.2	3.7	2.9	2.3
7	17088	30.0	22.1	16.0	11.7	8.1	6.8	5.1
	11792	21.0	15.6	11.6	7.8	6.2	4.4	3.3
	7936	14.2	10.3	7.4	5.6	3.7	3.3	2.6
8	17000	30.4	22.0	16.3	11.2	9.1	7.1	5.6
	11760	21.3	15.3	11.4	7.7	6.4	5.0	3.8
	7880	14.3	10.6	7.7	5.7	4.3	3.4	2.9
9	15920	33.6	23.5	17.3	12.6	9.2	7.0	5.4
	11632	23.7	16.4	12.1	8.6	6.4	4.9	3.8
	7896	16.4	11.5	8.4	6.2	4.5	3.4	2.6
10	16896	32.4	22.5	15.8	11.3	8.5	6.4	5.0
	11760	22.8	15.8	11.0	7.9	6.1	4.6	3.5
	7856	15.3	10.6	7.4	5.4	4.1	3.2	2.5

Table G.15--continued

Station No.	Applied Load (lbs.)	Measured Deflections (mils)						
		D ₁ (a)	D ₂	D ₃	D ₄	D ₅	D ₆	D ₇
		0 (b)	12	24	36	48	60	72
11	17232	23.2	19.2	15.0	11.2	8.4	6.5	4.9
	11880	16.2	13.4	10.4	7.7	5.9	4.5	3.4
	8104	11.0	9.1	7.1	5.3	4.1	3.1	2.5
1 (OWP)	17464	20.0	15.6	11.9	9.0	7.0	5.8	4.2
	11920	13.9	10.8	8.2	6.4	5.1	4.1	3.1
	7960	9.3	7.2	5.6	4.2	3.2	2.8	1.9
2 (OWP)	17360	29.9	20.9	15.4	11.0	8.1	6.6	4.8
	12032	21.0	14.7	10.8	7.8	5.7	4.6	3.4
	7920	14.2	10.1	7.4	5.4	4.1	3.2	2.5

(a) Sensor No. (b) Radial Distance in Inches From Center of FWD Load

Table G.16 Results of FWD Tests on Site 2 (Test 8)

Temperature (F): Air = 80 Pvm. Surf. = 88

Station No.	Applied Load (lbs.)	Measured Deflections (mils)						
		D ₁ (a)	D ₂	D ₃	D ₄	D ₅	D ₆	D ₇
		0 (b)	12	24	36	48	60	72
1	17200	29.9	21.8	15.9	11.4	8.4	6.4	5.1
	11776	20.6	15.0	11.1	8.1	6.0	4.5	3.5
	8040	13.8	10.1	7.5	5.5	4.1	3.1	2.5
2	17288	28.1	21.2	15.6	11.1	7.9	6.3	4.6
	11864	19.5	14.6	11.0	7.6	5.5	4.1	3.3
	8048	13.0	9.9	7.2	5.3	3.8	3.2	2.2
3	17200	29.1	21.5	15.5	11.1	8.1	6.2	4.8
	11856	20.3	14.8	10.7	7.9	5.8	4.4	3.4
	8040	13.5	9.9	7.2	5.3	3.9	3.0	2.3
4	17128	29.3	21.9	16.0	11.4	8.5	6.8	5.1
	11752	20.2	15.2	11.1	8.0	6.1	4.8	3.6
	8008	13.4	10.2	7.4	5.4	4.1	3.2	2.5
5	17176	30.1	22.0	15.8	11.1	8.4	6.6	5.1
	11768	21.0	15.2	11.1	7.8	6.0	4.6	3.5
	7976	14.1	10.2	7.4	5.2	4.0	3.2	2.5
6	17168	29.5	21.2	15.4	11.0	8.1	6.3	5.0
	11808	20.4	14.7	10.8	7.8	5.8	4.6	3.6
	7992	13.5	9.7	7.2	5.2	3.9	3.0	2.5
7	17152	28.9	21.0	15.7	11.4	8.5	6.6	5.0
	11728	20.0	14.6	10.8	8.0	6.0	4.7	3.6
	7992	13.4	9.8	7.4	5.4	4.1	3.2	2.5
8	17168	29.8	21.6	16.0	12.1	9.5	7.7	5.5
	11776	21.0	15.2	10.9	8.1	6.4	5.1	3.8
	8048	13.7	9.9	7.6	5.9	4.6	3.6	2.6
9	17107	30.0	21.4	15.7	11.8	9.0	7.2	5.3
	11864	21.0	15.0	11.0	8.4	6.4	4.9	3.8
	8024	13.9	9.9	7.2	5.6	4.4	3.2	2.5
10	17080	31.3	21.3	15.0	10.9	8.4	6.5	4.9
	11760	21.9	14.9	10.6	7.7	6.0	4.7	3.6
	7976	14.6	9.9	7.0	5.2	4.0	3.1	2.4

Table G.16--continued

Station No.	Applied Load (lbs.)	Measured Deflections (mils)						
		D_1 (a)	D_2	D_3	D_4	D_5	D_6	D_7
		0 (b)	12	24	36	48	60	72
11	17248	24.2	19.0	14.6	10.9	8.4	6.3	4.8
	11856	16.8	13.3	10.2	7.6	5.9	4.5	3.4
	8224	11.3	9.0	7.0	5.3	4.1	3.2	2.5
1 (OWP)	17512	21.6	16.1	12.0	8.8	6.9	5.5	4.2
	12016	14.9	11.2	8.4	6.1	4.8	3.7	3.0
	8088	10.0	7.6	5.7	4.3	3.3	2.7	2.0
2 (OWP)	17328	30.6	20.4	14.9	10.9	8.1	6.3	4.8
	11976	21.4	14.3	10.6	7.7	5.7	4.5	3.4
	7976	14.3	9.7	7.2	5.3	4.0	3.1	2.5

(a) Sensor No. (b) Radial Distance in Inches From Center of FWD Load

Table G.17 Results of FWD Tests on Site 3 (Test 1)

Temperature (F): Air = 60 Pvmt. Surf. = 55

Station No.	Applied Load (lbs.)	Measured Deflections (mils)						
		D ₁ (a)	D ₂	D ₃	D ₄	D ₅	D ₆	D ₇
		0(b)	12	24	36	48	60	72
1	17512	28.4	24.1	17.9	12.9	9.2	6.8	5.2
	17576	27.8	23.0	17.2	12.5	9.0	6.8	5.3
	17648	25.3	22.9	17.0	12.4	9.0	6.8	5.4
2	17456	26.6	21.9	16.0	11.5	8.	6.5	5.1
	17416	26.6	21.5	15.7	11.2	8.2	6.4	4.8
	17424	27.1	21.4	15.6	11.4	8.2	6.1	5.0
3	17400	27.9	22.9	16.2	11.5	8.2	6.2	4.8
	17464	27.1	21.9	15.6	11.1	8.1	6.2	4.9
	17424	27.5	21.6	15.5	11.0	8.1	6.2	5.0
4	17344	30.1	24.4	17.3	12.2	9.0	6.8	5.3
	17440	28.8	22.8	16.5	11.8	8.8	6.7	5.3
	17384	29.9	22.5	16.2	11.7	8.7	6.5	5.3
5	17376	28.5	23.5	17.3	12.4	9.0	6.5	5.1
	17416	27.7	22.2	16.4	11.9	8.7	6.4	5.1
	17392	24.9	21.8	16.2	11.8	8.7	6.5	5.3
6	17320	29.2	23.7	17.4	12.4	9.1	7.0	5.5
	17360	29.0	23.0	17.0	12.0	8.8	6.8	5.3
	17376	31.3	22.8	16.8	12.0	8.9	6.8	5.3
7	17320	34.2	31.2	12.9	9.7	7.3	5.5	4.4
	17424	31.6	28.3	12.5	9.6	7.4	5.8	4.7
	17368	32.0	27.5	12.5	9.7	7.3	5.6	4.7
8	17264	29.7	22.8	15.5	10.5	7.5	5.7	4.4
	17384	28.6	21.5	14.9	10.6	7.7	5.9	4.8
	17304	27.8	21.1	14.8	10.4	7.7	6.0	4.8
9	17400	25.4	20.7	15.2	10.7	7.8	6.0	4.6
	17472	29.3	20.0	14.7	10.4	7.7	6.1	4.7
	17376	22.8	19.7	14.6	10.2	7.5	5.9	4.7
10	17464	31.0	24.5	17.2	12.0	8.5	6.4	5.1
	17472	29.0	22.8	15.9	11.2	8.1	6.2	4.9
	17472	25.8	22.3	15.6	11.2	8.1	6.1	5.0

Table G.17--continued

Station No.	Applied Load (lbs.)	Measured Deflections (mils)						
		D ₁ (a)	D ₂	D ₃	D ₄	D ₅	D ₆	D ₇
		0 (b)	12	24	36	48	60	72
11	17496	25.6	21.3	15.3	10.9	8.1	6.3	4.9
	17512	24.8	20.1	14.8	10.6	7.9	6.2	4.8
	17472	23.0	19.7	14.8	10.6	7.8	6.1	4.8
1 (OWP)	17376	23.9	20.5	15.4	10.8	7.9	6.1	4.8
	17512	23.1	19.4	14.8	10.6	7.9	6.1	4.9
	17536	21.4	18.9	14.8	10.6	7.7	6.1	4.9
2 (OWP)	17416	25.7	20.2	14.8	10.9	8.3	6.4	5.1
	17480	25.8	20.0	14.8	10.9	8.3	6.3	5.0
	17456	24.1	19.9	14.8	10.9	8.3	6.3	4.9

(a) Sensor No. (b) Radial Distance in Inches From Center of FWD Load

Table G.18 Results of FWD Tests on Site 3 (Test 2)

Temperature (F): Air = 31 Pvmt. Surf. = 28

Station No.	Applied Load (lbs.)	Measured Deflections (mils)						
		D_1 (a)	D_2	D_3	D_4	D_5	D_6	D_7
		0(b)	12	24	36	48	60	72
1	18664	25.6	22.2	17.1	12.7	9.1	6.7	5.1
	18424	25.0	21.5	16.6	12.2	8.9	6.7	5.1
	18368	24.8	21.4	16.4	12.1	8.9	6.7	5.2
2	18656	25.8	21.5	16.0	11.4	8.3	6.2	4.7
	18504	25.2	20.9	15.6	11.2	8.4	6.3	4.9
	18464	25.5	20.7	15.5	11.1	8.3	6.3	4.8
3	18544	26.0	21.4	15.5	11.2	7.9	6.3	4.8
	18600	25.3	20.8	15.1	11.0	8.1	6.3	5.0
	18560	25.2	20.6	14.9	10.9	7.9	6.3	5.0
4	18384	27.6	22.6	16.6	11.8	8.5	6.6	4.8
	18432	26.9	22.0	16.2	11.6	8.6	6.6	5.3
	18512	26.6	21.7	16.0	11.5	8.4	6.6	4.8
5	18288	27.8	22.8	17.0	12.1	8.7	6.6	5.0
	18264	26.9	22.0	16.4	11.9	8.7	6.6	5.3
	18376	27.0	21.8	16.3	11.8	8.6	6.6	5.3
6	18240	30.7	23.9	17.4	12.0	8.9	6.9	5.3
	18288	29.5	22.8	16.7	11.8	8.8	6.9	5.5
	18320	29.4	22.7	16.6	11.5	8.9	6.9	5.5
7	18056	35.7	35.6	6.1	5.2	4.6	4.0	3.4
	18160	34.1	33.7	6.7	5.8	5.0	4.3	3.7
	18176	33.9	33.2	6.9	5.8	5.2	4.5	3.7
8	18184	27.0	21.5	15.4	10.9	8.0	6.1	4.8
	18288	26.0	20.6	14.8	10.6	7.8	6.1	4.8
	18264	24.2	20.5	14.5	10.4	7.9	6.0	4.8
9	18224	23.0	19.3	14.7	10.7	8.2	6.5	4.8
	18272	22.2	18.7	14.2	10.4	7.9	6.4	4.8
	18216	19.1	18.6	14.1	10.2	7.9	6.6	4.8
10	18232	27.4	21.7	15.7	11.1	8.4	6.3	5.0
	18256	26.9	21.1	15.2	10.9	8.2	6.3	5.1
	18248	26.6	20.9	15.1	10.8	8.1	6.2	5.0

Table G.18--continued

Station No.	Applied Load (lbs.)	Measured Deflections (mils)						
		D ₁ (a)	D ₂	D ₃	D ₄	D ₅	D ₆	D ₇
		0 (b)	12	24	36	48	60	72
11	18240	22.5	18.7	14.1	10.4	7.8	6.1	4.8
	18264	22.2	18.4	13.8	10.0	7.7	6.0	4.8
	18320	22.1	18.2	13.8	10.1	7.7	6.0	4.8
1 (OWP)	18168	18.8	16.4	13.0	9.8	7.6	6.3	5.2
	18232	18.5	16.0	12.7	9.6	7.5	6.1	5.2
	18184	18.5	15.9	12.6	9.5	7.5	6.1	5.2
2 (OWP)	18008	24.7	19.8	14.7	10.9	8.4	6.5	4.8
	18088	24.0	19.2	14.3	10.8	8.3	6.4	5.1
	18104	24.2	19.0	14.1	10.5	8.2	6.4	5.0

(a) Sensor No. (b) Radial Distance in Inches From Center of FWD Load

Table G.19 Results of FWD Tests on Site 3 (Test 3)

Temperature (F): Air = 54 Pvmnt. Surf. = 55

Station No.	Applied Load (lbs.)	Measured Deflections (mils)						
		D ₁ (a)	D ₂	D ₃	D ₄	D ₅	D ₆	D ₇
		0 (b)	12	24	36	48	60	72
1	26712	38.8	32.8	23.7	17.1	12.2	9.2	7.2
	17472	27.0	22.4	16.6	12.1	8.8	6.8	5.3
	9400	14.4	12.1	8.9	6.5	4.8	3.8	3.0
2	26736	39.5	31.6	22.7	16.0	11.7	9.0	7.0
	17528	27.3	21.8	15.8	11.3	8.3	6.4	5.0
	9392	14.6	11.7	8.4	6.1	4.4	3.5	2.8
3	26424	38.3	31.5	22.6	16.1	11.6	8.9	7.1
	17352	27.0	21.2	15.5	11.1	8.1	6.2	5.0
	9240	14.2	11.3	8.2	5.9	4.3	3.4	2.7
4	26280	41.5	33.8	23.8	16.6	12.2	9.3	7.4
	17296	29.3	22.8	16.5	11.6	8.6	6.6	5.2
	9200	15.7	12.2	8.9	6.2	4.6	3.6	2.9
5	26536	41.9	32.7	23.6	16.8	12.2	9.3	7.6
	17392	28.2	22.2	16.5	11.8	8.7	6.8	5.4
	9160	14.8	11.8	8.7	6.2	4.7	3.7	3.0
6	26368	44.6	35.2	25.0	17.3	12.3	9.4	7.4
	17392	30.2	23.7	17.2	12.0	8.7	6.8	5.4
	9096	16.2	12.7	9.2	6.4	4.8	3.8	3.0
7	26032	45.9	40.3	16.8	13.1	10.1	8.2	6.7
	17344	31.7	27.8	11.3	9.2	7.3	6.1	5.0
	8952	16.7	15.0	6.0	5.0	4.0	3.3	2.8
8	26152	41.2	31.8	22.0	15.5	11.3	8.8	7.2
	17224	28.2	21.7	15.1	10.9	8.0	6.3	5.2
	8888	14.7	11.4	7.8	5.7	4.3	3.4	2.8
9	26272	36.1	28.8	21.0	15.0	11.0	8.6	6.8
	17208	24.6	19.7	14.5	10.4	7.7	6.6	4.8
	8976	12.8	10.4	7.6	5.5	4.1	3.2	2.6
10	25624	42.5	32.2	22.3	15.7	11.5	8.9	7.1
	17024	28.7	21.9	15.4	10.9	8.0	6.2	5.0
	8904	15.1	11.7	8.1	5.8	4.3	3.4	2.7

Table G.19--continued

Station No.	Applied Load (lbs.)	Measured Deflections (mils)						
		D ₁ (a)	D ₂	D ₃	D ₄	D ₅	D ₆	D ₇
		0 (b)	12	24	36	48	60	72
11	26216	36.1	30.0	21.5	15.3	11.2	8.7	6.8
	17440	24.5	19.9	14.7	10.6	7.8	6.1	4.9
	8944	12.9	10.7	7.7	5.7	4.2	3.4	2.8
1 (OWP)	26264	33.3	28.0	21.2	14.9	10.8	8.6	7.0
	17632	21.8	19.1	14.5	10.2	7.5	6.0	4.9
	9064	11.2	10.0	7.5	5.3	4.0	3.2	2.5
2 (OWP)	26280	37.6	29.6	21.0	15.1	11.3	8.9	7.1
	17360	26.5	20.3	14.5	10.6	8.0	6.4	5.1
	9072	13.4	10.7	7.7	5.6	4.3	3.5	2.8

(a) Sensor No. (b) Radial Distance in Inches From Center of FWD Load

Table G.20 Results of FWD Tests on Site 3 (Test 4)

Temperature (F): Air = 75 Pvmt. Surf. = 73

Station No.	Applied Load (lbs.)	Measured Deflections (mils)						
		D_1 (a)	D_2	D_3	D_4	D_5	D_6	D_7
		0 (b)	12	24	36	48	60	72
1	25032	38.9	30.9	22.8	16.7	12.3	9.2	7.0
	17280	26.3	21.3	15.8	11.7	8.7	6.5	5.1
	8696	13.1	10.6	7.8	5.8	4.4	3.3	2.6
2	24992	40.4	30.9	21.6	15.3	11.3	8.4	6.7
	17288	27.4	20.9	14.9	10.6	7.9	5.9	4.7
	8664	13.6	10.7	7.5	5.4	4.0	3.0	2.4
3	24904	39.4	31.0	20.9	14.9	10.9	8.4	6.4
	17088	26.9	20.6	14.5	10.3	7.6	5.9	4.6
	8648	13.1	10.3	7.3	5.1	3.8	3.0	2.4
4	24888	41.2	31.8	22.7	16.1	12.1	9.1	7.2
	17064	28.4	21.4	15.7	11.1	8.5	6.4	5.1
	8528	14.0	10.9	7.8	5.6	4.3	3.3	2.6
5	24888	42.7	33.4	24.0	17.1	12.4	9.3	7.3
	17128	29.1	22.8	16.4	11.7	8.7	6.6	5.2
	8528	13.9	11.2	8.1	5.8	4.3	3.3	2.6
6	24840	44.3	32.9	23.3	16.7	12.2	9.4	7.6
	17000	30.0	22.4	16.0	11.5	8.5	6.6	5.4
	8520	15.0	11.4	8.0	5.8	4.3	3.3	2.7
7	24656	47.6	36.2	20.1	14.7	11.1	8.6	6.8
	16984	29.8	23.5	13.7	10.2	7.8	6.0	4.9
	8416	14.7	11.9	6.7	5.0	3.8	3.0	2.4
8	25000	41.5	32.0	21.8	15.4	11.3	8.7	6.8
	17024	27.9	21.0	14.9	10.7	7.9	6.0	4.8
	8536	13.7	10.3	7.3	5.3	4.0	3.0	2.4
9	25152	37.4	28.8	20.4	14.7	11.0	8.4	6.7
	17000	25.3	19.6	14.0	10.2	7.6	5.9	4.8
	8528	12.4	9.7	6.9	5.0	3.8	2.9	2.4
10	25088	40.4	30.8	21.4	15.0	10.9	8.4	6.4
	16912	27.2	20.8	14.7	10.4	7.6	5.9	4.6
	8592	13.6	10.5	7.3	5.2	3.9	3.0	2.4

Table G.20--continued

Station No.	Applied Load (lbs.)	Measured Deflections (mils)						
		D_1 (a)	D_2	D_3	D_4	D_5	D_6	D_7
		0 (b)	12	24	36	48	60	72
11	25360	35.7	28.7	20.2	14.4	10.7	8.4	6.8
	17152	24.4	19.4	13.8	10.0	7.5	5.8	4.7
	8640	12.1	9.7	6.9	5.0	3.7	2.9	2.3
1 (OWP)	25408	31.4	25.5	19.0	13.9	10.4	8.3	6.9
	17208	21.2	17.3	13.1	9.6	7.3	5.8	4.8
	8640	10.4	8.5	6.4	4.7	3.6	2.9	2.4
2 (OWP)	25408	37.1	29.1	21.1	15.8	11.9	9.2	7.2
	17312	25.1	19.9	14.5	10.9	8.3	6.5	5.1
	8548	12.0	9.9	7.2	5.5	4.2	3.3	2.6

(a) Sensor No. (b) Radial Distance in Inches From Center of FWD Load

Table G.21 Results of FWD Tests on Site 3 (Test 5)

Temperature (F): Air = 79 Pvm. Surf. = 85

Station No.	Applied Load (lbs.)	Measured Deflections (mils)						
		D ₁ (a)	D ₂	D ₃	D ₄	D ₅	D ₆	D ₇
		0(b)	12	24	36	48	60	72
1	25240	42.2	32.5	23.3	16.6	12.3	9.2	7.4
	11880	19.8	15.5	11.2	8.1	6.0	4.6	3.6
	8176	13.5	10.5	7.7	5.6	4.1	3.2	2.5
2	25088	41.7	30.3	21.2	14.6	10.8	8.6	6.7
	11968	19.5	14.6	10.1	7.1	5.3	4.2	3.4
	8128	13.2	9.9	6.8	4.9	3.6	2.8	2.3
3	25160	40.5	30.0	20.8	14.7	10.6	8.2	6.9
	12080	18.8	14.0	10.0	7.1	5.2	4.1	3.4
	8256	12.6	9.4	6.7	4.8	3.5	2.8	2.3
4	25064	44.5	32.2	22.8	15.8	11.6	9.3	7.3
	11904	20.9	15.4	11.0	7.8	5.7	4.5	3.6
	8144	14.1	10.4	7.4	5.3	3.9	3.1	2.5
5	25120	43.2	32.1	23.2	16.5	11.9	9.3	7.4
	12024	20.5	15.6	11.4	8.2	6.1	4.7	3.7
	8152	13.8	10.5	7.7	5.5	4.1	3.2	2.5
6	25080	46.7	33.0	23.3	16.1	11.7	9.0	7.6
	12000	21.8	16.1	11.4	7.9	5.9	4.6	3.7
	8112	14.9	10.8	7.6	5.6	4.1	3.2	2.5
7	25144	46.1	35.8	20.4	14.9	10.7	8.4	6.7
	11888	21.9	17.4	9.8	7.2	5.5	4.3	3.5
	8168	14.8	11.8	6.6	5.1	3.7	2.9	2.3
8	24984	43.5	30.7	22.0	15.4	11.2	8.8	7.3
	11832	20.1	14.5	10.3	7.3	5.4	4.3	3.5
	8016	13.5	9.7	7.0	4.9	3.7	2.8	2.4
9	25216	38.7	29.2	20.8	14.9	11.2	8.6	7.1
	11984	17.9	13.6	9.8	7.1	5.3	4.2	3.4
	8120	12.1	9.1	6.6	4.8	3.6	2.8	2.3
10	25904	43.6	30.3	20.8	14.5	11.4	8.6	6.9
	11728	20.3	14.3	10.0	7.1	5.3	4.2	3.4
	8096	13.7	9.6	6.8	4.8	3.7	2.9	2.3

Table G.21--continued

Station No.	Applied Load (lbs.)	Measured Deflections (mils)						
		D_1 (a)	D_2	D_3	D_4	D_5	D_6	D_7
		0 (b)	12	24	36	48	60	72
11	25672	31.6	25.2	19.0	13.9	10.3	8.3	6.9
	12136	14.8	11.9	9.1	6.7	5.0	4.1	3.4
	8296	9.9	8.0	6.1	4.5	3.4	2.7	2.3
1 (OWP)	25672	31.6	25.2	19.0	13.9	10.3	8.3	6.9
	12136	14.8	11.9	9.1	6.7	5.0	4.1	3.4
	8296	9.9	8.0	6.1	4.5	3.4	2.7	2.3
2 (OWP)	25360	40.7	30.2	22.0	15.2	11.4	9.1	7.7
	12056	19.1	14.6	10.2	7.4	5.5	4.5	3.9
	8264	13.0	9.2	7.5	5.1	4.2	3.2	2.2

(a) Sensor No. (b) Radial Distance in Inches From Center of FWD Load

Table G.22 Results of FWD Tests on Site 3 (Test 6)

Temperature (F): Air = 93 Pvm. Surf. = 118

Station No.	Applied Load (lbs.)	Measured Deflections (mils)						
		D ₁ (a)	D ₂	D ₃	D ₄	D ₅	D ₆	D ₇
		0(b)	12	24	36	48	60	72
1	25192	50.6	35.3	23.9	16.5	12.0	9.5	8.2
	11752	23.9	16.8	11.6	8.1	6.0	4.6	3.7
	7992	15.9	11.1	7.6	5.4	4.0	3.1	2.6
2	24800	49.3	32.0	21.2	14.6	10.8	8.7	6.9
	11968	23.4	15.5	10.4	7.1	5.3	4.2	3.4
	8024	15.6	10.4	6.9	4.7	3.5	2.8	2.3
3	24960	48.5	32.0	21.0	14.0	10.4	8.6	6.7
	12024	22.2	15.0	10.1	6.7	5.2	4.1	3.5
	8040	14.8	10.0	6.7	4.7	3.3	2.8	2.0
4	25048	55.1	34.2	23.1	16.1	11.8	9.3	7.5
	11928	24.1	16.2	11.1	7.8	5.8	4.5	3.6
	8000	16.0	10.8	7.4	5.2	3.9	3.0	2.5
5	24880	51.6	34.9	24.2	6.7	12.2	9.5	7.4
	11904	24.4	16.7	11.7	8.2	6.0	4.7	3.7
	8048	16.1	11.2	7.8	5.4	4.0	3.1	2.5
6	24856	50.5	34.9	23.7	16.0	11.3	9.7	7.4
	11920	24.3	16.8	11.4	7.9	5.7	4.6	3.6
	7936	16.2	11.2	7.6	5.3	3.9	3.0	2.4
7	24800	53.3	35.3	21.4	15.0	11.1	8.4	6.8
	11848	24.8	16.8	10.4	7.4	5.5	4.2	3.4
	7976	16.7	11.2	7.0	4.9	3.7	2.8	2.3
8	24904	48.0	33.1	22.2	14.5	10.8	9.4	7.0
	12008	22.1	15.5	10.5	7.0	5.3	4.3	3.4
	7936	14.6	10.2	6.9	4.7	3.5	2.7	2.2
9	25008	45.4	31.9	21.2	14.9	11.0	8.5	6.9
	12024	21.0	14.7	10.2	7.1	5.3	4.1	3.3
	8008	13.9	9.7	6.7	4.6	3.5	2.7	2.2
10	25584	44.5	31.6	21.2	14.4	10.8	8.5	6.9
	11624	20.8	15.2	10.3	7.1	5.3	4.2	3.4
	7896	13.9	10.2	6.9	4.8	3.5	2.8	2.3

Table G.22--continued

Station No.	Applied Load (lbs.)	Measured Deflections (mils)						
		D ₁ (a)	D ₂	D ₃	D ₄	D ₅	D ₆	D ₇
		0 (b)	12	24	36	48	60	72
11	25024	45.7	30.7	21.0	14.6	10.7	8.6	6.9
	11872	21.2	14.7	10.1	7.1	5.3	4.2	3.4
	7928	14.0	9.7	6.7	4.7	3.4	2.7	2.2
1 (OWP)	25128	42.6	29.0	20.1	13.6	10.5	8.5	7.0
	12168	18.7	13.5	9.5	6.6	5.1	4.2	3.4
	8088	12.3	8.8	6.2	4.3	3.3	2.7	2.3
2 (OWP)	24848	50.1	34.0	23.4	16.0	11.8	9.0	7.2
	12008	23.3	16.1	11.2	7.9	5.9	4.5	3.6
	7992	15.3	10.2	7.6	5.2	4.1	3.0	2.4

(a) Sensor No. (b) Radial Distance in Inches From Center of FWD Load

Table G.23 Results of FWD Tests on Site 3 (Test 7)

Temperature (F): Air = 80 Pvm. Surf. = 83

Station No.	Applied Load (lbs.)	Measured Deflections (mils)						
		D_1 (a)	D_2	D_3	D_4	D_5	D_6	D_7
		D_0 (b)	12	24	36	48	60	72
1	17120	28.7	22.1	15.8	11.3	8.4	6.4	5.1
	11856	19.9	15.4	11.1	7.9	5.9	4.6	3.7
	8120	13.4	10.4	7.5	5.4	4.0	3.1	2.4
2	17208	27.8	20.6	14.3	10.1	7.5	5.8	4.7
	11936	19.4	14.5	10.0	7.2	5.3	4.1	3.3
	8096	13.0	9.8	6.8	4.8	3.6	2.8	2.3
3	17240	26.4	19.6	14.0	9.9	7.4	5.8	4.8
	12048	18.4	13.6	9.9	6.9	5.3	4.2	3.5
	8160	12.1	9.2	6.4	4.7	3.4	2.8	2.3
4	17096	29.0	21.4	15.2	10.7	7.9	6.4	5.0
	11880	20.3	15.0	10.8	7.7	5.7	4.6	3.7
	8024	13.5	10.1	7.2	5.1	3.8	3.2	2.5
5	17192	29.9	22.8	16.4	11.7	8.6	6.6	5.3
	11992	20.8	15.9	11.6	8.3	6.1	4.7	3.8
	8016	14.0	10.6	7.8	5.6	4.1	3.2	2.6
6	17008	31.9	23.2	16.8	11.6	8.5	6.7	5.3
	11728	22.3	16.4	11.8	8.2	6.0	4.8	3.8
	7936	14.9	11.0	8.0	5.5	4.1	3.2	2.5
7	17176	31.7	25.4	13.6	10.1	7.6	5.9	4.8
	11864	22.1	18.0	9.5	7.1	5.4	4.3	3.5
	7936	14.8	12.1	6.3	4.7	3.6	2.8	2.3
8	17120	29.0	21.1	14.8	10.3	7.6	6.3	4.9
	11864	20.0	14.5	10.2	7.2	5.4	4.2	3.4
	7976	13.4	9.6	6.8	4.8	3.6	2.9	2.3
9	17200	25.0	18.9	13.8	9.9	7.6	6.0	4.8
	11904	17.2	13.1	9.6	7.0	5.3	4.1	3.3
	8040	11.5	8.8	6.4	4.7	3.5	2.7	2.2
10	17152	28.0	20.8	14.6	10.4	7.7	6.1	4.8
	11768	19.5	14.6	10.2	7.3	5.5	4.3	3.5
	7960	13.0	9.7	6.8	4.8	3.6	2.8	2.3

Table G.23--continued

Station No.	Applied Load (lbs.)	Measured Deflections (mils)						
		D ₁ (a)	D ₂	D ₃	D ₄	D ₅	D ₆	D ₇
		0 (b)	12	24	36	48	60	72
11	17256	24.1	18.0	13.1	9.5	7.4	5.7	4.7
	11912	16.8	12.7	9.4	6.7	5.2	4.0	3.4
	8080	11.1	8.5	6.2	4.5	3.4	2.7	2.2
1 (OWP)	17432	21.0	16.7	12.8	9.1	7.0	5.5	4.6
	12152	14.6	11.3	8.8	6.3	4.9	3.7	3.5
	8120	9.5	7.6	5.9	4.4	3.3	2.8	2.1
2 (OWP)	17280	28.1	20.8	15.2	11.0	8.4	6.7	5.5
	12000	19.6	14.4	10.5	7.4	5.8	4.6	4.0
	8112	13.0	9.6	7.0	4.9	3.7	3.4	2.7

(a) Sensor No. (b) Radial Distance in Inches From Center of FWD Load

Table G.24 Results of FWD Tests on Site 3 (Test 8)

Temperature (F): Air = 80 Pymt. Surf. = 88

Station No.	Applied Load (lbs.)	Measured Deflections (mils)						
		D_1 (a)	D_2	D_3	D_4	D_5	D_6	D_7
		D_0 (b)	12	24	36	48	60	72
1	16984	31.4	23.0	16.3	11.6	8.4	6.8	5.3
	11736	21.6	15.9	11.2	8.0	5.9	4.7	3.6
	7976	14.4	10.7	7.6	5.5	4.1	3.3	2.5
2	17064	29.8	21.3	14.6	10.2	7.5	6.1	4.8
	11856	20.6	14.7	10.1	7.1	5.3	4.2	3.3
	8032	13.7	9.8	6.7	4.7	3.5	2.8	2.3
3	17240	28.4	20.2	13.8	9.4	7.5	5.9	4.8
	11920	19.6	14.1	9.5	6.3	5.3	3.8	3.2
	8136	13.0	9.3	6.6	4.7	3.4	2.9	2.3
4	17040	31.5	22.2	15.6	11.1	8.3	6.5	5.1
	11768	21.8	15.4	10.9	7.8	5.9	4.6	3.7
	7960	14.4	10.2	7.6	5.4	4.0	3.1	2.5
5	17080	31.6	22.8	16.4	11.6	8.5	6.9	5.3
	11752	21.8	15.9	11.4	8.1	6.1	4.7	3.8
	7952	14.5	10.6	7.6	5.4	4.0	3.1	2.5
6	17024	34.0	23.6	16.8	11.3	8.4	6.6	5.3
	11752	23.5	16.5	11.6	8.2	6.1	4.7	3.8
	7968	15.7	11.0	8.0	5.3	4.1	3.2	2.6
7	17152	32.5	25.1	14.4	10.4	7.6	6.1	4.8
	11912	22.4	17.6	10.0	7.2	5.3	4.2	3.4
	8008	14.9	12.0	6.8	4.9	3.6	2.8	2.3
8	17152	29.7	20.8	14.5	10.2	7.6	5.9	4.7
	11864	20.6	14.4	10.1	7.1	5.3	4.1	3.3
	7920	13.5	9.5	6.7	4.7	3.5	2.8	2.2
9	17088	27.4	19.7	13.9	9.9	7.5	5.8	4.7
	11824	19.0	13.8	9.8	7.0	5.3	4.2	3.4
	8008	12.6	9.1	6.4	4.6	3.5	2.7	2.2
10	17008	29.7	21.2	14.4	10.2	7.6	6.3	4.9
	11712	20.6	14.8	10.2	7.2	5.4	4.3	3.5
	7912	13.7	10.0	6.7	4.9	3.5	3.1	2.4

Table G.24--continued

Station No.	Applied Load (lbs.)	Measured Deflections (mils)						
		D_1 (a)	D_2	D_3	D_4	D_5	D_6	D_7
		0 (b)	12	24	36	48	60	72
11	17176	26.6	19.2	13.4	9.8	7.3	5.7	5.1
	11880	18.4	13.1	9.5	6.8	4.9	3.8	3.6
	7976	12.2	8.7	6.4	4.5	3.4	2.8	2.1
1 (OWP)	17288	23.2	17.5	12.8	9.3	7.2	5.9	4.8
	12056	16.0	12.2	9.0	6.5	5.0	4.2	3.4
	8168	10.6	8.2	6.0	4.5	3.4	2.8	2.3
2 (OWP)	17176	28.6	20.6	14.8	10.8	8.2	6.6	5.1
	11960	19.8	14.4	10.4	7.7	5.8	4.7	3.7
	8064	13.1	9.6	6.8	5.1	3.9	2.9	2.3

(a) Sensor No. (b) Radial Distance in Inches From Center of FWD Load

REFERENCES

1. Brown, R.W., "The Mission of the Air Force Engineering and Services Center (AFESC)," lecture presented to Class TTE 5105, University of Florida, Gainesville, February 1986.
2. McVay, M.C., "A Micromechanical Study of Fabric and its Relationship with Macroscopic Stress and Deformation," Research Proposal, University of Florida, Gainesville, 1986.
3. Brabston, W.N., "Investigation of Compaction Criteria for Airport Pavement Subgrade Soils," Technical Report GL-81-U, Geotechnical Laboratory, U.S. Army Engineer Waterways Experiment Station, Vicksburg, Mississippi, October 1981.
4. Barker, W.R., and Brabston, W.N., "Development of a Structural Design Procedure for Flexible Airport Pavements," Final Report, U.S. Army Engineer Waterways Experiment Station, Vicksburg, Mississippi, September 1985.
5. "Navy Airfield Pavement Evaluation Manual," Unpublished Report, Vicksburg, Mississippi, 1987.
6. Himeno, K., Watanbe, T., and Maruyama, T., "Estimation of Fatigue Life of Asphalt Pavement," Proceedings, Sixth International Conference on the Structural Design of Asphalt Pavements, Cushing-Malloy, University of Michigan, Ann Arbor, Vol. 1, July 13-17, 1987, pp. 272-289.
7. Deacon, J.A., and Monismith, C.L., "Laboratory Flexural Fatigue Testing of Asphalt Concrete with Emphasis on Compound Loading Tests," Highway Research Record No. 158, HRB, Washington D.C., 1967, pp. 1-31.
8. Ruth, B.E., and Davis, A.S., "Fatigue and Fracture of Asphalt Concrete," Final Report D82, Department of Civil Engineering, University of Florida, Gainesville, December 1978.
9. Gerritsen, A.H., Van Gorp, C.A.P.M., Vander Heide, J.P.J., Moleenaar, A.A.A., and Pronk, A.C., "Prediction and Prevention of Surface Cracking in Asphalt Pavements," Proceedings, Sixth International Conference on the Structural Design of Asphalt Pavements, Cushing-Malloy, University of Michigan, Ann Arbor, Vol. I, July 13-17, 1987, pp. 378-391.
10. Lambe, T.W., and Whitman, R.V., Soil Mechanics, John Wiley & Sons, New York, 1969.

11. Monismith, C.L., and Finn, F.N., "Flexible Pavement Design: State-of-the-Art," *Journal of Transportation Engineering*, ASCE, Vol. 103, TE1, 1977, pp. 1-53.
12. Hicks, R.G., "Factors Influencing the Resilient Properties of Granular Materials," Ph.D. Dissertation, University of California-Berkeley, 1970.
13. Darter, M.I., Carpenter, S.H., Herin, M., Barenberg, E.J., Dempsey, B.J., and Marshall, M.R., "Techniques for Pavement Rehabilitation," Training Course, ERES, Inc., Champaign, Illinois, 1982.
14. Seed, H.B., and Fead, J.W.N., "Apparatus for Repeated Load Tests on Soils," Special Technical Publication No. 254, ASTM, Philadelphia, Pennsylvania, 1959.
15. McVay, M.C., and Taesiri, Y., "Cyclic Behavior of Pavement Base Materials," *Journal of the Geotechnical Engineering Division*, ASCE, Vol. 3, No. 1, January 1985, pp. 1-17.
16. Ishihara, K., "Soil Response in Cyclic Loading Induced by Earthquakes, Traffic, and Waves," presented to the Seventh Asian Regional Conference on Soil Mechanics and Foundation Engineering, Haifa, Israel, August 1983.
17. Peattie, K.R., "A Fundamental Approach to the Design of Flexible Pavements," Proceedings, First International Conference on the Structural Design of Asphalt Pavements, Cushing-Malloy, University of Michigan, Ann Arbor, August 20-24, 1962, pp. 403-411.
18. Edwards, J.M., and Valkering, C.P., Structural Design of Asphalt Pavement for Heavy Aircraft, Shell International Petroleum Co., London, England, 1970.
19. Witczak, M.W., "Design of Full-Depth Asphalt Airfield Pavements," Research Report 72-2, The Asphalt Institute, College Park, Maryland, April 1972.
20. Smith, R.E., and Lytton, R.L., "Synthesis Study of Nondestructive Testing Devices for the Use in Overlay Thickness Design of Flexible Pavements," Report FWHA/RD-83/097, Federal Highway Administration, Washington, D.C., 1983.
21. Smith, R.E., and Lytton, R.L., "Operating Characteristics and User Satisfaction of Commercially Available NDT Equipment," *Transportation Research Record* 1007, TRB, Washington D.C., 1985, pp. 1-9.
22. Nazarian, S., and Stokoe II, K.H., "Nondestructive Testing of Pavements Using Surface Waves," *Transportation Research Record* 993, TRB, Washington D.C., 1984, pp. 67-79.

23. Bretonniere, S., "Les Deflectometres a Boulet Pour L'etude des Deflections des Chaussees Sous Charges Dynamiques," Bulletin de Liaison No. 2, July-August 1963.
24. Sorensen A., and Hayven, M., "The Dynatest 8000 Falling Weight Deflectometer Test System," Proceedings, First International Symposium on Bearing Capacity of Roads and Airfields, Trondheim, Norway, June 23-25, 1982, pp. 464-470.
25. Uddin, W., Meyer, A.H., Hudson, W.R., and Stokoe II, K.H., "Project-Level Structural Evaluation of Pavement Based on Dynamic Deflections," Transportation Research Record 1007, TRB, Washington D.C., 1985, pp. 37-45.
26. Marchionna A., Cesarini, M., Fornaci, M.G., and Malgarini, M., "Pavement Elastic Characteristics Measured by Means of Tests Conducted with the Falling Weight Deflectometer," Transportation Research Record 1007, TRB, Washington D.C., 1985, pp. 46-53.
27. Lytton, R.L., Roberts, F.L., and Stoffels, S., "Determination of Asphaltic Concrete Pavement Structural Properties by Non-destructive Testing," Final Report RF7026, Texas A & M University, College Station, April 1986.
28. Uddin, W., Meyer, A.H., Hudson, W.R., and Stokoe II, K.H., "A Structural Evaluation Methodology for Pavements Based on Dynamic Deflections," Research Report 387-1, Center for Transportation Research, University of Texas at Austin, July 1985.
29. Ros, J., Pronk, A.C., and Eikelboom, J., "The Performance of Highway Pavements in the Netherlands and the Applicability of Linear Elasticity Theory to Pavement Design," Proceedings, Fifth International Conference on the Structural Design of Asphalt Pavements, Cushing-Malloy, University of Michigan, Ann Arbor, 1982.
30. Halim, A.O.A., Haas, R., and Phang, W.A., "Geogrid Reinforcement of Asphalt Pavements and Verification of Elastic Theory," Transportation Research Record 949, TRB, Washington D.C., 1983, pp. 55-65.
31. Waterhouse, A., "Stresses in Layered Systems Under Static and Dynamic Loading," Proceedings, Second International Conference on the Structural Design of Asphalt Pavements, Cushing-Malloy, University of Michigan, Ann Arbor, 1967, pp. 291-308.
32. Brown, S.F., and Pappin, J.W., "The Modelling of Granular Materials in Pavements," presented to the Symposium on Mechanics of Layered Systems, TRB, Washington D.C. 1985.

33. Ruth, B.E., Tia, M., and Badu-Tweneboah, K., "Structural Characterization of In-Place Materials by Falling Weight Deflectometer," Department of Civil Engineering, University of Florida, Gainesville, October 1986.
34. "BISAR Users Manual, Layered Systems Under Normal and Tangential Loads," Koninklijke/Shell Laboratorium, Amsterdam, Holland, 1972.
35. Finn, F.N., "Observations of Distress in Full-Scale Pavements," Special Report No. 126, Highway Research Board, Washington D.C., 1971.
36. Ruth, B.E., Roque, R., and Hardee, H.K., "Low-Temperature Pavement Response: Full Scale Pavement Testing," Final Report 245-D34, Department of Civil Engineering, University of Florida, Gainesville, February 1986.
37. Anderson, K.O., Shields, B.P., and Daeyczyn, J.M., "Cracking of Asphalt Pavements Due to Thermal Effects," Proceedings, Association of Asphalt Paving Technologists, Cushing-Malloy, Ann Arbor, Michigan, Vol. 35, 1966, pp. 247-262.
38. Hugo, F., and Kennedy, T.W., "Surface Cracking of Asphalt Mixtures in South Africa," Proceedings, Association of Asphalt Paving Technologists, Cushing-Malloy, Ann Arbor, Michigan, Vol. 54, 1985, pp. 454-501.
39. Yoder, E.J., and Witczak, M.W., Principles of Pavement Design, John Wiley & Sons, New York, 1975.
40. Pell, P.S., "Characterization of Fatigue Behavior," Special Report No. 140, Highway Research Board, Washington D.C., 1973, pp. 49-64.
41. Witczak, M.W., "Fatigue Subsystem Solution for Asphalt Concrete Airfield Pavements," Special Report No. 140, Highway Research Board, Washington D.C., 1973, pp. 112-129.
42. Barksdale, R.G., and Hicks, R.G., "Material Characterization and Layered Theory for Use in Fatigue Analysis," Special Report No. 140, Highway Research Board, Washington D.C., 1973, pp. 20-48.
43. Rauhut, J.B., and Kennedy, T.W., "Characterizing Fatigue Life for Asphalt Concrete Pavements," Transportation Research Record 888, TRB, Washington D.C., 1982, pp. 47-56.
44. Ruth, B.E., and Maxfield, J.D., "Fatigue of Asphalt Concrete," Final Report 245-D54, Department of Civil Engineering, University of Florida, Gainesville, 1977.

45. Ruth, B.E., Bloy, L.A.K., and Avital, A.A., "Low Temperature Asphalt Rheology as Related to Thermal and Dynamic Behavior of Asphalt Pavements," Final Report 245-U20, Department of Civil Engineering, University of Florida, Gainesville, 1981.
46. Ruth, B.E., Bloy, L.A.K., and Avital, A.A., "Prediction of Pavement Cracking at Low Temperatures," Proceedings, Association of Asphalt Paving Technologists, Cushing-Malloy, Ann Arbor, Michigan, Vol. 51, 1982, pp. 53-90.
47. Hills, J.F., and Brien, D., "The Fracture of Bitumens and Asphalt Mixes by Temperature Induced Stresses," Proceedings, Association of Asphalt Paving Technologists, Cushing-Malloy, Ann Arbor, Michigan, Vol. 35, 1966, pp. 292-309.
48. Monismith, C.L., Secor, B.A., and Secor, K.E., "Temperature Induced Stresses and Deformations in Asphalt Concrete," Proceedings, Association of Asphalt Paving Technologists, Cushing-Malloy, Ann Arbor, Michigan, Vol.34, 1965, pp. 248-279.
49. Finn, F.N., Nair, K., and Hilliard, J., "Minimizing Cracking of Asphalt Concrete Pavements," Proceedings, Association of Asphalt Paving Technologists, Cushing-Malloy, Ann Arbor, Michigan, Vol. 45, 1976, pp. 492-526.
50. Ruth, B.E., "Prediction of Low-Temperature Creep and Thermal Strain in Asphalt Concrete Pavements," Special Technical Publication No. 628, ASTM, Philadelphia, Pennsylvania, 1977.
51. Fabb, T.R.J., "The Influence of Mix Composition, Binder Properties, and Cooling Rate on Asphalt Cracking at Low Temperatures," Proceedings, Association of Asphalt Paving Technologists, Cushing-Malloy, Ann Arbor, Michigan, Vol. 43, 1974, pp. 285-319.
52. Schmidt, R.J., "The Relationship of the Low Temperature Properties of Asphalt to the Cracking of Pavements," Proceedings, Association of Asphalt Paving Technologists, Cushing-Malloy, Ann Arbor, Michigan, Vol. 36, 1966, pp. 263-269.
53. Hugo, F., "Catering For Long Term Changes in the Characteristics of Asphalt During the Design Life of a Pavement," Proceedings, Sixth International Conference on the Structural Design of Asphalt Pavements, Cushing-Malloy, University of Michigan, Ann Arbor, Vol. 1, July 13-17, 1987, pp. 290-304.
54. Haas, R., Thompson, E., Meyer, F., and Tessier G.R., "Study of Asphalt Cement Additives and Extenders," report prepared for the Roads and Transportation Association of Canada, 1983.

55. Ponniah, J., Haas, R., Phang, W.A., and Rothenburg, L., "Low-Temperature Reflection Cracking Through Asphalt Overlays," Proceedings, Sixth International Conference on the Structural Design of Asphalt Pavements, Cushing-Malloy, University of Michigan, Ann Arbor, Vol. 1, July 13-17, 1987, pp. 935-945.
56. Gerlach, A., Loizos, A., and Lucke, H., "The Influence of Stiffness-Progress of Different Pavement Layers on the Size and Shape of Rut Depth in the Pavement Surface," Proceedings, Sixth International Conference on the Structural Design of Asphalt Pavements, Cushing-Malloy, University of Michigan, Ann Arbor, Vol. 1, July 13-17, 1987, pp. 72-81.
57. Freeme, C.R., de Beer, M., and Viljoen, A.W., "The Behavior and Mechanistic Design of Asphalt Pavements," Proceedings, Sixth International Conference on the Structural Design of Asphalt Pavements, Cushing-Malloy, University of Michigan, Ann Arbor, Vol. 1, July 13-17, 1987, pp. 333-343.
58. Monismith, C.L., Finn, F.N., Ahlborn, G., and Markevich, N., "A General Analytically Based Approach to the Design of Asphalt Concrete Pavements," Proceedings, Sixth International Conference on the Structural Design of Asphalt Pavements, Cushing-Malloy, University of Michigan, Ann Arbor, Vol. 1, July 13-17, 1987, pp. 344-365.
59. Barber, V.C., "The Deterioration and Reliability of Pavements," Technical Report TR-S-78-8, U.S. Army Engineer Waterways Experiment Station, Vicksburg, Mississippi, July 1978.
60. Barker, W.R., "Prediction of Pavement Roughness," MP GL-82-11, Geotechnical Laboratory, U.S. Army Engineer Waterways Experiment Station, Vicksburg, Mississippi, September 1982.
61. Schweyer, H.E., "Asphalt Rheology in the Near Transition Temperature Range," Highway Research Record No. 628, HRB, Washington D.C., 1973, pp. 1-15.
62. Jongepier, R., and Kuilman, B., "Characteristics of the Rheology of Bitumens," Proceedings, Association of Asphalt Paving Technologists, Cushing-Malloy, Ann Arbor, Michigan, Vol. 38, 1969, pp. 98-122.
63. Teng, J., "Measurement of Low-Temperature Rheological Properties of Asphalt by Use of the Schweyer Rheometer," Master's Report, Department of Civil Engineering, University of Florida, Gainesville, 1986.
64. Duthie, J.L., "Proposed Bitumen Specifications Derived from Fundamental Parameters," Proceedings, Association of Asphalt Paving Technologists, Cushing-Malloy, Ann Arbor, Vol. 41, 1972, pp. 70-117.

65. Schweyer, H.E., Baxley, R.L., and Burns, A.M., "Low-Temperature Rheology of Asphalt Cements--Rheological Background," Special Technical Publication No. 628, ASTM, Philadelphia, Pennsylvania, 1976, pp. 5-42.
66. Schweyer, H.E., Smith, L.L., and Fish, G.W., "A Constant Stress Rheometer for Asphalt Cements - Rheological Background," Special Technical Publication No. 628, ASTM, Philadelphia, Pennsylvania, 1977, pp. 5-42.
67. Keyser, J.H., and Ruth, B.E., "Comparison of the Sensitivity of Asphalt Concrete Mixture Strength Tests to Changes in Asphalt Binder Properties," Proceedings, Association of Asphalt Paving Technologists, Cushing-Malloy, Ann Arbor, Michigan, Vol. 53, 1984, pp. 583-617.
68. Miller, J.S., Uzan, J., and Witczak, M.W., "Modification of the Asphalt Institute Bituminous Mix Modulus Predictive Equation," Transportation Research Record 911, TRB, Washington D.C., 1983, pp. 27-36.
69. "Structural Design of Asphalt Concrete Pavements," Special Report No. 126, Highway Research Board, Washington D.C., 1971.
70. Gonzalez, G., Kennedy, T.W., and Angnos, J.N., "Evaluation of the Resilient Elastic Characteristics of Asphalt Mixtures Using the Indirect Tensile Test," Research Report No. 183-6, Center for Highway Research, The University of Texas at Austin, 1975, pp. 1-71.
71. Kennedy, T.W., "Characterization of Asphalt Pavement Materials Using the Indirect Tensile Test," Proceedings, Association of Asphalt Paving Technologists, Cushing-Malloy, Ann Arbor, Michigan, Vol. 46, 1977, pp. 132-150.
72. Puyana, E., "Characterization of Asphalt Concrete Pavement Materials," Unpublished Master's Thesis, Department of Civil Engineering, University of Florida, Gainesville, 1983.
73. Mamlouk, M.S., "Characterization of Cold Mixed Asphalt Emulsion Treated Bases," Joint Highway Research Project IN/JHRP-79-19, School of Civil Engineering, Purdue University, West Lafayette, Indiana, 1979.
74. Deacon, J.A., "Materials Characterization - Experimental Behavior," Special Report No. 126, Highway Research Board, Washington D.C., 1971, pp. 150-179.
75. Bazin, P., and Saunier, J., "Deformability, Fatigue, and Healing Properties of Asphalt Mixes," Proceedings, Second International Conference on the Structural Design of Asphalt Pavements, Cushing-Malloy, University of Michigan, Ann Arbor, 1967, pp. 109-140.

76. Ruth, B.E., Kokomoor, K.W., Veitia, A.E., and Rumble, J.D., "Importance and Cost Effectiveness of Testing Procedures Related to Highway Construction," Final Report 245-U39, Department of Civil Engineering, University of Florida, Gainesville, April 1982.
77. Ruth, B.E., Schwyer, H.E., Davis, A.S., and Maxfield, J.D., "Asphalt Viscosity: An Indicator of Low Temperature Fracture Strain in Asphalt Mixtures," Proceedings, Association of Asphalt Paving Technologists, Vol. 48, 1979, pp. 221-237.
78. Finn, F.N., "Factors Involved in the Design of Asphaltic Pavement Surfaces," National Cooperative Highway Research Program Report No. 39, 1967.
79. Ruth, B.E., and Olson, G.K., "Creep Effects on Fatigue Testing of Asphalt Concrete," Proceedings, Association of Asphalt Paving Technologists, Cushing-Malloy, Ann Arbor, Michigan, Vol. 46, 1977, pp. 176-192.
80. Pavlovich, R.D., and Goetz, W.H., "Direct Tension Results for Some Asphalt Concretes," Proceedings, Association of Asphalt Paving Technologists, Cushing-Malloy, Ann Arbor, Michigan, Vol. 45 1976, pp. 400-424.
81. Page, G.C., Murphy, K.H., Ruth, B.E., and Roque, R., "Asphalt Binder Hardening - Causes and Effects," Proceedings, Association of Asphalt Paving Technologists, Cushing-Malloy, Ann Arbor, Michigan, Vol. 46, 1977, pp. 140-167.
82. Kumar, A., and Goetz, W.H., "Asphalt Hardening as Affected by Film Thickness, Voids, and Permeability in Asphalt Mixtures," Proceedings, Association of Asphalt Paving Technologists, Cushing-Malloy, Ann Arbor, Michigan, Vol. 46, 1977. pp. 571-605.
83. Tia, M., Ruth, B.E., Josephson, L.I., and Chari, C., "Preliminary Investigation of Original and In-Service Asphalt Properties for the Development of Improved Specifications," Final Report 245-D53, Department of Civil Engineering, University of Florida, Gainesville, August 1986.
84. Huffman, J.E., Discussion of Asphalt Durability Symposium, paper by J.B. Skog, "Effect of Changes in Asphalt Properties on Pavement Performance, Zaca-Wigmore Test Road," Proceedings, Association of Asphalt Paving Technologists, Vol. 50, 1981, pp. 538-560.
85. Potts, C.F., Schwyer, H.E., and Smith, L.L., "An Analysis of Certain Variables Related to Field Performance of Asphalt Pavements," Proceedings, Association of Asphalt Paving Technologists, Cushing-Malloy, Ann Arbor, Michigan, Vol. 42, 1973, pp. 564-588.

86. "Airfield Pavement Evaluation, Eglin AFB Aux. Field 3 (Duke Field), Florida," Air Force Engineering and Services Center, Tyndall AFB, Florida, January 1987.
87. "Highway Pavement Distress Identification for Highway Condition and Quality of Highway Construction, Survey," Federal Highway Administration, Washington D.C., March 1979.
88. "Airfield Pavement Condition Survey, Eglin AFB Aux. Field 3 (Duke Field)," Armament Division, Directorate of Civil Engineering (USAF), 1979.
89. Brown, W.D., "Airfield Survey", Duke Field, Florida, August 1987.
90. "Aircraft Characteristics for Airfield Pavement Design and Evaluation," Air Force Engineering and Services Center, Tyndall AFB, Florida, 1983.
91. Kablan, R. A. T., "Evaluation of Selected Methods for Determining Soil Hydraulic Conductivity," Unpublished Master's Thesis, Department of Soil Science, University of Florida, Gainesville, 1986.
92. Hillel, D., Introduction to Soil Physics, Academic Press, Orlando, Florida, 1980.
93. Schimmelpfennig, H., "Basic Thermocouple Thermometry," Abstract, Application Note W-15, Wescor, Inc.
94. Holman, J.P., Experimental Methods for Engineers, McGraw-Hill Book Co., New York, 1978.
95. Southgate, H.F., and Deen, R.C., "Temperature Distribution in Asphalt Pavements," Highway Research Record No. 549, HRB, Washington D.C., 1975, pp. 39-46.
96. Bush III, A.J., "Performance Prediction of Low Volume Airfield Pavements," Technical Report GL-86-14, Geotechnical Laboratory, U.S. Army Engineer Waterways Experiment Station, Vicksburg, Mississippi, September 1986.
97. Standard Specifications for Transportation Materials and Methods of Sampling and Testing, American Association of State Highway and Transportation Officials, Part II, Washington D.C., 1982.
98. Davidson, J.L., "Engineering Properties of Soils Laboratory Testing," Course CE 460, Department of Civil Engineering, University of Florida, Gainesville, pp. 2.1-2.7.
99. "Standard Specifications for Road and Bridge Construction," Florida Department of Transportation, Tallahassee, 1986.

100. "A Brief Introduction to Asphalt and Some of Its Uses," MS-5, The Asphalt Institute, College Park, Maryland, 1977.
101. Ruth, B.E., and Miller, M.D., "Shoving of Dense Graded Friction Courses at Intersections," Final Report 99700-7389, Department of Civil Engineering, University of Florida, Gainesville, December 1987.
102. Chari, C.T., "Evaluation of Age Hardening Methods on the Characteristics of Asphalts and Asphaltic Mixtures," Ph.D. Dissertation, Department of Civil Engineering, University of Florida, Gainesville, 1988.
103. "Model Construction Specifications for Asphalt Concrete and Other Plant-Mix Types," SS-1, The Asphalt Institute, College Park, Maryland, 1980.
104. "Instruction Manual for Strain Gage Conditioner and Amplifier System," Measurements Group, Raleigh, North Carolina, n.d.
105. Tia, M., "Characterization of Cold-Recycled Asphalt Mixture," Joint Highway Research Project FHWA/IN/JHRP-82/5, School of Civil Engineering, Purdue University, West Lafayette, Indiana, 1982.
106. Ruth, B.E., Roque, R., and Puyana, E., "Low Temperature Pavement Response: Verification of Pavement Response and Cracking Models," Final Report 245-U70, Department of Civil Engineering, University of Florida, Gainesville, September 1983.
107. Kennedy, T.W., "Pavement Design Characteristics of Inservice Asphalt Mixtures," presented to the Transportation Research Board Center for Highway Research, The University of Texas at Austin, 1976.
108. Badu-Tweneboah, K., "Evaluation of Layer Moduli in Flexible Pavement Systems Using Nondestructive and Penetration Testing Methods," Ph.D. Dissertation, University of Florida, Gainesville, 1987.
109. Ullidtz, P., and Stubstad, R.N., "Analytical-Empirical Pavement Evaluation Using the Falling Weight Deflectometer," Transportation Research Record 1022, TRB, Washington D.C., 1985, pp. 36-44.
110. Roque, R., "Low Temperature Response of Asphalt Concrete Pavements," Ph.D. Dissertation, Department of Civil Engineering, University of Florida, Gainesville, 1986.
111. Neville, A.M., Properties of Concrete, Pitman Publishing Inc., London, England, 1983.

BIOGRAPHICAL SKETCH

Charles William Manzione was born May 24, 1958, in South Plainfield, New Jersey. His family moved ten miles north to Berkeley Heights in 1961 where he attended both private and public schools. He graduated from Governor Livingston Regional High School in 1976 and entered The Citadel in the Fall of that year. While at the Citadel, he became active in several organizations including Air Force ROTC, the Junior Sword and Summerall Guard Drill Teams, and the student chapter of the American Society of Civil Engineers (ACSE). He graduated in May 1980 with a Bachelor of Civil Engineering degree, an Air Force commission, and the Distinguished Military designation. He received selection into Who's Who Among Students in American Universities and Colleges his senior year and subsequently into Tau Beta Pi.

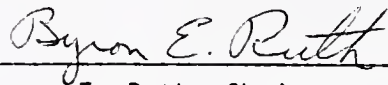
After a summer respite, Manzione entered the Air Force in September 1980 as a second lieutenant and was assigned to Keesler AFB, Mississippi. During his four years at Keesler, he served the civil engineering squadron in various capacities including design engineer, combat readiness officer, and resources and requirements chief.

In August 1984, Manzione moved to Gainesville to attend the University of Florida under the Air Force Institute of Technology Civilian Institute (AFIT/CI) Program. He received the Master of Engineering degree concentrating in the geotechnical field in December 1985 and was entered into the Phi Kappa Phi Honor Society. He started doctoral specialization in pavement/geotechnical engineering in January 1986.

Manziona is a registered professional engineer in the state of Mississippi and a member of the Society of Military Engineers (SAME). He has twice earned the Outstanding Young Men of America award.

Captain Manziona is married to the former Karen Cox of Ruston, Louisiana. They have a 21-month old son, Michael. They enjoy travel and family outings.

I certify that I have read this study and that in my opinion it conforms to acceptable standards of scholarly presentation and is fully adequate, in scope and quality, as a dissertation for the degree of Doctor of Philosophy.



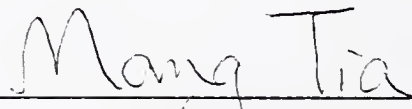
Byron E. Ruth, Chairman
Professor of Civil Engineering

I certify that I have read this study and that in my opinion it conforms to acceptable standards of scholarly presentation and is fully adequate, in scope and quality, as a dissertation for the degree of Doctor of Philosophy.



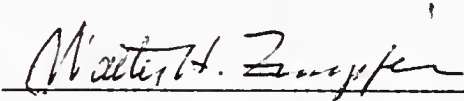
Michael C. McVay, Cochairman
Associate Professor of Civil
Engineering

I certify that I have read this study and that in my opinion it conforms to acceptable standards of scholarly presentation and is fully adequate, in scope and quality, as a dissertation for the degree of Doctor of Philosophy.



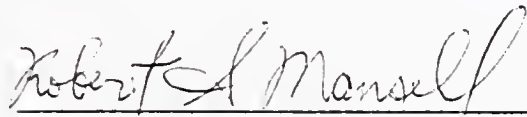
Mang Tia
Associate Professor of Civil
Engineering

I certify that I have read this study and that in my opinion it conforms to acceptable standards of scholarly presentation and is fully adequate, in scope and quality, as a dissertation for the degree of Doctor of Philosophy.



Walter H. Zimpfer
Associate Professor of Civil
Engineering

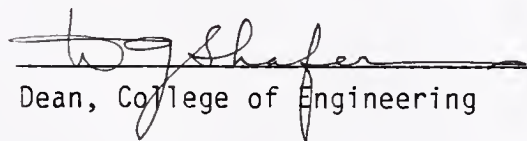
I certify that I have read this study and that in my opinion it conforms to acceptable standards of scholarly presentation and is fully adequate, in scope and quality, as a dissertation for the degree of Doctor of Philosophy.



Robert S. Mansell
Professor of Soil Science

This dissertation was submitted to the Graduate Faculty of the College of Engineering and to the Graduate School and was accepted as partial fulfillment of the requirements for the degree of Doctor of Philosophy.

April 1988



Dean, College of Engineering

Dean, Graduate School

66-1
D-745
#578